Identification of Novel Molecular Pathways Involved in Angiogenesis.

Ihsane Chrifi

Identification of Novel Molecular Pathways Involved in Angiogenesis.

Printed by 24-Drukwerk.nl
Cover design: Maarten Ebbelinghaus

Identification of Novel Molecular Pathways Involved in Angiogenesis.

Identificeren van nieuwe moleculaire signaaltransductie routes die een rol spelen in angiogenese.

Proefschrift

Ter verkrijging van de graad van doctor aan de Erasmus Universiteit Rotterdam op gezag van de rector magnificus

Prof. dr. R.C.M.E. Engels

En volgens besluit van het College voor Promoties.

De openbare verdediging zal plaatsvinden op

woensdag 16 januari 2019 om 11:30 uur

door

Ihsane Chrifi

geboren te Breda

Erasmus University Rotterdam

Promotiecommissie

Promotoren:	Prof. dr. D.J.G.M. Duncker
Overige leden:	Prof. dr. A.J.G. Horrevoets Prof. dr. J.M. Kros Dr. D. Merkus
Copromotor:	Dr. Kai Lai Cheng

The studies in this thesis have been performed at the laboratory of Experimental Cardiology, Erasmus Medical Center, Rotterdam, the Netherlands.

Financial support by the Dutch Heart Foundation for the publication of this thesis is gratefully acknowledged

Ter nagedachtenis aan mijn moeder Malika Rhazare
Zij zou trots zijn geweest
Bismillahi Rahmani Rahim

Table of Contents

Chapter 1 General Introduction and outline of this thesis.

General Introduction and outline of this thesis.

Multicellular organisms demand controlled access to oxygen and nutrients to efficiently conduct cellular processes. A highly developed vascular system has evolved during the evolution of complex multicellular organisms to ensure that all cells are within diffusion range of oxygen and nutrients. This triggers the expansion of the vasculature system to ensure that the developing organism reduces the functional diffusion distance, so that it can cope with the growing oxygen and nutrients demand (1). The development and expansion of the vasculature are mediated by a biological process called angiogenesis. In simple term, angiogenesis is the formation of blood vessels from pre-existing blood vessels. This complex process is subjected to a delicate balance between stimulatory and inhibitory signals of blood vessel growth. Dysregulation of the angiogenic balance leads to an uncontrolled vascular system in which vessel expansion and regression are abnormally affected. Whiteout therapeutic interference, abnormal angiogenesis proceed into a number of human diseases including malignant-, ischemic-, inflammatory-, infectious- and immune- disorders (2). In clinical therapy, restoring abnormal angiogenesis is based on pruning the vasculature to a normal balance of pro- and anti-angiogenic factors, which is also known as normalization. Agents that stimulate angiogenesis can improve blood flow in patients with ischemic diseases, whereas anti-angiogenic therapy can inhibit blood vessel growth during tumour angiogenesis. Adapting the concepts of vessel normalisation into therapy has not been proven to be as effective as originally hoped, because angiogenesis is regulated by multiple pathways. Therefore investigating these signalling pathways involved in angiogenesis is required for better understanding of the development of these diseases. In this thesis, we aim to provide a framework of the angiogenesis process by exploring and discovering prototypic regulatory mechanisms, which might shed light on failing normalisation therapies and offer novel pro- or anti-angiogenic therapies.

Capillary function

The majority of blood vessels are quiescent during adult life and are only activated during skeletal growth, wound healing, organ regeneration, inflammation, menstrual cycle and pregnancy (2). To cope with these functional demands blood vessels are recruited from activated capillary beds. The capillary beds form a bridge between the arteriole and venule in which gases, nutrients, immune cells are exchanged. They also help regulate blood pressures and play an important role in thermoregulation. Capillaries consist only of a basement membrane and a single endothelium layer, with scarce perivascular support of pericytes. Pericytes are cells of the connective-tissue family (mural cells), related to vascular smooth muscle cells, that wrap around small vessels at distinct functional locations of the capillary bed. The higher the blood pressure level, the more pericyte coverage is observed to compensate and regulate the vasomotion response of the vascular wall (4). During the initial phase of angiogenesis, pericytes interact with endothelial cells (ECs) to promote vascular permeability by

disrupting tight junctions between ECs, remodelling the extracellular matrix and by permeabilization of the basal membrane. In a later phase of angiogenesis, pericytes are recruited to the endothelium in favour of neovessel stabilization, maturation, and maintaining the endothelial barrier function (5). On the other hand, the single endothelium layer functions as a barrier between the blood circulation and surrounding tissue and regulate the exchange of substances between blood and interstitial fluid. ECs also control the vascular tone via endothelial nitric oxidase synthase (eNOS) mediated nitric oxide (NO) production, which acts as a modulator of vascular tone and on its turn the blood flow. High NO levels also prevent platelet coagulation through mediating the release of Von Willebrand factor (vWF) from its storage place, the Weibel-Palade bodies (WBP). The endothelium also plays an essential role in regulating the inflammatory response, for example by producing transcription factor nuclear factor kappa B (TNF-κB) to stimulate the ECs to secrete pro-inflammatory cytokines to recruit local immune cells.

Overall, the functional contribution of ECs and pericytes are recognized in physiological angiogenesis. To get a better understanding of the fundamental process involved in capillaries the molecular communication between ECs and pericytes should be addressed.

Hypoxia-induced angiogenesis

Angiogenesis is triggered by hypoxia as a response to cells exceeding their oxygen diffusion distance between tissue and capillary wall (>200 micrometres). In a low oxygen environment, cells start to produce hypoxia-inducible factor 1 alpha (HIF-1α), which is normally suppressed by oxygen-sensitive enzymes, namely prolyl hydroxylase domain-containing enzymes (PHDs). Consequently, the bioavailability of endogenous HIF-1α enhances transcriptional activation of pro-angiogenic factors. These pro-angiogenic factors are then secreted into the ECM and initiate communication with neighbouring capillaries to sprout towards the hypoxic cells (6). One of the major pro-angiogenic factors is vascular endothelial growth factor a (VEGFa) because it triggers or is involved in every known angiogenic pathway. The importance of VEGFa during angiogenesis is even highlighted in total and -heterozygous knockout studies of VEGFa in mice, which showed embryonic lethality due to multiple defects in vascular structure formation (7, 8). VEGFa forms several splice variants from which three crucial splice variant are well known to be secreted by hypoxic cells, namely $VEGFa^{121}$, $VEGFa^{165}$, and $VEGFa^{189}$. Depending on their amino acid size they differ in their diffusion distance through the ECM and therefore form a gradient of guidance cues for directional migration of the sprouting vessel (9). This established VEGFa gradient is recognised by the vascular endothelial growth factor receptor (VEGFR2) located on the membrane of vascular ECs. Thereby triggering the ECs to activate several molecular pathways involved in permeabilization, proliferation, migration, differentiation and pericytes detachment.

One of the molecular cascade activated by VEGFa is the eNOS pathway, which prevents blood leaking out of the permeable capillaries. eNOS stimulates NO production to dilate the capillary

wall and decrease its blood flow. Capillaries become permeable due to dimerization of activated VEGFR2 and VE-cadherin. VE-cadherin forms connections at the adherence junction site between ECs to support the endothelial barrier function. By forming dimers with VEGFR2 they undergo internalization which reduces the number of VE-cadherin-mediated adherens junctions and thus disrupting the endothelial barrier. VEGFa-VEGFr2 activation is also involved in the cross talk between EC and pericytes. VEGFa stimulates the ECs to synthesize and secrete Angiopoietin 2 (ANGPT2). ANGPT2 binds to its receptor TIE2 (Tyrosine kinase with Ig and epidermal growth factor homology domains 2) located on the pericytes, triggering pericytes to detach from the capillary wall. Destabilizing the capillary wall influences ECs and pericytes to enhance the production of metalloproteinases (MMP) in order to degrade the supporting basement membrane and surrounding extracellular matrix (ECM) enabling sprouting ECs to differentiate and migrate from the pre-existing vessel (figure 1).

Tip and stalk cell biology

Based on the differences in local VEGFa concentrations ECs are stimulated to differentiate into tip and stalk cells. Tip cells are selected by the responsiveness of ECs to the VEGFa gradient, which is dependent on the availability of VEGFR2. Chosen tip cells develop dynamic filopodia with accumulative VEGFR2 on the membrane, which detect the VEGFa gradient and lead the sprouting branch while migrating towards a denser VEGFa gradient (figure 1). Filopodia development is controlled by the Rho-guanosine-triphosphate (GTP) family, in particular cell division control protein 42 homologue (CDC42). CDC42 promotes filopodia–mediated movement by linking the cytoskeleton via its focal contacts to the ECM (10). Tip cell selection is also regulated via VEGFa-mediated activation of the Notch pathway, which is a key regulator of EC-fate, -differentiation and -survival. ECs compete for the tip cell position via the Notch receptor and its ligand Delta like 4 (DLL4), which both have an intracellular domain and an extracellular domain. The VEGFa gradient upregulates DLL4 expression in the nearest ECs and subsequently binds extracellularly to its Notch receptor on the membrane of neighbouring ECs. This forces the neighbouring ECs to downregulate their DLL4 expression and upregulate Notch signalling. High Notch signalling in the neighbouring cells promotes adaptation to a stalk cell phenotype which allows these cells to follow the tip cell, proliferate to support sprout elongation, undergo lumen formation, and recruit mural cells (pericytes or vascular smooth muscle cells) to stabilize the new vessel sprout. These processes are initiated by DLL4 stimulation of the Notch1 receptor on the stalk cells, leading to a downregulation of VEGFR2 receptors through direct binding of Hairy/Enhancer of split-related with YRPW motif protein 1 (HEY1) to the VEGFR2 promotor, whereas VEGFa antagonist receptor VEGFR1 (FLT1) is upregulated to restrict the VEGFa response. Another ligand of the Notch family is Jagged-1 which is manly expressed in stalk cells to promote stalk cell proliferation. Jagged-1/Notch signalling is also responsible for the maturation process by acting as a decoy ligand competing with DLL4 for the Notch receptors. This restricts the overall response (migration, proliferation,

ECM degradation, etc.) of ECs to DLL4/Notch signalling and stimulates recruitment of mural cells to stabilize the neovesse (figure 1) (2, 11).

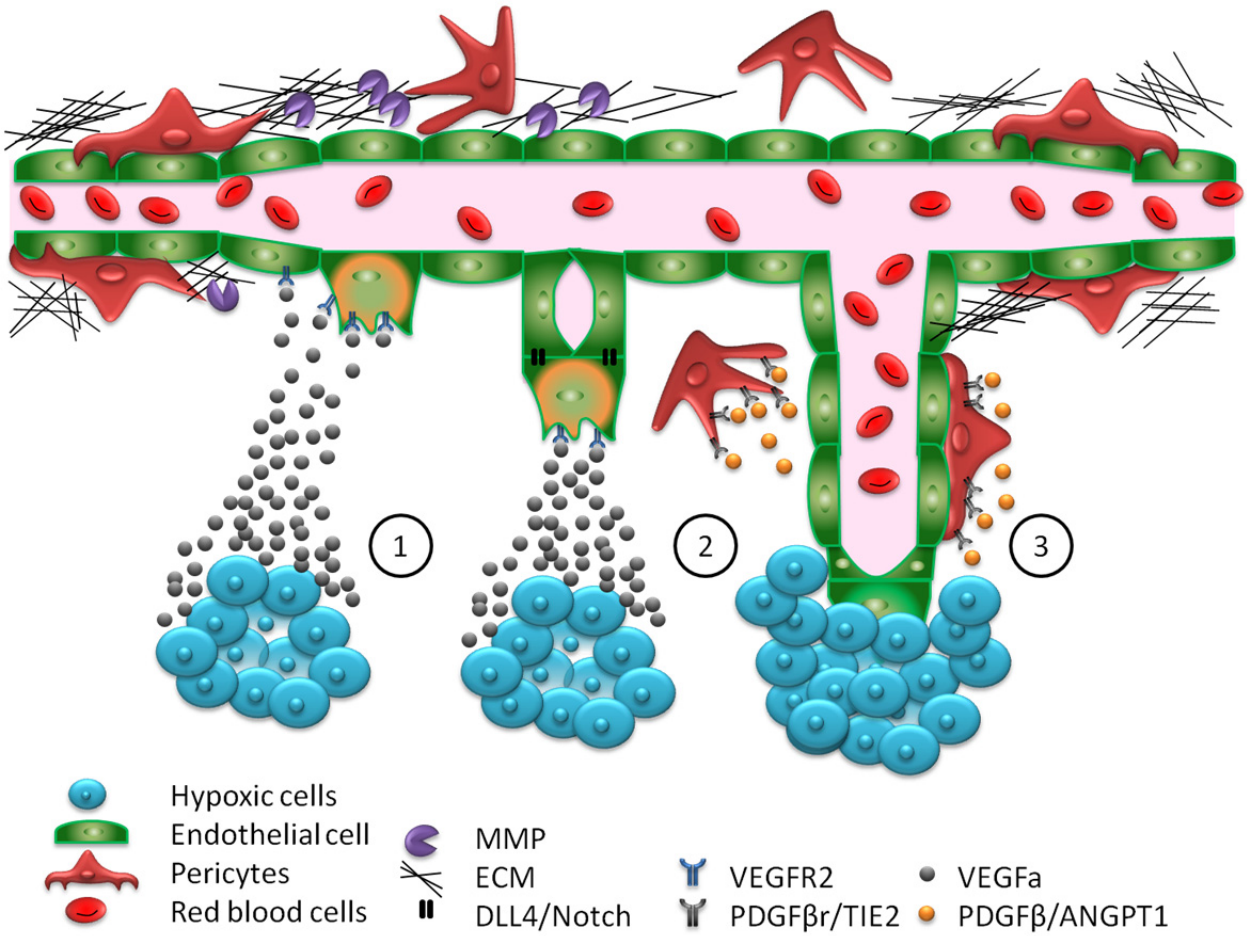

Figure 1: Schematic overview of the multistep process of angiogenesis. 1) Hypoxic cells secrete pro-angiogenic factors like VEGFa to activate ECs. ECs activate via its VEGFR2 and start releasing proteases like MMP to degrade the ECM and basement membrane. Pericytes detach from the basement membrane. 2) Tip and stalk cell selection based on the DLL4/Notch pathway. Tip cell migration towards hypoxic stimuli followed by stalk cell proliferation and lumen formation. 3) Stabilizing new sprout by attracting pericytes towards the sprout using PDGFβ-PDGFrβ and ANGPT1-TIE2 signalling. Rebuilding of the BM and ECM.

Lumen formation

Stalk cells luminize the established premature branch to allow blood perfusion. By adjusting their shape and rearranging EC junctions, an open structure (hollowing) is established within the sprout (figure 2). There are two proposed mechanisms for this hollowing process: cell hollowing and cord hollowing. In both processes, the ECs are polarized to determine the apical site for lumen development. This is initiated by direct interaction between integrins and ECM or adjacent ECs. Blockade of the α- or β-chain of the integrin family has been shown to result in improper polarity and complete absence of lumens *in vivo* and *in vitro* (12, 13). Lumen

formation triggers rearrangement of the actin cytoskeleton and the endosomal trafficking of adherence and tight junctions from the plasma membrane. Rearrangement of the cytoskeleton takes place through interaction between ECs and ECM-integrin, which signals downstream integrins to bind to F-actin and subsequently activate important cytoskeleton-rearrangement proteins, namely focal adhesion kinases (FAK) and Rho GTPases (CDC42 and RAC1). Endosomal trafficking plays a major role in the cell hollowing process by fusing vesicles into an elongated vacuole-like structure (VLS) spanning the length of the cell. Ultimately the VLS fuses with the plasma membrane to open up the exterior and establish luminal continuity between neighbouring ECs (figure 2) (14).

Endosomal trafficking during cord hollowing replaces the endothelial cell-cell adherens junctions VE-cadherin and E-cadherin with de-adhesive molecules podocalyxin (PODXL). Vesicles with negatively charged PODXL are released at the cell-cell contact to form an apical cell surface. This triggers the activation of negatively charged apical glycoproteins which lead to a repulsion of the apical cell surface (15). Small slits between interconnected ECs open up and develop into a lumen. The lumen is then further expanded by GTPase signalling that activates the formation of actomyosin complex. The actomyosin complexes together with the F-actin cytoskeleton induces the separation between the apical cell surfaces and generate the force that is required to widen the lumen (figure 2) (15).

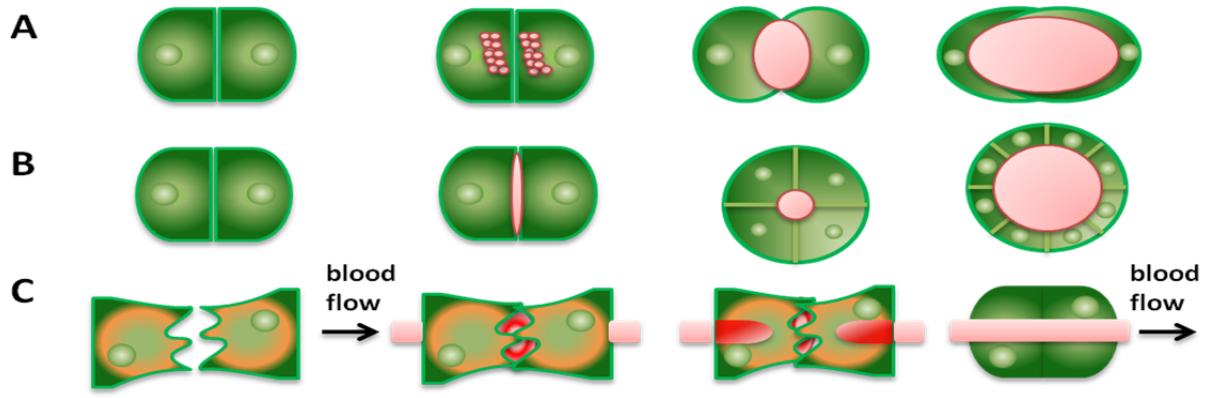

Figure 2: Lumen formation. A. Perpendicular view of cell hollowing: endosomal-induced vesicles fusion with plasma membrane which opens up a lumen. B. Perpendicular view of cord hollowing: apical membrane is established between two ECs by plasma membrane invagination. Anti-adhesive membrane molecules facilitate repulsion and thereby lumen formation. Cell division is essential for lumen expansion and maintenance of cell polarity. C. Longitudinal view of cord hollowing of anastomosing tip cells. Blood pressure stimulates plasma membrane invagination at the basal side of the tip cells whereas tip cell fusion stimulates vacuole formation at the apical side of the fused tip cells. Combining these hollowing processes results in extension of the lumen in which tip cells are connected to each other.

Perivascular cell recruitment and neovessel stabilization

Luminized neo-vessels still sustain limited endothelial barrier function, which makes them permeable and highly susceptible to vascular leakage and neo-vessel disintegration. Mural cells

are recruited to the neo-vessel wall, through paracrine communication mechanism between ECs and mural cells, which stabilize and mature the neo-vessel (figure 1). In response to VEGFa and MMP-mediated degradation of the ECM, ECs initiate the vascular stabilization process by releasing three crucial paracrine growth factors into the ECM: platelet-derived growth factor β (PDGF-β), Angiopoietin 1 (ANGPT1) and transforming growth factor β (TGF-β). Tip cells start secreting PDGF-β into the ECM to recruit surrounding mural cells expressing the receptor PDGFr-β. In a dose-dependent manner, PDGFr-β is being activated by PDGF-β to stimulate the mural cells to proliferate and migrate towards the PDGF-β stimuli. Stalk cells capture the secreted PDGF-β with their heparan sulfate proteoglycans and present them directly to mural cells. The high levels of PDGF-β in the ECM stimulate the Notch signalling pathway in mural cells to stimulate PDGFr-β on the cell surface. Ligand activation of the Notch1 receptor on mural cells leads to cleavage of the intracellular domain which able it to be transported to the nucleus and bind to the promotor of the PDGFr-β gene (16). The important role of PDGF-β signalling in neo-vascular stabilization is well demonstrated by studies, which report that PDGF-β or PDGFr-β knockout mice display decreased mural cell coverage in the vasculature. Contributing to dilated vessels and haemorrhaging, ultimately resulting in perinatal death (17). Whereas the paracrine PDGF-β/PDGFr-β communication mainly consists of signalling between ECs and mural cells, the ANGPT1/TIE2 paracrine signals mainly occur from mural cells to ECs. ANGPT1 is a ligand of the tyrosine kinase 2 receptor (TIE-2) and is known to act as an ANGPT2 antagonist. ANGPT1 is predominantly expressed by mural cells and promotes vascular stabilization and maturation by competing with ANGPT2 for a binding place on the TIE-2 receptor. This reduces ANGPT2–mediated upregulation of pro-angiogenic factors like VEGFa and MMPs, which promotes survival of the ECs, decreases the permeability of ECs barrier, and it results in basement membrane (BM) formation (18). ANGPT1 also stimulated ECs to increase production of mural cell recruitment factors like PDGF-β and TGF-β (19). Another multifunctional stabilization factor is TGF-β, which is a cytokine that can activate ECs and mural cells to proliferate, differentiate, migrate and determine their cell fate. The function of TGF-β is dependent on which activin receptor-like kinase receptor 1 or 5 (Alk-1 and Alk-5) it binds. Alk-1 signalling may occur in the early phase of TGF-β stimulation leading to cell proliferation and migration, whereas Alk-5 signalling dominates during stabilization, differentiation and extracellular matrix production. Activation of Alk-5 promotes Smad1/5 phosphorylation, which is transported into the nucleus to act as a transcription factor for target genes involved in cell cycle arrest leading to quiescence of ECs. It also acts as a transcription factor for target genes, which enhances differentiation of mesenchymal cells into smooth muscle cells and enhances co-activators for the build-up of the ECM. Alk-1 receptor activation leads to phosphorylation of Smad 1/5 and acts as a transcription factor of proliferation and migration genes, but also BM degradation markers. It is proposed that Akl1 signalling inhibits Alk5 signalling and vice versa, and is dependent on the amount of TGF-β secreted during interaction of ECs and mural cells.

Once the mural cells are recruited, they interact with ECs via TGFβ, PDGFβ and ANGPT1 pathways to establish the BM and the endothelial barrier function (figure 1). The BM separates the ECs from the pericytes and provides a meshwork of cell adhesion components consisting mainly of laminin, perlecan and nidogen 1 and 2. It also consists of fibronectin and collagen type IV which enhances the structural integrity of the neo-vessel. Previous studies have shown, that lack of pericytes leads to a decrease in the deposition of BM structural components and lead to failure of blood vessel stabilization. In addition, *in vivo* and *in vitro* studies have shown that pericyte interaction with ECs enhances the production of BM proteins (20, 21). The established BM is protected from MMP-mediated degradation by pericytes secretion of tissue inhibitor of metalloproteinase 3 (TIMP3) and metallopeptidase domain 15 (ADAM-15), thus increasing the survival and stability of the newly formed vascular BM.

Cell adhesion molecules

Pericytes and ECs are surrounded by the BM and maintain direct contact through micro pores at distinct points. One of the most well described contact morphologies are the peg- and-socket construction, in which pericytes filopodia (pegs) are inserted into endothelial invaginations (pockets). Peg-and-socket contacts are highly enriched in the gap junctions components Connexin-43 to allow exchange of ions and small molecules, which promotes TGF-β synthesis and differentiation of the mural cells into a smooth muscle like phenotype. They are also enriched in neuronal-(N)-cadherin-based adherence junctions. In combination with Notch signalling and mural cells secreted TGF-β activates sphingosine-1-phospate (S-1-P) signalling in ECs which leads to the transcription of N-cadherin. Cytoskeleton changes induced by RAC (Ras-related C3 botulinum toxin substrate 1) redistributes N-cadherin to facilitate a direct interaction with mural cells. N-cadherin-mediated adhesion of ECs-pericytes stimulates production of vascular endothelial-(VE)-cadherin to form tight junctions between ECs. This process thus strengthens the EC barrier function (cell-cell contacts) resulting in maturation and stabilization of the neo-vessel wal (22). In addition, VE-cadherin reduces the capacity of ECs to respond to proliferative stimuli by binding to VEGFR2 and inhibiting its pro-angiogenic signalling activity. Indeed, targeted inactivation of VE-cadherin in mice impairs vascular remodelling and maturation, causing lethality at 9.5 days of gestation.(23) Because of the reduced complex formation of VE-cadherin with VEGFR2, it induced endothelial apoptosis and abolished transmission of the endothelial survival signal (23). A reduction in responsiveness to pro-angiogenic factors in combination with EC-confluence and subsequently stabilization of VE-cadherin junctions ultimately leads to EC quiescence.

Endocytosis

During and after angiogenesis, highly complex signalling is being processed ranging from ligand-induced activation of cell surface receptors to rearrangement of cell-cell adhesion markers and regulating tight junctions. Downstream signalling of known pro-angiogenic factors such as

VEGFR2 and VE-cadherin signalling is partially regulated via endocytosis, which determines bio-availability, amplitude and duration of the downstream signalling. Disruption in intracellular trafficking of these membrane proteins leads to downstream signal termination and eventual impairment in angiogenesis (24). The molecular pathways involved in the complexity of multifaceted endocytosis pathways are still unclear and needs to be elucidated. In general plasma membrane proteins (cargo) are selected by adaptor protein complex family (AP-2) where it binds to sorting signals in the cytosolic tail of the protein (25). AP-2 also acts as an adaptor for clathrin-mediated endocytosis in which the AP-2 marked cargo is engulfed in clathrin-coated vesicles, forming what is also known as 'early endosomes'. In early endosomes, members of the RAB family of GTPases determine the fate of internalized cargo. Cargo can be recycled from the endosomes back to the plasma membrane or -under conditions of saturation- can be sorted into endosomes for degradation and retrograde transport to the trans-Golgi network (TGN). Around 60 RAB GTPases are known in literature involved in downstream membrane trafficking. RAB GTPases activate the trafficking kinetics by continuous cycles of GDP/GTP exchange through nucleotide exchange factor. Many types of endocytosis are mediated by RAB5, which promotes the internalization of transmembrane proteins by clathrin-coated vesicles (budding) and their transport to early endosomes. From the early endosomes RAB4 and RAB11 mediate transportation to the recycling endosomes. In contrast, RAB7 and RAB9 mediate trafficking towards the late endosomes to be fused with lysosomes for degradation and eventually retrograde transport to the TGN (22).
The regulatory mechanisms of membrane trafficking in vascular cells during angiogenesis remains incompletely understood. In this thesis, we have identified 2 putative proteins from the CKLF-like MARVEL Transmembrane domain family (CMTM) and Cingulin like 1 (cgnl1) as important regulators of VE-cadherin trafficking from the plasma membrane to recycling endosomes and lysosomes (see **chapter 2, 3 and 4**).

Identifying new genes involved in angiogenesis

Once blood vessels are stabilized and matured, the ECs and mural cells undergo tissue-specific changes to generate a functionally distinct vessel. As the new vessel is established oxygen-rich blood is being transported to the tissue eventually halting angiogenesis, because of a decline in HIF-1α and VEGF activity. Although, the general mechanistic overview of angiogenesis is well described the nature of angiogenesis during pathogenesis remains poorly understood. In particular, the influence of disease on the ability of pericytes to differentiate and stabilize the vessel, but also the nature of the pericyte–endothelial contacts, which vary in the course of vessel development, remain to be investigated in different pathological situations.
To identify new key regulators in angiogenesis and vascular homeostasis we previously conducted a micro-array screen on the transcriptome of murine embryos. We selected cells, which express Fetal liver kinase 1 (Flk1, murine orthologue of VEGFR-2) because they are known to be expressed in precursor ECs (angioblasts) and mature ECs, making them the ideal marker

for ECs development (26). Using fluorescent activated cell sorting FLK1 positive cells were sorted and measured during various stages of murine embryonic development. Total RNA was extracted from both FLK-positive and FLK-negative cells and their expression profile were compared using microarray analysis. A specified list of genes, that were significantly upregulated in FLK-positive cells were used for whole-mount *in situ* hybridization in zebrafish larvae, to validate their specific vascular expression. Hence, genes with a corresponding expression pattern in the vasculature were selected to investigate their function in *in vivo* and *in vitro* models. Candidate knockdown assays were conducted targeting the development of vasculature in zebrafish and mural retina *in vivo* in combination with *in vitro* knockdown assays, which were performed in 3D-collagen based co-culture of ECs and pericytes to assess blood vessel formation. Candidate genes with validated angiogenic function were further investigated in the context of disease.

Angiogenesis in pathology

Most of our blood vessel network is developed during embryogenesis and organ growth. In a healthy adult individual, most blood vessels remain quiescent and angiogenesis occurs only in a few circumstances: during the monthly cycle to build the lining of the uterus and during pregnancy to form the placenta. Moreover, angiogenesis is also triggered by a physiological stimuli such as hypoxia and inflammation during wound healing and repair. Previously, we described the tightly balanced range of angiogenic factors, which can act as stimulators or inhibitors of vessel formation. However, in pathophysiology conditions an imbalance can occur in these angiogenic factors resulting in loss of quiescence regulation of the vessels. This may result in excessive angiogenesis, which contributes to tumour development and metastasis, or insufficient endothelial repair, which leads to several cardiovascular conditions such as atherosclerosis.

Atherosclerosis (*thsd1*)

Endothelial dysfunction is one of the earliest events in atherosclerosis. Except from an imbalance in vascular tone, the deteriorated endothelium activates and features pro-vascular adhesion, pro-inflammatory, pro-oxidant, proliferative and pro-coagulation responses. Low-density lipoprotein (LDL) particles enter the damaged endothelium and undergo oxidative modification as a result of interaction with reactive oxygen species (ROS) to form oxidized LDL. Oxidized LDL triggers the ECs to produce vascular cell adhesion protein 1 (VCAM-1, ICAM-1, E-selectin, PCAM-1), chemotactic proteins (MCP-1) and growth factors (macrophage colony-stimulating factor, M-CSF) to recruit monocytes and lymphocytes to the vessel wall (36). Monocytes differentiate into macrophages and take up the oxidized LDL, resulting in foam cells that are trapped in the vascular wall and contribute to the formation of fatty streaks. The accumulation of fatty streaks results in a hypoxic environment with necrotic foam cells releasing their free cholesterol and modified lipids into the core matrix, forming what is known as the

necrotic core. The necrotic core expands into the intima due to the continuous influx of white blood cells further fuelling the entrapment of necrotic foam cells. Vascular smooth muscle cells are also stimulated to migrate from the media into the neo-intima to enclose the lipid-rich necrotic core and to deposit extracellular matrix to form a fibrous cap. As the fatty streak, expands it develops into a stable or unstable plaque. In stable plaques, the fibrous cap is thick and contains only small amounts of lipids. In contrast, in unstable plaques the fibrous cap is thin and contains a lipid-rich necrotic core with a severe accumulation of inflammatory cells, pericyte-mediated calcification, cell debris and signs of neovascularisation. (37) These unstable plaque (i.e. vulnerable) are prone to rupture, mostly due to activation of inflammatory cells in the plaque shoulder. T-cells secrete interferon type II (IFN-γ), which inhibits the production of the ECM by SMCs, whereas the enhanced activity of macrophages degrades the ECM of the fibrous cap via the production of various proteases, collagenases, gelatinases and stromelysin. (38) As the plaque advances in size, the hypoxic surface keeps increasing. To meet the oxygen-demand, the inflammatory cells secrete pro-angiogenic factors (VEGFa, FGF2, and PDGF-β) to promote neovascularization. The microvessels in the adventitia (vasa vasorum) sprout towards the plaque to supply a second route for inflammatory cells to enter the plaque and accelerate plaque growth. The newly formed microvessels in the plaque demonstrate an immature phenotype, due to high local VEGFa levels produced by activated inflammatory cells. Lack of PDGF-β mediated pericyte coverage further enables hyperproliferation and functional dedifferentiation of the endothelium. (37) Combined, this results in unstable neovessel structures that are more prone to intraplaque haemorrhaging and contribute to further weakening of the advanced lesion. Currently, our understanding of the working mechanism of intimal neovascularisation is incomplete, and further studies of the molecular pathways involved in intraplaque neovascular growth may contribute to novel drug targets for the treatment of unstable plaques. (37) In this thesis, we have identified Thrombospondin, type 1, domain containing 1 (*Thsd-1*) as a potential angiogenic factor and studied its role in murine vulnerable plaque model. The findings of this study are presented in **chapter 5** (39).

Vascular tone (Up_4A)

Insufficient angiogenesis is caused by exposure of the endothelium to risk factors, including smoking, dyslipidemia, hypertension or diabetes (27). These early risk factors contribute to endothelial dysfunction, which has a major effect on the vascular tone. ECs dysfunction causes an impaired balance of vasodilators and vasoconstrictors, making the arterial wall prone to damage and eventually atherosclerosis. Mediators of vascular tone are divided into endothelium-derived relaxing factors (EDRFs, vasodilators), including nitric oxide, prostacyclin, endothelium derived hyperpolarizing factors (EDHFs), and into endothelium-derived contracting factors (EDCFs, vasoconstrictors) such as endothelin and angiotensin (27, 28). Mechanisms that mediate the bioavailability of EDFRs and EDCFs are attractive drug targets to counter endothelial dysfunction. Jankowski et al. identified Uridine adenosine tetraphosphate (Up_4A) as

a novel target for EDCFs. Up_4A is synthesized by the VEGFR2 pathway and released by the ECs in response to acetylcholine, endothelin-1, adenosine triphosphate (ATP, uridine triphosphate (UTP) and mechanical stress. Up_4A contains both an adenosine and uridine moiety, which indicates that it is able to regulate the vascular tone via its purinergic and/or pyrimidinergic receptors. Several studies have investigated the vasomotor properties of Up_4A in different rat/mouse models and the results indicate that Up_4A levels are elevated in particular during hypertension suggesting a putative role in vascular dysfunction in pathophysiological conditions. (29-35) However, the physiological role of Up_4A during angiogenesis and through which purinergic receptor(s) it signals is currently unknown. In this thesis we investigate the role of Up_4A in angiogenesis. Findings of this study are discussed in **chapter 6**.

Tumour angiogenesis (Cecr1)

As mentioned earlier, the immune system is an essential regulator of angiogenesis in pathophysiological conditions. In the context of cancer, immune cells produce important pro-angiogenic factors (VEGF, ANGPT, PDGFβ etc.), which supports excessive activation of ECs resulting in the vascularization of tumour cells to facilitate tumour growth and metastasis. Until now anti-VEGFa therapy has not been very successful in treating tumour-mediated angiogenesis, because alternative pathways such as FGF2- and HIF1α- pathways, can bypass the treatment. In particular, macrophages located in the microenvironment of specific types of tumours are able to enhance the production of pro-angiogenic molecules (VEGFa, FGF, TNFα) in response to anti-VEGFa treatment (40). The highly pro-angiogenic microenvironment ``overstimulates'' ECs, which results in unevenly distributed tumour vessels that form chaotic tortuous networks of irregular branching patterns that cannot constantly be perfused (41). Over time, tumour cells are able to alter vessel morphology, physiology, and responsiveness to therapy which makes it hard to target common angiogenic pathways.

The critical role of the tumour associated macrophages (TAMs) has not been extensively investigated as a potential culprit of tumour progression. Many tumour cells produce colony-stimulating factors (CSF-1 also known as M-CSF) that prolong survival, proliferation, and differentiation of TAMs (42). TAMs are divided into M1 and M2 macrophages. M1 macrophages are primarily associated with acute tumour suppression because of their pro-inflammatory state. They are capable of tumour cell phagocytosis and antigen presenting to cytotoxic T-cells. M1-TAMs are in general characterised by the expression of CD40, CD80, CD16/32, CD86 (CD= cluster of differentiation), CCR7 (CC, chemotactic chemokines) and HLA-DR (human leukocyte antigen-antigen D related). In contrast, M2 macrophages are associated with immune modulation, wound heling, neovascularisation, tumour progression. M2 macrophages are characterised by IL-4, IL-10, IL-13 (IL, interleukin), CD163, CD204, CD14 and function in favour of neovessel formation and communicate with ECs and pericytes via VEGFa, EGF, PDGFβ pathways.

Clinical evidence indicates that in most tumours, an abundance of M2-TAMs mostly have a negative impact on patient survival (43-46).

In one of the studies described in this thesis, we focused on the most aggressive and vascularized form of a brain tumour, glioblastoma multiform (glioma or GBM). Glioma consists 30-50% of microglia and macrophages, with their densities positively correlated with glioma grade severity, vascularisation and malignancy (47). Microglia are mononuclear cells distributed throughout the brain where they function as key immune effector cells of the central nervous system (CNS). Together with monocytes, they form tumour associated macrophages (TAMs) who influence glioma growth and invasion, by generating high levels of oxygen radicals that induces genomic mutations and stimulate neovascularisation for oxygen and nutrients supply. Due to the hypoxic environment and impaired blood brain barrier, glial tumour cells secrete TAMs recruitment factors CSF-1, monocyte chemoattractant protein-1 (MCP-1 or CCCL2) MMP2, and periostin (POSTN). Analysis of human glioma samples by FACS has revealed that gliomas contain more recruited monocytes ($CD45^{high}$) than microglia ($CD45^{low}$) cells (48, 49). After TAMs invasion and infiltration, glioma cells take control of the phenotype of the TAMs by secreting factors to polarise them into more M2-like cells. IL-10 secretion creates an immunosuppressive microenvironment by reducing phagocytosis activity and by impairment of the antigen presenting properties by preventing MHC-class 2 expression. The polarised M2-TAMs start expressing MMP9, EGF, VEGF to promote neo-vascularisation so that oxygen, nutrients, and TAMs can be supplied to the glioma cells to promote expansion and metastasis. The precise mechanism by which M2-TAMs contributes to neo-vascularisation in glioma requires further study. In this thesis, we identified Cat Eye Syndrome Critical Region Protein 1 (CECR1) as a substantial factor in promoting TAMs polarization towards M2-like macrophages and supporting subsequent microvascular growth in glioblastoma. We also demonstrated that CECR1 activity promotes new vessel formation *in* vitro, via CECR1-PDGFβ-PDGFβr cross talk between macrophages and pericytes (see **chapter7**).

Outline of this thesis

Neovascularisation is a complex process that is involved in the development of a myriad of adult human diseases. The antiangiogenic agents currently tested have mainly targeted on inhibiting the VEGF pathway. However VEGF targeting alone has not been proven to be 100% effective in treatment, and it is becoming increasingly clear that many (yet unknown) interconnected and compensatory pathways also need to be targeted. Therefore identifying a new generation of multi-targeted anti-angiogenic agents will broaden and maximize the potential therapeutic approach. This thesis focuses on the discovery of novel molecular pathways that are involved in the development of neovascularisation *in vitro* versus *in vivo* studies, and in physiological conditions versus pathophysiological conditions. Using a genome-wide microarray screen of FLK-positive angioblasts during mouse embryogenesis, we have identified CKLF-like Marvel domain family (CMTM), Cingulin like 1 (Cgnl1), Thrombospondin type 1 domain containing 1

(Thsd-1) and Cat Eye Critical Region 1 (CECR1), as putative new candidates to target the angiogenic process. In **chapter 2 and 3** we describe how CKLF-like MARVEL domain family members CMTM3 and CMTM4 contributes to angiogenesis *in vitro* and in the development of zebrafish vasculature. We have shown that the CMTM family acts on the EC-EC barrier function by controlling the endocytic pathway of VE-cadherin internalisation. In **chapter 4** we demonstrate that Cgnl1 is specifically expressed in ECs and plays a crucial role in sustaining neovascular growth and stability *in vitro* and *in vivo* (murine based retina model). We discovered that Cgnl1 molecular function is based on the mechanism of regulating VE-cadherin association with the actin cytoskeleton, thereby stabilizing EC-EC adherence junctions. In **chapter 5** we identified Thsd-1 as a regulator of angiogenesis in different *in vivo* models including the zebrafish vascular development model, the postnatal retinal vascular development model in mice, and in the murine vulnerable plaque model. Our data shows that Thsd-1 plays an essential role in establishing and preserving the endothelial barrier function during angiogenesis *in vivo*. In **chapter 6** we explored the angiogenic potential of uridine adenosine tetraphosphate (Up_4A). Up_4A promotes tubule formation in a 3D-collagen based co-culture of ECs and pericytes. The proposed molecular mechanism appears to be activation of the purinergic receptors P2YRs and stimulation of the pro-angiogenic factors VEGFa and ANGPT2. Selective blockade of P2Y6R demonstrated that the pro-angiogenic properties of Up_4A are principally mediated via Up_4A-P2Y6R signalling. In **chapter 7** the role of CECR1 in glioma-based angiogenesis is described. We found that CECR1 polarizes macrophages into pro-angiogenic macrophages (M2-macrophages) which promotes cross talk between M2-macrophages and ECs-mural cells during angiogenesis. Finally, in **chapter 8** we integrate and discuss the results presented in this thesis and provide recommendations for future research.

Literature

1. Monahan-Earley R, Dvorak AM, Aird WC. Evolutionary origins of the blood vascular system and endothelium. J Thromb Haemost. 2013;11 Suppl 1:46-66.
2. Potente M, Gerhardt H, Carmeliet P. Basic and therapeutic aspects of angiogenesis. Cell. 2011;146(6):873-87.
3. Zhao Y, Adjei AA. Targeting Angiogenesis in Cancer Therapy: Moving Beyond Vascular Endothelial Growth Factor. Oncologist. 2015;20(6):660-73.
4. Armulik A, Genove G, Betsholtz C. Pericytes: developmental, physiological, and pathological perspectives, problems, and promises. Dev Cell. 2011;21(2):193-215.
5. van Dijk CG, Nieuweboer FE, Pei JY, Xu YJ, Burgisser P, van Mulligen E, et al. The complex mural cell: pericyte function in health and disease. Int J Cardiol. 2015;190:75-89.
6. Majmundar AJ, Wong WJ, Simon MC. Hypoxia-inducible factors and the response to hypoxic stress. Mol Cell. 2010;40(2):294-309.
7. Carmeliet P, Ferreira V, Breier G, Pollefeyt S, Kieckens L, Gertsenstein M, et al. Abnormal blood vessel development and lethality in embryos lacking a single VEGF allele. Nature. 1996;380(6573):435-9.
8. Ferrara N, Carver-Moore K, Chen H, Dowd M, Lu L, O'Shea KS, et al. Heterozygous embryonic lethality induced by targeted inactivation of the VEGF gene. Nature. 1996;380(6573):439-42.
9. Dvorak HF. Angiogenesis: update 2005. J Thromb Haemost. 2005;3(8):1835-42.
10. Fantin A, Lampropoulou A, Gestri G, Raimondi C, Senatore V, Zachary I, et al. NRP1 Regulates CDC42 Activation to Promote Filopodia Formation in Endothelial Tip Cells. Cell Rep. 2015;11(10):1577-90.
11. Phng LK, Gerhardt H. Angiogenesis: a team effort coordinated by notch. Dev Cell. 2009;16(2):196-208.
12. Drake CJ, Davis LA, Little CD. Antibodies to beta 1-integrins cause alterations of aortic vasculogenesis, in vivo. Dev Dyn. 1992;193(1):83-91.
13. Bayless KJ, Salazar R, Davis GE. RGD-dependent vacuolation and lumen formation observed during endothelial cell morphogenesis in three-dimensional fibrin matrices involves the alpha(v)beta(3) and alpha(5)beta(1) integrins. Am J Pathol. 2000;156(5):1673-83.
14. Lubarsky B, Krasnow MA. Tube morphogenesis: making and shaping biological tubes. Cell. 2003;112(1):19-28.
15. Lammert E, Axnick J. Vascular lumen formation. Cold Spring Harb Perspect Med. 2012;2(4):a006619.
16. Jin S, Hansson EM, Tikka S, Lanner F, Sahlgren C, Farnebo F, et al. Notch signaling regulates platelet-derived growth factor receptor-beta expression in vascular smooth muscle cells. Circ Res. 2008;102(12):1483-91.
17. Leveen P, Pekny M, Gebre-Medhin S, Swolin B, Larsson E, Betsholtz C. Mice deficient for PDGF B show renal, cardiovascular, and hematological abnormalities. Genes Dev. 1994;8(16):1875-87.
18. Uemura A, Ogawa M, Hirashima M, Fujiwara T, Koyama S, Takagi H, et al. Recombinant angiopoietin-1 restores higher-order architecture of growing blood vessels in mice in the absence of mural cells. J Clin Invest. 2002;110(11):1619-28.
19. Stoeltzing O, Ahmad SA, Liu W, McCarty MF, Wey JS, Parikh AA, et al. Angiopoietin-1 inhibits vascular permeability, angiogenesis, and growth of hepatic colon cancer tumors. Cancer Res. 2003;63(12):3370-7.

20. Stratman AN, Davis GE. Endothelial cell-pericyte interactions stimulate basement membrane matrix assembly: influence on vascular tube remodeling, maturation, and stabilization. Microsc Microanal. 2012;18(1):68-80.
21. Stratman AN, Malotte KM, Mahan RD, Davis MJ, Davis GE. Pericyte recruitment during vasculogenic tube assembly stimulates endothelial basement membrane matrix formation. Blood. 2009;114(24):5091-101.
22. Kawauchi T. Cell adhesion and its endocytic regulation in cell migration during neural development and cancer metastasis. Int J Mol Sci. 2012;13(4):4564-90.
23. Carmeliet P, Lampugnani MG, Moons L, Breviario F, Compernolle V, Bono F, et al. Targeted deficiency or cytosolic truncation of the VE-cadherin gene in mice impairs VEGF-mediated endothelial survival and angiogenesis. Cell. 1999;98(2):147-57.
24. Lampugnani MG, Orsenigo F, Gagliani MC, Tacchetti C, Dejana E. Vascular endothelial cadherin controls VEGFR-2 internalization and signaling from intracellular compartments. J Cell Biol. 2006;174(4):593-604.
25. Ohno H, Stewart J, Fournier MC, Bosshart H, Rhee I, Miyatake S, et al. Interaction of tyrosine-based sorting signals with clathrin-associated proteins. Science. 1995;269(5232):1872-5.
26. Nishikawa SI, Nishikawa S, Hirashima M, Matsuyoshi N, Kodama H. Progressive lineage analysis by cell sorting and culture identifies FLK1+VE-cadherin+ cells at a diverging point of endothelial and hemopoietic lineages. Development. 1998;125(9):1747-57.
27. Davignon J, Ganz P. Role of endothelial dysfunction in atherosclerosis. Circulation. 2004;109(23 Suppl 1):III27-32.
28. Duncker DJ, Koller A, Merkus D, Canty JM, Jr. Regulation of coronary blood flow in health and ischemic heart disease. Prog Cardiovasc Dis. 2015;57(5):409-22.
29. Matsumoto T, Tostes RC, Webb RC. The role of uridine adenosine tetraphosphate in the vascular system. Adv Pharmacol Sci. 2011;2011:435132.
30. Linder AE, Tumbri M, Linder FF, Webb RC, Leite R. Uridine adenosine tetraphosphate induces contraction and relaxation in rat aorta. Vascul Pharmacol. 2008;48(4-6):202-7.
31. Gui Y, Walsh MP, Jankowski V, Jankowski J, Zheng XL. Up4A stimulates endothelium-independent contraction of isolated rat pulmonary artery. Am J Physiol Lung Cell Mol Physiol. 2008;294(4):L733-8.
32. Hansen PB, Hristovska A, Wolff H, Vanhoutte P, Jensen BL, Bie P. Uridine adenosine tetraphosphate affects contractility of mouse aorta and decreases blood pressure in conscious rats and mice. Acta Physiol (Oxf). 2010;200(2):171-9.
33. Jankowski V, Meyer AA, Schlattmann P, Gui Y, Zheng XL, Stamcou I, et al. Increased uridine adenosine tetraphosphate concentrations in plasma of juvenile hypertensives. Arterioscler Thromb Vasc Biol. 2007;27(8):1776-81.
34. Zhou Z, Merkus D, Cheng C, Duckers HJ, Jan Danser AH, Duncker DJ. Uridine adenosine tetraphosphate is a novel vasodilator in the coronary microcirculation which acts through purinergic P1 but not P2 receptors. Pharmacol Res. 2013;67(1):10-7.
35. Zhou Z, de Wijs-Meijler D, Lankhuizen I, Jankowski J, Jankowski V, Jan Danser AH, et al. Blunted coronary vasodilator response to uridine adenosine tetraphosphate in post-infarct remodeled myocardium is due to reduced P1 receptor activation. Pharmacol Res. 2013;77:22-9.
36. Lusis AJ. Atherosclerosis. Nature. 2000;407(6801):233-41.

37. Cheng C, Chrifi I, Pasterkamp G, Duckers HJ. Biological mechanisms of microvessel formation in advanced atherosclerosis: the big five. Trends Cardiovasc Med. 2013;23(5):153-64.
38. Libby P. Changing concepts of atherogenesis. J Intern Med. 2000;247(3):349-58.
39. Haasdijk RA, Den Dekker WK, Cheng C, Tempel D, Szulcek R, Bos FL, et al. THSD1 preserves vascular integrity and protects against intraplaque haemorrhaging in ApoE-/- mice. Cardiovasc Res. 2016;110(1):129-39.
40. Bando H, Toi M. Tumor angiogenesis, macrophages, and cytokines. Adv Exp Med Biol. 2000;476:267-84.
41. Nagy JA, Chang SH, Shih SC, Dvorak AM, Dvorak HF. Heterogeneity of the tumor vasculature. Semin Thromb Hemost. 2010;36(3):321-31.
42. Murdoch C, Giannoudis A, Lewis CE. Mechanisms regulating the recruitment of macrophages into hypoxic areas of tumors and other ischemic tissues. Blood. 2004;104(8):2224-34.
43. Bingle L, Brown NJ, Lewis CE. The role of tumour-associated macrophages in tumour progression: implications for new anticancer therapies. J Pathol. 2002;196(3):254-65.
44. Balkwill F, Mantovani A. Inflammation and cancer: back to Virchow? Lancet. 2001;357(9255):539-45.
45. Pollard JW. Tumour-educated macrophages promote tumour progression and metastasis. Nat Rev Cancer. 2004;4(1):71-8.
46. Condeelis J, Pollard JW. Macrophages: obligate partners for tumor cell migration, invasion, and metastasis. Cell. 2006;124(2):263-6.
47. Rossi ML, Hughes JT, Esiri MM, Coakham HB, Brownell DB. Immunohistological study of mononuclear cell infiltrate in malignant gliomas. Acta Neuropathol. 1987;74(3):269-77.
48. Parney IF, Waldron JS, Parsa AT. Flow cytometry and in vitro analysis of human glioma-associated macrophages. Laboratory investigation. J Neurosurg. 2009;110(3):572-82.
49. Muller A, Brandenburg S, Turkowski K, Muller S, Vajkoczy P. Resident microglia, and not peripheral macrophages, are the main source of brain tumor mononuclear cells. Int J Cancer. 2015;137(2):278-88.

Chapter 2 CMTM3 mediates angiogenesis by regulating cell surface availability of Ve-cadherin in endothelial adherens junctions.

Ihsan Chrifi, Laura Louzao-Martinez, Maarten Brandt, Christian G.M. van Dijk, Petra Burgisser, Changbin Zhu MD, Johan M Kros MD, Dirk J. Duncker Caroline Cheng.

Published: Atherosclerosis Thrombosis Vascular Biology 2017 Jun; 37(6): 1098-1114

Abstract

Aim:
Decrease in Ve-cadherin adherens junctions (AJs) reduces vascular stability, whereas disruption of AJs is a requirement for neovessel sprouting during angiogenesis. Endocytosis plays a key role in regulating junctional strength by altering bio-availability of cell surface proteins, including Ve-cadherin. Identification of new mediators of endothelial endocytosis could enhance our understanding of angiogenesis.
Here we assessed the function of CKLF-like MARVEL Transmembrane domain 3 (CMTM3), which we have previously identified as highly expressed in Flk1+ endothelial progenitor cells during embryonic development.

Methods and Results:
Using a 3D co-culture of HUVECs-GFP and pericytes-RFP, we demonstrated that siRNA-mediated CMTM3 silencing in HUVECs impairs angiogenesis. *In vivo* CMTM3 inhibition by morpholino injection in developing zebrafish larvae confirmed that CMTM3 expression is required for vascular sprouting. CMTM3 knockdown in HUVECs does not affect proliferation or migration. Intracellular staining demonstrated that CMTM3 co-localizes with early endosome markers EEA1 and Clathrin+ vesicles, and with cytosolic Ve-cadherin in HUVECs. Adenovirus-mediated CMTM3 overexpression enhances endothelial endocytosis, shown by an increase in Clathrin+, EEA1+, Rab11+, Rab5+, and Rab7+ vesicles. CMTM3 overexpression enhances, whereas CMTM3 knockdown decreases internalization of cell surface Ve-cadherin *in vitro*. CMTM3 promotes loss of endothelial barrier function in thrombin-induced responses, shown by TEER measurements *in vitro*.

Conclusions:
In this study we have indentified a new regulatory function for CMTM3 in angiogenesis. CMTM3 is involved in Ve-cadherin turnover, and is a regulator of the cell surface pool of Ve-cadherin. Therefore, CMTM3 mediates cell-cell adhesion at AJs, and contributes to the control of vascular sprouting.

Introduction

Angiogenesis is a hypoxia-driven process that produces the vascular network during embryogenesis, mature wound healing, and disease progression in adult life[1]. Intercellular adhesion and signalling mediated by homophilic interaction of Ve-cadherin proteins in endothelial adherens junctions (AJs) play key roles in maintaining endothelial barrier function and vascular homeostasis during and after angiogenesis[2-5]. Gene ablation studies of VE-cadherin and associated proteins have revealed that junction strength dictates endothelial function and microvascular morphology and integrity[6, 7]. An important aspect in angiogenesis is the ability of endothelial cells (ECs) to dynamically modulate cell-cell adhesive state by regulating Ve-cadhrin availability at the cell membranes. Although reduced Ve-cadherin mediated cell-cell adhesion reduces microvascular stability, decrease in adhesive strength and disruption of endothelial AJs is required to allow ECs migration and neovessel sprouting during vascular expansion.

Endocytosis is a cellular process that is commonly used to alter bio-availability of cell surface proteins to modulate their functions. Endocytosis involves uptake of cell surface proteins in transport vesicles and sorting of vesicle cargo to either recycling or degradation compartments. By using Rab family GTPases as markers for intracellular vesicular compartments, the transport route of the membrane proteins can be actively monitored[8]. Previous studies have indicated that p120-catenin regulates Ve-cadherin lysosomal degradation by inhibiting endocytosis of the cell surface pool via interaction with the cytoplasmic tail of Ve-cadherin proteins[9]. Further analysis revealed that P102-catenin acts as a key protein in the plasma membrane retention mechanism of Ve-cadherin by preventing recruitment of Ve-cadherin into membrane domains enriched with endocytic machinery proteins, including Clathrin[10]. Other studies also indicate that cell surface availability of Ve-cadherin is regulated by VEGFA and is mediated by ß arrestin 2 and Clathrin-dependent endocytosis[4].

Although endothelial endocytosis plays such a critical role in Ve-cadherin and adherens junction regulation during and after angiogenesis, our overview of important regulators involved in these early endocytotic and subsequent intracellular transport processes, is still far from complete. To identify new key regulators in angiogenesis and vascular homeostasis we conducted a micro-array screen on the transcriptome of murine embryos, comparing Flk+ endothelial progenitor cells with Flk1- cell population. We identified CKLF-like MARVEL Transmembrane domain 3 (CMTM3) as a putative candidate gene enriched in the Flk1+ endothelial progenitor cell population. CMTM3 is a member of the chemokine-like factor super family(CKLFSF/CMTM) located on chromosome 16q22.1[11]. CMTM is a family of proteins linking chemokines and the Transmembrane 4 super family (TM4SF), encoded by nine genes in humans, CKLF and CKLFSF1-8[11]. Previous reports have indicated that CMTM members play important roles in cancer development[9, 12, 13]. Furthermore, some members of the CMTM family are highly expressed in immune cells[11, 14]. For CMTM3, more recent reports indicate involvement of the protein in

preventing growth and invasion of different types of cancer[15-17]. However, the putative function of CMTM3 in angiogenic regulation in ECs remains to be elucidated.

Here we studied the angiogenic potential of CMTM3 and investigated the molecular pathways that are mediated by CMTM3 in ECs. Our findings indicate that CMTM3 promotes neovessel formation *in vitro* in a 3D collagen matrix based co-culture of primary vascular cells. Loss-of function studies *in vivo* by morpholino-silencing of the orthologue of CMTM3 in developing zebrafish larvae validate CMTM3 pro-angiogenic capacities. *In vitro* studies demonstrate that CMTM3 co-localizes with the early endosomes markers (EEA1 and Clathrin) and internalized VE-cadherin. CMTM3 overexpression in HUVECs promotes endocytosis and intracellular vesicular trafficking, and augments basal and VEGFA-induced internalization of Ve-cadherin. In contrast, knockdown of CMTM3 in HUVECs significantly reduces Ve-cadherin internalization. Based on these findings, we propose a model in which CMTM3 contributes to early endocytosis of Ve-cadherin, a crucial step for reducing cell-cell adhesive strength in AJs in order to facilitate neovascular sprouting in the initial steps of angiogenesis. Our study provides new insights into the regulatory mechanisms by which endocytosis controls bio-availability of Ve-cadherin in endothelial AJs, and presents the first evidence of CMTM3-mediated control of early endocytosis of cell membrane surface proteins in vascular cells during angiogenesis.

Material and methods

Cell culture

All cells were cultured at 37°C in a 5% CO_2 humid atmosphere. HUVECs were obtained from Lonza and maintained in EGM2 medium (Lonza) with 100 Uml^{-1} penicillin-streptomycin (PS). Human brain vascular pericytes were obtained from ScienCell and maintained in DMEM supplemented with 10% FCS and 100 Uml^{-1} PS. Human aortic vascular smooth muscle cells (VSMC) were obtained from Lonza and maintained in $SMGM_2$ supplemented with 100 Uml^{-1} PS. All cells were used between passages 3 and 6. Co-culture experiments were performed in basal EBM medium supplemented with 2% FCS, rhFGF-B, ascorbic acid, and 100 Uml^{-1} PS. HUVEC and pericytes were transfected with lentivirus GFP and RFP expression constructs respectively, obtained from Sanbio. For this, cells (passage 1) were plated on gelatine coated culture plates, and transfection was performed when cells reached 60% confluence. Lentivirus was added to the cells at MOI 5 in the presence of 6 µg/ml polybrene in basal medium with 0.2% FCS. After 6 hours of transduction, the cells were incubated for 72 hours in fresh growth medium. Blasticidin (2.5 µg/ml) was added to the cells as a selection marker. After 10 days of selection, GFP-positive HUVECs and RFP-positive pericytes were harvested and propagated for storage by cryopreservation.

Trans-membrane co-culture

HUVEC were seeded on top of a 0.4 µM polycarbonate membrane (Transwell® Costar) and mural cells on the downside of the membrane. After 24 hours incubation in serum low condition (EBM+0.2% FCS+PS) cells were separately harvested using a cell-scraper and processed for mRNA isolation.

QPCR analysis

Total RNA was extracted from treated cells using RNAeasy kit (Qiagen) and was checked for quality and quantity by spectrophotometer (Nanodrop; ND-1000) and/or capillary electrophoresis (Agilent 2100 Bioanalyser). Reverse transcription was conducted with iScript synthesis kit (Brad) according to manufacturer instructions. Quantitative real-time PCR was performed using SYBR-Green-Cycler IQ5 detection system (Biorad). All results were normalised for the expression of the house keeping gene ß actin. The primers of target genes are summarized in table 1.

Short interference RNA

Silencing CMTM3 in HUVEC and HUVEC-GFP was conducted by using a mixture of 4 complementary siRNA sequences directed against the mRNA of CMTM3 (Thermo Fisher): 5'-GCCCUCAUCUACUUUGCUA-3'; 5'-GCAACUGAUUUCUACCUGA-3'; 5'-CAAGACAGAAGAAGAGAGAAU-3'; 5'-UUAACGACGUGGCCAAAUU-3' (siCMTM3). As a negative control a pool of 4 non-

targeting siRNA sequences were used (siSham). Cells were grown to 60% confluence and transfected with 20 µM siRNA using lipofectamine (Dharmafect, Thermo Scientic) according to manufacturer's instructions. The miRNA silencing was validated 48-72 hours post transfection using qPCR and Western blotting. Optimal CMTM3 silencing was obtained 72 hours post transfection.

Subcellular fractioning and protein extraction

Cells were harvested 72 hours post siRNA transfection. To distinguish cytoplasmic proteins (soluble fraction) from the membrane proteins (insoluble fraction), cells were washed twice with PBS and harvested in lysisbuffer (140 mM NaCl, 10 mM Tris pH 7.6, 1 mM EDTA, 1% Triton X-100 [TX-100], 0.05% sodium dodecyl sulfate, 1x protease inhibitor cocktail, 1 mM PMSF). The lysates were incubated for 20 minutes on ice and centrifuged at 13000*g* for 12 minutes to separate the soluble fraction from the insoluble fraction. The insoluble fraction was then solubilised in lysis buffer with 2% SDS. Both fractions were loaded onto SDS-PAGE followed by Western blot analysis.

Western blot

Before protein samples were loaded on sodium dodecyl sulfate-polyacrylamide gel electrophoresis (SDS-PAGE), the protein concentration was determined using Pierce BCA Protein Assay according manufacturer's protocol. Samples were denatured for 10 minutes at 95°C, followed by separation with a 10% or a 4-15% gradient SDS-PAGE gel (Biorad). Subsequently, proteins were transferred to a nitrocellulose membrane (Pierce) and incubated for 1 hour in Odyssey (Li-Cor) blocking buffer (diluted 1:1 in PBS). The membranes were incubated overnight with anti-CMTM3, ß actin, and anti-Ve-cadherin (Santa Cruz) in concentrations recommended by the manufacturer. Protein bands were visualized with the Li-Cor detection system (Westburg).

Collagen based 3D co-culture

The microvessel networks were established by seeding HUVEC-GFP and pericyte-RFP at a density of $6X10^4$ HUVEC-GFP and $1.2X10^4$ pericytes-RFP in 50 µl of 2.5 mg/ml type 1 collagen (BD Bioscience). Stem cell factor, stromal-derived factor-1α, and interleukin-3 (BD-Bioscience) were each added at 400 ng/µl in the collagen matrix to promote angiogenesis, followed by collagen cross-linking for 1 hour at 37°C and 5% CO_2 after supplementing the gel with 100 µl EBM_2+2%FCS+ascorbic acid + fibroblast growth factor-2 (obtained from the EGM_2 bulletkit) in a 96-wells plate setup. Co-cultures were recorded by fluorescence microscopy at day 2 and day 5. Total tubule length, mean tubule length and the number of vascular junctions and tubules were quantified using the Angiosys software program.

Ve-cadherin internalization assay and immunofluorescence

The internalization assay was performed as described previously by Gavard *et al*[36]. Briefly, HUVECs were grown on coverslips to confluence before incubation in EGM with anti-human VE-cadherin (BV9 clone, ab7047, Abcam) antibody (5 µg/ml) at 4°C for 1 hour to label cell-surface exposed VE-cadherin. Subsequently, cells were placed at 37°C for 30 minutes to track VE-cadherin movement, in either basal medium (control) or basal medium supplemented with VEGFA (50 ng/ml; cat#100-20, Peprotech). Cells were either washed with PBS (PBS supplemented with 1.8 mM $CaCl^2$ and 1 mM $MgCl^2$) and fixed with 4% paraformaldehyde at room temperature for 30 minutes, or exposed to an additional mild acid wash (2mM PBS-glycine [pH 2.0], 15 minutes) prior to washing and fixation to remove membrane bound antibodies. This treatment reveals internalized anti-VE-cadherin antibodies. Blocking and permeabilization was conducted for 30 minutes at room temperature in PBS with 1% BSA and 0.5% Triton-X. Secondary antibody (Alexa Fluor 488 goat anti-mouse IgG, cat#A11029, Invitrogen) incubation was performed for 2 hours at room temperature, followed by an incubation step with phalloidin-rhodamine for 30 minutes at room temperature to label cytoskeletal F-actin. DAPI was used as a nuclear counterstain. Images of fluorescent-labeled markers were acquired by a ZEISS LSM700 microscope and a 63 oil immersion objective lens. Images were acquired by using the manufacturer's standard software. 3D images were obtained by scanning several XY planes in the Z direction with enough depth to scan the entire cell (±10 µm). Serial pictures along the Z-axis were combined, creating a stacked XY image. The total area of VE-cadherin from multiple stacked images was determined by using imageJ 1.47v.

Flow cytometry

CMTM3 silenced HUVEC were seeded at a density of $0.5X10^5$ cells/well in a 6 wells plate in co-culture medium. After 24, 48,and 72 hours cells were harvested for proliferation and apoptosis assay. The single cell suspension for each condition were stained for Propidium Iodide and Annexin V (BD Pharmingen) according to manufacturer's protocol and analyzed by flowcytometry (BD Facs Canto). Cells were counted for 2 minutes at medium speed to determine the average cell amount. Cell cycle analysis was performed after 48 hours incubation at 37°C in 5% CO2 and fixed overnight in 70% ethanol at 4°C. After washing the cells with ice-cold PBS, cells were stained with PI and treated with 0.5mg/ml RNase for 30 min at 37°C and analyzed by flowcytometry.

Migration assay

CMTM3 was silenced in HUVEC and after 24 hours seeded at a density of $5X10^4$ cells/well in a 96 wells plate with cell seeding stoppers of Oris™ Universal Cell Migration (Platypus Technologies). Cells were allowed to adhere for 24 hours and after that the seeding stoppers were removed to reveal a cell-free detection zone into which cells migrate in serum low condition EBM with 2% FCS for 16 hours. The cells were washed and stained with Calcein-AM (BD-Bioscience) according

manufacturer`s instructions and imaged by fluorescence microscopy. Quantification of the images was assessed by Clemex vision software to measure the percentage of the mean surface area of the migrated cells.

Intracellular immunostaining

24 hours post transfection with siRNA, HUVEC were seeded in a 48 wells plate $1X10^5$ cells/well. Cells adhere for 24 hours after which they were fixed in 4% paraformaldehyde (PFA) for 10 min, followed by 15 min permeabilization in 0.1% Triton-X100. This was followed by overnight 4°C incubation with primary antibody (see supplementary table 2), secondary antibody Alexa Fluor 488 or Alexa Fluor 594, and vectashield with dapi, all according to manufacturer`s protocol. In some experiments, cells were also co-stained with phalloidin-rhodamin or a second primary antibody. Samples were imaged by fluorescence or confocal microscopy. For quantification of area and assessment of co-localization, the signal of multiple stacked images was analyzed using imageJ 1.47v.

CMTM3 adenovirus

Recombinant adenoviruses were produced using Gateway pAd/CMV/V5-DEST vector and ViraPower™ Adenoviral Expression System, according manufacturer's instructions (Invitrogen). Fully sequenced Human CMTM3 cDNA clone was obtained from Lifesciences, which contains the coding sequence (cds) of CMTM3 in a pCMV-SPORT6. Full-length cDNAs of CMTM3 with attB-site was amplified by PCR using specific forward oligos 5`-GGGGACAAGTTTGTACAAAAAAGCAGG CTTCACCATGTGGCCCCCAGACCCCGACC-3` and reverse oligo`s 5`-GGGGACCACTTTGTACAAGAAAGCTGGGTTTCAGTCAGAGTCCGAGTCGGAATTCTC-3`. Moreover a HIS tag was placed at the C-terminal region of CMTM3 (CMTM3-HA) using the RV primer 5`-GGGGACCACTTTGTACAAGAAAGCT GGGTGGTCAGAGTCCGAGTCGGAATTCTC-3`. Amplicons of CMTM3 and CMTM3-HA were cloned into a pDONR™ 221 vector via BP Clonase™ II enzyme mix to create an entry clone. The fidelity of CMTM3 and CMTM3-HA was confirmed by DNA sequencing. Subsequently, the CMTM3 expression cassette was cloned from the entry vectors into pAd/CMV/V5-DEST (Invitrogen) expression vectors (pAd CMV) using LR-reaction II (invitrogen). After verification by DNA sequencing, the pAd/CMV plasmids were linearized by Pac1 restriction and subsequently transfected with Lipofectamine 2000 (Invitrogen) in 293A cells. Infected cells were harvested until 80% of the cells detached from plates followed by three cycles of freeze/thawing to get crude viral lysate (CVL).

Transendothelial resistance measurements

HUVEC were transfected with adenovirus or siRNA 24 hours before seeding on a pre-coated (0,1% gelatin) semi-permeable filter insert (0.4um pore size, Falcon). Before seeding, the blank resistance (R_{blank}) of each insert was measured in an Endohm-SNAP chamber (World Precision Instruments, Berlin) filled with 5 ml of EGM-2, which was coupled to an EVOMX resistance

meter (World Precision Instruments). The Transendothelial resistance (TEER) was measured daily for a total of 3 days post transfection. At day 2 the monolayers were treated with 1 U/ml thrombin for 30 minutes and the TEER was recorded every 5 min. After thrombin-induced decrease in TEER the cells were washed with fresh medium and the TEER was recorded every 15 min for 2 hr. The electrical resistance was calculated by Ohm`s law and expressed in $\Omega*cm^2$, (resistance of experimental insert minus resistance of corresponding blank insert) times 4.2 (area of the insert membrane in cm^2).

Results

CMTM3 silencing in ECs impairs vascular growth in a 3D collagen matrix vascular co-culture system in vitro.

CMTM3 function in angiogenesis was assessed in loss-of-function studies, conducted by transfection of CMTM3 targeting siRNA in HUVECs with GFP marker expression. QPCR analysis validated efficient silencing of CMTM3 in cells treated with CMTM3 targeting siRNA (siCMTM3) versus non-transfected controls (control) or cells transfected with a pool of non-targeting siRNA sequences (sisham) (Figure 1A). Expression levels of the other CMTM-family members did not differ between groups, indicating that the siRNA mediated silencing of CMTM3 was specific (Figure 1B). Next, the angiogenic capacities of these CMTM3-silenced ECs were evaluated in an *in vitro* 3D angiogenesis assay that was previously developed for studying the formation of lumenized micro-capillary structures (Figure 1C) [18, 19]. In this assay, GFP labelled HUVECs and RFP labelled pericytes were co-cultured in a collagen matrix, which enabled direct interaction between the two cell types. EC sprouting and onset of tubule formation can be observed after 1 day of co-culture. At the same time, stabilization of neovascular structures is triggered by perivascular recruitment of pericytes. Both processes proceed till up to 5 days post-seeding, eventually forming micro-capillaries with pericyte coverage and clear distinction of open luminal areas (Figure 1C). Imaging and quantification of the vascular structures were conducted at day 2 and 5.

Data obtained at day 2 and 5 showed that CMTM3 silencing in GFP-HUVECs severely impaired formation of neovascular structures in the 3D vascular assay, as compared to non-treated and sisham controls (Figure 1D and E). CMTM3 silencing reduced total tubule length (by 4.6 and 3.9 fold at day 2 and by 2.7 and 2.6 fold at day 5), number of tubules (by 3.6 and 3.1 fold at day 2 and by 2.2 and 2.1 fold at day 5), number of junctions (by 10.2 and 7.5 fold at day 2 and by 4.8 and 4.7 fold at day 5), and mean tubule length (by 1.3 and 1.2 fold at day 2 and by 1.4 and 1.3 fold at day 5), compared to control and sisham respectively. In contrast CMTM3 silencing in RFP-pericytes did not affect neovascular growth, demonstrated by lack of differences between groups in vascular parameters at both time points (Figure 1F). Similarly, CMTM3 silencing in GFP-HUVECs using a second siRNA sequence significantly decreased total tubule length, and the number of junctions and tubules in the 3D vascular assay. (Sup. Figure I).

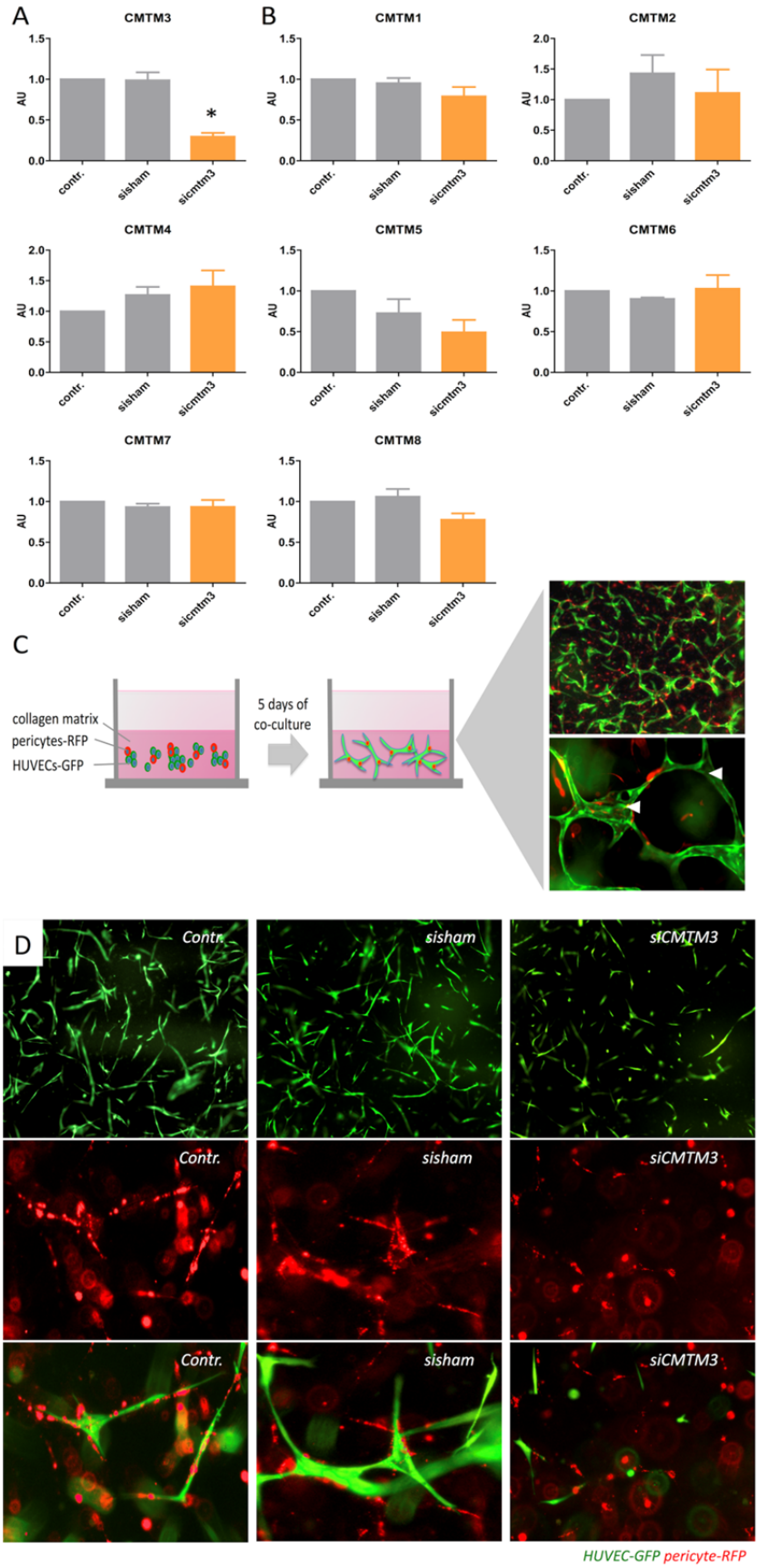
A
CMTM3
B
CMTM1
CMTM2
CMTM4
CMTM5
CMTM6
CMTM7
CMTM8
AU
contr.
sisham
sicmtm3
*
C
collagen matrix
pericytes-RFP
HUVECs-GFP
5 days of
co-culture
D
Contr.
sisham
siCMTM3
HUVEC-GFP pericyte-RFP

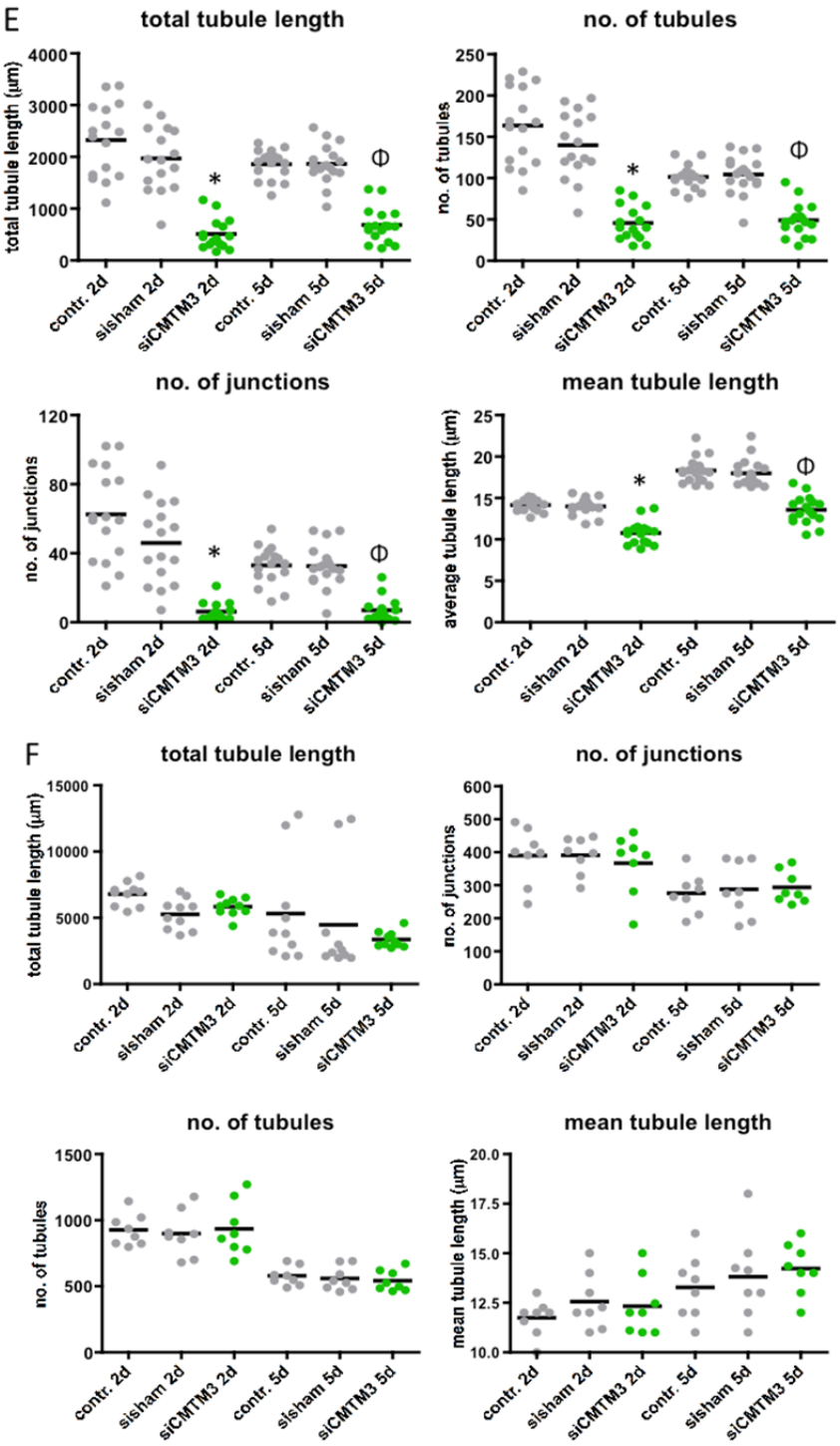

Figure 1. CMTM3 silencing in ECs impairs vascular growth in a 3D collagen matrix vascular co-culture system *in vitro.*

(A) QPCR analysis of CMTM3 expression levels in HUVECs treated with CMTM3-targeting siRNA (siCMTM3) compared to non-targeting scrambled siRNA treated cells (sisham) or non-treated controls (contr.). (B) QPCR analysis of mRNA expression levels of CMTM family members in HUVECs treated with HUVECs treated with CMTM3-targeting siRNA (siCMTM3) compared to non-targeting scrambled siRNA

treated cells (sisham) or non-treated controls (contr.). For A and B, Gene expression levels are shown in target gene/house keeping gene (ß actin) ratio (AU), mean ± SEM. *P<0.05 versus sisham and control. N≥6. (C) Schematic figure showing the 3D collagen matrix co-culture set up. Depicted in the right panel are representative confocal microscopy images taken at low (upper image) and high magnification (lower image) at 5 days of co-culture. HUVECS are labelled with GFP (in green); Pericytes are labelled with dsRED (in red). Arrowheads indicate neovascular structures with open lumen. (D) Representative low (upper row) and high (two lower rows) magnification images of 3D collagen matrix HUVECs-GFP and pericytes-dsRED co-cultures in which HUVECs-GFP were treated with CMTM3-targeting siRNA (siCMTM3) compared to non-targeting scrambled siRNA treated cells (sisham) or non-treated controls (contr.). Images displayed were taken at day 5. (E) Quantification of total tubule length, number of tubules and junctions, and mean tubule length at day 2 and 5 of co-culture. Values are Mean ± SEM. *P<0.05 versus control and sisham at day 2 and 5. $^{\Phi}$P<0.05 versus control and sisham at day 2 and 5. N≥15 co-cultures. (F) Data from co-culture experiments in which pericytes-dsRED were treated with CMTM3-targeting siRNA (siCMTM3) compared to non-targeting scrambled siRNA treated cells (sisham) or non-treated controls (contr.). Quantification of total tubule length, number of tubules and junctions, and mean tubule length at day 2 and 5 of co-cultures. Values are Mean ± SEM. N≥8 co-cultures.

Mural cell interaction induces expression of CMTM3 and CMTM-family members CKLF1, CMTM2, CMTM4 and CMTM8 in human endothelial cells.

To investigate the CMTM3 expression in vascular cells, QPCR analysis was conducted on single cultured vascular cells and compared to co-cultured human vascular cells that mimicked the physiological *in vivo* and co-culture condition in which pericytes and endothelial cells are in direct contact during angiogenesis and vascular homeostasis. CMTM3 was significantly upregulated in HUVECs in response to co-culture with pericytes and VSMCs (Figure 2A-B). Further evaluation of the other CMTM family members showed upregulation of CMTM4 and CMTM8 in response to co-culture with VSMCs or pericytes, whereas CMTM2 and CLKF1 were only upregulated in the VSMCs co-culture condition (Figure 2B). CMTM3 expression was not altered in mural cells exposed to endothelial co-stimulation, whereas CMTM2, CMTM4, and CMTM8 expressions in mural cells were responsive to co-culture with ECs. These findings indicate that CMTM3 and CMTM-family members are upregulated in response to endothelial and mural cell contact.

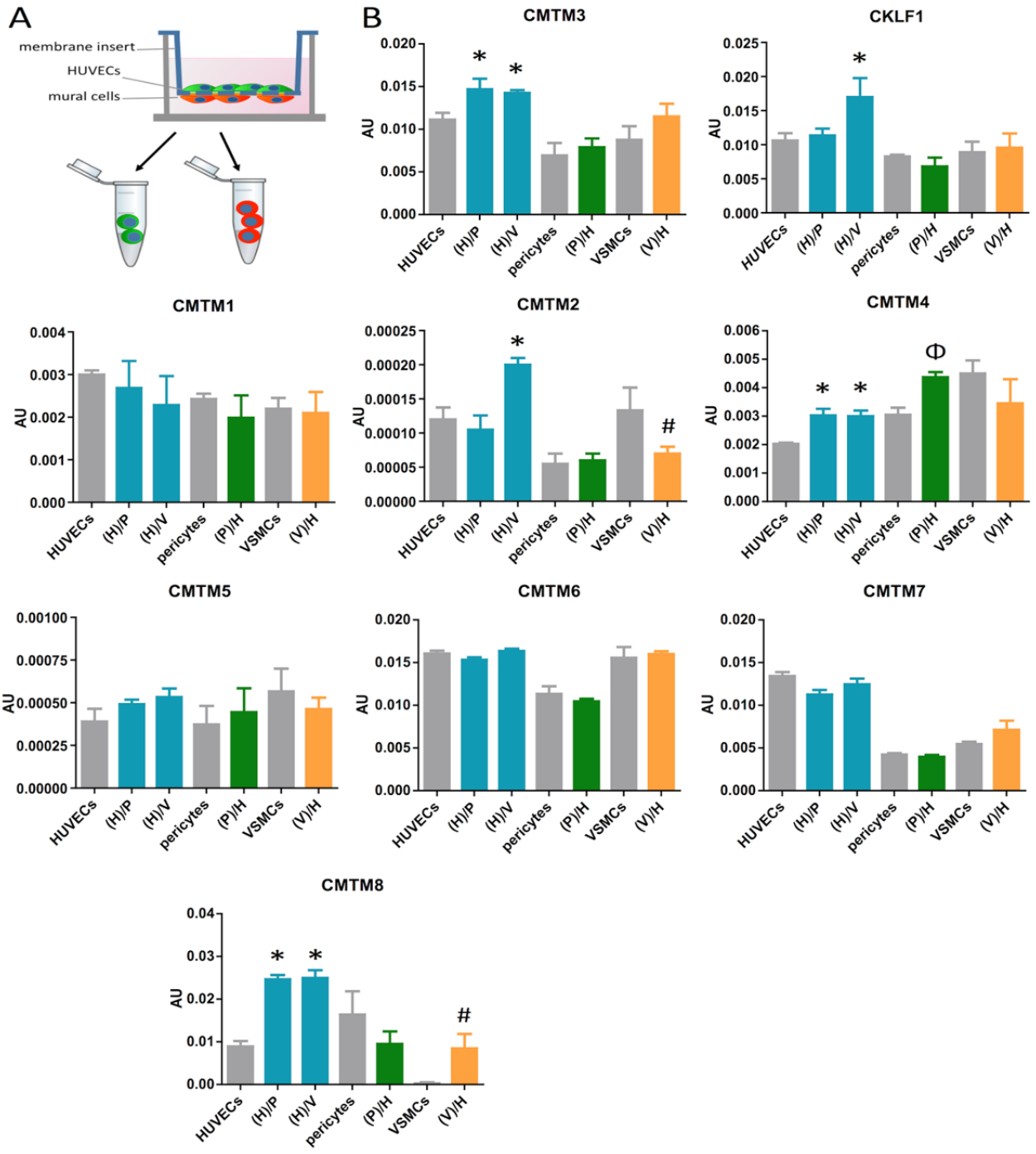

Figure 2. Amongst the CMTM-family members, CMTM3, CKLF1, CMTM2, CMTM4, and CMTM8 expression in HUVECs respond to mural cell interaction. (A) Schematic representation of the protocol. (B) QPCR analysis of the expression level of CMTM-family members in single culture (HUVECs, pericytes, VSMCs) and co-culture conditions in HUVECs (HUVECs with pericytes indicated as (H)/P; HUVECs with VSMCs indicated as (H)/V), and in mural cells (pericytes with HUVECs indicated as (P)/H; VSMCs with HUVECs indicated as (V)/H). Gene expression levels are shown in target gene/house keeping gene (ß actin) ratio (AU), mean ± SEM. *P<0.05 versus other HUVECs single culture. $^{\Phi}$P<0.05 versus pericyte single culture. $^{\#}$P<0.05 versus VSMC single culture. N≥6.

Silencing of CMTM3 during zebrafish development inhibits intersomitic vessel growth.

To assess the involvement of CMTM3 in angiogenesis *in vivo*, the gene was silenced in developing zebrafish larvae of the transgenic zebrafish lines Tg(fli1:eGFP)^{y1}, using morpholino (MO) knockdown technology. CMTM3 and its family members are highly conserved in most species including the zebrafish. Two morpholinos were designed for silencing of the zebrafish CMTM3 orthologue based on the splice modification principle of the pre-mRNA target and were validated to produce (non-functional) alternative spice products (Sup. Figure IIA-C). The first morpholino construct targeting the splice site located on CMTM3 exon 3 – intron 3 (E3-I3), diminished intersomitic vessel (ISV) formation at 24 hours post fertilization compared to uninjected controls (UICs). Quantification of zebrafish phenotype showed that in the E3-I3 group, 47% of the larvae displayed the ISV defect phenotype, versus 0% in the control group (Figure 3A and C). Functional validation of the E3-I3 morpholino was shown by PCR analysis of mRNA extracted from injected pools of larvae, indicated by the presence and absence of the non-spliced pre-mRNA band in E3-I3 and UIC groups respectively (Figure 3B). Similarly, the second morpholino construct targeting the splice site on exon 2 – intron 2 (E2-I2) inhibited the growth of ISVs, with the defect phenotype consistently observed in 67% of the E2-E2 group versus 0% in the UIC group, further validating the negative effect of CMTM3 silencing on angiogenesis during zebrafish development (Figure 3C and Sup. Figure IIA-F).

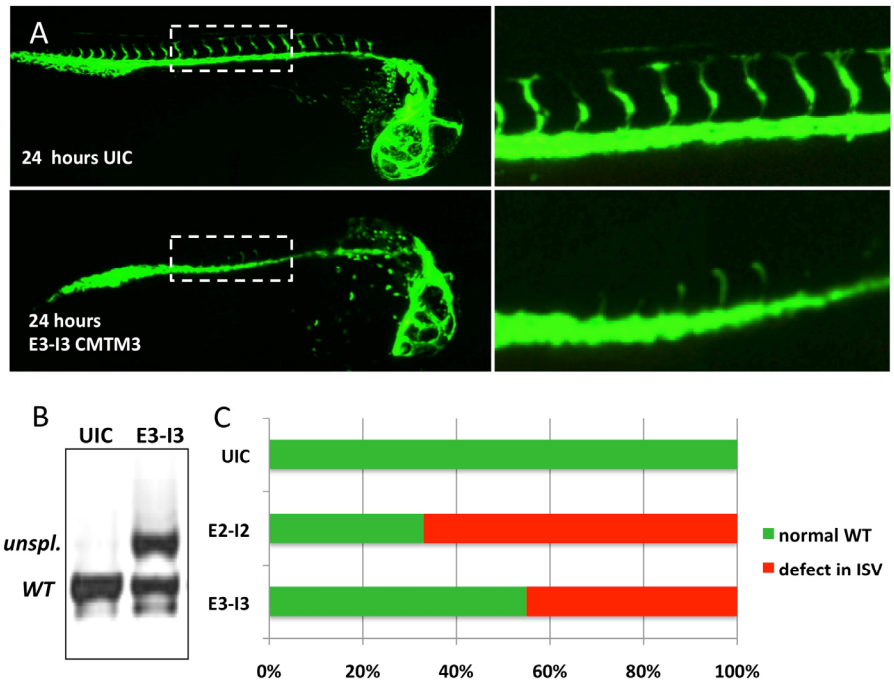

Figure 3. Morpholino-induced silencing of CMTM3 in zebrafish affects vascular growth of intersomitic vessels. (A) Tg(fli1:eGFP)^{y1} embryos at 24 hpf, lateral view, anterior to the right. Distinct reduction of intersomitic vascular sprouting in the trunk region was observed in *CMTM3* targeting morpholino-

injected (morpholino targeting splice site E3-I3 of CMTM3, indicated as *E3-I3 CMTM3*) embryos compared to uninjected controls (UIC). The zebrafish vasculature is highlighted by the eGFP marker (in green). Right hand panel shows high magnification images showing intersomitic outgrowth in the indicated the trunk region. (B) PCR validation of morpholino targeting of splice site E3-I3. Shown are the PCR bands of unspliced (unpl.) and spliced wildtype (WT) zebrafish CMTM3 mRNAs in uninjected and E3-I3 morpholino treated larvae. (C) Quantification of the defective intersomitic vasculature (ISV) phenotype and wildtype (normal) phenotype in zebrafish larvae injected with E3-E3 or E2-I2 morpholinos versus uninjected controls. Data represent percentage of counted larvae.

CMTM3 silencing does not affect endothelial cell proliferation and cell migration.

Previous studies in gastric cancer cells imply that CMTM3 functions as a tumor suppressive gene with overexpression of CMTM3 leading to inhibition of cell proliferation and migration. Here we investigated the effect of CMTM3 silencing on these specific parameters in HUVECs. Knockdown of CMTM3 mediated by siRNA targeting (siCMTM3) did not affect cell proliferation compared to non-transfected and scrambled non-targeting siRNA transfected controls (sisham), indicated by a lack of difference in cell count during HUVEC expansion over the course of 2 days (Figure 4A). In line with these results, no difference in cell cycle progression was observed between the groups (Figure 4B and C). In addition, cell migration capacity was investigated in a transwell migration assay, but showed no effect of CMTM3 silencing (Figure 4D and E). Similarly, migration and proliferation was not affected by CMTM3 overexpression in HUVECs, which was induced by transfection with a recombinant adenovirus encoding for human CMTM3 cDNA (adCMTM3) (Sup. Figure III). These data indicate that decrease in physiological levels of CMTM3 does not affect the proliferative and migratory capacity of human endothelial cells.

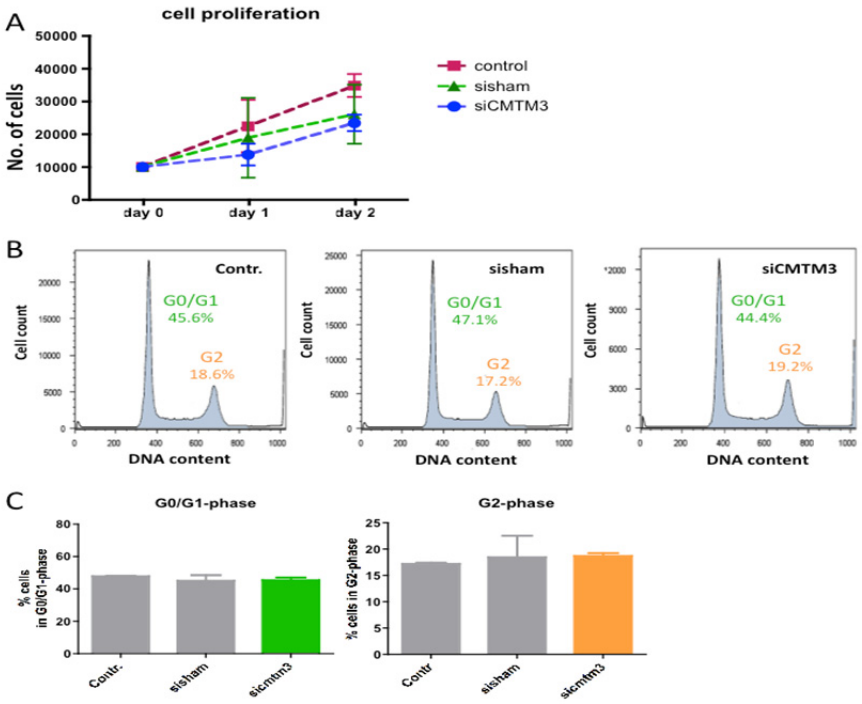

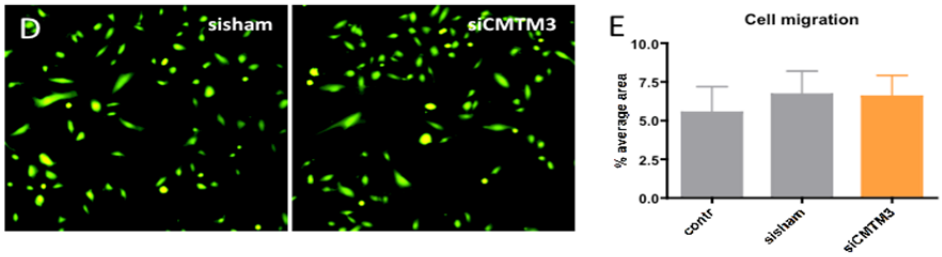

Figure 4. CMTM3 inhibition does not affect endothelial cell proliferation and migration.
(A) Number of counted cells at day of seeding (day 0) and after 1 and 2 days of cell proliferation in siCMTM3 treated HUVECs compared to sisham and non-transfected controls. Shown is mean ± SEM. N=6 (B) Representative flow cytometry profiles showing the distribution of G0/G1 and G2 phase cells at 2 days post seeding in siCMTM3 treated HUVECs compared to sisham and non-transfected controls stained for DNA content with PI. (C) Quantification of % cells in G0/G1 and % cells in G2 phase in siCMTM3 treated HUVECs compared to sisham and non-transfected controls. Shown is mean ± SEM. N=6. (D) Representative results of trans-membrane migration assays after 24 hours of migration in siCMTM3 treated HUVECs compared to sisham controls. Cells are visualized by Calcein-AM (Green) uptake. (E) Quantification of % area within image field covered by HUVECs compared to sisham controls. Shown is mean ± SEM. N=8.

CMTM3 localizes in distinct vesicle-like structures and co-localizes with Ve-cadherin in the endothelial cytosol.

To further elucidate the mechanistic function of CMTM3, HUVECs were transfected with a recombinant adenovirus encoding for human CMTM3 cDNA (adCMTM3). Transgene expression was validated by qPCR and compared with HUVECs transfected with sham virus (adsham; Figure 5A). CMTM3 protein was detected by immuno-fluorescence staining in the cytosol where it accumulated in vesicle-like structures (Figure 5B). Western blot analysis also demonstrated that CMTM3 was present in the soluble cytosolic fraction, and not in the insoluble actin bound fraction of HUVEC lysates (Figure 5C). To further elucidate the intracellular function of CMTM3, we assessed the co-localization of CMTM3 with markers of the different intracellular vesicular transport compartments. Double immuno-fluorescent staining of EEA1 (a marker of early endosomes) and CMTM3 in HUVECs transfected with an adenoviral expression vector of CMTM3 cDNA, showed significant co-localization between the two signals in the larger sized cytosolic vesicles (Figure 5D). Similarly, CMTM3 co-localized with larger vesicles that were positive for Clathrin (Figure 5E). In contrast co-localizations between CMTM3 and Rab11 or Rab4 (both markers of recycling vesicles), and between CMTM3 and Rab7 (marker for vesicles destined to transport proteins to the lysosomal degradative pathway), or Rab5 (late endosome/lysosome protein) were limited (Figure 5F-I). Intracellular trafficking of endocytic vesicles plays a crucial regulatory role in controlling cell surface presentation of Ve-cadherin, a cell-cell adherens junction protein that is critical for vascular barrier function and angiogenesis[10]. Immuno-fluorescence staining of Ve-cadherin in confluent endothelial

monolayers of adCMTM3 transfected HUVECs (adCMTM3) showed that CMTM3 overexpression increased cytosolic localization of Ve-cadherin compared to the mainly cell-cell junctional localization that was observed in controls transfected with sham adenovirus (adsham) (Figure 5J). Western blot analysis indicated that total protein levels of Ve-cadherin remained unchanged (Figure 5K). Double staining of CMTM3 and Ve-cadherin in adCMTM3 HUVECs showed significant co-localization of CMTM3 with cytosolic Ve-cadherin (Figure 5L). Quantification of the co-localization signals represented in Pearson's correlation coefficient values confirms our visual observations, showing higher values for CMTM3/EEA1 and CMTM3/Ve-cadherin compared to CMTM3/Rab11, CMTM3/Rab7, CMTM3/Rab4 or CMTM3/Rab5 co-localizations (Figure 5M). CMTM3/EEA1 was also significantly more observed compared to CMTM3/Clathrin. For CMTM3/Clathrin, the correlation value was significantly higher compared to CMTM3/Rab4 and CMTM3/Rab5. Colocalization of endogenous CMTM3 with EEA1 was also detected (Sup. Figure IV).

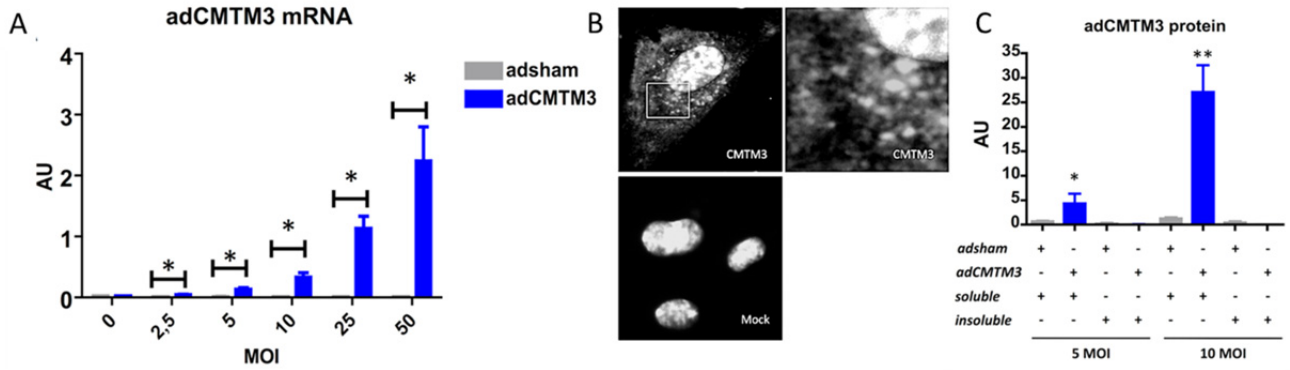

Figure 5. CMTM3 localizes in distinct vesicle-like structures and co-localizes with Ve-cadherin in the endothelial cytosol, but not at adherens junctions.

(A) QPCR analysis of human CMTM3 expression levels in HUVECs transfected with different MOI of adenovirus containing an expression vector for CMTM3 cDNA (adCMTM3) or with sham virus containing an empty expression vector (adsham). Gene expression levels are shown in target gene/house keeping gene (ß actin) ratio (AU), mean ± SEM. *P<0.05 in student T-test comparisons between adsham and adCMTM3 group of equal MOI. N=3. (B) Representative low and higher magnification immunofluoresence microscope images of HUVECs transfected with adCMTM3, immunostained for CMTM3 and visualized using a secondary rhodamin (red) labelled antibody. Mock image shows the background signal of secondary labelling antibody. (C) Western blot quantification of CMTM3 protein levels in adsham and adCMTM3 transfected HUVECs, in the soluble (cytosol) and insoluble (actin cytoskeleton bound) cell lysates fraction at different MOIs. Protein levels are shown in CMTM3/loading control protein (ß actin) ratio (AU), mean ± SEM. *P<0.05 versus other all other groups. **P<0.001 versus all other groups. N=4

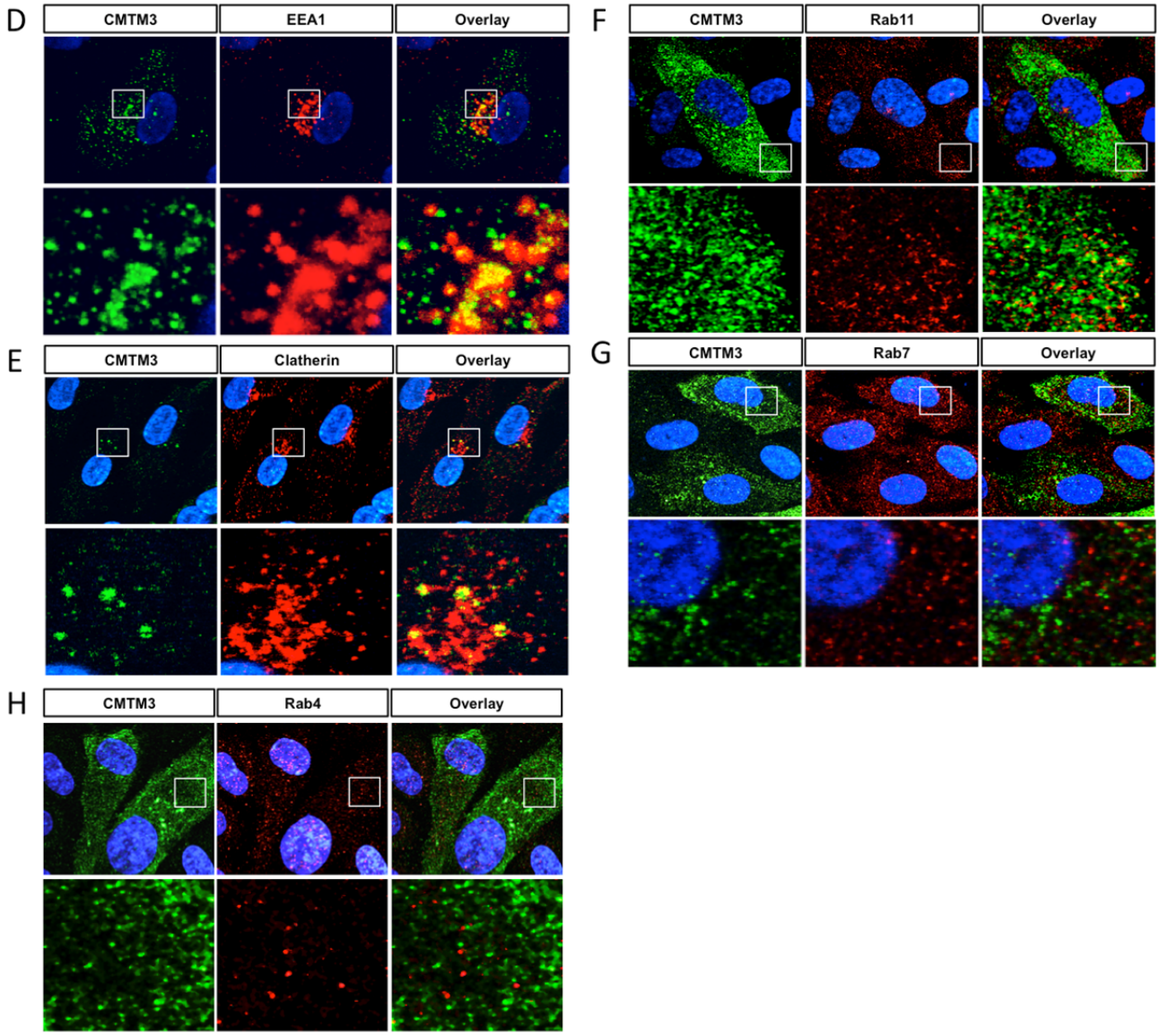

Figure 5.(D) Representative low and higher magnification confocal microscope images of HUVECs transfected with adCMTM3, immunostained for CMTM3 (green) and EEA1 (red), (E) CMTM3 (green) and clathrin (red), (F) CMTM3 and Rab11, (G) CMTM3 and Rab7, (H) CMTM3 and Rab4. Co-localization of CMTM3 and endocytic compartment protein markers in overlay images in yellow.

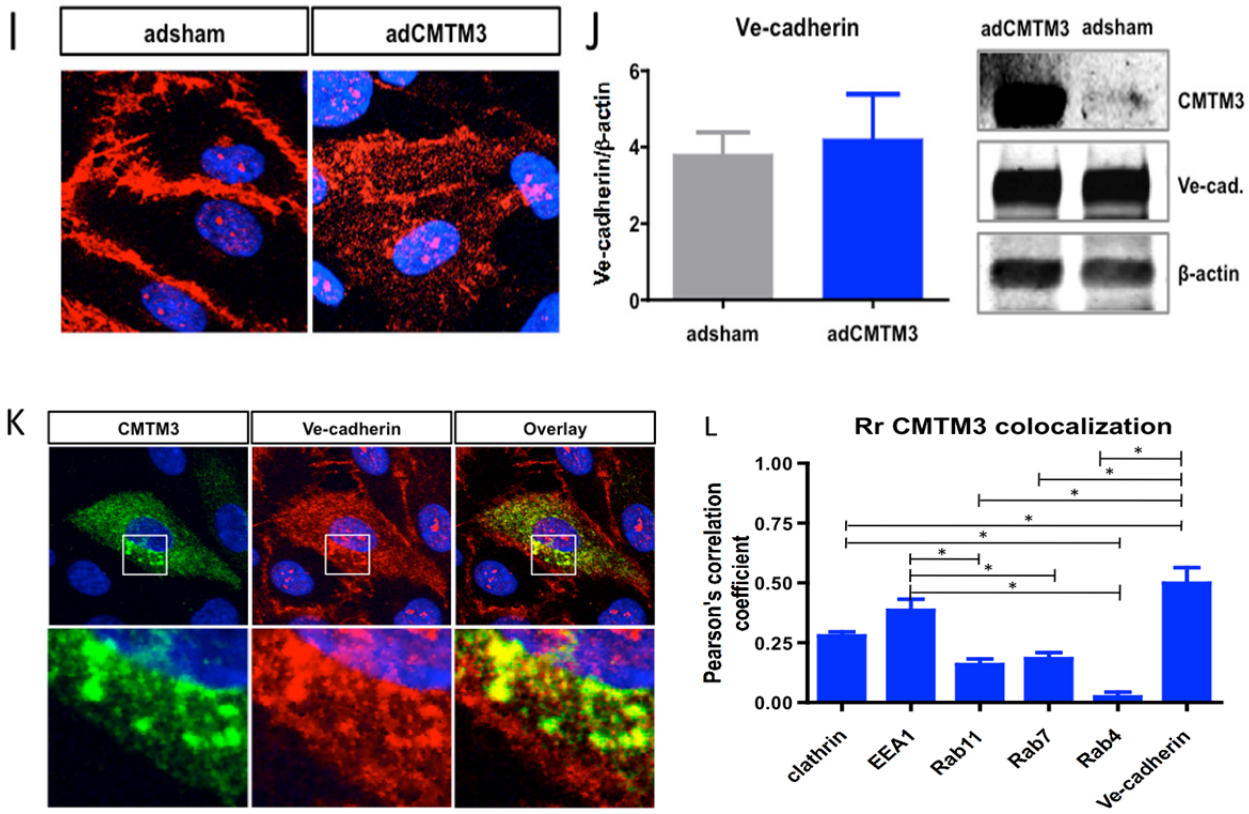

Figure 5. (I) Representative immunofluoresence microscope images of HUVECs transfected with adsham and adCMTM3, immunostained for Ve-cadherin (red). Co-localization in overlay image is in yellow. (J) Western blot quantification of Ve-cadherin protein bands in adsham and adCMTM3 transfected HUVECs, protein levels are shown in Ve-cadherin/loading control protein (ß actin) ratio, mean ± SEM. N=3. Representative Western blot bands for CMTM3, Ve-cadherin and ß actin are shown for adCMTM3 and adsham HUVECs. (K) Representative low and higher magnification immunofluoresence microscope images of HUVECs transfected with adCMTM3, immunostained for CMTM3 (green) and Ve-cadherin (red). (L) Quantificantion of co-localization of CMTM3 with Ve-cadherin and endocytic compartment markers in confocal micrographs based on Pearson's correlation coefficient (Rr), mean ± SEM. *P<0.05. N≥8.

Quantification of the immuno-fluorescence signals of Clathrin, EEA1, Rab11, Rab7, Rab5 and Rab4 indicated that Clathrin+, EEA1+, Rab11+, Rab5+ and Rab7+ vesicles were significantly increased in adCMTM3 versus adsham treated HUVECs (Figure 6A-F). Combined, these data indicate that CMTM3 is localized in early endosomes and could be involved in regulating Ve-cadherin transport in cytosolic vesicles during endocytosis. Functional involvement of these endocytosis-related proteins in angiogenesis was shown in the 3D collagen matrix vascular co-culture system: Knockdown of Clathrin and Rab5 in GFP-HUVECs mimicked the CMTM3 phenotype, significantly diminishing the numbers of junctions and tubules, as well as decreasing total tubule length (Sup. Figure V and VI for Clathrin and Rab5 respectively).

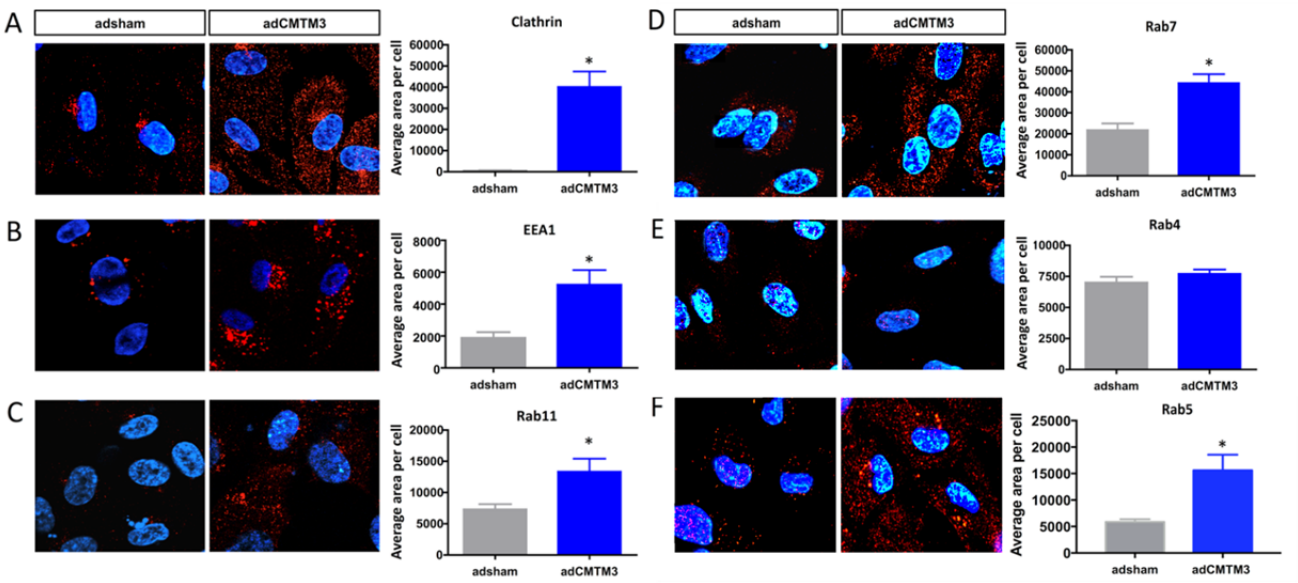

Figure 6. CMTM3 expression significantly upregulates the endocytic pathway.

(A) Representative confocal micrographs of HUVECs transfected with adsham and adCMTM3, immunostained for clathrin (red). Quantification of clathrin+ area per cell in adsham and adCMTM3 transfected HUVECs. (B) Representative confocal micrographs of HUVECs transfected with adsham and adCMTM3, immunostained for EEA1 (red). Quantification of EEA1+ area per cell in adsham and adCMTM3 transfected HUVECs. (C) Representative confocal micrographs of HUVECs transfected with adsham and adCMTM3, immunostained for Rab11 (red). Quantification of Rab11+ area per cell in adsham and adCMTM3 transfected HUVECs. (D) Representative confocal micrographs of HUVECs transfected with adsham and adCMTM3, immunostained for Rab7 (red). Quantification of Rab7+ area per cell in adsham and adCMTM3 transfected HUVECs. (E) Representative confocal micrographs of HUVECs transfected with adsham and adCMTM3, immunostained for Rab4 (red). Quantification of Rab4+ area per cell in adsham and adCMTM3 transfected HUVECs. For all data displayed, mean ± SEM. *P<0.05 versus adsham. N≥8.

CMTM3 mediates Ve-cadherin endocytosis and barrier function of endothelial (adherens) junctions.

To elucidate the role of CMTM3 in the internalization of Ve-cadherin, we conducted an internalization assay in which adsham and adCMTM3 transfected confluent HUVEC monolayers were compared. Quantification of the total Ve-caderin+ areas per cell (before acid wash procedure that removes extracellular Ve-cadherin signal, see sup. material and methods for details) demonstrates that CMTM3 overexpression did not alter the signal (data not shown). In contrast, assessment of Ve-cadherin and cell cytoskeleton actin represented in Pearson's correlation coefficient values shows a significant reduction in VE-cadherin/actin co-localization in adCMTM3 versus adsham groups (Figure 7A, B), indicating that Ve-cadherin connections with the actin cytoskeleton, which are necessary for adherens junction formation and stabilization, are affected. Furthermore, quantification following acid wash treatment demonstrates that internalization of Ve-cadherin is significantly increased in adCMTM3 versus adsham treated

HUVECs under both basic conditions and VEGFA stimulation (Figure 7C-E). Visa versa, siRNA mediated knockdown of CMTM3 (siCMTM3) significantly decreases Ve-cadherin internalization compared to sisham treated HUVECs in response to VEGFA stimulation (Figure 7F-H). SiRNA or adenoviral transfection did not significantly affect Ve-cadherin uptake, as shown by comparison between adsham/sisham versus non-transfected controls (Sup. Figure VII). Thus, these data confirm that CMTM3 is indeed involved in Ve-cadherin internalization. To investigate if Ve-cadherin uptake was mediated by direct binding to CMTM3, co-immunoprecipitation experiments were conducted using magnetic beads coated with an antibody against Ve-cadherin to isolate Ve-cadherin-complexes in protein lysate of adCMTM3 transfected HUVECs. Ve-cadherin protein pull down was successful, but no CMTM3 was detected in the co-immunoprecipitate, implying that direct binding between CMTM3 and Ve-cadherin does not take place in HUVECs (Sup. Figure VIII).

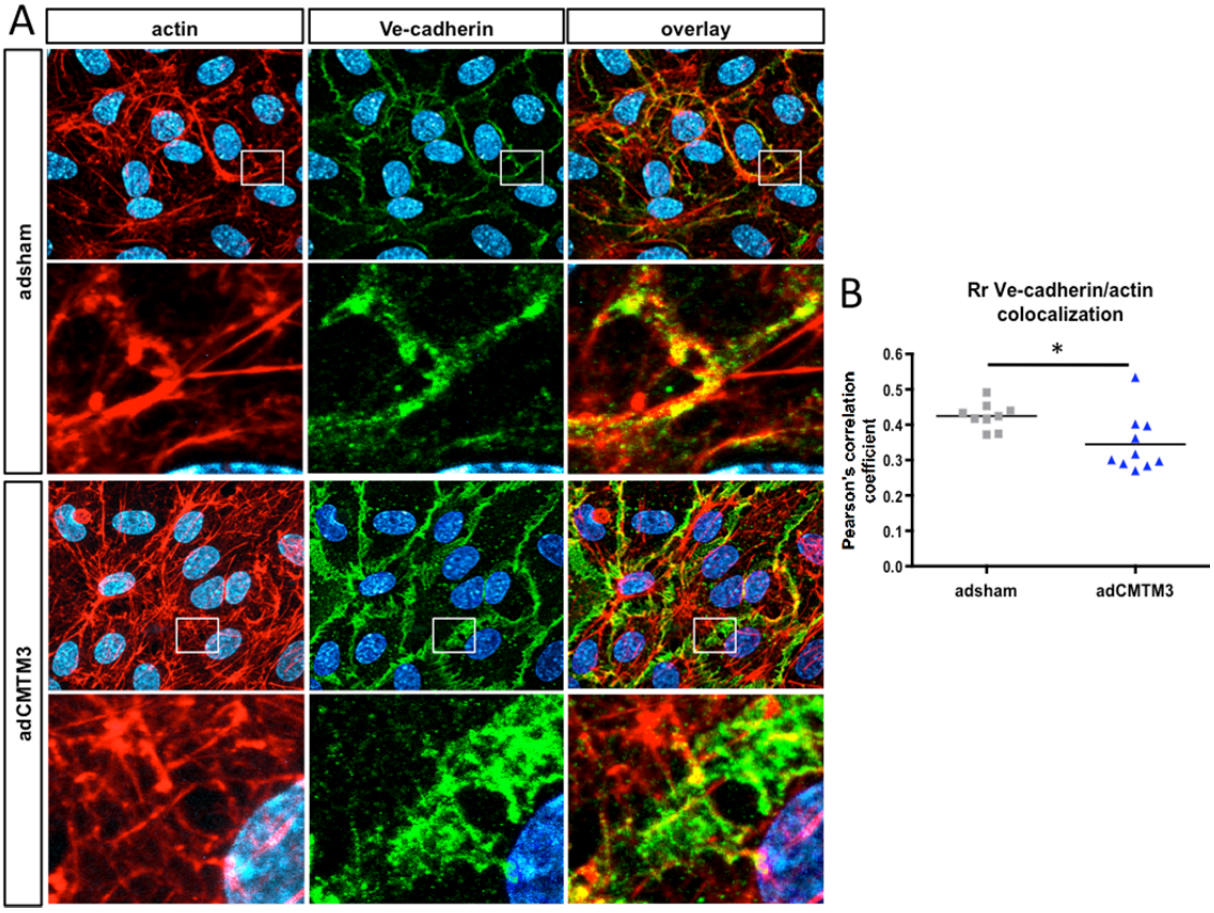

Figure 7. CMTM3 promotes internalization of cell-surface Ve-cadherin.

(A) Representative low and high magnification confocal micrographs of confluent grown HUVECs immunostained for actin (red) and Ve-cadherin (green), in adsham and adCMTM3 transfected cultures. Co-localization in overlay image is in yellow. (B) Quantificantion of co-localization of Ve-cadherin and actin in confocal micrographs based on Pearson's correlation coefficient (Rr), mean ± SEM. *P<0.05. N≥9.

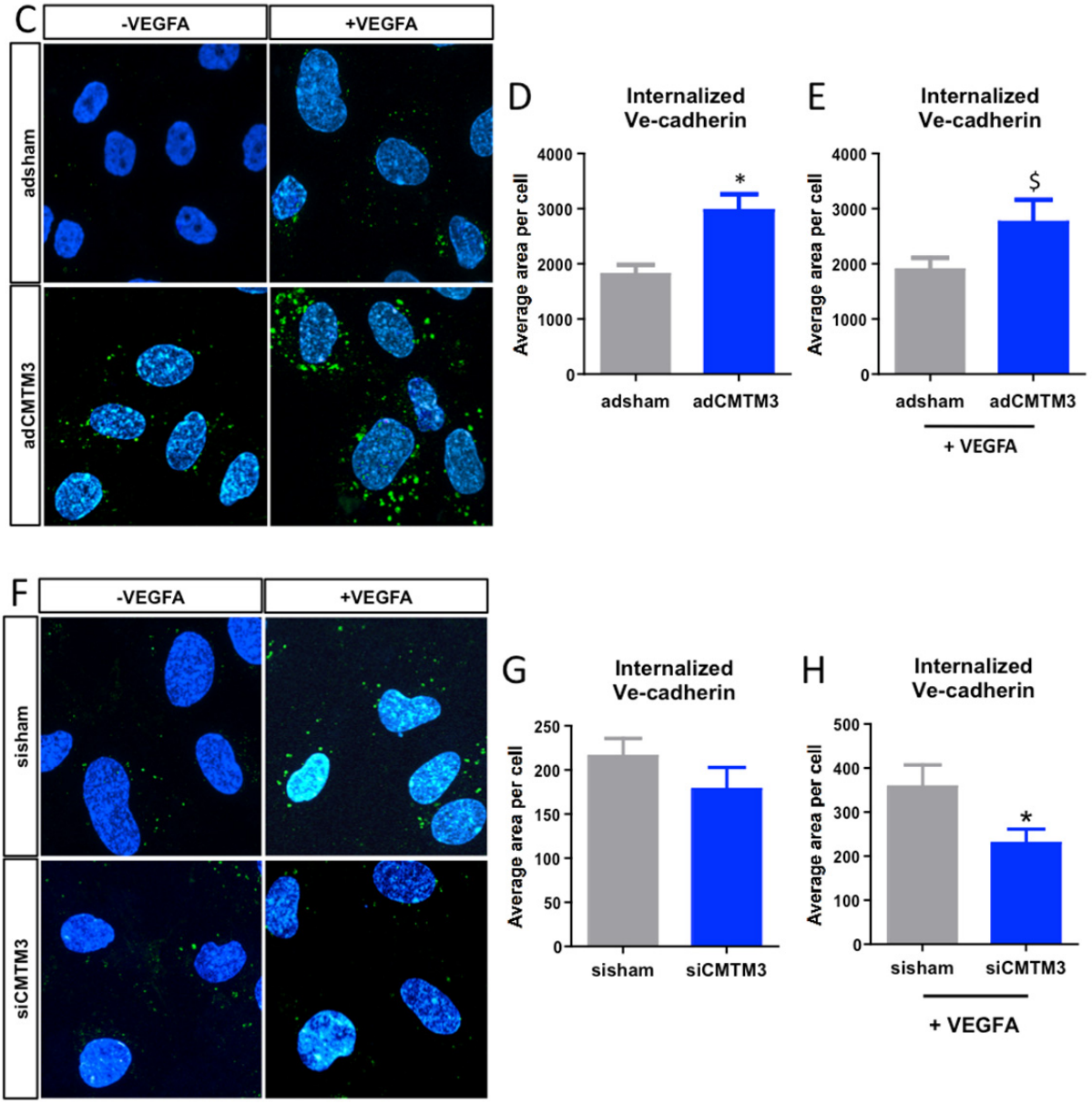

Figure 7. (C) Representative confocal micrographs of confluent grown HUVECs in adsham and adCMTM3 cultures, labelled with VE-cadherin antibodies at 4ºC, followed by 37ºC incubation for 30 minutes with and without exogenous VEGFA to track VE-cadherin movement, followed by a low pH wash to remove surface bound antibodies, before proceeding with immunostaining to visualize internalized Ve-cadherin (green). (D) Quantification of internalized Ve-cadherin+ area per cell in adsham and adCMTM3 HUVECs without VEGFA, and (E) with VEGFA stimulation, mean ± SEM. *P<0.05 versus adsham. $^{\$}$P<0.1 versus adsham. N≥8. (F) Representative confocal micrographs of confluent grown HUVECs in sisham and siCMTM3 cultures showing internalized Ve-cadherin (green) following a protocol similar to C. (G) Quantification of internalized Ve-cadherin+ area per cell in sisham and siCMTM3 HUVECs without VEGFA, and (H) with VEGFA stimulation, mean ± SEM. *P<0.05 versus adsham. N≥8.

Shifts in Ve-cadherin endocytosis directly alter cell-surface bio-availability of Ve-cadherin to form intercellular homophilic bonds at AJs, and may therefore impact endothelial barrier function. To evaluate the effect of CMTM3 on the barrier function, we conducted transendothelial electrical resistance (TEER) measurements on HUVEC monolayers exposed to thrombin induced endothelial junction disruption. Basal levels of electrical resistance did not differ between siCMTM3 and sisham groups. However, the thrombin-induced response in CMTM3 knockdown was significantly decreased compared to sisham controls (Figure 8A): The decrease in resistance during the initial phase (0-30 minutes, exposure to thrombin) was less for siCMTM3 ($P<0.1$; Figure 8B), whereas the increase in resistance during the recovery phase (30-120 minutes, after removal of thrombin at 30 minutes), was not significantly different between the two groups (Figure 8C). In contrast, whereas basal levels were similarly not affected, CMTM3 overexpression significantly increased the thrombin-induced response (Figure 8D): The decrease in resistance during the initial phase was significantly higher for adCMTM3 compared to adsham controls (Figure 8E). Similarly, the increase in resistance during the restoration phase was more pronounced in the adCMTM3 group (Figure 8F).

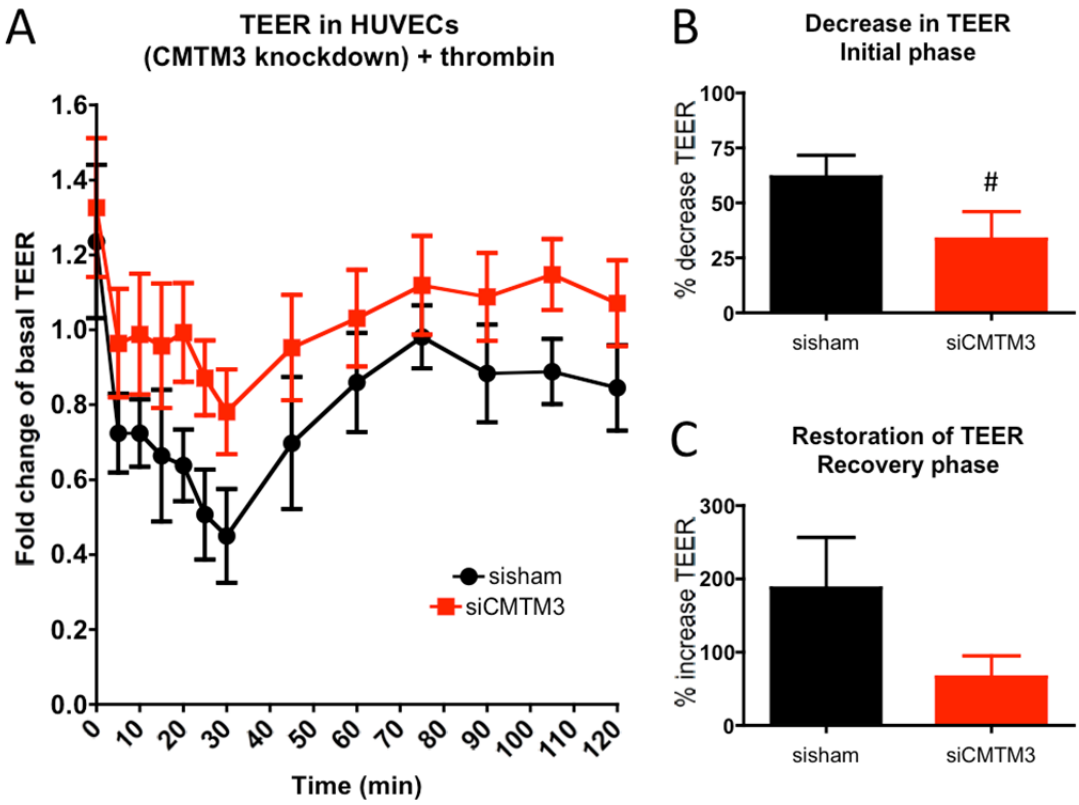

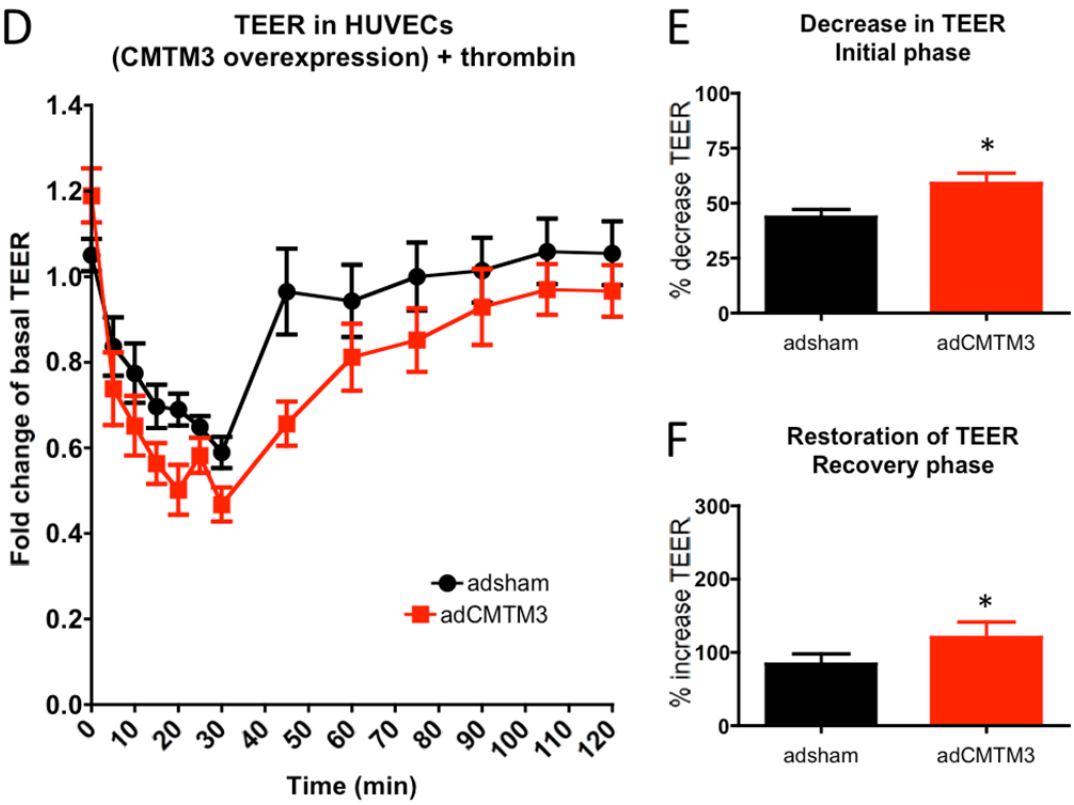

Figure 8. CMTM3 promotes loss of endothelial electric resistance in thrombin-induced response. (A) Thrombin response (presented in fold change compared to basal resistance of non-transfected group: Y axes) of confluent HUVECs monolayers during (0-30 minutes) and after (30-120 minutes) thrombin (1 U/ml) stimulation in siCMTM3 versus sisham conditions. At 0 minutes, thrombin was added and at 30 minutes thrombin was removed. Mean ± SEM. N≥8 per time series. $P<0.05$; Two-way ANOVA. (B) Decrease in resistance during initial phase (0-30 minutes) in sisham and siCMTM3 groups. (C) Increase in resistance during recovery phase (30-120 minutes) in sisham and siCMTM3 groups. For B and C; mean ± SEM. $^{\#}P<0.1$ versus sisham. N≥8. (D) Thrombin response (presented in fold change compared to basal resistance of non-transfected group: Y axes) of confluent HUVECs monolayers during (0-30 minutes) and after (30-120 minutes) thrombin (1 U/ml) stimulation in adCMTM3 and adsham conditions. At 0 minutes, thrombin was added and at 30 minutes thrombin was removed. Mean ± SEM. N≥8 per time series. $P<0.1$; Two-way ANOVA. (E) Decrease in resistance during initial phase (0-30 minutes) in adsham and adCMTM3 groups. (F) Increase in resistance during recovery phase (30-120 minutes) in adsham and adCMTM3 groups. For E and F; mean ± SEM. *$P<0.05$ versus adsham. N≥8.

Discussion

We have previously found that CMTM3 expression is enriched in endothelial progenitor cells during murine embryonic development. In this study, we assessed the endothelial function of this putative angiogenic regulator. The most important findings of our current study are: (1) CMTM3 in endothelial cells is crucial for new vessel formation, as shown in an *in vitro* 3D collagen based co-culture assay with human endothelial cells and pericytes by siRNA mediated CMTM3 silencing. (2) CMTM3 inhibition *in vivo* by morpholino injection in developing zebrafish larvae confirms that CMTM3 expression is required for (intersomitic) vascular growth. (3) CMTM3 knockdown does not affect endothelial cell proliferation or migration. (4) However CMTM3 is localized in early endosome markers EEA1 and Clathrin positive intracellular vesicles. (5) Furthermore, CMTM3 co-localizes with internalized Ve-cadherin. (6) CMTM3 overexpression enhances the endothelial endocytic pathway. (7) CMTM3 overexpression enhances whereas CMTM3 knockdown decreases Ve-cadherin internalization. (8) Knockdown of CMTM3 increases junctional resistance during exposure to thrombin. This effect is reversed in CMTM3 overexpression conditions.

CMTM3 regulation of Ve-cadherin turnover in angiogenesis

Previously, CMTM-family members have been shown to regulate tumor cell growth and migration in different types of cancers[9, 12, 13]. For CMTM3, it has been reported that the protein was highly expressed in testis, leukocytes and spleen[11]. In cancer cells, CMTM3 was silenced by CpG methylation in carcinomas, and restoration of CMTM3 expression inhibited tumor cell growth and promoted apoptosis[17]. CMTM3 silencing or down regulation was also reported for testicular and gastric cancer cells. Similarly, restoration of CMTM3 expression inhibited cancer cell growth by inducing cell cycle arrest and reducing cancer cell migration[15, 20]. However, the function of CMTM3 in normal cell types, and in particularly, in vascular cells, remained yet to be defined.

In this study, we demonstrated that CMTM3 plays an important role in angiogenesis *in vivo* and *in vitro*. In contrast to the main CMTM3 function in various cancer cell types, our data showed that CMTM3 does not influence cell cycle progression and proliferation in endothelial cells. Furthermore, CMTM3 does not affect endothelial cell migration. Rather, our data demonstrated that the angiogenic capacity of CMTM3 is associated with the regulation of cell surface Ve-cadherin bio-availability mediated by mechanisms of endocytosis.

Endocytosis-mediated internalization of Ve-cadherin removes the protein from adherens junction sites and reduces formation of intercellular complexes. This decrease in cell-cell connections is vital for the initial phases of angiogenic sprouting, as destabilization of intercellular contacts promotes EC migration and tip and stalk cell differentiation, followed by vascular expansion from the pre-existing origin vessel. For example, knockdown of Ve-cadherin in zebrafish embryos has been shown to increase intersomitic vessel sprouting[21]. Previous studies have also shown that adherens junction turnover involves endocytic trafficking

pathways that essentially control the rate of Ve-cadherin turnover: Ve-cadherin internalization in response to e.g. VEGDA stimulation, is mediated by Ve-cadherin targeting for Clathrin-mediated endocytosis by binding of (beta-arrestin) adaptor protein-mediated complexes, which further recruits endocytic machinery protein clusters into Clathrin-coated pits situated in the membrane[4]. This is followed by dynamin-mediated scission of the plasma membrane, followed by inward membrane budding to form Clathrin-coated vesicles[22]. After internalization, these vesicles fuse into early endosomes where Ve-cadherins are either sorted into late endosomes and subsequently degraded in lysosomes[23], or are transported back to the cell surface pool directly, or via further processing by recycling endosomes[16, 22].

Here we demonstrated that CMTM3 could promote the endocytosis pathway: Clathrin+ subcellular vesicles and early endosomes marked by EEA1 were increased in CMTM3 expressing endothelial cells compared to adsham controls. Furthermore, CMTM3 expression increased recycling endosomes marked by Rab11 and late endosomes marked by Rab7. We also showed that CMTM3 expression promotes internalization of Ve-cadherin at basal level and in response to VEGFA stimulation, whereas CMTM3 knockdown inhibited Ve-cadherin internalization in response to VEGFA. Furthermore, CMTM3 reduced junctional resistance in endothelial monolayers, indicating that CMTM3 regulates endothelial barrier function and vascular integrity.

In relation to endocytic mechanisms and subcellular vesicles trafficking, Eswaran *et al.* reported that the CMTM-family genes were homologous to myelin and lymphocyte (MAL) proteins tricellulins, plasmolipins and occluding families, which comprise the tetra-spanin trans-membrane domain (MAL and related protein for vesicle trafficking and membrane linking, or MARVEL). These proteins have been functionally linked to cell communication and intracellular transport[24]. They also demonstrated that CMTM7 interacts with BLNK in a membrane protein complex in B-cell precursor acute lymphoblastic leukemia cell lines[24]. Overexpression of CMTM8 in tumor cell lines enhanced the endocytosis rate of EGFR[25]. Further studies are required to assess if the other family members, like CMTM3, are also involved in endocytosis regulation.

Based on our findings and previous reports, we interpret from our data that CMTM3 is involved in turnover of the cell surface Ve-cadherin pool. In an angiogenic environment, formation of vascular sprouts from pre-existing vessels is mediated by VEGFA. Endocytosis of Ve-cadherin following VEGFA stimulation is one of the main mechanisms by which VEGFA promotes vascular sprouting[4]. As indicated by our findings, CMTM3 appears to be an important regulator in this process as it significantly enhances VEGFA-mediated Ve-cadherin, thereby reducing junctional adhesion strength between the cells. The exact mechanism by which CMTM3 facilitates Ve-cadherin internalization remains to be further investigated. Given our findings that also demonstrated that CMTM3 is co-localized with Clathrin, CMTM3 could function as an adaptor protein that is involved in Ve-cadherin targeting and positioning in the protein complex of Clathrin-mediated endocytosis. Similarly, CMTM3 could be involved in regulating the fusion of Clathrin coated vesicles into EEA1+ endosomes, as CMTM3 also co-localized with EEA1 in our

studies. Currently, we are conducting further studies to elucidate the contribution of CMTM3 in subcellular trafficking of Ve-cadherin.

In conclusion, in this study we have identified, for the first time to our knowledge, a regulatory function for CMTM3 in angiogenesis. CMTM3 is involved in Ve-cadherin turnover, and is a regulator of the cell surface pool of Ve-cadherin. Therefore, CMTM3 mediates cell-cell adhesion at AJs, and contributes to the control of vascular sprouting. Further studies that elucidate the exact mechanisms by which CMTM3 regulates endocytic transport of plasma membrane proteins in endothelial cells could lead to the identification of new drug targets and contribute to new therapies to block vascular growth in tumors, or enhance angiogenesis in tissue regeneration.

References

1. Eelen G, de Zeeuw P, Simons M, Carmeliet P. Endothelial cell metabolism in normal and diseased vasculature. Circ Res 2015;**116**(7):1231-44.
2. Vestweber D. VE-cadherin: the major endothelial adhesion molecule controlling cellular junctions and blood vessel formation. Arterioscler Thromb Vasc Biol 2008;**28**(2):223-32.
3. Wallez Y, Huber P. Endothelial adherens and tight junctions in vascular homeostasis, inflammation and angiogenesis. Biochim Biophys Acta 2008;**1778**(3):794-809.
4. Gavard J, Gutkind JS. VEGF controls endothelial-cell permeability by promoting the beta-arrestin-dependent endocytosis of VE-cadherin. Nat Cell Biol 2006;**8**(11):1223-34.
5. Lampugnani MG, Orsenigo F, Gagliani MC, Tacchetti C, Dejana E. Vascular endothelial cadherin controls VEGFR-2 internalization and signaling from intracellular compartments. J Cell Biol 2006;**174**(4):593-604.
6. Gory-Faure S, Prandini MH, Pointu H, Roullot V, Pignot-Paintrand I, Vernet M, Huber P. Role of vascular endothelial-cadherin in vascular morphogenesis. Development 1999;**126**(10):2093-102.
7. Cattelino A, Liebner S, Gallini R, Zanetti A, Balconi G, Corsi A, Bianco P, Wolburg H, Moore R, Oreda B, Kemler R, Dejana E. The conditional inactivation of the beta-catenin gene in endothelial cells causes a defective vascular pattern and increased vascular fragility. J Cell Biol 2003;**162**(6):1111-22.
8. Stenmark H. Rab GTPases as coordinators of vesicle traffic. Nat Rev Mol Cell Biol 2009;**10**(8):513-25.
9. Xiao K, Garner J, Buckley KM, Vincent PA, Chiasson CM, Dejana E, Faundez V, Kowalczyk AP. p120-Catenin regulates clathrin-dependent endocytosis of VE-cadherin. Mol Biol Cell 2005;**16**(11):5141-51.
10. Chiasson CM, Wittich KB, Vincent PA, Faundez V, Kowalczyk AP. p120-catenin inhibits VE-cadherin internalization through a Rho-independent mechanism. Mol Biol Cell 2009;**20**(7):1970-80.
11. Zhong J, Wang Y, Qiu X, Mo X, Liu Y, Li T, Song Q, Ma D, Han W. Characterization and expression profile of CMTM3/CKLFSF3. J Biochem Mol Biol 2006;**39**(5):537-45.
12. Li T, Cheng Y, Wang P, Wang W, Hu F, Mo X, Lv H, Xu T, Han W. CMTM4 is frequently downregulated and functions as a tumour suppressor in clear cell renal cell carcinoma. J Exp Clin Cancer Res 2015;**34**:122.
13. Li H, Li J, Su Y, et al. A novel 3p22.3 gene CMTM7 represses oncogenic EGFR signaling and inhibits cancer cell growth. Oncogene 2014;**33**(24):3109-18.
14. Han W, Ding P, Xu M, Wang L, Rui M, Shi S, Liu Y, Zheng Y, Chen Y, Yang T, Ma D. Identification of eight genes encoding chemokine-like factor superfamily members 1-8 (CKLFSF1-8) by in silico cloning and experimental validation. Genomics 2003;**81**(6):609-17.
15. Li Z, Xie J, Wu J, Li W, Nie L, Sun X, Tang A, Li X, Liu R, Mei H, Wang F, Wang Z, Gui Y, Cai Z. CMTM3 inhibits human testicular cancer cell growth through inducing cell-cycle arrest and apoptosis. PLoS One 2014;**9**(2):e88965.
16. Yan Z, Wang ZG, Segev N, Hu S, Minshall RD, Dull RO, Zhang M, Malik AB, Hu G. Rab11a Mediates Vascular Endothelial-Cadherin Recycling and Controls Endothelial Barrier Function. Arterioscler Thromb Vasc Biol 2016;**36**(2):339-49.

17. Wang Y, Li J, Cui Y, et al. CMTM3, located at the critical tumor suppressor locus 16q22.1, is silenced by CpG methylation in carcinomas and inhibits tumor cell growth through inducing apoptosis. Cancer Res 2009;**69**(12):5194-201.
18. Lei Z, van Mil A, Brandt MM, Grundmann S, Hoefer I, Smits M, El Azzouzi H, Fukao T, Cheng C, Doevendans PA, Sluijter JP. MicroRNA-132/212 family enhances arteriogenesis after hindlimb ischaemia through modulation of the Ras-MAPK pathway. J Cell Mol Med 2015;**19**(8):1994-2005.
19. Stratman AN, Malotte KM, Mahan RD, Davis MJ, Davis GE. Pericyte recruitment during vasculogenic tube assembly stimulates endothelial basement membrane matrix formation. Blood 2009;**114**(24):5091-101.
20. Su Y, Lin Y, Zhang L, et al. CMTM3 inhibits cell migration and invasion and correlates with favorable prognosis in gastric cancer. Cancer Sci 2014;**105**(1):26-34.
21. Abraham S, Yeo M, Montero-Balaguer M, Paterson H, Dejana E, Marshall CJ, Mavria G. VE-Cadherin-mediated cell-cell interaction suppresses sprouting via signaling to MLC2 phosphorylation. Curr Biol 2009;**19**(8):668-74.
22. Mellman I, Yarden Y. Endocytosis and cancer. Cold Spring Harb Perspect Biol 2013;**5**(12):a016949.
23. Xiao K, Allison DF, Kottke MD, Summers S, Sorescu GP, Faundez V, Kowalczyk AP. Mechanisms of VE-cadherin processing and degradation in microvascular endothelial cells. J Biol Chem 2003;**278**(21):19199-208.
24. Eswaran J, Sinclair P, Nakjang S, Harrision CJ. Identification of Cmtm Family Proteins As Tumor Suppressor and Membrane Regulator in B Cell Precursor Acute Lymphoblastic Leukemia. Blood 2014;**124**(21):3582.
25. Jin C, Ding P, Wang Y, Ma D. Regulation of EGF receptor signaling by the MARVEL domain-containing protein CKLFSF8. FEBS Lett 2005;**579**(28):6375-82.

Supplemental data

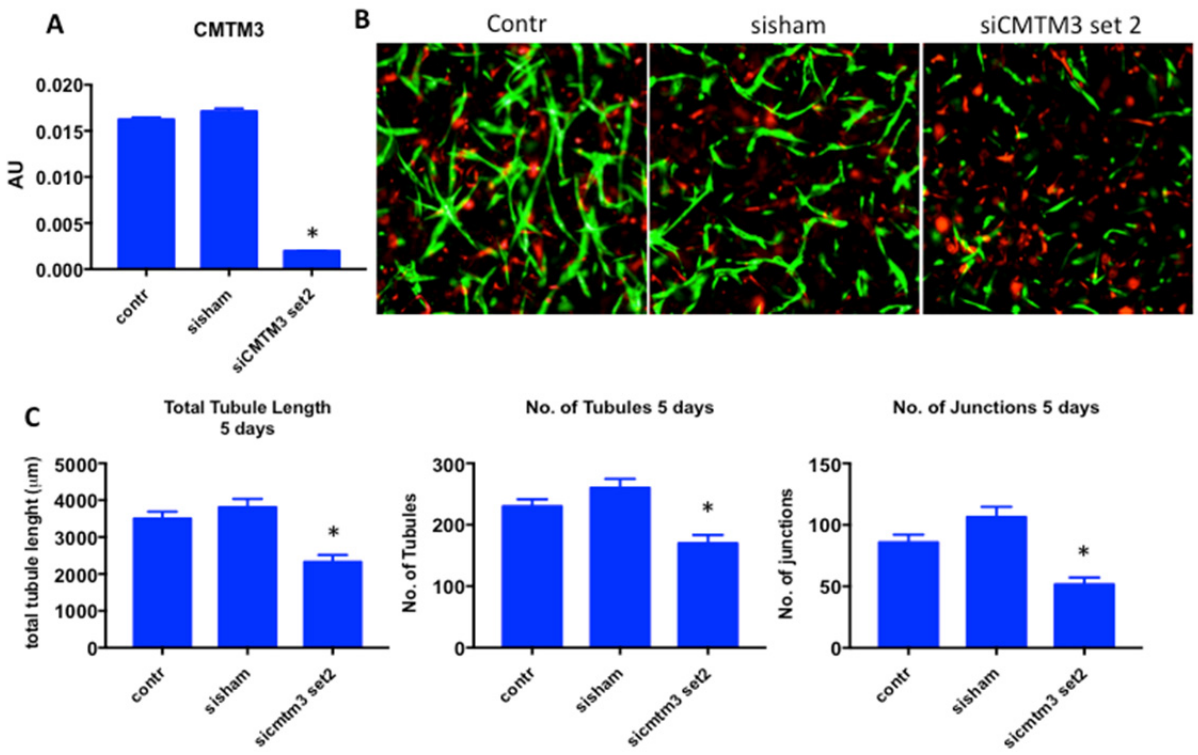

Sup. Figure I. CMTM3 silencing using a second siRNA sequence in ECs impairs vascular growth in a 3D collagen matrix vascular co-culture system *in vitro.* (A) QPCR analysis of CMTM3 expression levels in HUVECs treated with a second sequence of CMTM3-targeting siRNA (siCMTM3) compared to non-targeting scrambled siRNA treated cells (sisham) or non-treated controls (contr.). Gene expression levels are shown in target gene/house keeping gene (ß actin) ratio (AU), mean ± SEM. *P<0.05 versus sisham and control. N≥3. (B) Representative images of 3D collagen matrix HUVECs-GFP and pericytes-GFP co-cultures in which HUVECs-GFP were treated with a second sequence of CMTM3-targeting siRNA (siCMTM3) compared to non-targeting scrambled siRNA treated cells (sisham) or non-treated controls (contr.). Images displayed were taken at day 5. (C) Quantification of total tubule length, number of tubules and junctions at day 5 of co-culture. Values are Mean ± SEM. *P<0.05 versus control and sisham at day 5. N≥15 co-cultures.

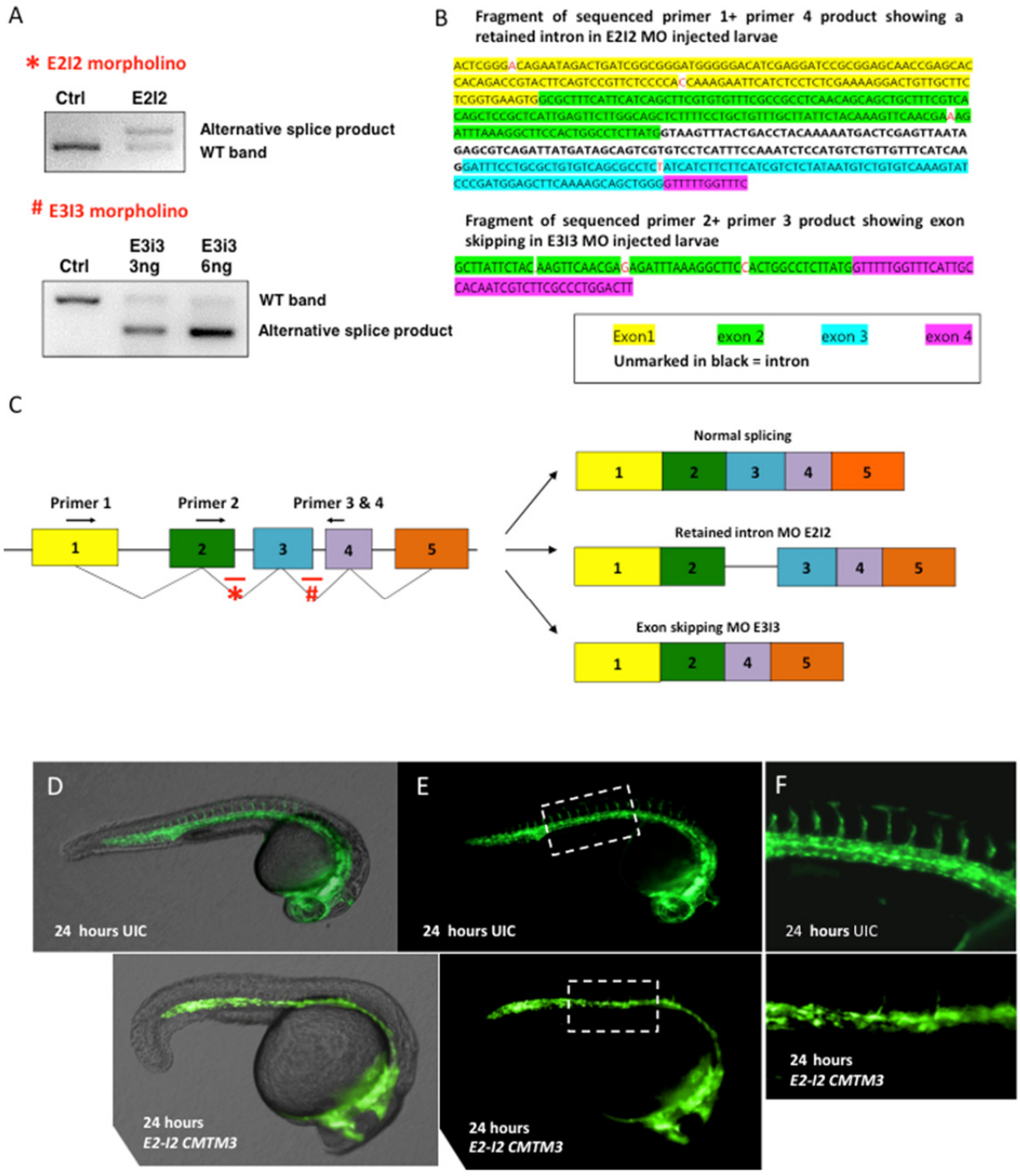

Sup. Figure II. Morpholino-induced silencing of CMTM3 in zebrafish affects vascular growth of intersomatic vessels.

(A) PCR validation of the morpholino targeting of splice sites E2-I2 and E3-I3. Shown are the PCR bands of wildtype (WT) and alternatively spliced (non-functional) zebrafish CMTM3 mRNAs in uninjected (contr.) and E2-I2 or E3-I3 morpholino (MO) treated larvae. (B) PCR bands were isolated from gel and sequenced to reveal the composition of the alternative spliced products. (C) Diagram showing the alternative spliced mRNA products of (1) MO E2I2: Larger product with retained intron compared to WT, and (2) MO E3I3:

Smaller product with exon skipping. (D) Tg(fli1:eGFP)^{y1} embryos at 24 hpf, lateral view, anterior to the right. (E) Distinct reduction of intersomatic vascular sprouting in the trunk region was observed in CMTM3 targeting morpholino-injected (morpholino targeting splice site E2-I2 of CMTM3 (indicated as E2-I2 CMTM3) embryos compared to uninjected controls (UIC). The zebrafish vasculature is highlighted by the eGFP marker (in green). (F) Panel shows high magnification images of intersomatic outgrowth in the indicated trunk region in UIC and E2-I2 CMTM3 group.

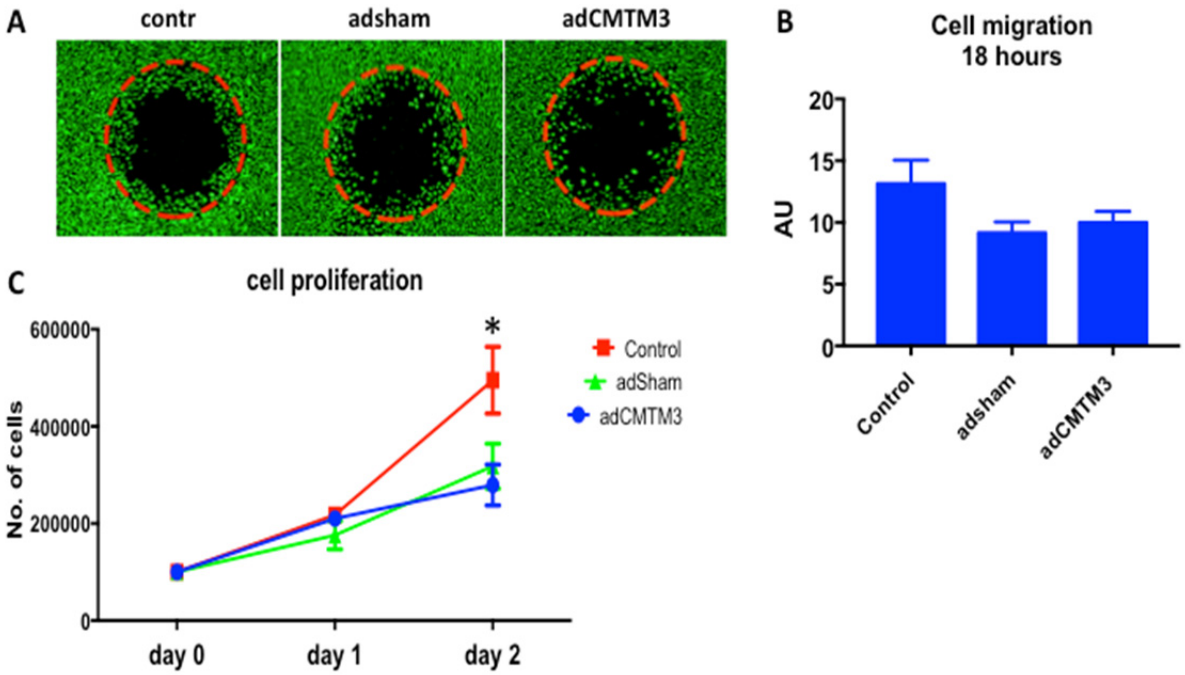

Sup. Figure III. CMTM3 overexpression does not affect endothelial cell migration and proliferation.
(A) Representative results of plug-based migration assays after 24 hours of migration in adCMTM3 treated HUVECs compared to adsham and nontransfected controls. Cells are visualized by Calcein-AM (Green) uptake. The red circle indicates the area occupied by a plug during seeding. Plug was removed to allow free migration of cells into the circle zone for 18 hours. (B) Quantification of % area within circle zone covered by HUVECs compared to sisham and nontransfected controls. Shown is mean ± SEM. N>4. (C) Number of counted cells at day of seeding (day 0) and after 1 and 2 days of cell proliferation in adCMTM3 treated HUVECs compared to adsham and non-transfected controls. Shown is mean ± SEM. N>4. *P<0.05 control versus adsham and adCMTM3.

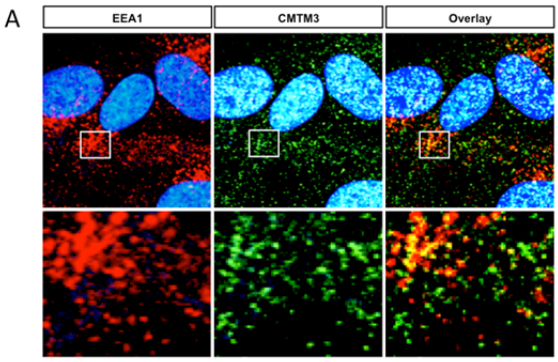

Sup. Figure IV. Endogenous CMTM3 colocalizes with EEA1. (A) Representative immunofluoresence microscope images of HUVECs immunostained for endogenous CMTM3 (green), EEA1 (red) and dapi. Co-localization in overlay image is in yellow.

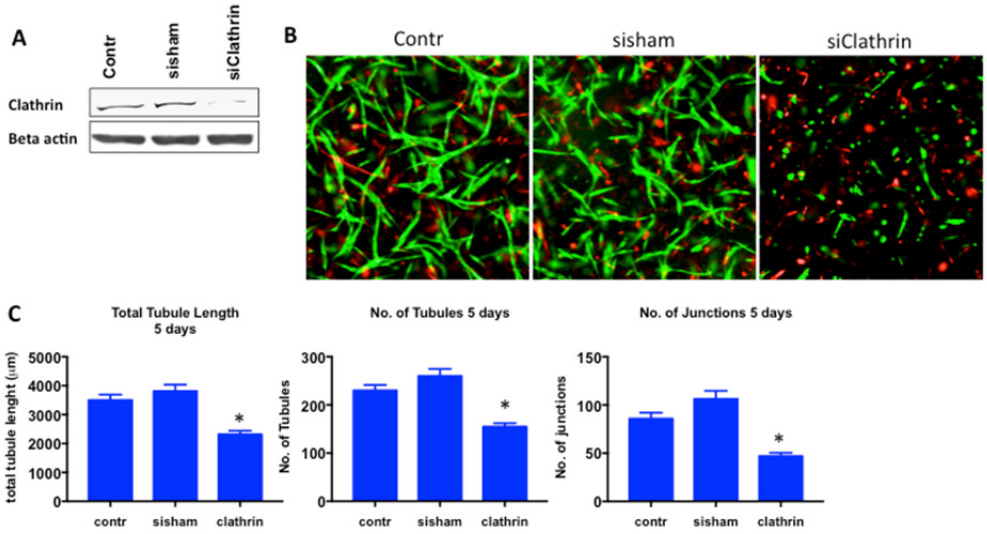

Sup. Figure V. Clathrin silencing in ECs impairs vascular growth in a 3D collagen matrix vascular co-culture system *in vitro*. (A) Western blot analysis of clatherin protein levels in HUVECs treated with clathrin-targeting siRNA (siclathrin) compared to non-targeting scrambled siRNA treated cells (sisham) or non-treated controls (contr.). ß actin blotting was used as a loading control. Shown is a representative blot of 2. (B) Representative images of 3D collagen matrix HUVECs-GFP and pericytes-GFP co-cultures in which HUVECs-GFP were treated with siclatherin compared to non-targeting scrambled siRNA treated cells (sisham) or non-treated controls (contr.). Images displayed were taken at day 5. (C) Quantification of total tubule length, number of tubules and junctions at day 5 of co-culture. Values are Mean ± SEM. *P<0.05 versus control and sisham at day 5. N≥15 co-cultures.

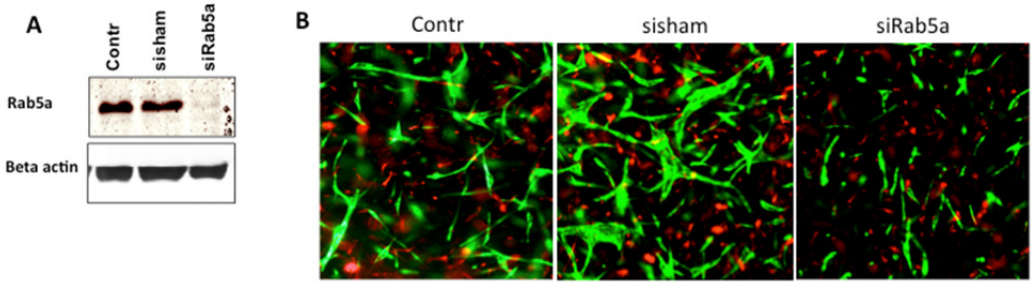

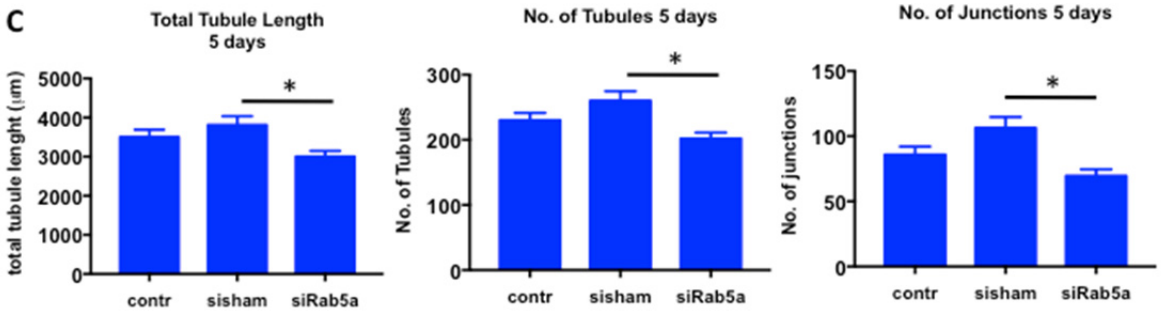

Sup. Figure VI. Rab5(a) silencing in ECs impairs vascular growth in a 3D collagen matrix vascular co-culture system *in vitro.* (A) Western blot analysis of clatherin protein levels in HUVECs treated with Rab5-targeting siRNA (siRab5a) compared to non-targeting scrambled siRNA treated cells (sisham) or non-treated controls (contr.). ß actin blotting was used as a loading control. Shown is a representative blot of 2. (B) Representative images of 3D collagen matrix HUVECs-GFP and pericytes-GFP co-cultures in which HUVECs-GFP were treated with siRab5 compared to non-targeting scrambled siRNA treated cells (sisham) or non-treated controls (contr.). Images displayed were taken at day 5. (C) Quantification of total tubule length, number of tubules and junctions at day 5 of co-culture. Values are Mean ± SEM. *P<0.05 versus sisham at day 5. N≥15 co-cultures.

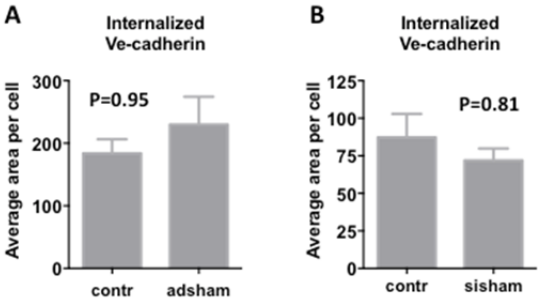

Sup. Figure VII. Internalization of cell-surface Ve-cadherin in adsham or sisham transfected HUVECs versus non-transfected controls.
(A) Quantification of internalized Ve-cadherin+ area per cell in adsham and non-transfected HUVECs, mean ± SEM. N≥6. (B) Quantification of internalized Ve-cadherin+ area per cell in sisham and non-transfected HUVECs, mean ± SEM. N≥6.

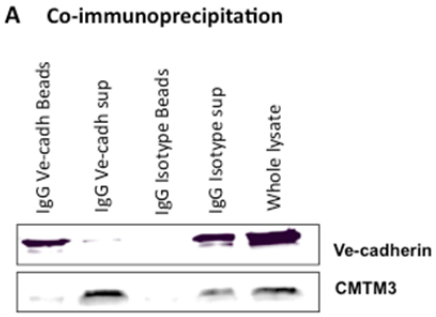

Sup. Figure VIII. Co-immunoprecipitation experiments show successful pull-down of targeted Ve-cadherin but no direct binding of Ve-cadherin with CMTM3. (A) Western blot analysis of Ve-cadherin and CMTM3 bands detected in (from left to right): (1) pull-down lysate of beads coated with an antibody against Ve-cadherin, (2) the flush-through lysate treated of IgG Ve-cadherin coated beads condition, (3) pull-down lysate of beads coated with a non-specific IgG isotype, (4) flush-through lysate of IgG isotype coated beads condition, and (5) whole lysate. Blot shows representative result of 3 experiments.

Chapter 3 CMTM4 regulates angiogenesis by promoting cell surface recycling of VE-cadherin to endothelial adherens junctions.

Ihsan Chrifi*, Laura Louzao-Martinez*, Maarten M. Brandt, Christian G.M. van Dijk, Petra E. Burgisser, Changbin Zhu, Johan M. Kros, Marianne C. Verhaar, Dirk J. Duncker, Caroline Cheng.

** These authors contributed equally.*

Published: Angiogenesis 2018 Aug; [ahead of print]

Abstract

Aim:
Vascular endothelial (VE) cadherin is a key component of endothelial adherens junctions (AJs) and plays an important role in maintaining vascular integrity. Endocytosis of VE-cadherin regulates junctional strength and a decrease of surface VE-cadherin reduces vascular stability. However, disruption of AJs is also a requirement for vascular sprouting. Identifying novel regulators of endothelial endocytosis could enhance our understanding of angiogenesis. Here, we evaluated the angiogenic potential of (CKLF-like MARVEL transmembrane domain 4) CMTM4 and assessed in which molecular pathway CMTM4 is involved during angiogenesis.

Methods and Results:
Using a 3D vascular assay comprised of GFP-labeled HUVECs and dsRED-labeled pericytes, we demonstrated *in vitro* that siRNA-mediated CMTM4 silencing impairs vascular sprouting. *In vivo*, CMTM4 silencing by morpholino injection in zebrafish larvae inhibits intersomitic vessel growth. Intracellular staining revealed that CMTM4 colocalizes with Rab4 and Rab7 positive vesicles, both markers of the endocytic trafficking pathway. CMTM4 colocalizes with both membrane-bound and internalized VE-cadherin. Adenovirus-mediated CMTM4 overexpression enhances the endothelial endocytic pathway, in particular the rapid recycling pathway, shown by an increase in early endosomal antigen-1 positive (EEA1+), Rab4+, Rab11+ and Rab7+ vesicles. CMTM4 overexpression enhances membrane-bound VE-cadherin internalization, whereas CMTM4 knockdown decreases internalization of VE-cadherin. CMTM4 overexpression promotes endothelial barrier function, shown by an increase in recovery of trans-endothelial electrical resistance (TEER) after thrombin stimulation.

Conclusion:
We have identified in this study a novel regulatory function for CMTM4 in angiogenesis. CMTM4 plays an important role in the turnover of membrane-bound VE-cadherin at AJs, mediating endothelial barrier function and controlling vascular sprouting.

Introduction

Angiogenesis is a critical process that occurs during embryonic development, is re-activated in wound healing, and is often disturbed in disease. Abnormalities in new vessel formation, represented by either excessive or insufficient growth, contribute to a wide range of disorders, including cancer and cardiovascular diseases [1].

Acquiring and maintaining vascular homeostasis is crucial for the formation and stabilization of new blood vessels during angiogenesis. In order for the endothelial cells (ECs), that form the inner lining of new blood vessels, to function in an integrated manner, specific junctions consisting of cell-adhesion molecules are required. From these junctions, adherens junctions (AJs) are critical for cell-cell adhesion and are tightly regulated by complex molecular pathways. Vascular endothelial (VE) cadherin is the main cell-adhesion molecule found in endothelial AJs and plays an important role in maintaining endothelial barrier function [2,3]. Blocking VE-cadherin by the use of antibodies has a negative effect on endothelial survival and increases vascular permeability[4]. In addition, VE-cadherin-deficient mice suffer from severe vascular defects, including impaired vascular sprouting, limited organization of ECs into large mature vessels, and vessel regression, resulting in death at mid-gestation [5,6].

AJs are dynamic structures from which the amount of membrane-bound VE-cadherin that can undergo homophilic interactions with neighboring cells can be actively regulated, thereby modulating the junctional adhesive strength. A reduction in membrane-bound VE-cadherin will result in microvascular destabilization and loss of barrier function. However, a decrease in adhesive strength is required for the disruption of AJs in order to allow EC migration and morphological adaptation into tip and stalk cells during vascular sprouting.

Endocytosis is a form of active transport that is commonly used by cells to take up large secreted molecules or membrane-bound proteins, such as VE-cadherin, into the cytosol for processing. VE-cadherin is taken up in specialized regions called clathrin-coated pits that bud from the membrane to form clathrin-coated vesicles. These vesicles then fuse with early endosomes in which the endocytosed cargo is sorted for recycling, lysosomal, or other trafficking routes [7]. Each distinct trafficking step is controlled by a subset of Rab GTPases, making these enzymes ideal markers to monitor the transport route of endocytosed proteins [8]. Rapid endocytosis of VE-cadherin and the subsequent disassembly of AJs is promoted by vascular endothelial growth factor A (VEGF-A), making the ligand for the VEGF Receptor 1 and 2 (VEGFR1 and 2) an active regulator of vascular permeability [9].

Whereas endocytosis plays a vital role in modulating vascular permeability by controlling the adhesive strength in AJs, little is known about important regulators involved in the early endocytic and subsequent trafficking routes in ECs. Moreover, the exact contribution of endocytosis regulators to the angiogenic process remains to be further elucidated. To identify novel regulators of angiogenesis, we performed a transcriptome analysis of mouse embryos, comparing VEGFR2 positive endothelial progenitor cells with the VEGFR2 negative cell population. We identified an enriched expression of several members of the CKLF-like Marvel

Transmembrane Domain-containing gene (CMTM) family in the VEGFR2 positive population. In humans, this family comprises 9 genes (CKLF and CMTM1-8) that all contain a MAL (myosin and lymphocyte) And Related proteins for Vesicle trafficking and membrane Link (MARVEL) domain [10]. Several studies on CMTM members reveal that they can prevent growth and invasion of different cancer types [11-18]. In a recent study, we revealed that CMTM3 has a specialized function in ECs, where it is involved in regulating the early endocytosis of VE-cadherin during vascular growth [19]. However, the putative function of other CMTM members in endothelial endocytosis, regulation of vascular permeability, and angiogenesis remains to be elucidated. Increasing our understanding of other regulators of angiogenesis is highly important for the development of novel therapeutic targets.

In this study, we investigated the angiogenic potential of CMTM4 and assessed in which molecular pathways CMTM4 is involved in ECs. To our knowledge, CMTM4 is until now only known for its potential to act as a tumor suppressor gene [14]. Our data demonstrated that CMTM4 regulates angiogenesis by promoting cell surface recycling of VE-cadherin to endothelial AJs.

Material and methods

Cell culture

Primary human umbilical vein endothelial cells (HUVECs) were purchased from Lonza and maintained in EGM2 medium (Lonza) with 100 Uml^{-1} penicillin-streptomycin (PS). Primary human brain derived vascular pericytes were purchased from ScienCell and maintained in DMEM+10%FCS with 100 Uml^{-1} PS. At passage 1, HUVECs were transduced with lentiviral GFP construct (HUVECs-GFP) and pericytes with lentiviral dsRED construct (pericytes-dsRED) and selected for puromycin (2.5ug/ml) resistance as previously described [19]. All cells were used between passages 3 and 6 and cultured at 37ºC in a humidified atmosphere containing 5% CO_2.

qPCR analysis

Total RNA was isolated from cultures (single cell monolayers and co-cultured HUVECs and pericytes) using RNeasy kit (Qiagen) according to manufacturer's instructions. The purity and concentrations of RNA were quantified by using Nanodrop (ND-1000) absorbance measurements at 260/280nm and/or capillary electrophoresis (Agilent 2100 Bioanalyser). The iScript synthesis kit (Biorad) was used for cDNA synthesis according to manufacturer's instructions. Gene expression was determined using quantitative real-time PCR (qPCR) according to the SYBR-Green-Cycler IQ5 detection protocol (Biorad). The primer sequences are listed in Supp. Table 1. All results were normalized for the expression of housekeeping gene β-actin.

Short interference RNA (siRNA)

CMTM4 or CMTM3 knockdown in HUVECs and HUVECs-GFP was achieved by using either a mix of 4 complementary siRNA sequences or 2 sets of individual siRNA sequences directed against the mRNA of CMTM4 or CMTM3 (ThermoScientific). As a negative control, cells were either untreated or transfected with a mix of 4 non-targeting siRNA sequences. The sequences are listed in Supp. Table 2.

Adenoviral transduction

Human recombinant CMTM4 or CMTM3 adenovirus were produced using the Gateway pAd/CMV/V5-DEST vector kit and ViraPower™ Adenoviral Expression System kit, according manufacturer's instructions (Invitrogen). Fully sequenced Human CMTM4 or CMTM3 cDNA were obtained from OriGene and Lifesciences, respectively, cloned in a pCMV-SPORT6 vector. To amplify the CMTM4 gene from the obtained clone and simultaneously convert it with *att*B sites, a PCR was conducted with full length *att*B-CMTM4 specific primers: forward oligo's 5`-GGGGACAAGTTTGTACAAAAAAGCAGGCTTCACCATGCGGAGCGGCGAGGAGCTGGACGG-3` and reverse oligo`s 5`-GGGGACCACTTTGTACAAGAAAGCTGGGTTTCACGTGTCCAGGCGCTGGATCTC AGG-3`. The full length *att*B-CMTM4 amplicons was then cloned into a pDONR™ 221 vector to create an entry clone, according to BP Clonase™ II protocol. Full-length cDNAs of CMTM3 with attB-site was amplified by PCR using specific forward oligos 5`- GGGGACAAGTTTGTACAAAA AAGCAGGCTTCACCATGTGGCCCCCAGACCCCGACC-3` and reverse oligo`s 5`- GGGGACCACTTTGT ACAAGAAAGCTGGGTTTCAGTCAGAGTCCGAGTCGGAATTCTC-3`. Moreover a HIS tag was placed at the C-terminal region of CMTM3 (CMTM3-HA) using the RV primer 5`- GGGGACCACTTTGTAC AAGAAAGCT GGGTGGTCAGAGTCCGAGTCGGAATTCTC-3`. Amplicons of CMTM3 and CMTM3-HA were cloned into a pDONR™ 221 vector via BP ClonaseTM II enzyme mix to create an entry clone. DNA sequencing validated the obtained CMTM4 or CMTM3 sequence. Using LR-reaction II (Invitrogen), the CMTM4 or CMTM3 reading frame cassettes were cloned into pAd/CMV/V5-DEST (Invitrogen) expression vectors according to manufacturer's protocol. After verification by DNA sequencing, the pAd/CMV/V5-DEST plasmids were linearized by *Pac*1 restriction and transfected with Lipofectamine 2000 (Invitrogen) into 293A cells. When 80% of the infected cells formed crude viral vesicles, the cells were harvested, followed by three cycles of freeze/thawing to get crude viral lysate (CVL), and the virus was purified using cesium chloride gradient.

Subcellular fractioning and protein extraction

To separate cytoplasmic proteins from the membrane-bound proteins, i.e. the soluble and insoluble fraction, respectively, HUVECs received a PBS wash twice and were harvested in lysis buffer (140 mM NaCl, 10 mM Tris [pH 7.6], 1 mM EDTA, 1% Triton X-100, 0.05% SDS, 1X protease inhibitor cocktail, 1 mM PMSF) 48 hours post-transfection. The lysates were incubated on ice for 20 minutes and were centrifuged at 13,000 g for 12 minutes to separate

the soluble from the insoluble fraction. The pellet was then solubilised in lysis buffer with 2% SDS. Both fractions were subjected to SDS-PAGE and immunoblotting.

Western blot

Protein concentration was determined by the Bradford method (Pierce BCA Protein Assay kit). Equal amounts of sample were loaded on a sodium dodecyl sulfate-polyacrylamide gel electrophoresis (SDS-PAGE) and transferred onto a nitrocellulose membrane (Pierce) at 4ºC overnight. Membranes were blocked and probed with primary antibodies according to manufacturer's instructions (Supp. Table 3). Protein bands were visualized with Li-Cor secondary antibodies and detection system (Westburg) according to manufacturer`s instructions. The detected protein expressions were normalized with β-actin.

Collagen based 3D co-culture

HUVEC-GFP and pericyte-dsRed were co-cultured at a 5:1 ratio in a 3D bovine collagen type 1 (2 mg/ml) environment (Gibco), supplemented with EBM-2 medium (Lonza), ascorbic acid, fibroblast growth factor, 2% FCS, SCF-1, SDF-1α and IL-3 (i.e. co-culture medium), as previously described [20]. Images were taken 2 days after seeding to assess the sprouting capacities of ECs and at day 5, when lumenized micro-capillary structures are formed. Images were taken with fluorescence microscopy with a 2x objective. Images were analyzed based on the number of junctions, the number of tubules and the tubule length using AngioSys 2.0 software.

VE-cadherin internalization assay and immunofluorescence

The internalization assay was performed at 48 hours post-transfection as previously described [9]. Briefly, HUVECs were grown on coverslips to confluence before labeling the cell-surface exposed VE-cadherin by incubation with mouse anti-human VE-cadherin (Supp. Table 3) at 4°C for 1 hour. Movement of labelled VE-cadherin was monitored by placing the cells at 37°C for 1 hour, in basal medium with or without VEGF (50ng/ml; Preprotech), after which the cells were either washed with PBS (PBS supplemented with 1.8 mM CaCl2 and 1 mM MgCl2) or with a mildly acidic buffer (2mM PBS-glycine [pH 2.0], 15 minutes) to remove membrane bound antibodies and revealing the internalized labelled VE-cadherin. Cells were fixed with 4% paraformaldehyde for 30 min, followed by a blocking and permeabilization step for 30 min in PBS with 1% BSA and 0.5% Triton-X. Secondary antibody (Supp. Table 3) incubation was performed for 1 hour at room temperature, followed by a 30 minutes incubation step to label cytoskeletal F-actin with rhodamine phalloidin (Supp. Table 3). For labelling of Rab proteins (Supp. Table 3), an extra primary antibody step was performed after fixation instead of labelling cytoskeletal F-actin. DAPI was used as a nuclear counterstain. Images of fluorescent-labeled markers were obtained with a Leica TCS SP8 X microscope and a 63x oil immersion objective lens. 3D images were obtained by scanning multiple XY planes in the Z direction with a depth of ±10 µm. Serial pictures along the Z-axis were combined to create a stacked XY image. The total

internalized VE-cadherin area was determined by using ImageJ 1.47v.

Morpholino injection in developing zebrafish larvae

Zebrafish (Danio rerio) were maintained under standard laboratory conditions. Morpholinos (MO) against the zebrafish orthologue of CMTM4 were obtained from Gene Tools (Philomath, USA) and suspended in Danieau buffer (58mM NaCl, 0.7mM
KCl, 0.4mM MgSO4, 0.6 mM Ca(NO3)2, 5.0 mM HEPES pH 7.6) containing 0.2% phenol red. Different doses of the MO were injected into single-cell stage zebrafish embryos as previously described [21]. The sequences are listed in Supp. Table 4.

Flow cytometry

CMTM4 silenced HUVECs were seeded at a density of $50x10^3$ cells/well in co-culture medium. After 24, 48, and 72 hours cells were harvested for proliferation and apoptosis analysis. Each harvested sample was stained with Propidium Iodide (PI) and Annexin V (BD Pharmingen) according to manufacturer's protocol and analyzed by flowcytometry (BD Facs Canto). Cells were counted for 2 minutes at medium speed to determine the average cell amount. Cell cycle analysis was conducted after the cells were cultured for 48 hours at 37°C in 5% CO2 and fixed overnight in 70% ethanol at 4°C. Cells were washed with ice-cold PBS and were stained with PI and treated with 0.5 mg/ml RNase for 30 minutes at 37°C before analysis by flow cytometry.

Migration assay

HUVECs were seeded at a density of $75x10^3$ cells/well in a 24 wells plate and after 24 hours, CMTM4 was either silenced or overexpressed. EC migration was assessed 24 hours post-transfection by scratching the HUVEC layer using a 200 µl pipette tip. Loose cells were removed by a PBS wash. Images were taken at t=0, t=4 and t=8 hours, after which the scratch area reduction was determined using Adobe Photoshop CS6.

Intracellular immunostaining

HUVECs were seeded at a density of $10x10^4$ cells/well 24 hour prior to transfection. Cells were fixed 48 hours post-transfection with 4% paraformaldehyde for 30 minutes, followed by a blocking and permeabilization step for 30 minutes in PBS with 1% BSA and 0.5% Triton-X. This was followed by incubation with a primary and secondary antibody (Supp. Table 3) at room temperature for 1.5 and 1 hour, respectively. Cytoskeletal F-actin was labelled with rhodamine phalloidin and DAPI was used as a nuclear counterstaining. Images of fluorescent-labeled markers were obtained with a Leica TCS SP8 X microscope and a 63x oil immersion objective lens. For quantification of the total area, 3D images were obtained by scanning multiple XY planes in the Z direction with a depth of ± 10 µm. Serial pictures along the Z-axis were combined to create a stacked XY image that was further analyzed using ImageJ 1.47v.

Transendothelial resistance measurements

HUVECs were transfected with CMTM4 siRNA or adenovirus 24 hours prior seeding on a 0.1% gelatin permeable filter insert (0.4 μm pore, Falcon). Before the experiment, the resistance (R_{blank}) was measured by placing unseeded inserts in an Endohm-SNAP chamber filled with 5 ml of EGM-2 medium (World Precision Instruments, Berlin). The chamber was coupled to an EVOMX resistance meter (World Precision Instruments, Berlin). The trans-endothelial electrical resistance (TEER) was measured daily to monitor resistance buildup during growth towards full confluence. At day 2, confluent monolayers were treated with 1U/ml thrombin for 20 minutes during which the TEER was measured every 5 minutes. After 20 minutes, the thrombin solution was washed away and replaced with normal medium. TEER was measured every 15 minutes during the restoration phase for 2 hours.

Statistical analysis

The statistical analyses were performed using Graphpad Prism version 7.02. To test if values came from a Gaussian distribution, the D'Agostino-Pearson omnibus or Shapiro-Wilk normality test were used. The unpaired t-test and the ordinary one-way ANOVA test were used if the values were normally distributed. In case the values did not pass the normality test, either the Mann-Whitney test or Kruskal-Wallis were used as non-parametric tests. $P \leq 0.05$ was accepted as statistically significant. Values are shown as mean ± SEM.

Results

CMTM4 expression is essential for vascular growth in an in vitro 3D angiogenesis assay

The function of CMTM4 was investigated *in vitro* using siRNA mediated silencing in HUVECs. Both qPCR and Western blot analysis confirmed efficient silencing of CMTM4 in cells transfected with two different siRNA sets specific for CMTM4 (siCMTM4 set 1 and set 2), compared to untreated cells (control) and cells transfected with a pool of non-targeting siRNA sequences (siSHAM) (Fig. 1a-b). The mRNA levels of the other CMTM family members were not significantly downregulated by both CMTM4 targeting siRNA sets when comparing siCMTM4 versus siSHAM, indicating that the siRNA mediated silencing was specific for CMTM4 (Fig. 1c).

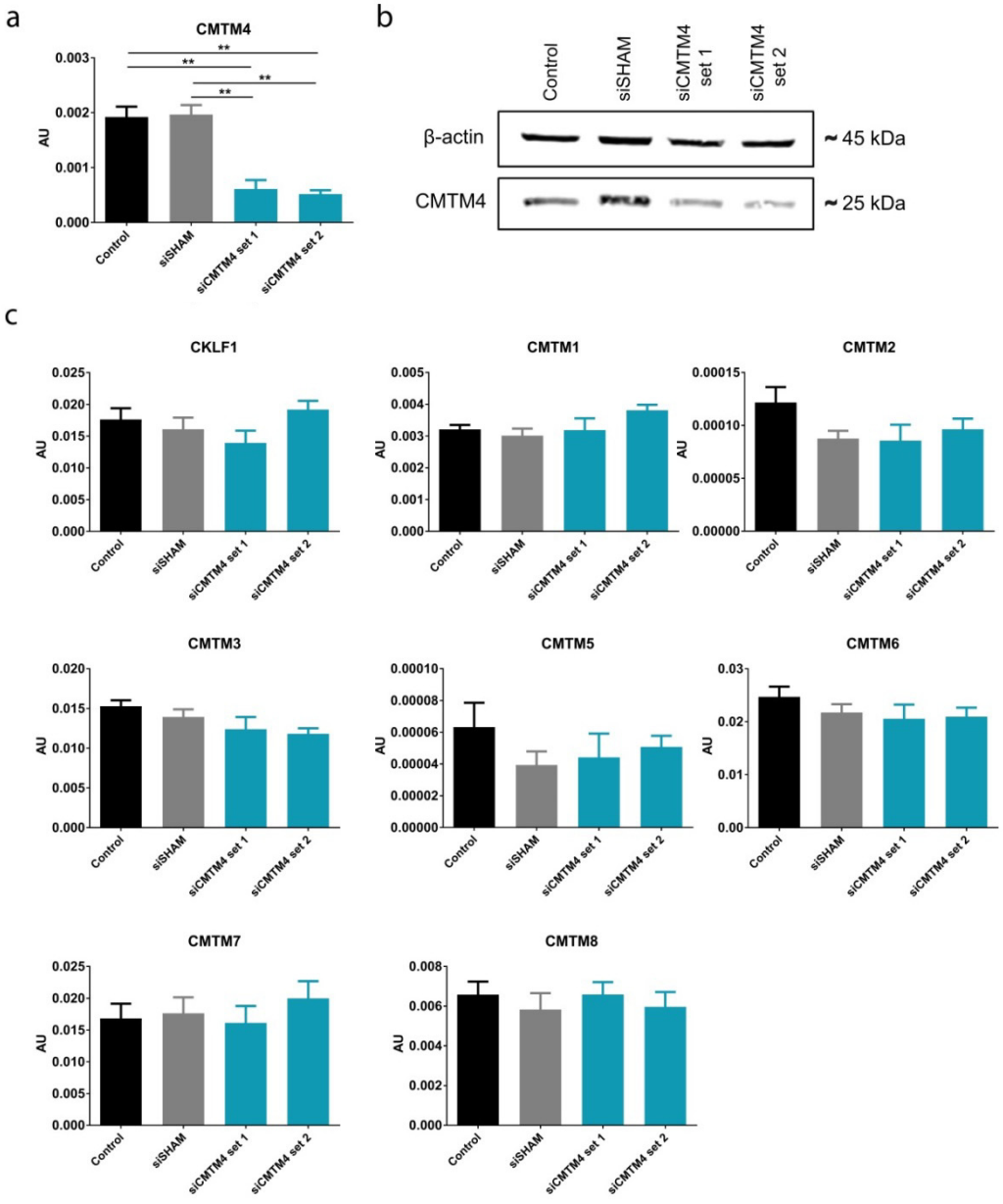

Fig 1. CMTM4-targeting siRNA induced significant and specific silencing of CMTM4 expression

a Gene expression levels of CMTM4 in HUVECs transfected with CMTM4-targeting siRNA (siCMTM4), non-targeting siRNA (siSHAM) and in non-transfected HUVECs (control). **b** Representative Western blot of CMTM4 and β-actin protein levels in siCMTM4, siSHAM and control HUVECs. Shown is a representative blot of 3 blots. **c** Gene expression levels of CMTM family members in siCMTM4, siSHAM and control HUVECs. For **a** and **c**, gene expression levels were normalized to β-actin (AU); values are mean ± SEM, **P<0.01; N≥8 qPCRs.

Next, the angiogenic potential of these CMTM4-silenced HUVECs was assessed *in vitro* in a 3D angiogenesis assay developed for studying the formation of lumenized micro-capillary structures [22]. In this assay, GFP-expressing HUVECs and dsRED-expressing pericytes directly interact in a collagen type I matrix. After one day of co-culture, EC sprouting and tubule formation can be observed and these neovascular structures are stabilized by perivascular recruitment of pericytes. After 5 days, micro-capillaries with distinct luminal areas and pericyte coverage can be observed. Imaging and quantification of these vascular structures was conducted at day 2 and 5. This assay has been well validated in previous studies [23-25]. Endothelial silencing of CMTM4 severely impaired the formation of neovascular structures in the 3D angiogenesis assay when compared to control and siSHAM (Fig. 2a). Quantification revealed a significant reduction in the number of junctions, the number of tubules and the total tubule length of HUVECs after both 2 and 5 days of coculture (Fig. 2b). In contrast, CMTM4 silencing in pericytes did not affect tubule formation at 2 or 5 days of coculture (Supp. Fig. 1a-d).

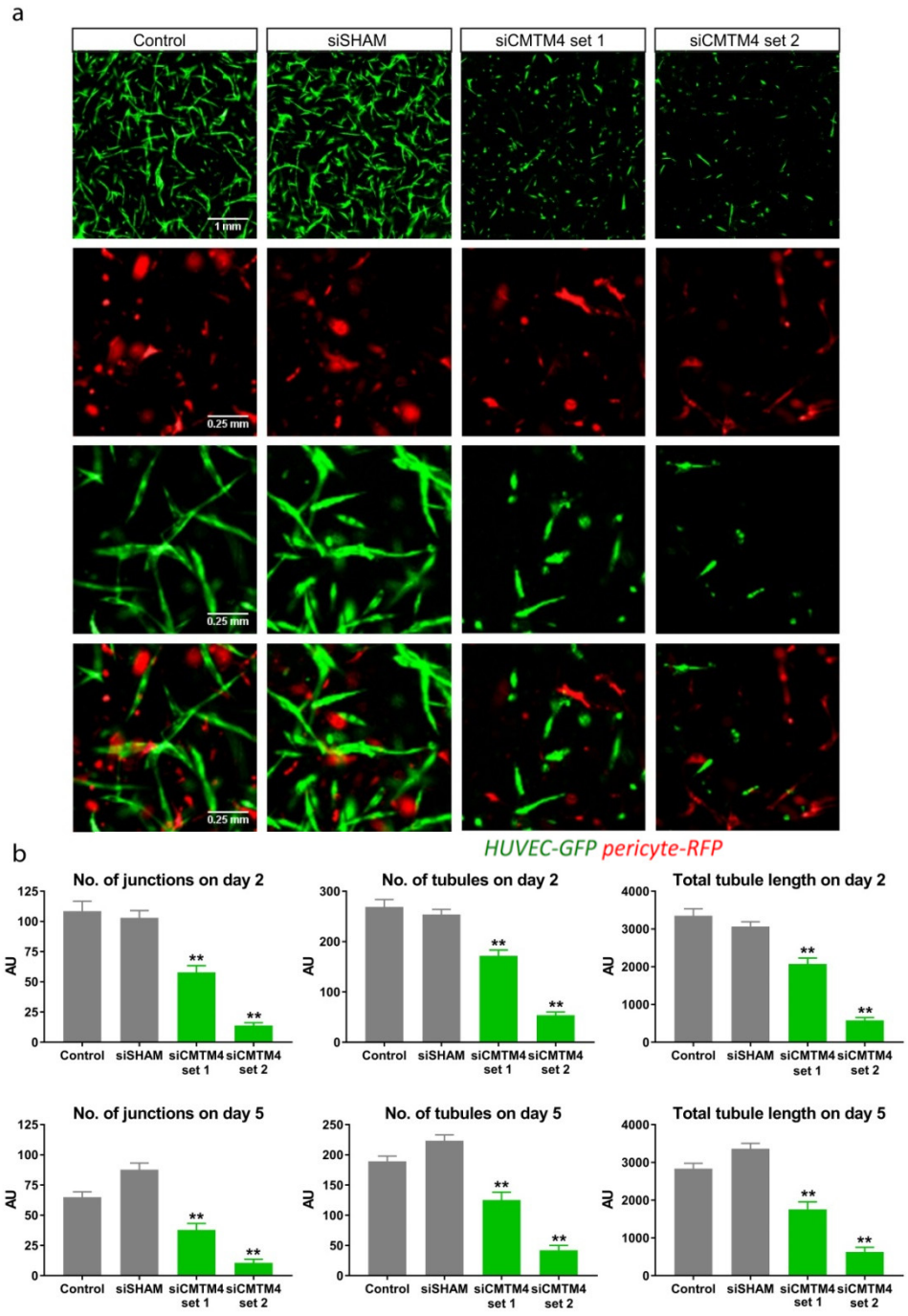

Fig 2. CMTM4 silencing is essential for vascular growth *in vitro*

a Representative immunofluorescent images taken at 2x magnification (upper row) and zoomed-in images (three lower rows) of GFP-labelled HUVECs (green) and dsRED-labelled pericytes (red) cultured for 5 days in a 3D collagen matrix, in which the HUVECs-GFP were transfected with either CMTM4-targeting siRNA (siCMTM4) or non-targeting siRNA (siSHAM) or not transfected (control). Scale bar represents 1 mm for the upper row and 0.25 mm for the three lower rows. **b** Quantification of the number of junctions, number of tubules and total tubule length of siCMTM4, siSHAM and control HUVECs at day 2 and 5 of co-culture. Values are mean ± SEM, **P<0.01 compared to all other conditions; N≥6 co-cultures, ± 7 images each.

Silencing of CMTM4 in developing zebrafish larvae inhibits intersomitic vessel growth

In order to evaluate CMTM4 function during *in vivo* angiogenesis, the zebrafish orthologue of the gene was silenced in developing larvae of the transgenic zebrafish line Tg(fli1:eGFP)$_{y1}$ by morpholino knockdown. CMTM4 was highly conserved in the zebrafish genome and two morpholinos were designed to target the CMTM4 zebrafish orthologue with knockdown based on the splice modification principle of the pre-mRNA target. Injection with a morpholino construct that targeted the splice site located on CMTM4 intron 2-exon 3 (i2-e3) affected intersomitic vessel (ISV) formation versus uninjected larvae at 24 hours post-fertilization (Fig. 3a). Phenotype quantification showed in the 3ng i2-e3 morpholino group that 36% of larvae displayed defects in ISV formation versus 0% in the control group. Injection with 6ng i2-e3 increased the number of larvae with affected ISVs to 48% (Fig. 3b). In line with these findings, injection of the second morpholino construct that targeted the splice site on CMTM4 intron 1-exon 2 (i1-e2) affected ISV formation in 56% of the larvae in the i1-e2 group versus 0% in the control population (Supp. Fig. 2a, b). These data clearly demonstrate a negative effect of CMTM4 silencing on angiogenesis in developing zebrafish larvae *in vivo.*

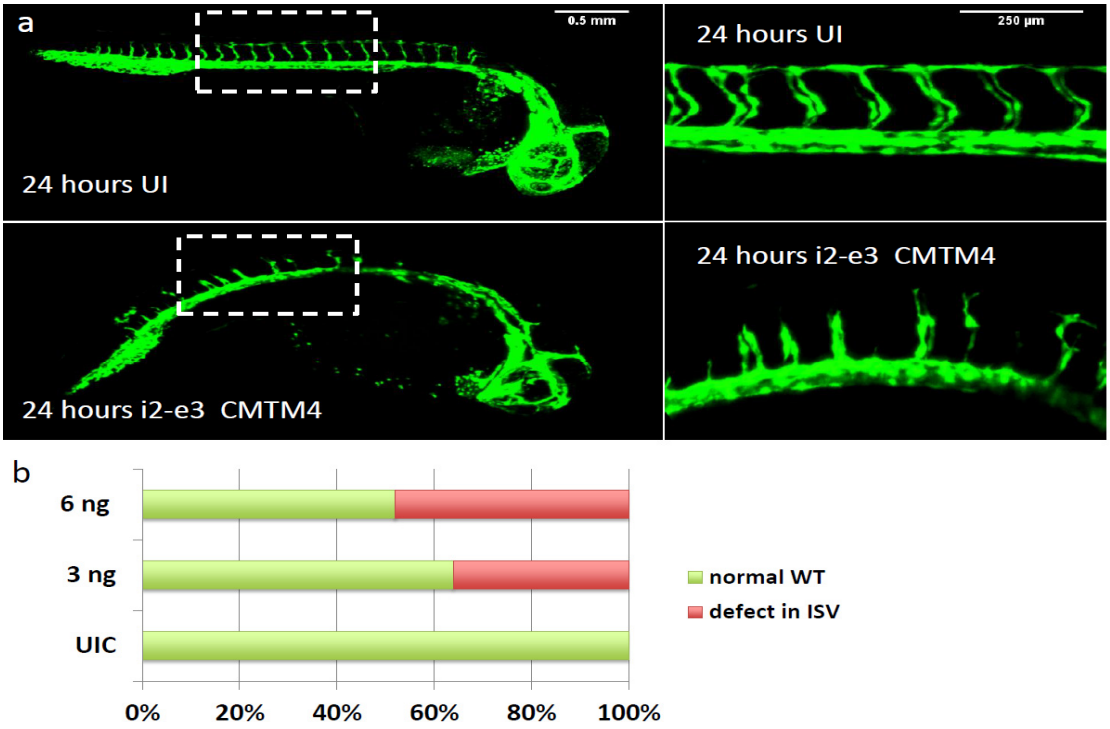

Fig 3. Morpholino silencing of CMTM4 in developing zebrafish larvae induced defects in intersomitic vessels. a Tg(fli1:eGFP)$_{y1}$ larvae at 24 hours post fertilization, anterior to the right, lateral view. Defects in intersomitic vessel (ISV) formation was observed in the trunk region in specimens injected with morpholinos targeting the splice site of i2-e3 of CMTM4 (indicated as i2-e3 CMTM4) compared with uninjected controls (UIC). The vasculature is highlighted by eGFP (green). Left hand panels show 2x magnification images with 0.5 mm scale bar, right hand panels show 10x images with 0.25 mm scale bar. **b** Quantification of ISV defect phenotype versus wildtype (WT) phenotype in i2-e3 injected group at different doses versus UIC. Data represents percentage of counted larvae (~100 per group).

Effect of CMTM4 on cell cycle progression, migration and proliferation

Previous studies in HeLa and clear cell renal cell carcinoma cells imply that CMTM4 functions as a tumor suppressive gene, with expression of CMTM4 leading to cell migration and inhibition of cell proliferation via G2/M phase accumulation [14,15]. We investigated the effects of CMTM4 silencing in HUVECs on these parameters. CMTM4 silencing using either siRNA set 1 or 2 did not affect cell proliferation as shown by comparison with siSHAM treated and non-treated control groups based on cell count and PI analysis of the G0/G1-phase and G2 phase in fixed cells (Supp. Fig. 3a, b). Migration capacity was also assessed by scratch assay and showed a significant decrease in response to CMTM4 silencing by set 2, but not by set 1, in HUVECs compared to siSHAM treated or non-treated controls after 4 and 8 hours of migration (Supp. Fig. 3c-e).

Next, we investigated the effects of CMTM4 overexpression on the same parameters. HUVECs were transfected with a recombinant adenovirus that encodes for human CMTM4 cDNA (adCMTM4). qPCR analysis validated significant transgenic expression of CMTM4 in HUVECs compared to HUVECs transfected with sham virus (adSHAM) (Fig. 4a). In contrast with CMTM4 silencing, cell count and cell cycle progression was decreased in adCMTM4 HUVECs versus adSHAM or non-transfected groups, as shown by reduced cell count and an increase of cells in G0/G1 versus G2 phase (Fig. 4b, c). However, overexpression of CMTM4 did not affect migration capacity of HUVECs (Fig. 4d-f). These findings indicate that increased levels of CMTM4 limit cell proliferation, but do not affect cell migration.

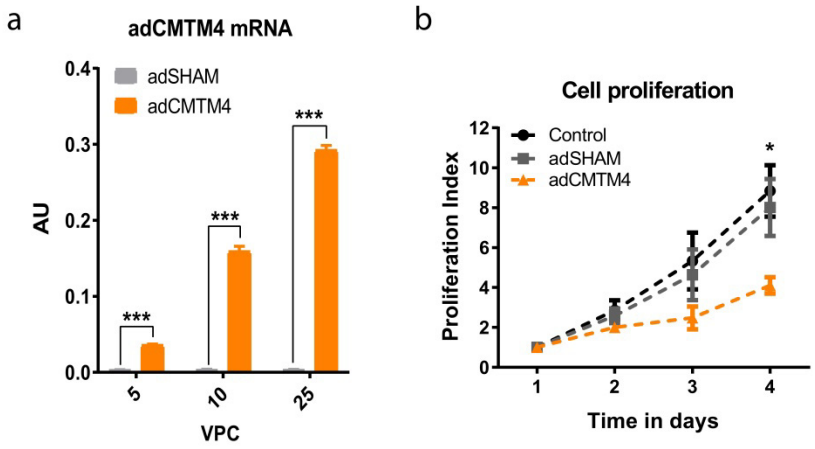

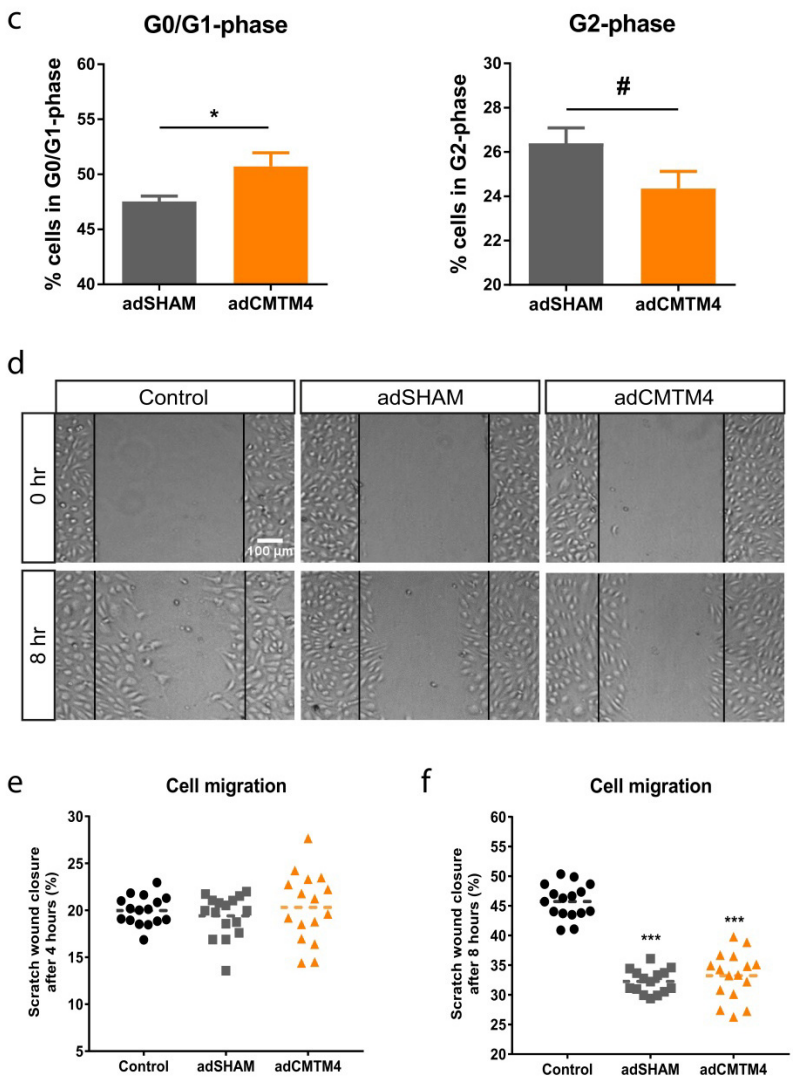

Fig 4. CMTM4 overexpression limited endothelial cell proliferation, but did not affect cell migration

a Quantitative polymerase chain reaction (qPCR) of human CMTM4 expression in HUVECs transfected with different (5, 10, 25) virus particles per cell (VPC) of adenovirus containing an expression vector for CMTM4 cDNA (adCMTM4) or with sham virus containing an empty expression vector (adSHAM). Shown are target gene/house-keeping gene (β actin) ratio (AU). Mean ± SEM, ***P<0.001 in comparisons between adSHAM and adCMTM4 group of equal VPC; N=4 qPCRs. **b** The number of cells counted at day of seeding (day 1), and at day 2, 3 and 4 of cell proliferation in adCMTM4 HUVECs compared with adSHAM and non-transfected controls. Shown is mean ± SEM, N=6; *P<0.05. **c** Bar graphs showing the % of G0/G1 and G2 phase cells at day 2 after transfection in adCMTM4 versus adSHAM HUVECs and non-transfected controls. Shown is mean ± SEM, *P<0.05, #P<0.10; N=4. **d** Representative brightfield microscope images (4x magnification) of a scratch migration assay after 8 hours of migration of adCMTM4 HUVECs compared to adSHAM and non-treated controls. Scale bar represents 100 µm. Bar graphs of the quantified results of the scratch migration assay showing the % area within the scratched region covered by adCMTM4 HUVECs compared to adSHAM and non-treated controls after 4 hours (**e**) and 8 hours (**f**). Shown is mean, ***P<0.001; N=2, 8 wells each.

CMTM4 colocalizes with endocytic vesicle structures and VE-cadherin in adherens junctions

In a recent study, we revealed that CMTM3 is mainly localized in the cytosol, where it is involved in regulating the early endocytosis of the AJ protein VE-cadherin [19]. Therefore, we evaluated in this study the intracellular function of CMTM4 in ECs. Western blot analysis demonstrated that CMTM4 was mainly present in the soluble cytosolic fraction and not in the insoluble more actin enriched fraction of the HUVEC lysates (Fig. 5a). Similarly, VE-cadherin was mainly enriched in the soluble fraction (Fig. 5a).

Double immuno-fluorescent staining of CMTM4 with different markers of intracellular vesicular transport compartments showed limited colocalization with early endosome markers EEA1 and Clathrin (Fig. 5b-d). In contrast, examination of CMTM4 with markers of recycling vesicles showed significant colocalization between CMTM4 and Rab4, but not Rab11 (Fig. 5b, e, and f). Furthermore, colocalization between CMTM4 and Rab7, a marker for vesicles destined for the lysosome pathway, was also significantly increased compared to EEA1, clathrin, and Rab11 (Fig. 5b, g). These findings indicated that CMTM4 was colocalized in (Rab4 marked) recycling and (Rab7 marked) lysosome destined vesicles and may contribute to recycling and lysosome activity in the process of endocytosis. Further analysis of CMTM4 intracellular localization showed cytosolic and cell-cell junction localization of the protein. Dual immunostaining analysis demonstrated that the CMTM4 signal colocalized with VE-cadherin, both at the AJs and in cytosolic vesicle structures (Fig. 5b, h). Transgenic overexpression of CMTM4 in ECs appeared to alter the junctional pattern of VE-cadherin into plaque-like structures (Fig. 5i). Studies have shown that Junction-Associated-Intermittent-Lamellipodia (JAIL) structures appear at established endothelial junctions and induce an overlap with the plasma membrane of the neighboring cell, forming subsequent VE-cadherin plaques that, after retraction of JAIL, are incorporated into the junctions [26,27]. Overexpression of CMTM4 did not affect the total VE-cadherin+ area (Fig. 5j). Similarly, Western blot analysis of adCMTM4 or adSHAM transfected HUVECs showed no difference in total protein concentration of VE-cadherin (Fig. 5k).

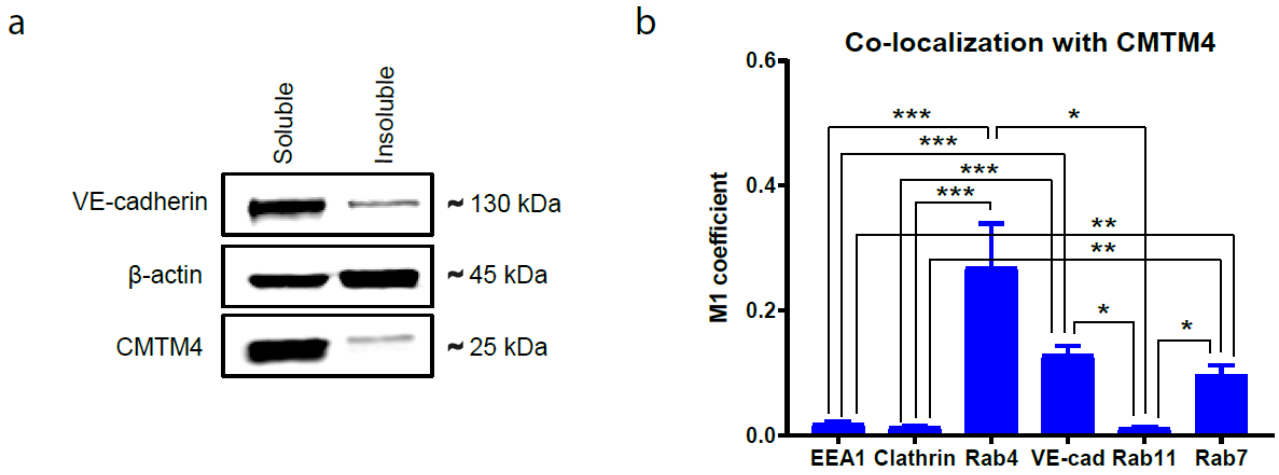

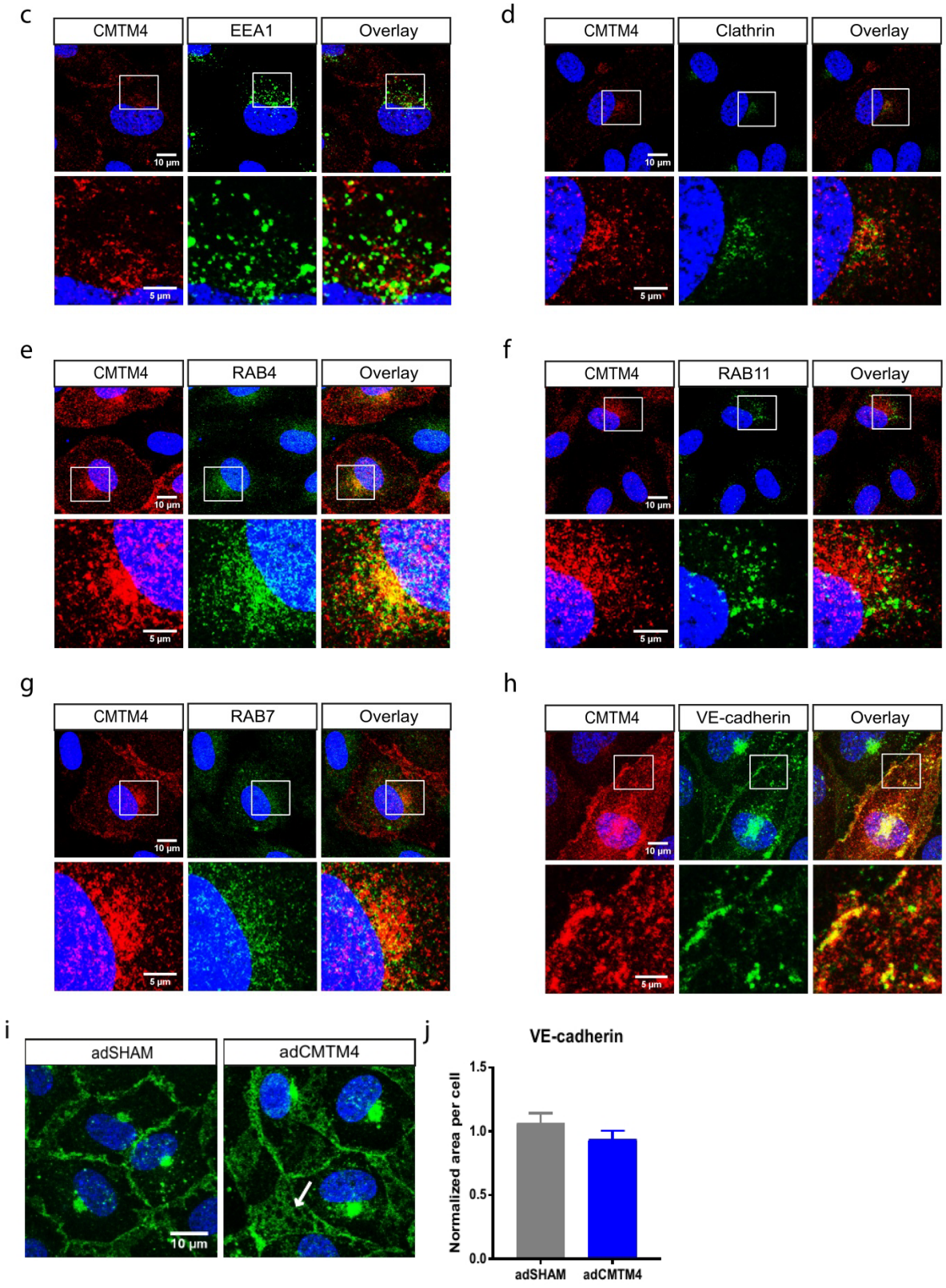
c
CMTM4
EEA1
Overlay
10 µm
5 µm
d
CMTM4
Clathrin
Overlay
10 µm
5 µm
e
CMTM4
RAB4
Overlay
10 µm
5 µm
f
CMTM4
RAB11
Overlay
10 µm
5 µm
g
CMTM4
RAB7
Overlay
10 µm
5 µm
h
CMTM4
VE-cadherin
Overlay
10 µm
5 µm
i
adSHAM
adCMTM4
10 µm
j
VE-cadherin
Normalized area per cell
1.5
1.0
0.5
0.0
adSHAM
adCMTM4

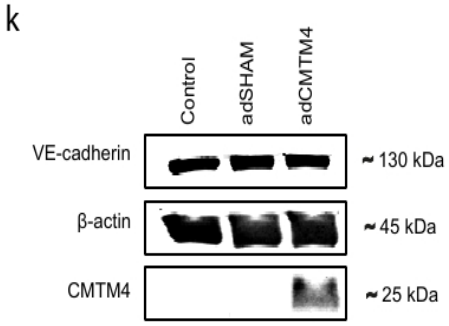

Fig 5. CMTM4 localizes with different vesicle compartments of the intracellular endocytosis pathway and VE-cadherin+ adherens junctions

a Representative Western blot of CMTM4, β-actin and VE-cadherin protein levels in the soluble and insoluble cell lysates fraction of HUVECs. **b** Quantification of colocalization of CMTM4 with VE-cadherin and endocytic compartment markers in confocal micrographs based on M1 coefficient. Mean ± SEM, *P<0.05, **P<0.01, ***P<0.001; N=3, 5 fluorescent images each. Representative 63x magnification (upper row) and zoomed-in (lower row) confocal microscope images of HUVECs transfected with adCMTM4 (VPC10), immunostained for CMTM4 (red) and EEA1 (green) (**c**) Clathrin (green) (**d**), Rab4 (green) (**e**), Rab11 (green) (**f**), Rab7 (green) (**g**) and VE-cadherin (green) (**h**). Colocalization of CMTM4 and endocytic compartment protein markers or VE-cadherin in overlay images is displayed in yellow. Scale bars represent 10 µm for the upper rows and 5 µm for the lower rows. **i** Representative immunofluorescence microscope images of VE-cadherin (green) in adSHAM and adCMTM4 HUVECs (VPC10). White arrow marks the altered VE-cadherin junctional pattern into a plaque-like structure. Scale bar represents 10 µm. **j** Quantification of total VE-cadherin+ area per cell in adSHAM or adCMTM4 transfected HUVECs (VPC10). Mean ± SEM; N=3, 5 fluorescent Z-stacks each. **k** Representative Western blot bands for total CMTM4, VE-cadherin and β-actin expression of adCMTM4 and adSHAM HUVECs (VPC5). Shown is a representative blot of 2 blots.

Quantification of EEA1, Clathrin, Rab4, Rab11, and Rab7 immunofluorescence signals showed that EEA1+, Rab4+ and Rab11+ vesicles, were significantly increased in adCMTM4 versus adSHAM-treated HUVECs and a similar trend was visible for Rab7+ vesicles. In contrast, the amount of Clathrin+ vesicles was not affected (Fig. 6a-e). These data indicate that CMTM4 enhances endocytosis processes in ECs.

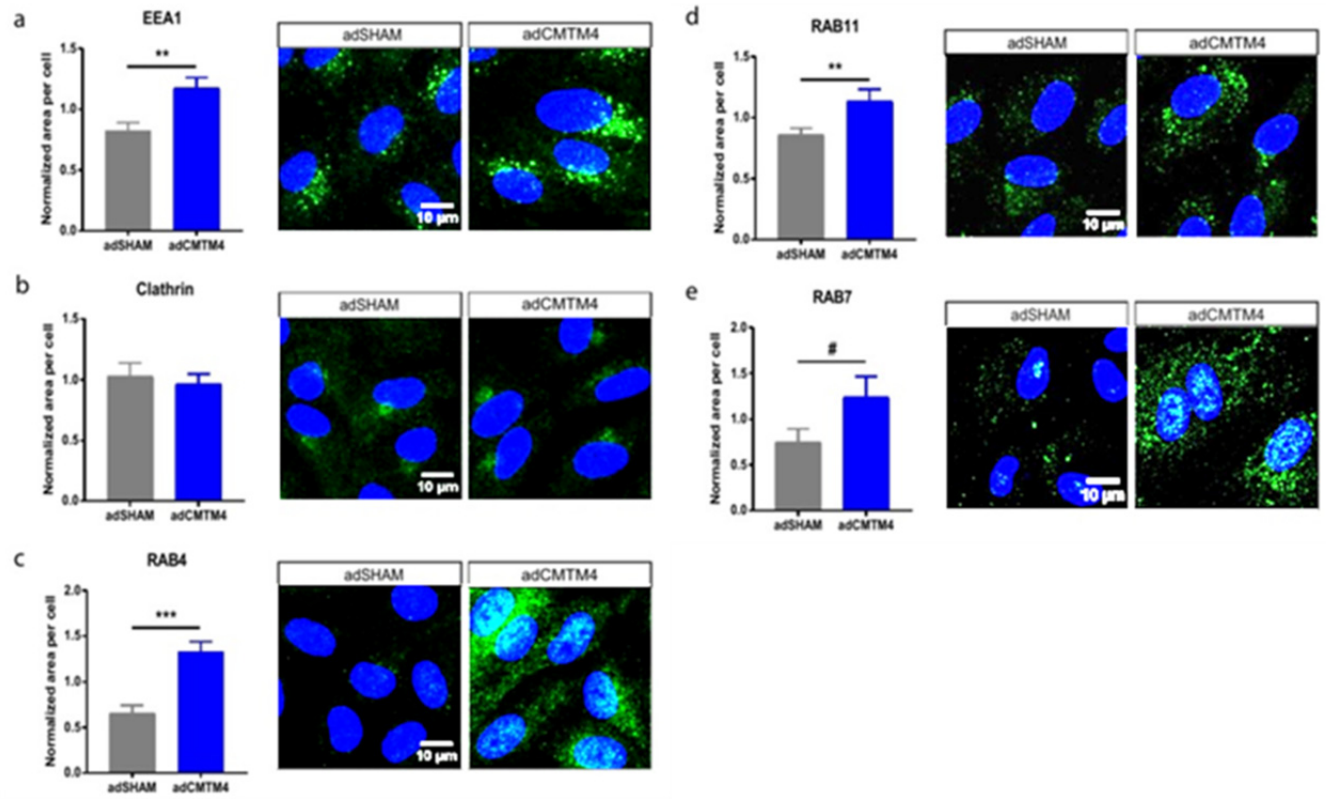

Fig 6. CMTM4 overexpression significantly upregulates the endothelial endocytic pathway
Quantification of area per cell in adCMTM4 and adSHAM transfected HUVECs (VPC10). Representative confocal micrographs (63x magnification) of HUVECs transfected with adCMTM4 and adSHAM (VPC10), immunostained (green) for EEA1 (**a**), Clathrin (**b**), Rab4 (**c**), Rab11 (**d**) and Rab7 (**e**). For all data displayed, mean ± SEM, #P<0.1, **P<0.01, ***P<0.001; N=3, 5 Z-stacks each; scale bars represent 10 µm.

CMTM4 regulates VE-cadherin endocytosis and promotes endothelial barrier function of endothelial adherens junctions

The putative role of CMTM4 in endocytosis processing of VE-cadherin was evaluated with an internalization assay, where confluent HUVECs transfected with adSHAM or adCMTM4 were exposed to a low temperature shock (1 hour at 4°C) followed by an 1 hour incubation at 37°C. Assessment of VE-cadherin in relation to the actin cytoskeleton showed a significant increase in colocalization in adCMTM4 treated versus adSHAM confluent HUVEC monolayers, as demonstrated by an increase in Pearson correlation coefficient (Fig. 7a-b). This finding indicates that CMTM4 promotes VE-cadherin connections with the actin cytoskeleton that are vital for AJ stabilization.

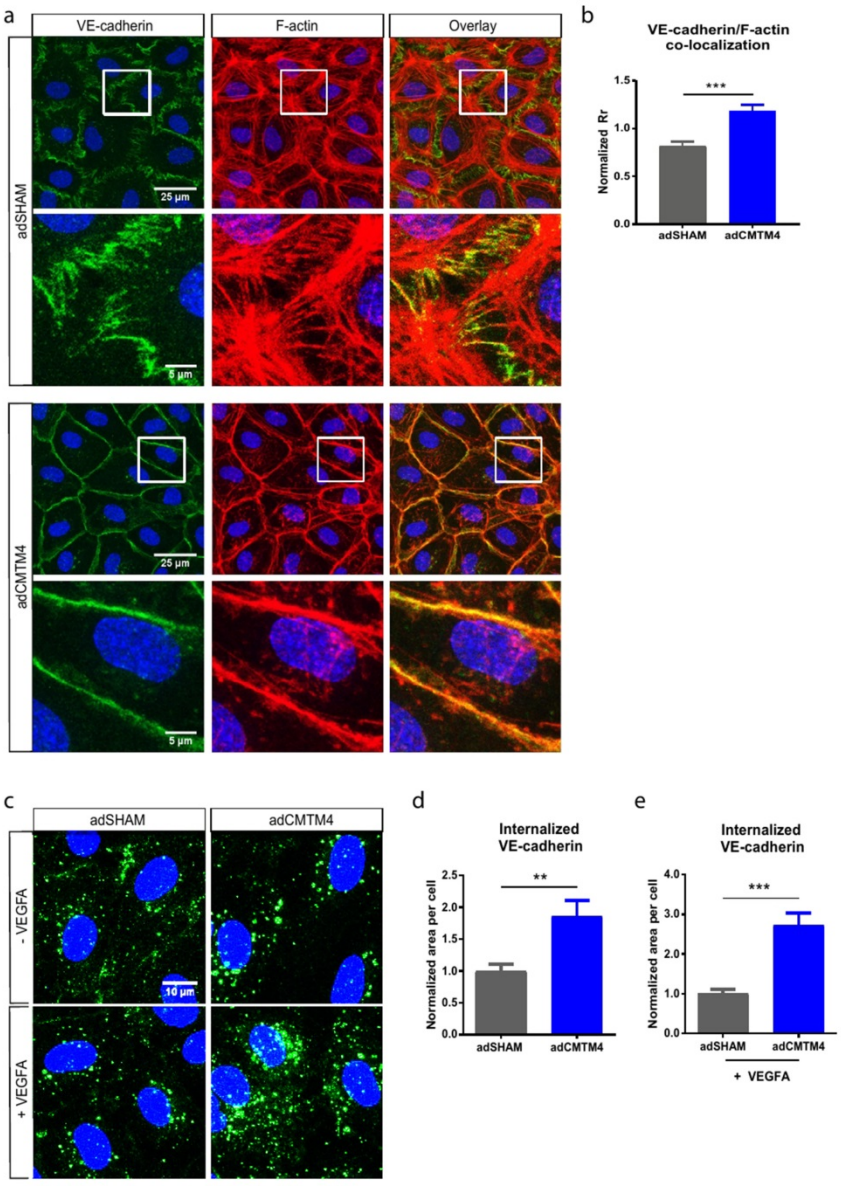
a
VE-cadherin
F-actin
Overlay
adSHAM
adCMTM4
25 µm
5 µm
b
VE-cadherin/F-actin
co-localization
Normalized Rr
***
adSHAM
adCMTM4
c
adSHAM
adCMTM4
- VEGFA
+ VEGFA
10 µm
d
Internalized
VE-cadherin
Normalized area per cell
**
adSHAM
adCMTM4
e
Internalized
VE-cadherin
Normalized area per cell
***
adSHAM
adCMTM4
+ VEGFA

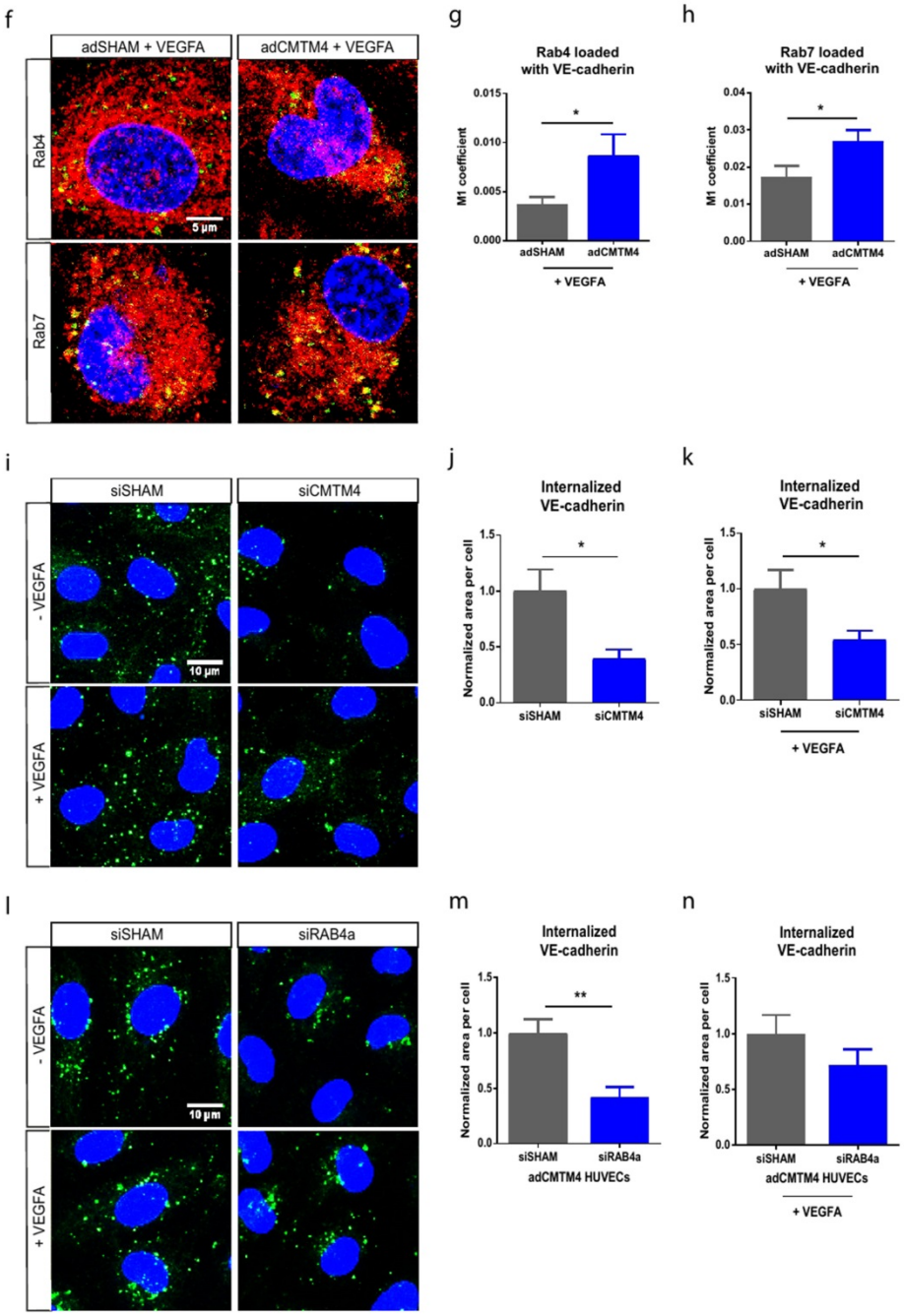

Fig 7. CMTM4 upregulates endocytosis and subsequent recycling of VE-cadherin

a Representative 63x magnification (upper row) and zoomed-in (lower row) confocal microscope images of confluent HUVEC cultures that were immunostained for F-actin (red) and VE-cadherin (green) in adSHAM and adCMTM4 transfected cells (VPC10) that were exposed to low temperature shock (1 hour at 4°C) followed by 1 hour incubation at 37°C. Adherens junctions were quicker restored in adCMTM4 condition versus adSHAM conditions (zigzagged VE-cadherin signal in adSHAM versus linear VE-cadherin junctions). Colocalization signal in overlay is in yellow. Scale bars represent 25 µm for the upper rows and 5 µm for the lower rows. **b** Quantification of the colocalization signal between VE-cadherin and F-actin in confocal micrographs based on normalized Pearson correlation coefficient (Rr). Mean ± SEM, ***P<0.001 versus adSHAM; N=4, 5 Z-stacks each. **c** Representative confocal micrographs (63x

magnification) of confluent adSHAM and adCMTM4 cultures (VPC10) labeled with VE-cadherin antibodies at 4°C to track VE-cadherin movement, followed by 37°C incubation for 1 hour with and without VEGFA stimulation. Surface bound VE-cadherin antibodies were removed by an acid-wash, before proceeding with immunostaining for visualization of internalized VE-cadherin (green). Scale bar represents 10 µm. Quantification of internalized VE-cadherin area per cell in adSHAM and adCMTM4 HUVECs without VEGFA (**d**) and with VEGFA (**e**) stimulation. Mean ± SEM, **P<0.01, ***P0.001 versus adSHAM; N=4, 5 Z-stacks each. **7f** Representative zoomed-in confocal micrographs (63x magnification) of confluent adSHAM and adCMTM4 cultures (VPC10) labeled with VE-cadherin antibodies at 4°C to track VE-cadherin movement, followed by 37°C incubation for 1 hour with and without VEGFA stimulation. Surface bound VE-cadherin antibodies were removed by an acid-wash, before proceeding with immunostaining for visualization of internalized VE-cadherin (green) and either Rab4 or Rab7 (red). Scale bar represents 5 µm. Quantification of colocalization of either Rab4 (**g**) or Rab7 (**h**) with VE-cadherin in confocal micrographs based on M1 coefficient. Mean ± SEM, *P<0.05; N=2, 5 fluorescent images each. **i** Representative confocal micrographs (63x magnification) of confluent siSHAM and siCMTM4 cultures labeled with VE-cadherin antibodies at 4°C to track VE-cadherin movement, followed by 37°C incubation for 1 hour with and without VEGFA stimulation. Surface bound VE-cadherin antibodies were removed by an acid-wash, before proceeding with immunostaining for visualization of internalized VE-cadherin (green). Scale bar represents 10 µm. Quantification of internalized VE-cadherin area per cell in siSHAM and siCMTM4 HUVECs without VEGFA (**j**) and with VEGFA (**h**) stimulation. Mean ± SEM, *P<0.05 versus adSHAM; N=2, 5 Z-stacks each. **l** Representative confocal micrographs (63x magnification) of confluent siSHAM HUVECs and HUVECs transfected with Rab4a-targeting siRNA (siRAB4a) labeled with VE-cadherin antibodies at 4°C to track VE-cadherin movement, followed by 37°C incubation for 1 hour with and without VEGFA stimulation. Surface bound VE-cadherin antibodies were removed by an acid-wash, before proceeding with immunostaining for visualization of internalized VE-cadherin (green). Scale bar represents 10 µm. Quantification of internalized VE-cadherin area per cell in siSHAM and siRAB4a HUVECs without VEGFA (**m**) and with VEGFA (**n**) stimulation. Mean ± SEM, **P<0.01 versus adSHAM; N=2, 7 Z-stacks each.

Next, the role of CMTM4 in VE-cadherin endocytosis was assessed. For this, confluent adSHAM or adCMTM4 HUVECs were incubated with VE-cadherin antibody at 4°C before an acid wash treatment to remove all extracellular VE-cadherin signal. Subsequent analysis following 1 hour incubation at 37°C without and with VEGFA stimulation showed a significant increase of internalized VE-cadherin in adCMTM4 versus adSHAM conditions (Fig. 7c-e). The internalized VE-cadherin upon VEGF stimulation is present in both Rab4+ and Rab7+ vesicles, with significantly more Rab4+ and Rab7+ vesicles loaded with VE-cadherin in adCMTM4 HUVECs when compared to adSHAM HUVECs (Fig. 7f-h). In line with these findings, siRNA mediated knockdown of CMTM4 significantly decreased the signal of internalized VE-cadherin in siCMTM4 treated HUVECs with and without VEGFA stimulation (Fig. 7i-k). This effect of CMTM4 is dependent on Rab4, since adCMTM4 HUVECs transfected with siRNA specific for Rab4a (siRAB4a) also show significantly less internalized VE-cadherin when compared to siSHAM HUVECs. The trend is still visible under VEGF stimulation (Fig. 7l-n and Supp. Fig. 4a).

Findings so far indicate that CMTM4 could regulate the bio-availability of VE-cadherin at cell-cell AJs, which implies that it could impact endothelial barrier function. We used transendothelial electric resistance (TEER) measurements to evaluate the response of HUVEC monolayers transfected with adSHAM or adCMTM4 to thrombin-induced junction disruption. Basal levels (before thrombin stimulation) of TEER were not affected by CMTM4 overexpression. However, the recovery of TEER post thrombin stimulation was significantly increased in adCMTM4 conditions compared to adSHAM (Fig. 8a-c). In line with these findings, basal TEER levels were similarly not affected by siRNA mediated silencing of CMTM4, but TEER recovery after thrombin removal was significantly decreased in siCMTM4 versus siSHAM conditions (Supp. Fig. 4 a, b).

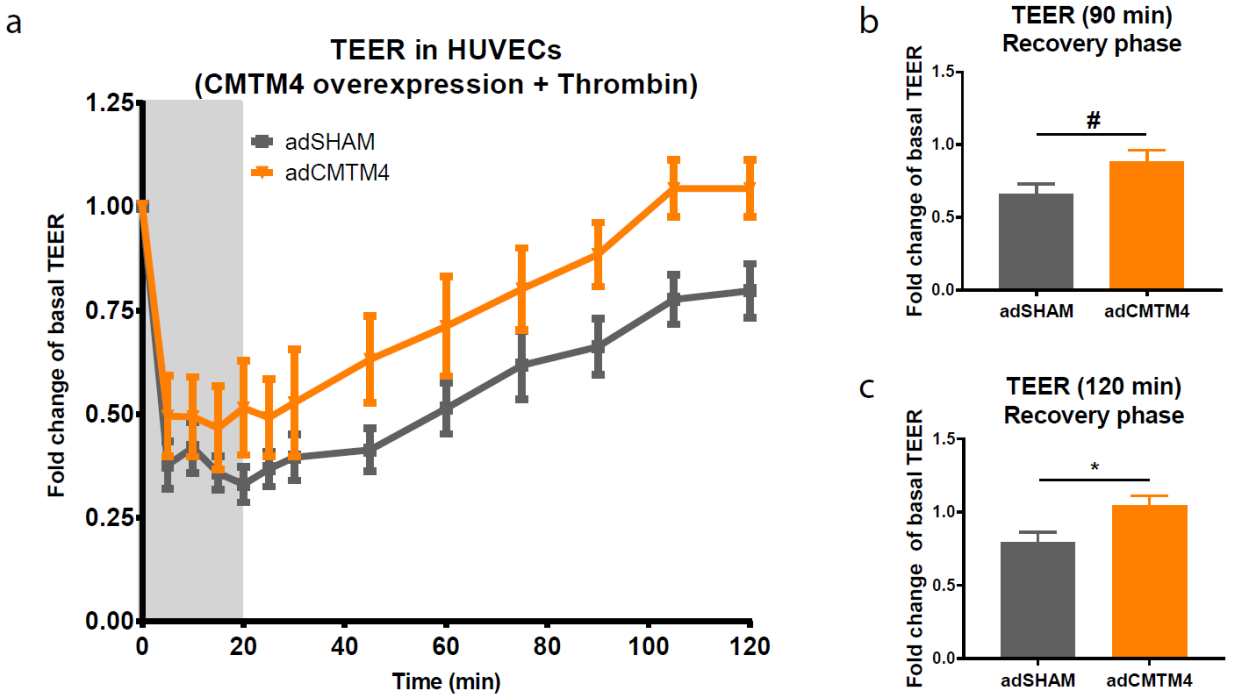

Fig 8. CMTM4 promotes restoration of endothelial electric resistance in thrombin-induced response
a Thrombin response (presented in fold change compared with basal resistance of nontransfected group: Y axes) of confluent HUVEC monolayers during (0–20 minutes) and after (20–120 minutes) thrombin (1 U/mL) stimulation in adCMTM4 and adSHAM conditions. At 0 minutes, thrombin was added and after 20 minutes thrombin was removed (gray area). Mean ± SEM. N≥4 per time series. Increase in resistance during recovery phase at 90 minutes (**b**) and 120 minutes (**c**) in adSHAM and adCMTM4 groups. Mean ± SEM, #P<0.10 versus adSHAM; N≥6.

Discussion

In this study, we investigated the angiogenic potential of CMTM4 and evaluated in which molecular pathways CMTM4 is involved in ECs. The most important findings of this study are: 1) CMTM4 silencing impairs vascular growth in an *in vitro* 3D angiogenesis assay. 2) Silencing of CMTM4 in developing zebrafish larvae inhibits intersomitic vessel growth. 3) Intracellular staining reveals that CMTM4 colocalizes with Rab4 and Rab7 positive vesicles, and with both membrane-bound and internalized VE-cadherin. 5) CMTM4 enhances the endothelial endocytic pathway, in particular the Rab4 recycling pathway. 6) CMTM4 also enhances VE-cadherin internalization and increases endothelial barrier function recovery.

Several previous studies have revealed that CMTM family members can prevent growth and invasion of different cancer cell types [11-18]. CMTM4 has been reported to be frequently downregulated in clear cell renal cell carcinoma where it functions as a tumor suppressor. Thus, restoration of CMTM4 suppressed the tumorigenicity of these cancer cells, whereas knockdown of CMTM4 led to enhanced tumor growth [14]. Furthermore, overexpression of CMTM4 inhibits HeLa cell growth via G2/M phase accumulation [15]. In a recent study, we demonstrated that CMTM3 has a specialized function in ECs, where it is involved in the regulation of early endocytosis of VE-cadherin during vascular growth [19]. However, the putative function of CMTM4 in endothelial endocytosis and the contribution of CMTM4 to the regulation of vascular permeability have not been elucidated to date.

In the present study, we demonstrated that CMTM4 plays an important role in angiogenesis. Loss of CMTM4, as shown *in vitro* with a 3D vascular assay and *in vivo* with zebrafish larvae, results in a significant reduction of vascular sprouting. ECs can actively modulate their junctional adhesive strength by regulating the amount of bioavailable VE-cadherin on the cell membrane. A reduction in membrane-bound VE-cadherin will result in microvascular destabilization that is required for EC migration and vascular sprouting. Vascular sprouting from pre-existing vessels is mediated by VEGFA by stimulating the endocytosis of VE-cadherin [9]. Similar to CMTM3, we have shown that the angiogenic capacity of CMTM4 is associated with the regulation of cell-surface VE-cadherin. CMTM4 overexpression promotes the internalization of VE-cadherin, both at basal levels and in response to VEGFA stimulation. Vice versa, CMTM4 knockdown inhibits VE-cadherin internalization. In line with our findings, it has been shown that a reduction of VE-cadherin both *in vitro* and *in vivo* increases vascular permeability and stimulates vascular sprouting [4,28].

After these initial stages of neovessel formation, VE-cadherin is eventually required for the formation of a stable vasculature by preventing disassembly. This is demonstrated in VE-cadherin-deficient mice, who suffer from severe vascular defects, resulting in death at mid-gestation [5,6]. In line with those observations, our data indicate that CMTM4 overexpression promotes VE-cadherin connections with the actin cytoskeleton that are vital for AJs stabilization. The VE-cadherin/catenin complex interacts with actin filaments to ensure adequate junction adhesion and barrier function. Usually, the boundaries between adjacent ECs

display a stable linear morphology and are regulated by cortical F-actin. However, endothelial AJs are highly dynamic and reorganize continually in response to external stimuli [27]. These linear cell-cell junctions can convert into dynamic discontinuous cell-cell junctions, characterized by the appearance of stress fibers and zigzagged junctions where VE-cadherin aligns with the end of these stress fibers. Discontinuous junctions are characteristic for an activated and permeable endothelium [29]. Our data indicate that AJs are quicker restored in adCMTM4 HUVECs after a cold stimulus, showing a stable resting condition pattern with linear VE-cadherin junctions that colocalize with the cortical F-actin belt, when compared to sham treated cells. adSHAM HUVECs appear to be at a different stage of cell-cell junction remodeling in response to the cold stimulus, showing a zigzagged VE-cadherin pattern and stress fibers. This discontinuous pattern seen in adSHAM HUVECs will contribute to a rapid increase in endothelial permeability and subsequently a longer recovery phase. In concordance, TEER measurements revealed a fast recovery after thrombin induced endothelial junction disruption in ECs with overexpression of CMTM4 when compared to sham treated cells, whereas knock-down of CMTM4 resulted in a lower recovery rate. Taken together, these results are consistent with the concept that CMTM4 is responsible for a fast turn-over of VE-cadherin from the plasma membrane and back, thereby regulating the junctional adhesive strength of ECs and hence the endothelial barrier function.

The turnover of cell surface VE-cadherin involves endocytic trafficking pathways, in which VE-cadherin is transferred into the cytosol in clathrin-coated vesicles and is further sorted for recycling or lysosomal trafficking routes, among others [7]. Cargo proteins can be recycled back to the plasma membrane through two distinct recycling pathways: The Rab4-mediated rapid recycling pathway and the Rab11-mediated slow endosome pathway [30]. Rapid recycling occurs directly from the early endosomal compartment, whereas the slow recycling route involves protein cargo trafficking from either early endosomes or the trans-Golgi network through the pericentriolar recycling endosomal compartment, before returning to the cell surface [31,32].

In the present study, we demonstrated that CMTM4 strongly colocalized with Rab4 and VE-cadherin, suggesting that CMTM4 is involved in regulating the rapid recycling of VE-cadherin back to the plasma membrane at AJs. Furthermore, overexpression of CMTM4 significantly increased Rab4+ vesicles in the cytosol, but did not increase the total protein amount of VE-cadherin, indicating that CMTM4 regulates the localization, but not the synthesis or degradation of VE-cadherin. It has been shown that overexpression of Rab4 increases the recycling of various receptors back to the cell surface. For example, Rab4 overexpression in CHO (Chinese Hamster Ovary) cells raised the number of transferrin receptors on the cell surface from 20% to 80% [33]. Recycling and activation of the β-Adrenergic receptor was also enhanced by overexpression of Rab4 in cardiac myocytes [34]. Furthermore, Rab4 activation increased the expression of VE-cadherin at the cell surface of lung microvascular endothelial cells (LMVECs), whereas Rab4 inhibition reduced VE-cadherin levels, thereby increasing vascular permeability [35]. More specifically, Rab4 activation enhanced EC migration, adhesion, and tube formation [36].

Besides Rab4, CMTM4 overexpression also significantly enhances Rab11+ and EEA1+ vesicles in the cytosol. EEA1 colocalizes exclusively to early endosomes, from which cargo is further sorted into trafficking routes. Silencing of Rab11a in LMVECs prevented VE-cadherin recycling and expression at the plasma membrane and blocked junctional reannealing after vascular inflammation [37]. CMTM4 does not colocalize with either EEA1 or Rab11, however, our findings do imply that the slow endosome pathway is activated as well in response to CMTM4 overexpression. Sorting endosomes leaving the recycling pathways are organized in different Rab domains, created through the recruitment of specific effector proteins [30]. These recycling endosomes are comprised of multiple combinations of Rab proteins, creating distinct endosome populations. Fast recycling is achieved by rapid sorting into Rab4+ domains within one endosome and recycling slows down once the cargo arrives to the pericentriolar membranes consisting mainly of Rab4+Rab11+ domains [30,38]. After Rab4 depletion, Rab11+ vesicles fuse with the plasma membrane to release the protein cargo [38]. Rab4 is not involved in exocytosis, but acts as a regulator in the formation of recycling vesicles from early endosomes, since removal of Rab4 strongly inhibits the formation of these vesicles [39]. Our findings imply that CMTM4 may function as an effector protein for creating Rab4+ domains in rapid and slow recycling endosome populations. CMTM4 may also serve as an adaptor protein for targeting and positioning VE-cadherin in these Rab4+ recycling vesicles, since our findings indicate that CMTM4 is also involved in VE-cadherin endocytosis and recycling.

Instead of recycling back to the plasma membrane, VE-cadherin can also be targeted to the lysosomal trafficking route for degradation. In our dataset, CMTM4 also localizes with Rab7, which is involved in the regulation of late endosomal trafficking to lysosomes [40]. Furthermore, overexpression of CMTM4 enhances Rab7+ vesicles in the cytosol, indicating that the lysosomal trafficking route is also activated in response to CMTM4 overexpression.

In a recent paper, we have shown that family-member CMTM3 regulated the endocytosis of VE-cadherin and localized with EEA1 and Clathrin, both markers of the early endocytic pathway, but not with Rab4 [19]. This generates the perception that the CMTM-family may play an important role in the endocytosis and recycling of VE-cadherin in ECs, with each member of the gene family having their own specialized function along the various endocytic trafficking routes. All 9 CMTM-family members contain a MARVEL domain, which is characterized by a four transmembrane-helix architecture, that has been associated with proteins involved in vesicle trafficking [41]. In line with this notion, overexpression of CMTM8 in tumor cell lines enhanced the endocytosis of the epidermal growth factor receptor (EGFR), whereas knockdown delayed endocytosis [42]. We addressed if there is a functional relationship between CMTM4 and family-member CMTM3 by performing an internalization assay with double CMTM4 + CMTM3 overexpression. Results demonstrate that there is a small trend visible that double CMTM4 + CMTM3 overexpression has an additive effect on single CMTM overexpression; however, this is not significant (Supp. Fig. 6a, b, and g). Both single and double CMTM overexpression internalize significantly more VE-cadherin when compared to sham treated cells, implying that CMTM3 and

CMTM4 do not interfere and abolish each other's effect. In addition, we tested if CMTM4 and CMTM3 regulate each other's localization by performing immunostainings for CMTM4 and CMTM3 with and without the presence of the other family member. In normal conditions, CMTM4 localizes both at the cytosol and cell border, whereas CMTM3 only localizes at the cytosol. In the knock down conditions, this pattern does not change, implying that CMTM4 and CMTM3 do not regulate each other's localization (Supp. Fig. 6 c-f and h). Further studies are required to assess if other family members are involved in the endocytosis regulation of ECs.

In conclusion, we have identified in this study for the first time to our knowledge, a regulatory function for CMTM4 in angiogenesis. CMTM4 plays an important role in the turnover of surface VE-cadherin, thereby mediating endothelial barrier function and controlling vascular sprouting. Further studies are needed to elucidate the exact mechanism by which CMTM4 regulates the endocytosis and trafficking of EC surface proteins. Increasing our understanding of the regulators of endothelial endocytosis could help find novel therapeutic targets for the treatment of various diseases associated with vascular leakage, to block vascular growth in tumors, or to overcome the problem of poor vascularization in tissue engineering.

References

1. Carmeliet P (2003) Angiogenesis in health and disease. Nature medicine 9 (6):653-660. doi:10.1038/nm0603-653
2. Wallez Y, Huber P (2008) Endothelial adherens and tight junctions in vascular homeostasis, inflammation and angiogenesis. Biochimica et biophysica acta 1778 (3):794-809. doi:10.1016/j.bbamem.2007.09.003
3. Vestweber D (2008) VE-cadherin: the major endothelial adhesion molecule controlling cellular junctions and blood vessel formation. Arteriosclerosis, thrombosis, and vascular biology 28 (2):223-232. doi:10.1161/atvbaha.107.158014
4. Corada M, Liao F, Lindgren M, Lampugnani MG, Breviario F, Frank R, Muller WA, Hicklin DJ, Bohlen P, Dejana E (2001) Monoclonal antibodies directed to different regions of vascular endothelial cadherin extracellular domain affect adhesion and clustering of the protein and modulate endothelial permeability. Blood 97 (6):1679-1684
5. Carmeliet P, Lampugnani MG, Moons L, Breviario F, Compernolle V, Bono F, Balconi G, Spagnuolo R, Oosthuyse B, Dewerchin M, Zanetti A, Angellilo A, Mattot V, Nuyens D, Lutgens E, Clotman F, de Ruiter MC, Gittenberger-de Groot A, Poelmann R, Lupu F, Herbert JM, Collen D, Dejana E (1999) Targeted deficiency or cytosolic truncation of the VE-cadherin gene in mice impairs VEGF-mediated endothelial survival and angiogenesis. Cell 98 (2):147-157
6. Gory-Faure S, Prandini MH, Pointu H, Roullot V, Pignot-Paintrand I, Vernet M, Huber P (1999) Role of vascular endothelial-cadherin in vascular morphogenesis. Development (Cambridge, England) 126 (10):2093-2102
7. Xiao K, Garner J, Buckley KM, Vincent PA, Chiasson CM, Dejana E, Faundez V, Kowalczyk AP (2005) p120-Catenin regulates clathrin-dependent endocytosis of VE-cadherin. Molecular biology of the cell 16 (11):5141-5151. doi:10.1091/mbc.E05-05-0440
8. Stenmark H (2009) Rab GTPases as coordinators of vesicle traffic. Nature reviews Molecular cell biology 10 (8):513-525. doi:10.1038/nrm2728
9. Gavard J, Gutkind JS (2006) VEGF controls endothelial-cell permeability by promoting the beta-arrestin-dependent endocytosis of VE-cadherin. Nature cell biology 8 (11):1223-1234. doi:10.1038/ncb1486
10. Han W, Ding P, Xu M, Wang L, Rui M, Shi S, Liu Y, Zheng Y, Chen Y, Yang T, Ma D (2003) Identification of eight genes encoding chemokine-like factor superfamily members 1-8 (CKLFSF1-8) by in silico cloning and experimental validation. Genomics 81 (6):609-617
11. Li Z, Xie J, Wu J, Li W, Nie L, Sun X, Tang A, Li X, Liu R, Mei H, Wang F, Wang Z, Gui Y, Cai Z (2014) CMTM3 inhibits human testicular cancer cell growth through inducing cell-cycle arrest and apoptosis. PloS one 9 (2):e88965. doi:10.1371/journal.pone.0088965
12. Wang Y, Li J, Cui Y, Li T, Ng KM, Geng H, Li H, Shu XS, Li H, Liu W, Luo B, Zhang Q, Mok TS, Zheng W, Qiu X, Srivastava G, Yu J, Sung JJ, Chan AT, Ma D, Tao Q, Han W (2009) CMTM3, located at the critical tumor suppressor locus 16q22.1, is silenced by CpG methylation in carcinomas and inhibits tumor cell growth through inducing apoptosis. Cancer research 69 (12):5194-5201. doi:10.1158
13. Hu F, Yuan W, Wang X, Sheng Z, Yuan Y, Qin C, He C, Xu T (2015) CMTM3 is reduced in prostate cancer and inhibits migration, invasion and growth of LNCaP cells. Clinical & translational oncology : official publication of the Federation of Spanish Oncology Societies and of the National Cancer Institute of Mexico 17 (8):632-639. doi:10.1007/s12094-015-1288-9

14. Li T, Cheng Y, Wang P, Wang W, Hu F, Mo X, Lv H, Xu T, Han W (2015) CMTM4 is frequently downregulated and functions as a tumour suppressor in clear cell renal cell carcinoma. Journal of experimental & clinical cancer research : CR 34:122. doi:10.1186/s13046-015-0236-4
15. Plate M, Li T, Wang Y, Mo X, Zhang Y, Ma D, Han W (2010) Identification and characterization of CMTM4, a novel gene with inhibitory effects on HeLa cell growth through Inducing G2/M phase accumulation. Molecules and cells 29 (4):355-361. doi:10.1007/s10059-010-0038-7
16. Xiao Y, Yuan Y, Zhang Y, Li J, Liu Z, Zhang X, Sheng Z, Xu T, Wang X (2015) CMTM5 is reduced in prostate cancer and inhibits cancer cell growth in vitro and in vivo. Clinical & translational oncology : official publication of the Federation of Spanish Oncology Societies and of the National Cancer Institute of Mexico 17 (6):431-437. doi:10.1007/s12094-014-1253-z
17. Li H, Li J, Su Y, Fan Y, Guo X, Li L, Su X, Rong R, Ying J, Mo X, Liu K, Zhang Z, Yang F, Jiang G, Wang J, Zhang Y, Ma D, Tao Q, Han W (2014) A novel 3p22.3 gene CMTM7 represses oncogenic EGFR signaling and inhibits cancer cell growth. Oncogene 33 (24):3109-3118. doi:10.1038/onc.2013.282
18. Gao D, Hu H, Wang Y, Yu W, Zhou J, Wang X, Wang W, Zhou C, Xu K (2015) CMTM8 inhibits the carcinogenesis and progression of bladder cancer. Oncology reports 34 (6):2853-2863. doi:10.3892/or.2015.4310
19. Chrifi I, Louzao-Martinez L, Brandt M, van Dijk CGM, Burgisser P, Zhu C, Kros JM, Duncker DJ, Cheng C (2017) CMTM3 (CKLF-Like Marvel Transmembrane Domain 3) Mediates Angiogenesis by Regulating Cell Surface Availability of VE-Cadherin in Endothelial Adherens Junctions. Arteriosclerosis, thrombosis, and vascular biology 37 (6):1098-1114. doi:10.1161/atvbaha.116.308792
20. Zhu C, Mustafa D, Zheng PP, van der Weiden M, Sacchetti A, Brandt M, Chrifi I, Tempel D, Leenen PJM, Duncker DJ, Cheng C, Kros JM (2017) Activation of CECR1 in M2-like TAMs promotes paracrine stimulation-mediated glial tumor progression. Neuro-oncology 19 (5):648-659. doi:10.1093
21. Nasevicius A, Ekker SC (2000) Effective targeted gene 'knockdown' in zebrafish. Nature genetics 26 (2):216-220. doi:10.1038/79951
22. Stratman AN, Malotte KM, Mahan RD, Davis MJ, Davis GE (2009) Pericyte recruitment during vasculogenic tube assembly stimulates endothelial basement membrane matrix formation. Blood 114 (24):5091-5101. doi:10.1182/blood-2009-05-222364
23. Jorgensen CB (1988) Nature of moulting control in amphibians: effects of cortisol implants in toads Bufo bufo. General and comparative endocrinology 71 (1):29-35
24. Zhou Z, Chrifi I, Xu Y, Pernow J, Duncker DJ, Merkus D, Cheng C (2016) Uridine adenosine tetraphosphate acts as a proangiogenic factor in vitro through purinergic P2Y receptors. American journal of physiology Heart and circulatory physiology 311 (1):H299-309. doi:10.1152/ajpheart.00578.2015
25. Zhu C, Chrifi I, Mustafa D, van der Weiden M, Leenen PJM, Duncker DJ, Kros JM, Cheng C (2017) CECR1-mediated cross talk between macrophages and vascular mural cells promotes neovascularization in malignant glioma. Oncogene 36 (38):5356-5368. doi:10.1038/onc.2017.145
26. Cao J, Ehling M, Marz S, Seebach J, Tarbashevich K, Sixta T, Pitulescu ME, Werner AC, Flach B, Montanez E, Raz E, Adams RH, Schnittler H (2017) Polarized actin and VE-cadherin dynamics regulate junctional remodelling and cell migration during sprouting angiogenesis. Nature communications 8 (1):2210. doi:10.1038/s41467-017-02373-8

27. Abu Taha A, Schnittler HJ (2014) Dynamics between actin and the VE-cadherin/catenin complex: novel aspects of the ARP2/3 complex in regulation of endothelial junctions. Cell adhesion & migration 8 (2):125-135
28. Abraham S, Yeo M, Montero-Balaguer M, Paterson H, Dejana E, Marshall CJ, Mavria G (2009) VE-Cadherin-mediated cell-cell interaction suppresses sprouting via signaling to MLC2 phosphorylation. Current biology : CB 19 (8):668-674. doi:10.1016/j.cub.2009.02.057
29. Millan J, Cain RJ, Reglero-Real N, Bigarella C, Marcos-Ramiro B, Fernandez-Martin L, Correas I, Ridley AJ (2010) Adherens junctions connect stress fibres between adjacent endothelial cells. BMC biology 8:11. doi:10.1186/1741-7007-8-11
30. Sonnichsen B, De Renzis S, Nielsen E, Rietdorf J, Zerial M (2000) Distinct membrane domains on endosomes in the recycling pathway visualized by multicolor imaging of Rab4, Rab5, and Rab11. The Journal of cell biology 149 (4):901-914
31. Van Der Sluijs P, Hull M, Zahraoui A, Tavitian A, Goud B, Mellman I (1991) The small GTP-binding protein rab4 is associated with early endosomes. Proceedings of the National Academy of Sciences of the United States of America 88 (14):6313-6317
32. Ullrich O, Reinsch S, Urbe S, Zerial M, Parton RG (1996) Rab11 regulates recycling through the pericentriolar recycling endosome. The Journal of cell biology 135 (4):913-924
33. van der Sluijs P, Hull M, Webster P, Male P, Goud B, Mellman I (1992) The small GTP-binding protein rab4 controls an early sorting event on the endocytic pathway. Cell 70 (5):729-740
34. Filipeanu CM, Zhou F, Lam ML, Kerut KE, Claycomb WC, Wu G (2006) Enhancement of the recycling and activation of beta-adrenergic receptor by Rab4 GTPase in cardiac myocytes. The Journal of biological chemistry 281 (16):11097-11103. doi:10.1074/jbc.M511460200
35. Chichger H, Braza J, Duong H, Boni G, Harrington EO (2016) Select Rab GTPases Regulate the Pulmonary Endothelium via Endosomal Trafficking of Vascular Endothelial-Cadherin. American journal of respiratory cell and molecular biology 54 (6):769-781. doi:10.1165/rcmb.2015-0286OC
36. Chichger H, Braza J, Duong H, Stark M, Harrington EO (2015) Neovascularization in the pulmonary endothelium is regulated by the endosome: Rab4-mediated trafficking and p18-dependent signaling. American journal of physiology Lung cellular and molecular physiology 309 (7):L700-709.
37. Yan Z, Wang ZG, Segev N, Hu S, Minshall RD, Dull RO, Zhang M, Malik AB, Hu G (2016) Rab11a Mediates Vascular Endothelial-Cadherin Recycling and Controls Endothelial Barrier Function. Arteriosclerosis, thrombosis, and vascular biology 36 (2):339-349. doi:10.1161/atvbaha.115.306549
38. Ward ES, Martinez C, Vaccaro C, Zhou J, Tang Q, Ober RJ (2005) From sorting endosomes to exocytosis: association of Rab4 and Rab11 GTPases with the Fc receptor, FcRn, during recycling. Molecular biology of the cell 16 (4):2028-2038. doi:10.1091/mbc.E04-08-0735
39. Pagano A, Crottet P, Prescianotto-Baschong C, Spiess M (2004) In vitro formation of recycling vesicles from endosomes requires adaptor protein-1/clathrin and is regulated by rab4 and the connector rabaptin-5. Molecular biology of the cell 15 (11):4990-5000. doi:10.1091/mbc.E04-04-0355
40. Bucci C, Thomsen P, Nicoziani P, McCarthy J, van Deurs B (2000) Rab7: a key to lysosome biogenesis. Molecular biology of the cell 11 (2):467-480
41. Sanchez-Pulido L, Martin-Belmonte F, Valencia A, Alonso MA (2002) MARVEL: a conserved domain involved in membrane apposition events. Trends in biochemical sciences 27 (12):599-601
42. Jin C, Ding P, Wang Y, Ma D (2005) Regulation of EGF receptor signaling by the MARVEL domain-containing protein CKLFSF8. FEBS letters 579 (28):6375-6382. doi:10.1016/j.febslet.2005.10.021

Supplemental figures

Supp. Fig. 1

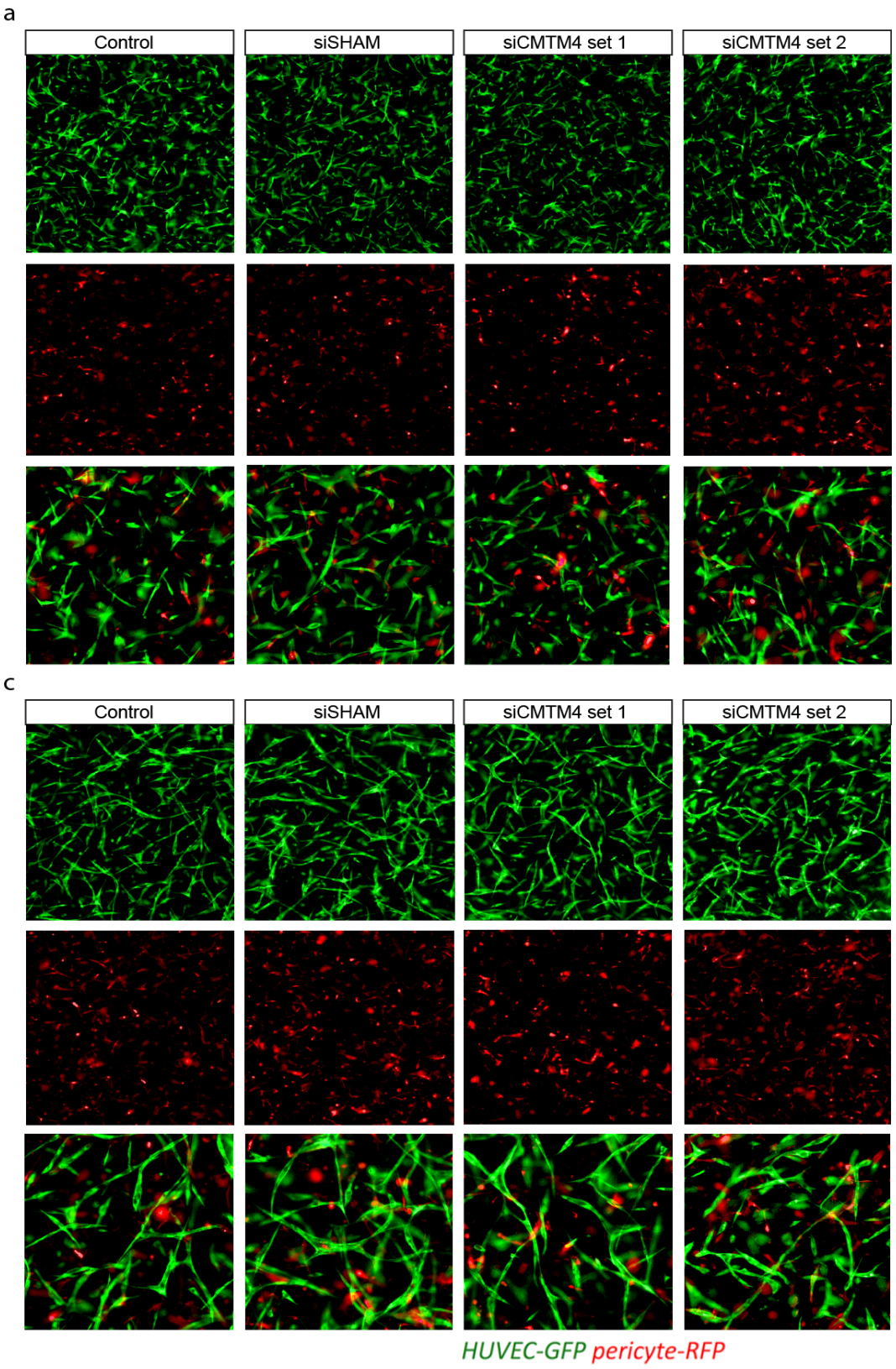

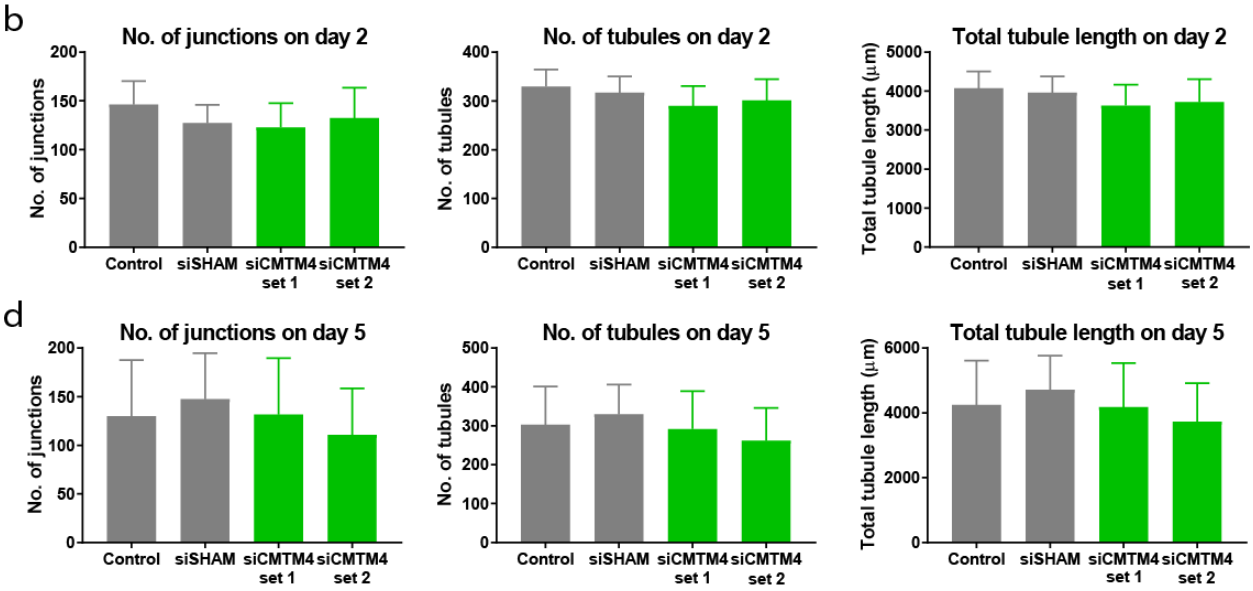

Supp. Fig. 1. CMTM4 silencing in pericytes does not affect vascular growth *in vitro*

a Representative immunofluorescent images taken at 2x magnification (upper rows) and zoomed-in images (lower row) of GFP-labelled HUVECs (green) and dsRED-labelled pericytes (red) cultured for 2 days in a 3D collagen matrix, in which the dsRED labeled pericytes were transfected with either CMTM4-targeting siRNA (siCMTM4 set 1 or set 2), non-targeting siRNA (siSHAM) or not transfected (control). **b** Quantification of the number of junctions, number of tubules and total tubule length of siCMTM4 set 1 and set 2, siSHAM and control HUVECs at day 2 of co-culture. Values are mean ± SEM; N=4 co-cultures. **c** Representative immunofluorescent images taken at 2x magnification (upper rows) and zoomed-in images (lower row) of GFP-labelled HUVECs (green) and dsRED-labelled pericytes (red) cultured for 5 days in a 3D collagen matrix, in which the dsRED labeled pericytes were transfected with either CMTM4-targeting siRNA (siCMTM4 set 1 or set 2), non-targeting siRNA (siSHAM) or not transfected (control). **d** Quantification of the number of junctions, number of tubules and total tubule length of siCMTM4 set 1 and set 2, siSHAM and control HUVECs at day 5 of co-culture. Values are mean ± SEM; N=4 co-cultures.

Supp. Fig. 2

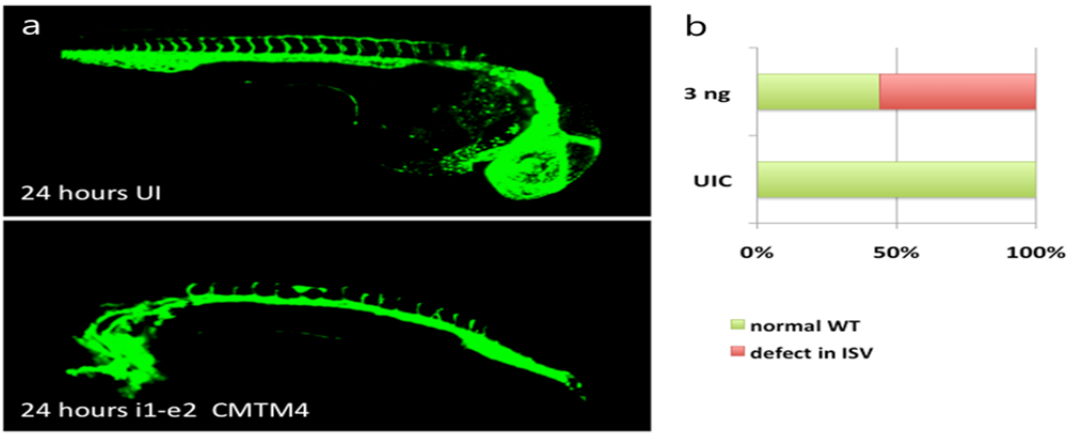

Supp. Fig. 2. Silencing of CMTM4 by morpholino targeting in developing zebrafish larvae trigger defects in intersomitic vessels

a Tg(fli1:eGFP)$_{y1}$ larvae at 24 hours post fertilization. Defects in intersomitic vessel formation were detected in the trunk region in larvae injected with morpholinos targeting the splice site of i1-e2 of CMTM4 (indicated as i1-e2 CMTM4) (lower image) compared to uninjected controls (UIC) (upper image). Vasculature is visualized with eGFP (green). 2x magnification **b** Quantification of intersomitic vessel defect phenotype versus wildtype phenotype in i1-e2 injected group versus UICs. Data represents percentage of counted larvae (~100 counted per group).

Supp. Fig. 3

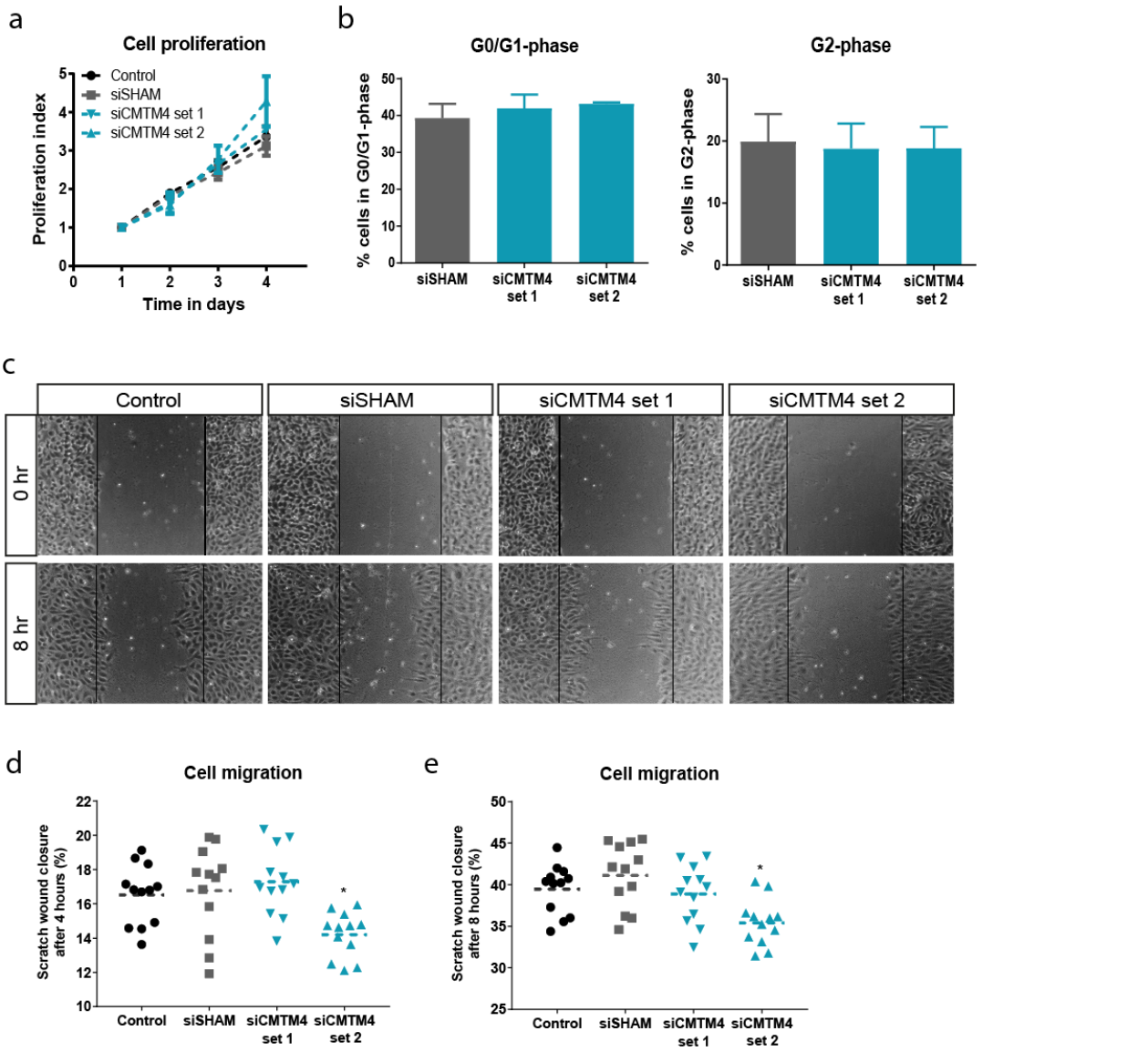

Supp. Fig. 3. CMTM4 silencing did not affect endothelial cell proliferation, but had a small effect on cell migration

a The number of cells counted at day of seeding (day 1), and at day 2, 3 and 4 of cell proliferation in siCMTM4 HUVECs (set 1 and set 2) compared with siSHAM and non-transfected controls. Shown is mean ± SEM, N=4. **b** Bargraphs showing the % of G0/G1 and G2 phase cells at day 2 after transfection in siCMTM4 versus siSHAM and non-transfected controls. Shown is mean ± SEM, N≥3. **c** Representative brightfield microscope images (4x magnification) of a scratch migration assay after 8 hours of migration of siCMTM4 HUVECs (set 1 and set 2) compared with siSHAM and non-treated controls. Bargraphs of the quantified results of the scratch migration assay showing the % area within the scratched region covered by siCMTM4 (set 1 and set 2) HUVECs compared with siSHAM and non-treated controls after (**d**) 4 hours and (**e**) 8 hours. Shown is mean; N=2, 6 wells each.

Supp. Fig. 4

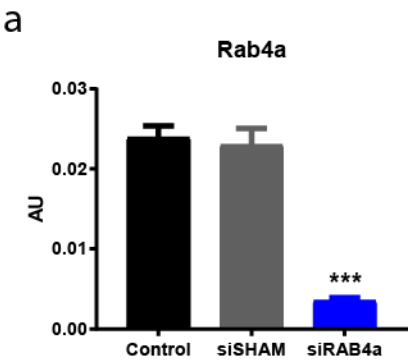

Supp. Fig. 4. Rab4a-targeting siRNA induced significant silencing of Rab4a expression

a Gene expression levels of Rab4a in HUVECs transfected with Rab4a-targeting siRNA (siRAB4a), non-targeting siRNA (siSHAM) and in non-transfected HUVECs (control). Gene expression levels were normalized to β-actin (AU); values are mean ± SEM; N=4 qPCRs; ***P<0.001 compared to both control and siSHAM.

Supp. Fig. 5

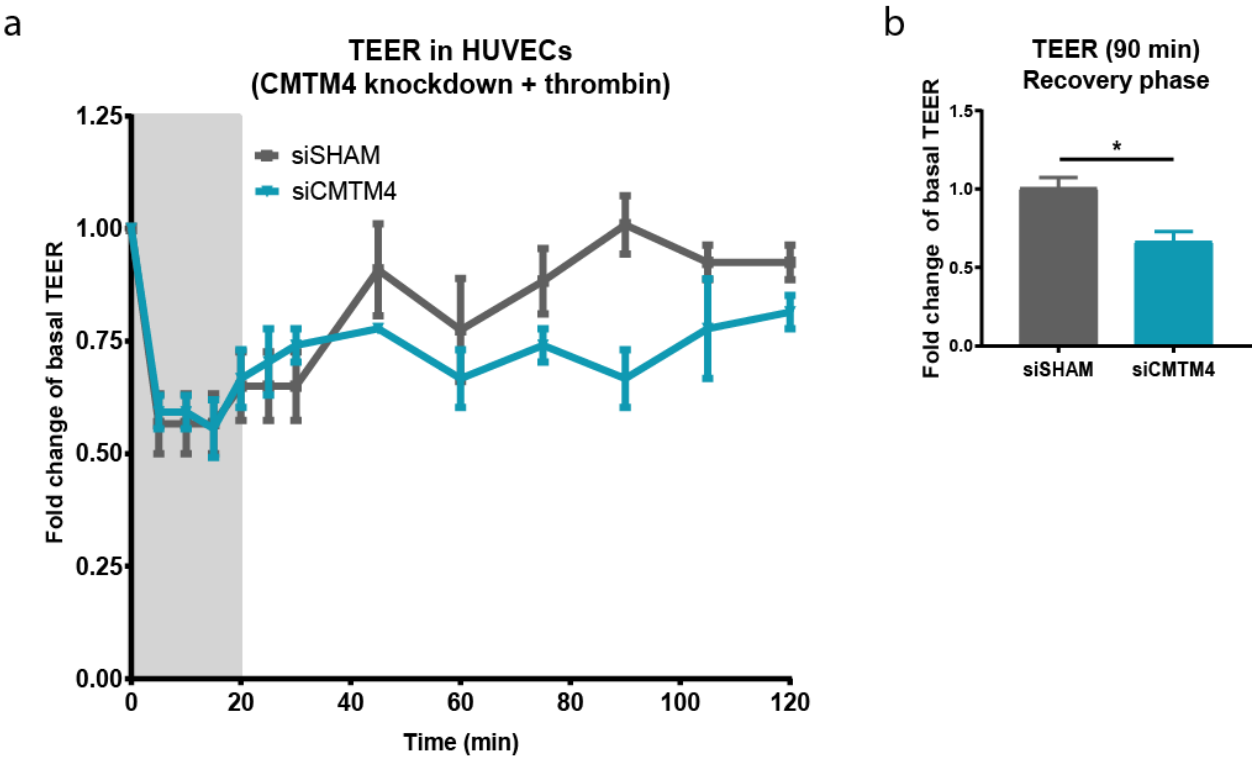

Supp. Fig. 5. CMTM4 promotes restoration of endothelial electric resistance in thrombin-induced response

a Thrombin response (presented in fold change compared with basal resistance of

nontransfected group: Y axes) of confluent HUVEC monolayers during (0–20 minutes) and after (20–120 minutes) thrombin (1 U/mL) stimulation in siCMTM4 and siSHAM conditions. At 0 minutes, thrombin was added and at 20 minutes thrombin was removed (gray area). Mean ± SEM. N=3 per time series. **b** Increase in resistance during recovery phase at 90 minutes in siSHAM and siCMTM4 groups. Mean ± SEM. *P≤0.05 versus siSHAM. N=3.

Supp. Fig. 6

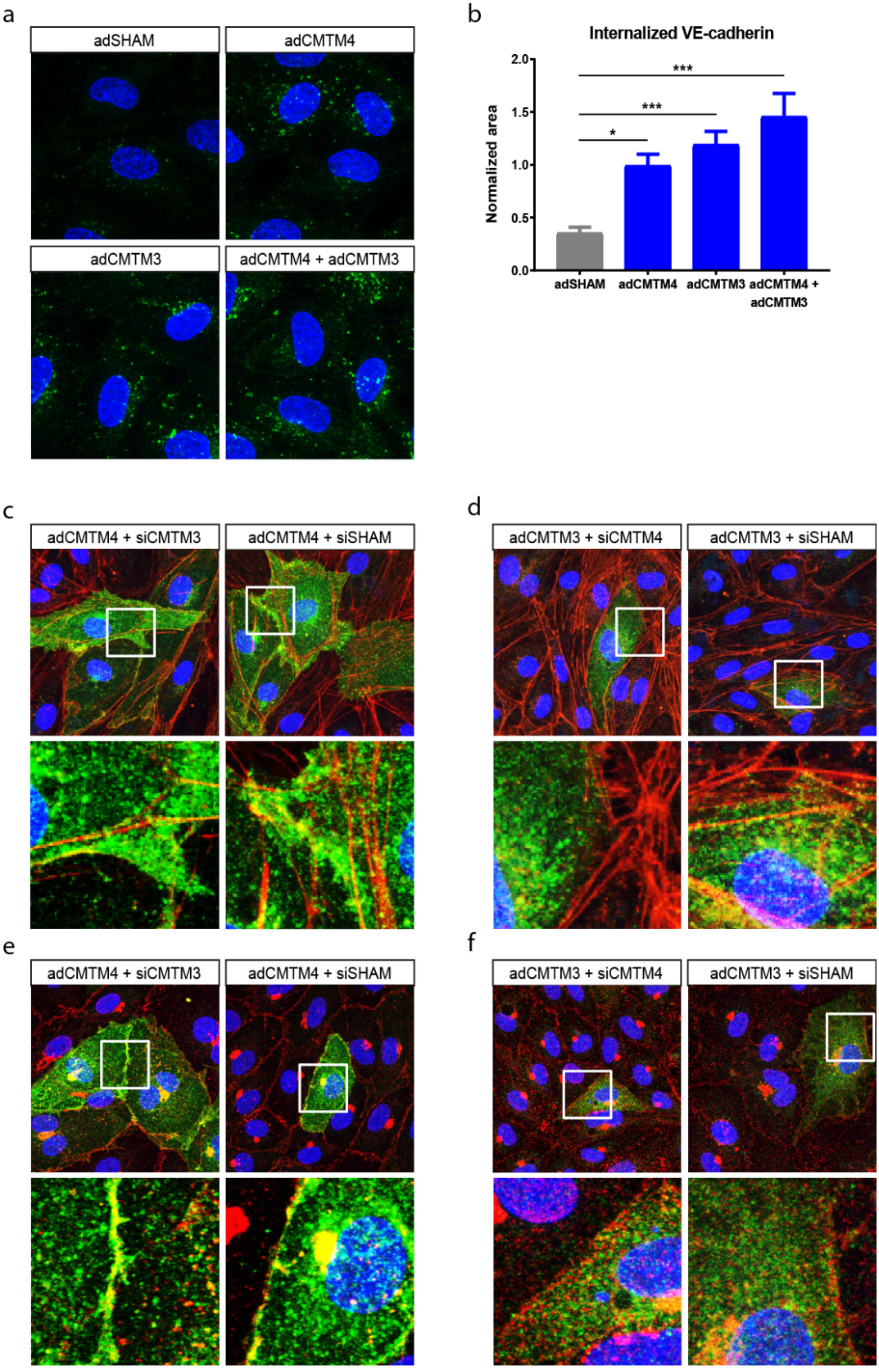
a
adSHAM
adCMTM4
adCMTM3
adCMTM4 + adCMTM3
b
Internalized VE-cadherin
Normalized area
2.0
1.5
1.0
0.5
0.0
***
***
*
adSHAM
adCMTM4
adCMTM3
adCMTM4 + adCMTM3
c
adCMTM4 + siCMTM3
adCMTM4 + siSHAM
d
adCMTM3 + siCMTM4
adCMTM3 + siSHAM
e
adCMTM4 + siCMTM3
adCMTM4 + siSHAM
f
adCMTM3 + siCMTM4
adCMTM3 + siSHAM

g

	CMTM3 (AU)		CMTM4 (AU)	
adSHAM	0.018972	0.019645	0.004082	0.004148
adCMTM4	0.021615	0.023672	0.317889	0.304525
adCMTM3	1.905051	1.902983	0.004664	0.004623
adCMTM4 + adCMTM3	1.007529	1.072234	0.186527	0.182948

h

	CMTM3 (AU)		CMTM4 (AU)	
adCMTM4 + siCMTM3	0.001536	0.001832	0.068990	0.093618
adCMTM4 + siSHAM	0.012848	0.018171	0.073897	0.091932
adCMTM3 + siCMTM4	1.383564	2.560715	0.000740	0.000494
adCMTM3 + siSHAM	1.194415	1.531579	0.004066	0.003358

Supp. Fig. 6. CMTM4 and CMTM3 do not interfere or enhance each other's function and localization

a Representative zoomed-in confocal micrographs (63x magnification) of confluent adSHAM, adCMTM4 (VPC20), adCMTM3 (VPC20) and adCMTM4 + adCMTM4 double overexpression (VPC10 each) HUVECs labeled with VE-cadherin antibodies at 4°C, followed by 37°C incubation for 1 hour to track VE-cadherin movement. Surface bound VE-cadherin antibodies were removed by an acid-wash, before proceeding with immunostaining for visualization of internalized VE-cadherin (green). **b** Quantification of internalized VE-cadherin area per cell in adSHAM, adCMTM4 (VPC20), adCMTM3 (VPC20) and adCMTM4 + adCMTM4 double overexpression (VPC10 each) HUVECs. *P<0.05, ***P0.001 versus adSHAM. N=2, 5 Z-stacks each. **c** Representative 63x magnification (upper row) and zoomed-in (lower row) confocal microscope images of adCMTM4 + siCMTM3 and adCMTM4 + siSHAM HUVECs immunostained for CMTM4 (green) and F-actin (red) (VPC10). **d** Representative 63x magnification (upper row) and zoomed-in (lower row) confocal microscope images of adCMTM3 + siCMTM4 and adCMTM3 + siSHAM HUVECs immunostained for CMTM3 (green) and F-actin (red) (VPC10). **e** Representative 63x magnification (upper row) and zoomed-in (lower row) confocal microscope images of adCMTM4 + siCMTM3 and adCMTM4 + siSHAM HUVECs immunostained for CMTM4 (green) and VE-cadherin (red) (VPC10). **f** Representative 63x magnification (upper row) and zoomed-in (lower row) confocal microscope images of adCMTM3 + siCMTM4 and adCMTM3 + siSHAM HUVECs immunostained for CMTM3 (green) and VE-cadherin (red) (VPC10). **g** Gene expression levels of CMTM3 and CMTM4 in adSHAM, adCMTM4 (VPC20), adCMTM3 (VPC20) and adCMTM4 + adCMTM4 double overexpression (VPC20) HUVECs. Gene expression levels were normalized to β-actin (AU); N=2 qPCRs. **h** Gene expression levels of CMTM3 and CMTM4 in adCMTM4 + siCMTM3, adCMTM4 + siSHAM, adCMTM3 + siCMTM4 and adCMTM3 + siSHAM HUVECs. Gene expression levels were normalized to β-actin (AU); N=2 qPCRs; VPC10.

Chapter 4 Cgnl1, an endothelial junction complex protein, regulates GTPase mediated angiogenesis.

Ihsan Chrifi*, Dorien Hermkens*, Maarten Brandt, Christian van Dijk, Petra E. Bürgisser, Remco Haasdijk, Jiayi Pei, Esther van de Kamp, Changbin Zhu, Lau Blonden, Johan, M. Kros, Dirk Jan Duncker, Henricus J. Duckers[4#], Caroline Cheng[1,2#]

*These *first and # last authors contributed equally to the paper.*

Published: Cardiovascular Research 2017 Dec. 1;113(14): 1776-1788

Abstract

Aims: The formation of cell-cell and cell-extra cellular matrix contacts by endothelial cells is crucial for the stability and integrity of a vascular network. We previously identified cingulin-like 1 (Cgnl1) in a transcriptomic screen for new angiogenic modulators. Here we aim to study the function of the cell-cell junction associated protein Cgnl1 during vessel formation.

Methods and Results: Unlike family member cingulin, Cgnl1 expression is enriched in endothelial cells during vascular growth. Cgnl1 is important for the formation of multicellular tubule structures, as shown *in vitro* using loss-of function assays in a 3D matrix co-culture system that uses primary human endothelial cells and supporting mural cells. Further studies revealed that Cgnl1 regulates vascular growth by promoting Ve-cadherin association with the actin cytoskeleton, thereby stabilizing adherens junctions. Cgnl1 also regulates focal adhesion assembly in response to extracellular matrix contact, promoting vinculin and paxillin recruitment and focal adhesion kinase signalling. *In vivo*, we demonstrate in a postnatal retinal vascular development model in mice that Cgnl1 function is crucial for sustaining neovascular growth and stability.

Conclusions: Our data demonstrate a functional relevance for Cgnl1 as a defining factor in new vessel formation both *in vitro* and *in vivo*.

Introduction

New vessel formation plays a critical role in embryonic development and disease progression of adult organisms. The mechanism is complex and consists of multiple stages that include primary plexus formation, network expansion, and vascular remodelling.[1, 2] During the initial phase of new vessel formation, maturing endothelial cells (ECs) establish cell-cell interaction to form multi-cellular structures that are gradually remodelled into microvascular tubules with open lumina. This critical step is orchestrated by mobilizing the EC's actin cytoskeleton to facilitate cell-morphological adaptations that are crucial for intercellular junction assembly. The importance of small GTPases in these processes has been previously investigated:[3] Rac1 is implied to be the predominant GTPase involved in VEGFA mediated angiogenesis,[4] and is crucial for lumen and tubule formation. Rac1 also facilitates migration as it controls actin polymerization during the formation of lamellopodia,[5] and knockdown of Rac1 in mice led to embryonic lethality as a result of defects in vascular growth.[6] In addition, cdc42 and Rac1 regulate endothelial barrier function by modulating the interaction between the actin cytoskeleton and junctional proteins like Ve-cadherin, located at adherence junctions.[7, 8] Rho family GTPases constantly cycle between the guanine diphosphate (GDP) bound inactive state and the guanine triphosphate (GTP) bound active state. Their activity is tightly regulated by their activators Guanine-Exchange-Factors (GEF), and their inhibitors, which include GTPase activation proteins and guanine-diphosphate-disassociation inhibitors.[9]

Cingulin is a 140 kDa protein, which is ubiquitously expressed in different cell types with high expression levels detected in epithelial cells of various origins. *In vitro* studies in canine renal epithelial cells demonstrates that cingulin is localized at the cytoplasmatic surface of tight junctions where it functions as an adaptor protein for GEFs.[10] Cingulin binds to actin filament bundles, suggesting that cingulin may be a linking protein between tight junction complexes and the actin cytoskeleton. However, although cingulin depletion promotes RhoA activity, it does not affect tight junction complex formation or actin cytoskeleton assembly.[10, 11] Cingulin-like 1 (Cgnl1), a 150-160 kDa paralogue of cingulin, also known as JACOP and PCING, was recently discovered to be localized in both adherens and tight junctions. Cgnl1 was shown to be an inhibitor of RhoA activity, but was also involved in the activation of Rac1 by the GEF Tiam1 in epithelial cells.[10, 12] Like cingulin, Cgnl1 is co-localized with actin filament bundles, implying that it could be a cross-road modulator that links intercellular junction assembly to actin cytoskeleton-regulated morphogenesis, both key processes in angiogenesis. Indeed, Cngl1 mRNA expression has been detected in CD31+ cells isolated from mouse embryos on days 8.5 and 9.5, in which it was preferentially expressed in endocardial cells, but not yolk sac endothelial cells.[23] Previously, we conducted a genome-wide transcriptomic screen with the goal to identify new molecular regulators of vascular development during murine embryogenesis.[13] In line with the previous report, we found that unlike cingulin, Cgnl1 was mainly expressed in Flk1+ endothelial precursor cells during embryonic development. Cgnl1 has been indicated to be actively involved in tight junction regulation of endothelial cells.[14] Here we

further assessed the role of Cgnl1 in endothelial cell biology and angiogenesis.
Our data demonstrate that Cgnl1 promotes angiogenesis by strengthening adherens junctions via Rac1 activation, which leads to stabilization and further elongation of newly formed vascular tubules.

Methods

Mouse retinal angiogenesis model
Approval was granted by the institutional ethics review board (DEC 109-11-12). All animal procedures were conducted conform the guidelines from Directive 2010/63/EU of the European Parliament on the protection of animals used for scientific purposes. Two or 8 days old C57bl/6 pups were anesthetized by placement on ice. For Cgnl1 silencing experiments, 100 nmol accel siRNA targeting murine Cgnl1 was intra-vitreally injected in the left, and 100 nmol accel scrambled non-tageting siRNA in the right eye (Dharmacon, Netherlands) in a volume of 0.5 μl using a 33-gauge needle. At day 6 or 12 post-transfection, pups were sacrificed by decapitation, and retinas were stained with FITC isolectin IB4 (1:200). Angiosys analysis software (Angiosystems, UK) was used to determine total tubule length, and the number of tubules and junctions per field of view. Adequate target mRNA inhibition was validated by qPCR analysis and western blot analysis.

In vitro culture
Human Umbilical Vein Endothelial Cells (HUVECs; Lonza) and Human Brain Vascular Pericytes (HBVPs; Lonza) were cultured on gelatine-coated plates in EGM2 medium (EBM2 medium supplemented with EGM2 bullet kit and 2% FCS; Lonza) and DMEM (10% FCS; Lonza) respectively, in 5% CO_2 at 37 ˚C. The experiments were performed with cells at passage 3-5. Lentiviral transfected HUVECs that express green fluorescent protein (GFP) were used at passage 6-8.

Statistical analysis
Results are expressed as the mean ± SD and statistical analysis was performed by one-way ANOVA followed by tukey's post-hoc test, or Student's t-test where appropriate. $p<0.05$ was considered significant.

Small GTPase activation assay
For measuring small GTPase activity, HUVECs were serum starved in EBM-2/0.2% FCS overnight, followed by cell seeding in full supplemented EGM2 medium on gelatin/collagen coated surface for 20 and 40 minutes, before cells were harvested in NP40 buffer. proGTP-RhoA, Rac1, and cdc42 activation levels in the cell lysaters were measured using the G-lisa detection system (Tebu-Bio, Netherlands) following the manufacturer's protocol.

Flow cytometric analysis

BRDU incorporation assay: HUVECs were synchronized in the G0/G1 phase by serum deprivation in EGM-2/0.2% FCS for 12 hours, followed by incubation in EGM-2 with 10µM BRDU for 4 hours at 37°C/5% CO2. Afterwards, cells were harvested, washed in PBS, fixed in 70% ethanol, treated with pepsin, and stained for BRDU incorporation using a direct FITC labeled mouse antibody directed against BRDU (Abcam, UK) and propidium-iodide (PI 1:300), followed by FACS analysis (FACScanto, BD Biosciences, The Netherlands) and subsequent data analysis by use of Flowjo® -software (Tree Starinc., US).

Cell cycle analysis: Cells were harvested at 0, 4 and 12 hours post activation, fixed in 70% ethanol/PBS for 15 min on ice, stained with propidium-iodide (PI 1:300), and analyzed by flow cytometry (FACScanto, BD Biosciences, Netherlands) with subsequent data analysis by use of Flowjo®-software (Tree Star inc., US).

Apoptosis analysis: Cells were harvested at 0, 4 and 12 hours post activation, stained for Annexin V and PI signals using an Annexin V apoptosis detection kit (BD Biosciences, The Netherlands), followed by analysis of the samples by flow cytometry (FACScanto, BD Biosciences, Netherlands) and subsequent data analysis by use of Flowjo®-software (Tree Star inc., US).

In vitro assays

2D matrigel assay: HUVECs were seeded at a density of 3×10^4 cells/ml in 200 µl EGM2 medium in a 96-well plate on serum-reduced Matrigel (BD Biosciences, The Netherlands) and incubated for 24 hours. Viable cells were visualized by Calcein-AM uptake according to the manufacturer's protocol (BD Biosciences, The Netherlands) and fluorescence microscopy.

3D collagen monoculture and coculture assay: HUVECs (GFP labelled) were either suspended alone (monoculture in 3D collagen matrix) or with pericytes (RFP labelled) in 2,5 mg/ml collagen type 1 and assays were performed confirm the protocol developed by Stratman et al[1]. Live imaging was conducted using the Incucyte live cell analysis system(Essen Bioscience, The Netherlands).

Cell adhesion assay: HUVECs were harvested with accutase and seeded at density of 10000 cells per well of a 12 wells plate on gelatine coated glass slides. After 10, 20, 30, 60, or 120 minutes of incubation at 37°C/5% CO2 in EGM2 medium, the cells were washed with PBS and fixed with 4% PFA, followed by Rhodamine Phalloidin staining, and/or immunofluorescent staining of the FA components, paxillin, vinculin, and FAK using the protocol that was earlier described.

Quantification of the 2D matrigel, monoculture, and ccoculture assay, and time lapse imaging data: Angiosys analysis software (Angiosystems, UK) was used for 2D matrigel, monoculture and coculture assay to determine mean and total tubule length, and the number of tubules and junctions per field of view. FIJI (Image J) was used to analyze AR, roundness and GFP+ structure area data from time lapse imaging.

SiRNA mediated gene silencing

Targeted knockdown of genes was achieved by transfer of a mix of 4 specific siRNAs sequences directed against the target mRNA (Smartpool, Dharmacon, The Netherlands) in 50-60% sub-confluent HUVEC cultures, at 3 days prior to inclusion in experiments. As a control, cells were transfected with a mix of 4 scrambled non-targeting siRNAs (Dharmacon, The Netherlands). siRNA transfection efficiency of >80% of HUVECs was achieved at 72 hours, as validated by FITC-labelled siRNA (siglow, Dharmacon, The Netherlands, data not shown). Adequate overexpression or knockdown of the target genes was validated by qPCR and western blot analysis at 2 and 3 days post transfection respectively.

Quantitative PCR and western blot analysis

RNA was isolated using the RNAeasy kit (Qiagen, The Netherlands) and was checked for quality and quantity by capillary electrophoresis (Agilent 2100 Bioanalyzer, Agilent Technologies, The Netherlands), followed by reverse transcription into cDNA. qPCR reactions were performed by real-time assessment of the sybergreen signal using the iCycler iQ Detection System (Bio-Rad, The Netherlands). qPCR analysis was performed for the murine transcripts of Cgnl1, and for the human transcripts of Cgnl1, cingulin, VEGFA, VEGFR2, angtp1, angtp2, Tie1, and Tie2. Target mRNA expression levels are reported relative to the housekeeping genes, hypoxanthine guanine phosphoribosyl transferase (Hprt1) in murine samples, and β actin in the human samples, as previously described[2]. For Western blot analysis, samples were lysed in NP40 buffer, and analysed on a 1.5% SDS-PAGE gel followed by western blotting using 1:1000 rabbit anti-FAK, rabbit anti-FAK phosphoY397, rabbit anti-ß actin (Abcam, UK), rabbit anti-CSrc, rabbit anti-CSrc phospho Y418 (Sigma, Netherlands), 1:500 mouse anti-vinculin, and mouse anti-paxillin (Abcam, UK), and 1:500 mouse anti-paracingulin/Cgnl1 (Invitrogen, Netherlands) and 1:500 rabbit anti-cingulin (Atlas Antibodies, Netherlands) for protein detection. Protein bands were visualized using the Li-Cor detection system (Westburg, The Netherlands), as previously described[3-5]. Tissue extracts were separated in Triton-X soluble and insoluble fractions following a modified protocol of Lampugnani et al. before Western blot analysis[6].

Primary cell culture condition and intracellular staining

Primary human umbilical vein endothelial cells (HUVECs, Lonza, Netherlands) were cultured on gelatin-coated plates at 37°C/5% CO2 in EGM2 medium (EBM2 medium supplemented with commercial bullet kit and 2% FCS) with penicillin/streptomycin (Lonza, The Netherlands). Only cell cultures of passages 3-6 were used throughout the experiments. For intracellular staining, HUVECs were grown on coverslips and fixed in 4% paraformaldehyde (Sigma, Netherlands) for 5 minutes, followed by membrane permeabilization in 0.2% tritonX/PBS for 10 minutes, incubation with 1:100 mouse anti-Cgnl1 (Invitrogen, Netherlands), and subsequent detection of the signal by using a 1:200 FITC labeled goat anti-mouse IgG antibody (Invitrogen, Netherlands). For dubbelstaining, the Cgnl1 staining protocol was followed by incubation with Rhodamine

Phalloidin (Sigma, Netherlands) for visualization of the actin cytoskeleton. For the detection of FA components, fixed and permeabilized cells are incubated with 1:100 mouse anti-vinculin, or mouse anti-paxillin antibodies (Abcam, UK), followed by detection of the signal using a 1:200 dilution of a FITC labelled goat anti-mouse IgG antibody (Invitrogen, Netherlands) and subsequent Rhodamine Phalloidin staining (Sigma, Netherlands). For detection of adherens junction protein Ve-cadherin, fixed and permeabilized cells are incubated with 1:100 mouse anti-Ve-cadherin followed by detection using a 1:200 dilution of FITC labelled goat anti mouse IgG antibody (Invitrogen, Netherlands) followed by Rhodamine Phalloidin staining (Sigma, Netherlands). Coverslips were mounted using Vectashield/DAPI (Brunschwig, Netherlands) and stained cells were imaged by fluorescence microscopy (Carl Zeiss Inc., Netherlands). Quantification of Ve-cadherin at AJs was conducted by quantifying Ve-cadherin+ area per image view, presetting the dectection threshold on high to capture only the high fluorescent signal of Ve-cadherin accumulated at the AJs, excluding the weak Ve-cadherin signal in the cytoplasma. Theobtained values were corrected for the number of cells per view. For 2D coculture staining, pericytes were seeded 24 hours prior adhesion of HUVECs-GFP on top of coverslips. Pericytes were visualized by phalloidin-blue staining, imaging of Ve-cadherin and paxillin distribution in HUVECs-GFP was monitored by confocal microscopy, using Zstack analysis of Ve-cadherin and paxillin immuno signals in GFP+ cells.

Results

Cgnl1 shows predominant expression in developing vascular structures.

Cgnl1 was mainly expressed in the (fetal kinase receptor 1) Flk1+ cell population during embryonic development in mice as shown by qPCR validation of microarray screen data (Fig. 1A). Cgnl1 was predominantly expressed in Flk1+ endothelial precursor cells at 9.5 days post coitus during which the majority of the vascular structures in the embryo are established (Fig. 1A). This finding was further confirmed by data-mining of public expression databases (NCBI, Gene Expression Omnibus: Supplemental data Fig. 1A, B), which showed higher expression levels of Cgnl1 in primary endothelial cells of different origins compared to the more epithelial enriched expression of cingulin.

Next, whole mount *in situ* hybridization was conducted using a probe that targeted the zebrafish orthologue of Cgnl1 in the larval stages. At 24 hours post fertilization (hpf), Cgnl1 expression was observed in the trunk region in the dorsal aorta and post cardinal vein with low expression in the intersegmental vessels (Fig. 1B and D). In the head region, Cgnl1 was clearly expressed in the bi-lateral aorta Y-trunk and the cranial vasculature (Fig. 1E and C). From 48 hpf onward, Cgnl1 expression was also observed in the heart (Fig. 1F). The vascular expression pattern of Cgnl1 was similar to the vascular GFP pattern of Tg(kdrl;eGFP)^{y1} zebrafish larvae (Sup.Fig. 1C). This vascular pattern of Cngl1 gradually declined during larvae maturation (Fig. 1F-I). Specific targeting of Cgnl1 by anti-sense probe was validated by comparing the anti-sense and sense probe signal (Sup.Fig.1D,E). To assess if this vascular expression pattern was conserved in

mammals, qPCR analysis was conducted on different organs in mature C57/bl6 mice. Endogenous murine Cgnl1 expression was significantly higher in the aorta and kidney as compared to heart, lung, liver, skeletal muscle, eye and brain tissue (Fig. 1J). In contrast, cingulin expression was not enriched in murine aorta (Fig. 1K). Human umbilical vein derived endothelial cells (HUVECs) showed significant higher expression of Cgnl1 as compared to human pericytes, renal epithelial cells and fibroblasts (Sup.Fig. 1F). In contrast, cingulin expression was more prominent in renal epithelial cells (Sup.Fig. 1G). Immunohistological analysis demonstrated selective Cgnl1 expression in the endothelial lining of large blood vessels and microvessels in human samples (Fig. 1L).

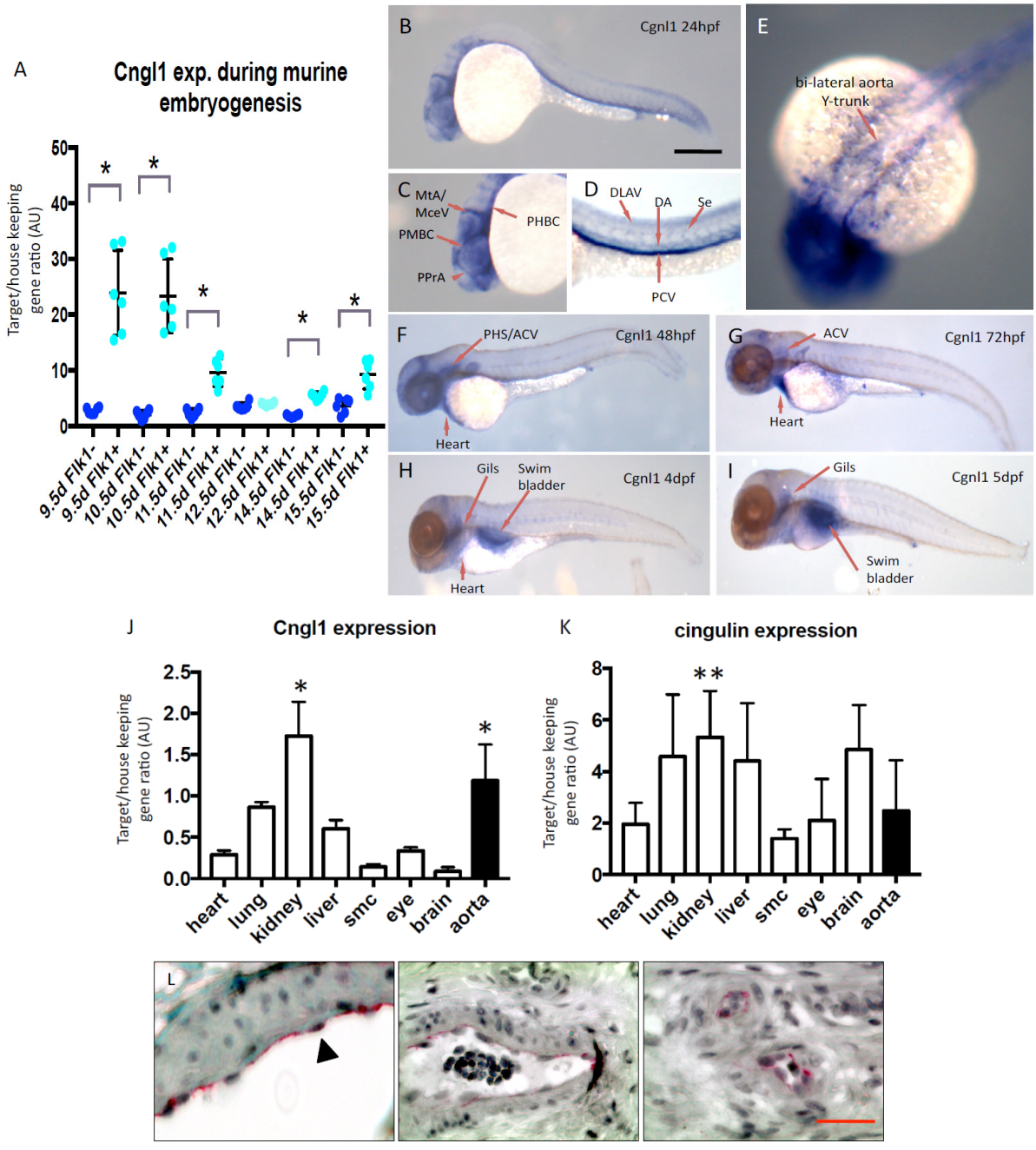

Figure 1: Cgnl1 is mainly expressed in vascular endothelial cells.
(A) Cgnl1 expression in Flk1+ and Flk1- cells during embryonic development of C57/bl6 mice from 9.5 to 15.5 days post coital analyzed by qPCR. Mean ± SD, n=6 for each time point, *p<0.05 versus time point matched Flk1- cells. Student's t-test. (B) Whole-mount *in situ* hybridization of wild type zebrafish larvae at different time points. Scale bar represents 5 mm. Lateral view: Cgnl1 targeting antisense probe signal (blue) detected in the vasculature at 24 hpf. (C) Cgnl1 expression is visible in the cranial vessels, including the middle cerebral vein (MceV), metencephalic artery (MtA), primordial midbrain channel (PMBC), primitive prosencephalic artery (PPrA), and primordial hindbrain channel (PHBC). (D) In the trunk region, Cgnl1 signal is in the posterior cardinal vein (PCV), dorsal longitudinal anastomotic vessel (DLAV), dorsal aorta (DA), and intersegmental vessel (Se). (E) Dorsal view: Expression of Cgnl1 in the bilateral aorta Y-trunk. (F) Regression of Cgnl1 signal during larvae maturation: Lateral view: Cgnl1 expression at 48 hpf is mainly located in cranial vessels, primary head sinus (PHS) and anterior cardinal vein (ACV), and heart region. (G) Cgnl1 expression at 72 hpf is still detected in the ACV, and remains visible in the heart, whereas expression of Cgnl1 at (H) 4 dpf and (I) 5 dpf is mainly in the gills and swimbladder. QPCR analysis of (J) Cgnl1 and (K) cingulin expression in various tissues of mature C57/bl6 mice. Mean ± SD, n=5, *p<0.05 aorta or kidney versus expression in all other tissues. **p<0.05 kidney versus expression in skeletal muscle (smc). One-way ANOVA, followed by post hoc test with aorta or kidney set as control. (L) Immunostaining of Cgnl1 in human paraffin sections: From left to right, Cgnl1 expression is observed in the endothelium of macrovessels (first and second micrograph, indicated by black arrowhead) and microvessels (third micrograph). Scale bar represents 50 µm. Red signal = VEGFR2 immuno-staining, black = nucleus staining.

Cgnl1 is essential for neovascular tubule formation.

Based on the vascular enriched expression profile of Cgnl1, we hypothesized that Cgnl1 contributes to vascular development. A standard 2D-matrigel sprouting assay was conducted in which sprouting capacity of ECs was assessed. In this assay, ECs form cordlike structures consisting of 1-3 cells within 18 hours, after which this initial network disintegrates due to the lack of stabilizing cues. Using siRNA that targeted endogenous Cgnl1 (siCgnl1) and scrambled siRNA as controls (sisham) in human primary HUVECs, the effect of Cgnl1 silencing on angiogenic sprouting potential was investigated.

SiCgnl1 transfection significantly reduced endogenous Cgnl1 mRNA and protein levels as compared to sisham-transfected and non-transfected (control) HUVECs (Sup.Fig. 2A-D). In addition, siRNA targeting of Cgnl1 did not affect family member cingulin on either protein or mRNA level (Sup.Fig. 2E, F). Quantitative comparison between siCgnl1-transfected and sisham-transfected cells showed no difference in sprouting capacity in the 2D-matrigel assay (Sup.Fig. 2G, H).

As Cgnl1 did not seem to affect initial vascular sprouting, we proceeded to study Cgnl1 function in vascular tubule construction in the presence of mural cells that provide vascular stabilizing cues. Tubule formation experiments were conducted in a well-validated 3D collagen type I gel coculture system. In this assay, GFP marked HUVECs are cocultured with RFP labelled pericytes to enable assessment of a number of critical steps, including assembly of multicellular,

lumenized branching vessels. The multicellular nature of neovessels obtained with this 3D coculture assay is demonstrated in Sup.Fig. 3A,B, and is shown in a time lapse movie (Sup. Movie 1). The effect of Cgnl1 silencing by siRNA targeting in HUVEC was assessed at day 2 and day 5 (Fig. 2A, B, and Sup.Fig.3C). Cgnl1 silencing (siRNA set 1) severely impeded the formation of new tubule structures as compared to non-transfected and sisham-transfected controls (Fig. 2B). These results were further confirmed by using a second set of siRNA that targets Cgnl1 on different sequences (Fig. 2C, D). In contrast, monocultures of HUVECs in 3D collagen matrix did not affect new tubule formation, indicating that pericyte interaction with ECs is important for the process of Cgnl1-mediated tubule formation (Sup.Fig. 4A-D). Cgnl1 expression was significantly upregulated in HUVECs that were cocultured with mural cells (VSMCs or pericytes) as compared to HUVECs monocultures (Sup Fig. 4E). Evaluation of the expression profile of the HUVECs in coculture with pericytes revealed that downregulation of Cgnl1 in HUVECs diminished Angiopoietin 1 (Angpt1) and increased VEGFA expression, whereas VEGFR2, Angiopoietin 2 (Angpt2), Tie1, and Tie2 expression levels remained unaffected (Sup.Fig. 4F). In contrast, western blot analysis revealed no significant effect of Cgnl1 silencing on VEGFA and Angpt1 protein levels (Sup.Fig. 4G). Cgnl1 silencing in HUVECs did not affect pericyte numbers (Sup.Fig. 5A). Next, we assessed if induction of Cgnl1 expression in HUVECs is induced either by direct cell contact or paracrine stimulation by pericytes. HUVECs cultured on a thin porous membrane with direct contact of pericytes that are cultured on the other side show enhanced Cgnl1 expression versus HUVECs cultured without pericyte direct contact (Sup.Fig. 5B, C). In contrast, HUVECs cultured in the bottom well of a thin porous membrane insert in which percytes were seeded, allowing paracrine stimulation of HUVECs without direct pericyte contact, did not enhance Cngl1 expression versus HUVECs cultured in a similar setup without pericytes (Sup.Fig. 5D) These data indicate that induction of Cgnl1 expression in HUVECs in response to pericytes is mediated via direct contact between the two cell types. Endothelial cell and pericyte interaction can take place in peg-and-socket contacts via (CX43-mediated) gap and (N-cadherin-based) adherence junctions.[15] To further investigate via which interaction mechanism pericyte activation of Cngl1 in endothelial cells is mediated, we evaluated Cngl1 expression in HUVECs in response to pericyte direct contact stimulation with siRNA mediated knockdown of CXC43 and N-cadherin. Silencing of these peg-and-socket enriched proteins in HUVECs and pericytes did not affect induction of Cgnl1 expression in HUVECs by pericyte contact (Sup.Fig. 5E, F). Recent findings also indicate endothelial cells and mural cells communicate via cross-cell type Notch ligand presentation,[16-18] initiating Notch signalling that promotes strong cell-cell contacts by Ve-cadherin immobalization at adherens junctions.[17-19] Indeed, siRNA mediated silencing of Notch1 and Notch4 and DLL4 in HUVECs and pericytes abolished Cgnl1 mRNA upregulation mediated by pericyte coculture (Sup.Fig. 5G-I). These data demonstrate that Cngl1 expression in endothelial cells is enhanced via direct contact with pericytes via Notch signalling between the two cell types.

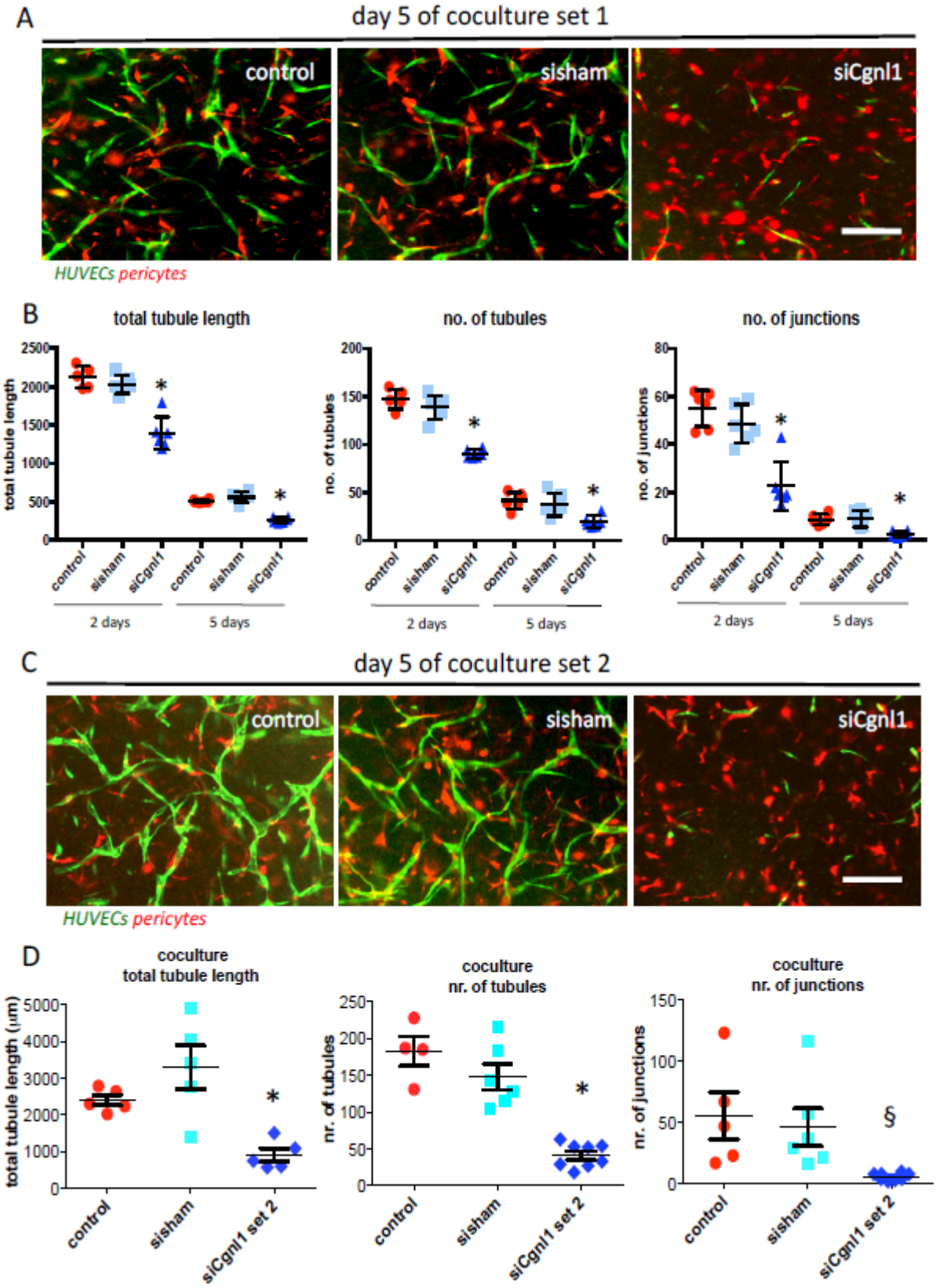

Figure 2: Cgnl1 knockdown impairs vascular network stabilization *in vitro*.

(A) Representative results at day 5 in 3D collagen matrix coculture following Cgnl1 silencing or sham

siRNA transfection in HUVEC-GFP (green). Pericytes are marked by RPF (red). Scale bars in A and C represent 100µm. (B) Quantitative analysis shows the number of total tubule length, and number of tubules and junctions in coculture conditions (n=5). Values represent means ± SD. *p<0.05 siCgnl1 versus time-corresponding control and sisham. Black bars indicate 2 days and white bars indicate data of 5 days coculture. One-way ANOVA for comparisons within one time point. (C) Representative results at day 5 in 3D collagen matrix coculture following Cgnl1 silencing with siRNA set 2. (D) Data of quantified coculture conditions at day 5, following silencing with Cngl1 targeting siRNA set 2 (N>5). Values represent means ± SD, *p<0.05, §p<0.1, siCgnl1 versus time-corresponding control and sisham. One-way ANOVA for comparisons within one time point.

Cgnl1 silencing in vivo impedes retinal vasculature development in postnatal mice.

To assess the *in vivo* relevance of these findings, the effect of Cgnl1 knockdown was studied in the developing retinal vasculature of post-natal C57/bl6 wildtype mice. Cgnl1 was silenced by injection of murine Cgnl1 targeting siRNA in the left and non-targeting siRNA in the right eye of 2 days old pups. Injection of the non-targeting siRNA sequences did not affect retinal vascularization (data not shown). Silencing of Cgnl1 was verified by qPCR and western blot (Sup.Fig. 6A and B). At day 6, the retinas were dissected and the vasculature was visualized by isolectin IB4 staining. Expansion of the vascular network from the neural plexus towards the retinal borders was impeded by Cgnl1 knockdown (Fig. 3A). Assessment on higher magnification showed frequent malformation in the vascular structures and lower vessel density in siCgnl1 treated retinas (Fig. 3A). Quantification of the vasculature showed decline in the number of vascular tubules, junctions, and in total tubule length (Fig. 3B). Likewise, Cgnl1 silencing during a later timeframe (with injection at day 8 after birth, during which a high density vascular network is well-established) compromised integrity of the vascular network, and further quantification showed a similar reduction in the number of tubules, junctions, and total tubule length at day 12 (Fig. 3A and Sup.Fig. 6C).

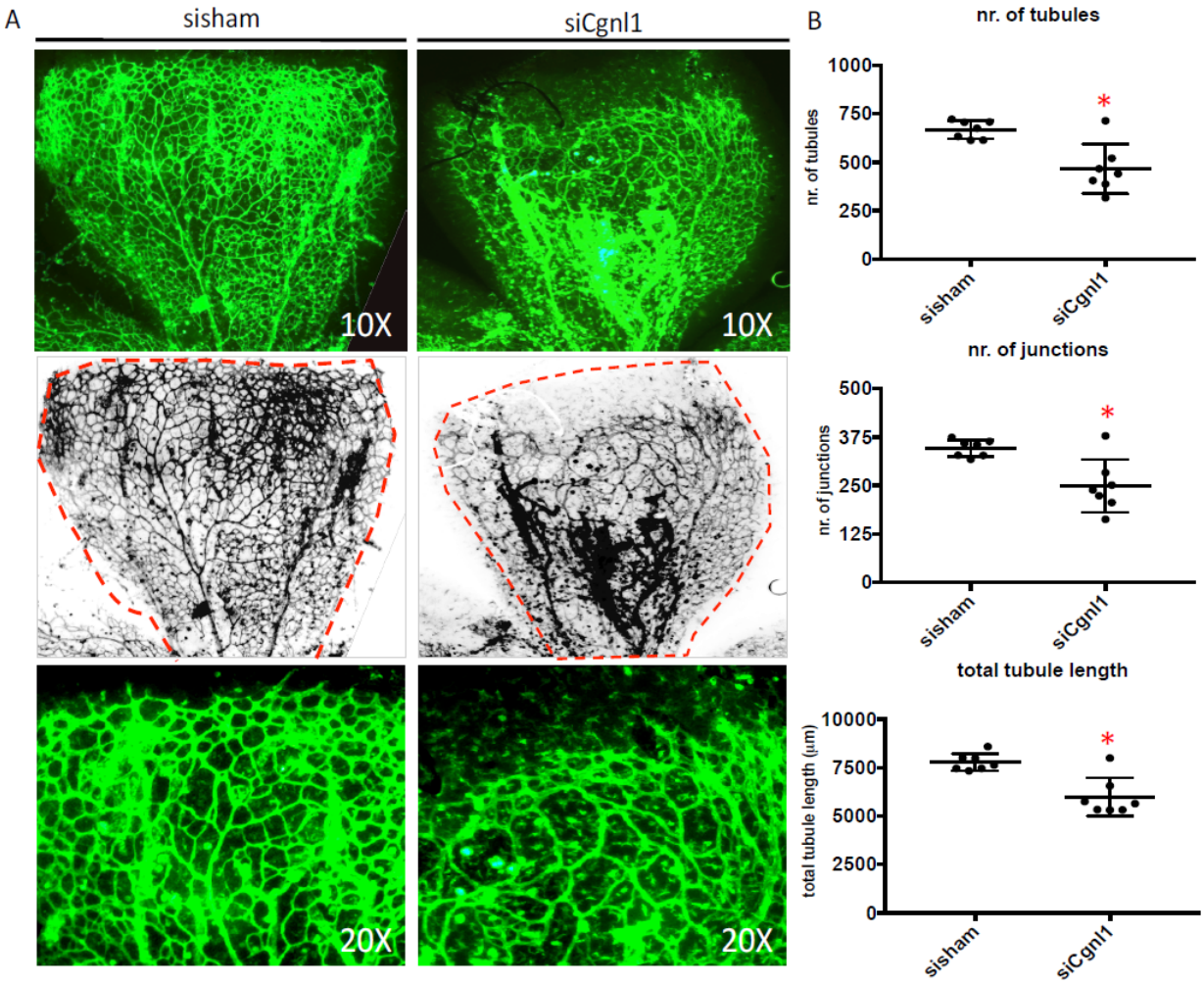

Figure 3: Cgnl1 silencing impedes vasculature development *in vivo*.
(A) Top row of images show representative micrographs of the developing retinal vasculature visualized by whole mount isolectin IB4 staining (FITC signal) at day 6. Second row of images show inverted version of micrographs used for quantification, red broken lines indicate retinal borders. 10X magnification. Third row of images show high magnification micrographs of the angiogenic front. 20X magnification. (B) Quantified results of retinal vascularization at day 6 after siCgnl1 injection at day 2 as compared to sisham-injected controls. Mean ± SD per group is indicated in scatter plots. *p<0.05 versus sisham-injected eyes. n=7 pups per group. Student's t-test.

Cgnl1 silencing affects Rac1 and RhoA activity and decreases actin cytoskeleton assembly.
It was previously reported that Cgnl1 is involved in the regulation of Rho-family GTPases activity in epithelial kidney cells.[12] Consequently, we assessed RhoA, cdc42 and Rac1 activities using ELISA-based activity assays. HUVECs were seeded on a thin layer of gelatin/collagen coating to provide an integrin-ECM contact trigger for GTPase activation, and were harvested after 20 and 40 minutes of stimulation for analysis. Cgnl1 silencing in HUVECs significantly reduced Rac1 activation early after cell seeding (Fig. 4A), whereas RhoA activity was increased (Fig. 4A). In contrast, no significant effect was observed in the activation of the small GTPase cdc42 in

comparison to sisham-transfected controls (Fig. 4A). Western blot analysis showed no difference in total Rac1, RhoA and cdc42 protein levels (Sup.Fig. 7A). In line with the observation that Cgnl1 expression is increased in HUVECs in response to pericyte stimulation, HUVECs cocultured with pericytes showed a significant increase in Rac1 activation versus single culture HUVECs (Sup.Fig. 7B). In addition, silencing of Cngl1 in HUVECs abolished these effects of pericyte stimulation (Sup.Fig. 7C). Our data showed that upregulation of Cgnl1 expression by pericyte contact in HUVECs was mediated via Notch signalling. Indeed silencing of Notch4 abolished the effects on Rac1 activity by pericyte stimulation of HUVECs (Sup.Fig. 7C). These data demonstrate that Cngl1 upregulation in HUVECs by pericyte cross talk with HUVECs via Notch signalling enhances endothelial Rac1 activity.

A delay in cell-morphological adaptation during adhesion of Cgnl1 silenced HUVECs implied that actin-cytoskeletal assembly in these cells was affected. To study this in more detail, siCgn1 and sisham transfected HUVECs were seeded on gelatin/collagen-coated glass slides, and morphological changes in the actin-cytoskeleton during cell adhesion were studied by phalloidin-Rhodamine staining at 10 and 20 minutes after seeding Fig. 4B). Cgnl1 knockdown caused a delay in actin-adaptation, identified by a significant decrease in the number of cells with a distinct flat morphology with clear actin-distribution at the cell periphery, and an increased in rounded cells with limited actin redistribution after 10 minutes of adhesion (Fig. 4C). To further validate these findings, live imaging was conducted in the previously described 3D collagen type I gel coculture system. Cellular adaptation of GFP marked HUVECs was monitored for up to 50 time points post-initiation of the assay (1 time point = 1 hour). Silencing of Cgnl1 in HUVECs-GFP reduced the morphological adaptive capacity of these cells, shown by a significant reduction in the siCgnl1 treated group in natural increase of *aspect ratio* (AR = major axis/minor axis) per GFP+ structure as observed in sisham treated controls, indicating a defect in cell elongation (Fig. 4D,E). Similarly, the natural decrease in *roundness* per GFP+ structure was significantly reduced in the siCngl1 treated group (Fig. 4D,E). These results were further confirmed by using a second set of siRNA that targeted Cgnl1 on different sequences (Sup.Fig. 7B).

The observed effects of Cgnl1 silencing on neovessel formation could be caused by changes in EC proliferation or apoptosis. However, Cgnl1 silencing did not immediately affect EC proliferation, as shown by lack of difference in BRDU incorporation and cell cycle progression (Sup.Fig. 8A, B) between the sisham and siCgnl1 treated groups at 4 and 12 hours post cell cycle initiation respectively. In addition, PI/AnnexinV analysis by flow cytometry showed that Cgnl1 silencing in HUVECs *in vitro* did not affect EC apoptosis at 4 hours post cell cycle activation (Sup.Fig. 8C). Together, these data imply that the inhibitory effect of Cgnl1 silencing on vascular formation is not direct dependent on cell proliferation and apoptosis, but may be mediated by Rho-family GTPase regulation of cell morphology via modification of the cytoskeleton.

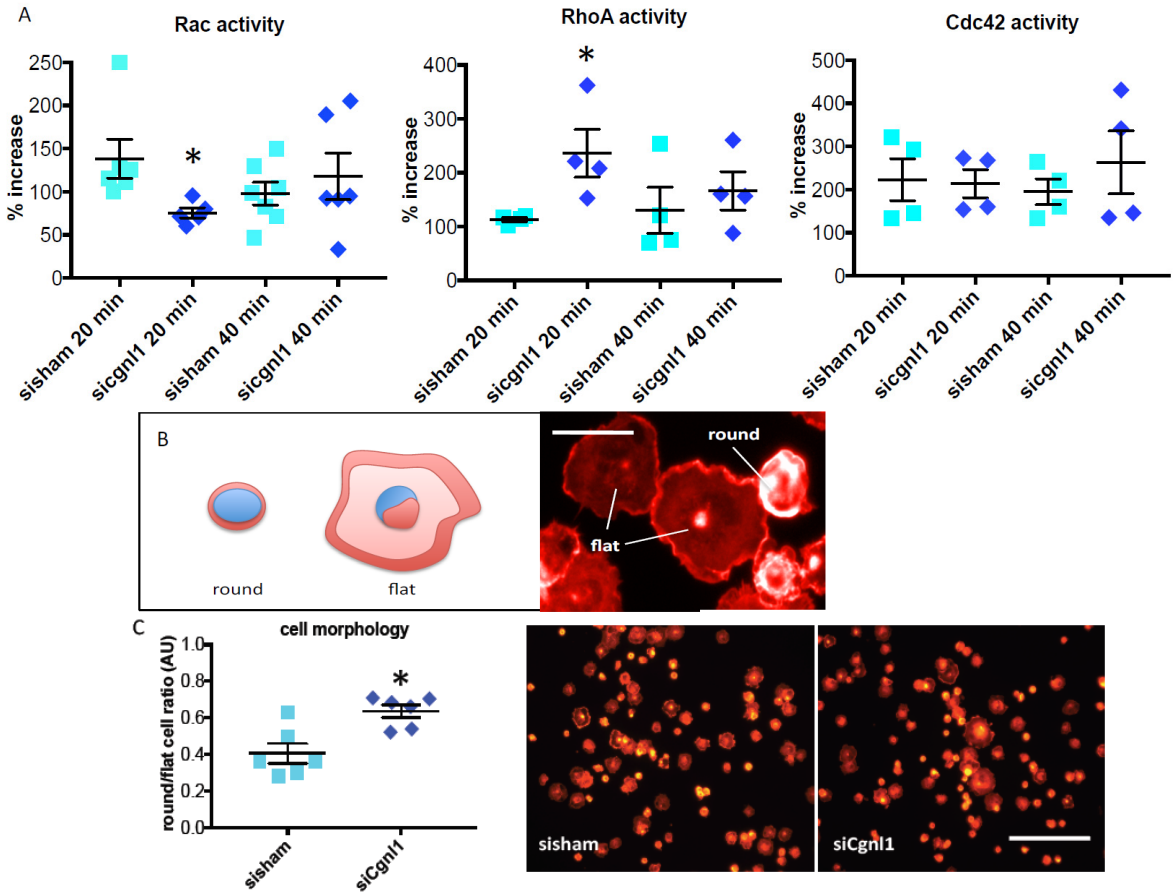

Figure 4: Cgnl1 regulates Rac1 and RhoA signalling and actin cytoskeleton dynamics

(A) Chemo-luminescence measurement of the GTP-bound small G-proteins in cell lysates from siCgnl1 or sisham-transfected HUVECs after 20 and 40 minutes of cell seeding, showing the levels of GTP-Rac1, GTP-Rho-A, and GTP-cdc42. Values represent means ± SD. *p<0.05 versus sisham in corresponding time group. n>4. Student's t-test. (B) Micrographs of typical results of a cell adhesion assay in which sisham and siCgnl1 treated HUVECs are seeded on a gelatine/collagen coated surface and analyzed for cell-spreading after 10 minutes adhesion. Scale bar represents 10 µm. (C) Actin visualized by phalloidine staining enables distinction between adherent cells (flat cell morphology) and non-adherent cells (round cell morphology). Scale bar represents 100 µm. Bargraph shows round/flat cell ratio in the siCgnl1 and sisham transfected groups. Values represent means ± SD. *p<0.05 versus sisham in corresponding group. n=6. Student's t-test.

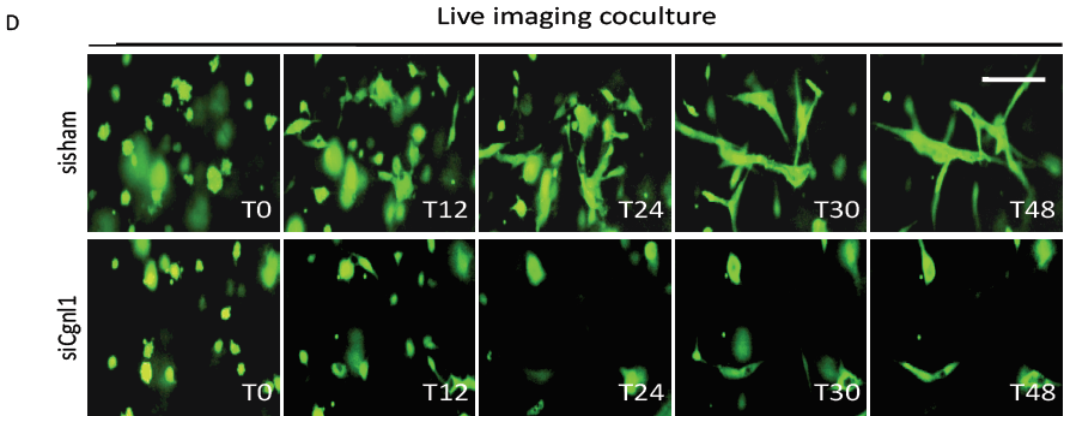

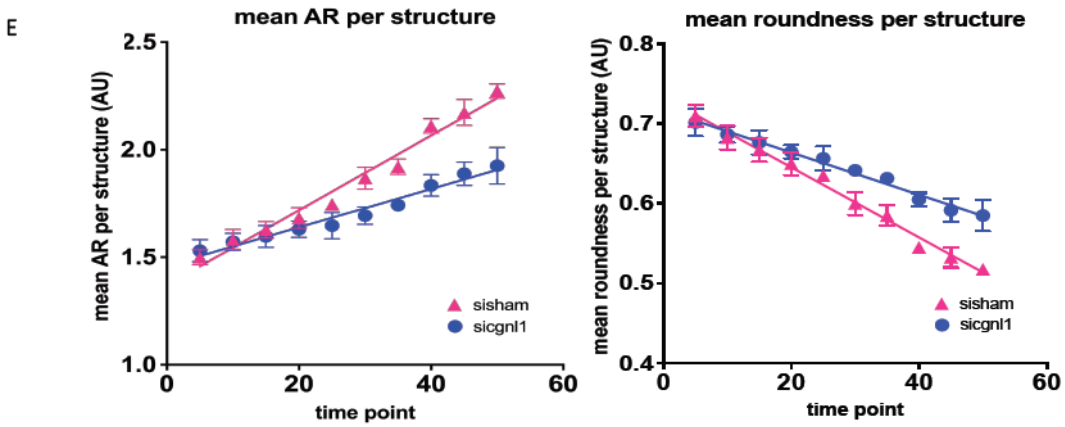

Figure 4: (D) Serial images of time-lapse imaging of HUVECs GFP cells seeded in 3D collagen coculture with pericytes in siCgnl1 and sisham group. Different time points (T) are shown. 1 time point represents 1 hour post seeding. Scale bar represents 50 μm. (E) Quantification of aspect ratio (AR) and roundness per HUVEC-GFP+ structure (from T = 0 to T = 50 post seeding). Each symbol represents average ± SD of 5 time points. Each time point is composed of 5 individual measurements. $p<0.0001$ for AR and roundness, siCngl1 versus sisham group, linear regression analysis, overall comparison.

Cgnl1 silencing disrupts Ve-cadherin association with the actin cytoskeleton and impairs Ve-cadherin adherens junction stabilization.

Co-localization of Cgnl1 with the actin cytoskeleton in kidney epithelial cells was previously reported. Here we assessed the intracellular localization of Cgnl1 in human endothelial cells. Cgnl1 antibody staining showed co-localization of Cgnl1 with phalloidin-stained actin filaments in HUVEC cultures (Fig. 5A). Protein association with the cytoskeleton can be evaluated by comparing the TritonX-100 insoluble with the TritonX-100 soluble fractions of cell extracts.[20] Comparison between the TritonX-100 soluble and insoluble compartment of confluent HUVEC cultures clearly showed a predominant presence of Cgnl1 in the Triton-X100 insoluble (cytoskeleton associated) fraction (Fig. 5B). Soluble and insoluble fractions were adequately separated, as shown by predominant enrichment of VEGFA in the soluble fraction (Sup.Fig. 9A).

Cgnl1 was previously shown to affect adherence junction stability via Rac1 activation in kidney epithelial cells[12]. Actin cytoskeleton association with Ve-cadherin is crucial for adherens junction formation and survival of the neovasculature. Hence, we evaluated the levels of Ve-cadherin in endothelial soluble and insoluble fractions. No difference was observed in the soluble fraction between the groups (Fig. 5C). In contrast, Cgnl1 silencing in confluent HUVEC monolayers significantly reduced the level of Ve-cadherin protein in the Triton-X100 insoluble (actin cytoskeleton associated) fraction as compared to the controls (Fig. 5D). Immunofluorescent microscopy revealed that Cgnl1 silencing affected Ve-cadherin localization at cell-cell contacts in confluent HUVEC monolayers *in vitro.* Thus, a significant decrease in Ve-cadherin+ adherens junction formation at the cell-cell borders was observed (Fig. 6A,B). This decrease in Ve-cadherin recruitment at adherens junctions in the Cngl1 silenced condition was also observed when the confluent layer of HUVECs was in contact with mural cells (pericytes) (Fig. 6C,D).

These data indicate that Cgnl1 promotes Ve-cadherin adherens junctions formation in endothelial cells.

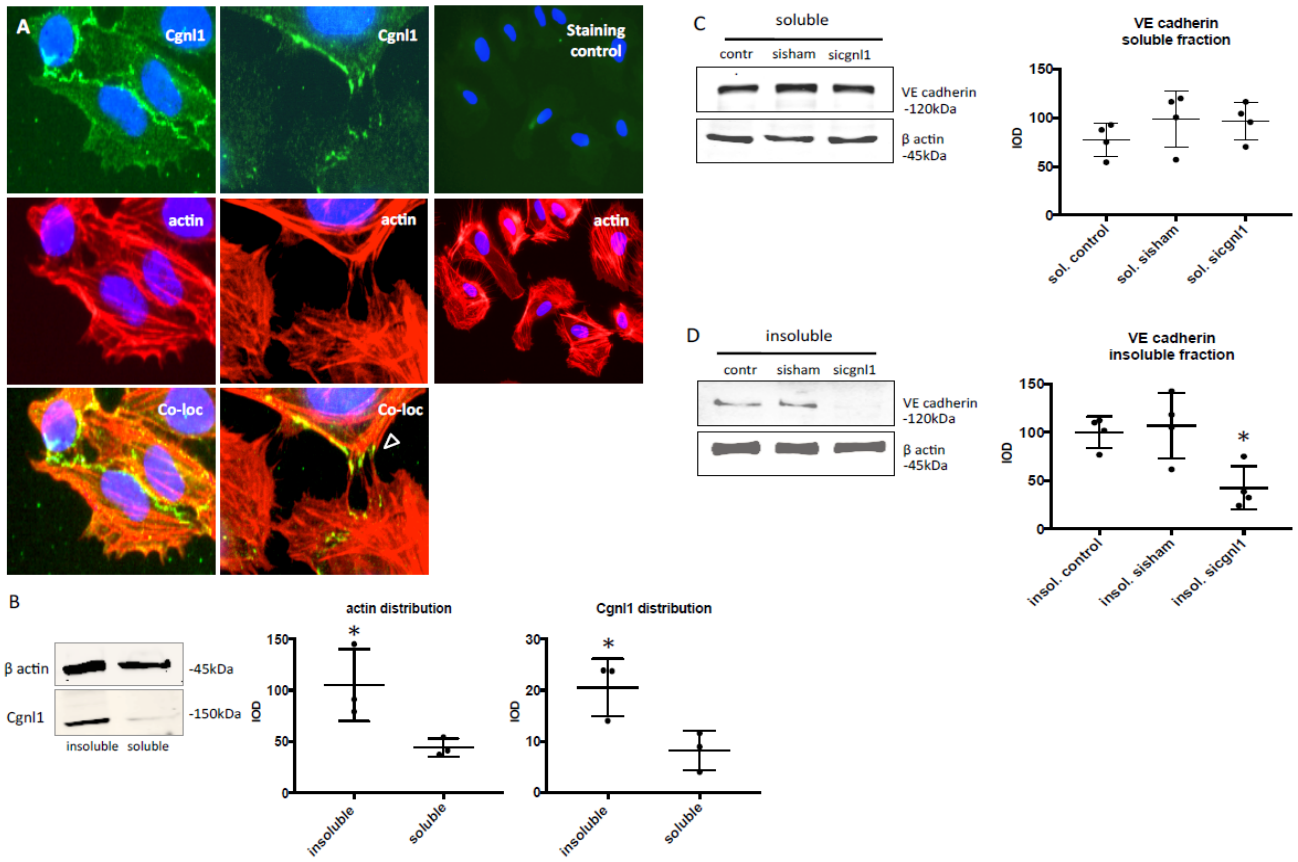

Figure 5: Cgnl1 silencing disrupts Ve-cadherin association with the actin cytoskeleton.

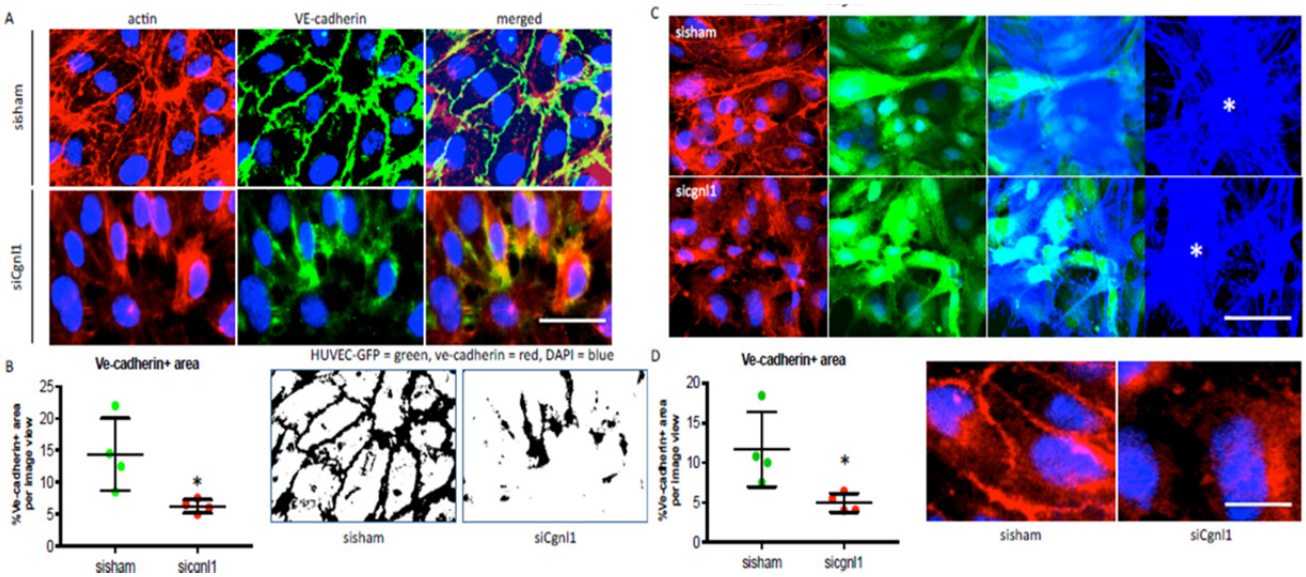

Figure 6: Cgnl1 silencing impairs Ve-cadherin adherens junction stabilization.

Figure 5: Cgnl1 silencing disrupts Ve-cadherin association with the actin cytoskeleton.
(A) Intracellular staining of HUVECs for Cgnl1 (green signal), DAPI (blue signal) and actin cytoskeleton filaments (red signal), arrowhead indicates Cgnl1 signal colocalized with actin fibers in filopodia during interaction with neighbouring cells. Immunostaining using a species-matched isotypic control validated Cgnl1 signal specificity, as shown in the third column. Micrographs are depicted at 40X (first two columns), and 20X magnification (third column). n=4. (B) Cgnl1 protein levels in HUVECs in the Triton-X insoluble fraction (the actin cytoskeleton associated compartment) versus the soluble fraction. Shown are representative Western blots for β actin and Cgnl1 (left). Graphs show quantified results (right). Values represent mean integrated optical density (IOD) ± SD corrected for β actin loading controls. *p<0.05 versus soluble. n=3. Student's t-test.
(C-D) Western blot results show Ve-cadherin protein level in the Triton-X soluble and insoluble fraction in siCgnl1-treated confluent HUVEC monolayers versus sisham or non-treated controls. Graphs show quantified results. Values represent mean integrated optical density (IOD) ± SD corrected for β actin loading controls. *p<0.05 versus sisham and control. n=4. One-way ANOVA.

Figure 6: Cgnl1 silencing impairs Ve-cadherin adherens junction stabilization.
(A) Representative micrographs of fluorescent immunostaining for actin (red) and Ve-cadherin (green) distribution in confluent HUVEC monolayers treated with set 1 siCngl1 versus sisham control. Scale bar represents 10 μm. (B) Quantification analysis of percentage of the Ve-cadherin+ area at cell junctions. Values represent means ± SD. *p<0.05 versus sisham. Images (right) show inverted version of micrographs used for quantification. Data obtained from 4 different experiments, with analysis of 12 different micrographs per group per experiment. One-way ANOVA. (C) Representative micrographs of z stack analysis of HUVEC-GFP culture on top of pericyte-RFP, showing the fluorescent signal of Ve-cadherin (shown in red, first column) in confluent HUVEC-GFP+ (GFP shown in green, second column) layer treated with siCngl1 versus sisham. DAPI signal in blue. Third column shows composite images of the phalloidin blue+ (Alexa Fluor 350) pericyte layer beneath the HUVECs-GFP (green). Last column shows isolated Z-stack layer of phalloidin blue+ pericytes (asterisk indicated). Scale bar represents 20 μm. (D) Quantification analysis of percentage of the Ve-cadherin+ area at cell junctions. Values represent means ± SD. *p<0.05 versus sisham and control. Images (right) show high details of Ve-cadherin at adherens junctions. Scale bar represents 5 μm. Data obtained from 4 different experiments, with analysis of 6 different micrographs per group per experiment. One-way ANOVA.

Cgnl1 silencing impairs FAK signalling and focal adhesion complex assembly.

Except for modulation of cell-cell junctions, Rac1 is a known key modulator of integrin-focal adhesion complex assembly, a process that plays a prominent role in endothelial cell morphological adaptation during tubule formation. Indeed activated (GTP bound) Rac1 was found to be recruited to initial focal adhesion sites.[21] As Cgnl1 modulates Rac1 activation, and endothelial cell adhesion was affected in Cgnl1 silenced HUVECs, we hypothesized that Cgnl1 may also affect focal adhesion complex assembly in response to endothelial cell-extracellular matrix (ECM) contact. We investigated the effect of Cgnl1 silencing on focal adhesion-assembly in the response to cell-ECM interaction. Immunofluorescent intracellular staining was

conducted on siCgnl1 or sisham treated HUVECs at 30, 60 and 120 minutes after seeding on gelatin/collagen coated glass slides. A significant defect in assembly of focal adhesion-structural proteins paxillin and vinculin (Fig. 7C-F) were observed in Cgnl1 silenced HUVECs at 60 minutes post seeding as compared to sisham controls (Fig. 7C-F). Recruitment and activation of FAK at nascent focal adhesion sites is required to strengthen and maturate the focal adhesion complex. Intracellular staining revealed that Cgnl1 silencing inhibited FAK recruitment at focal adhesion sites at 30, 60 and 120 minutes post seeding (Fig. 7A,B). This decrease in focal adhesion assembly in Cgnl1 silenced condition was also observed when the confluent layer of HUVECs was cultured in contact with mural cells (pericytes) (Sup.Fig. 9B,C), as shown by paxillin analysis. Western blot analysis also showed a significant decrease in vinculin, but not paxillin protein levels (Sup.Fig. 9D), indicating that the effects observed for vinculin may be directly linked to a reduction in vinculin protein. Western blot analysis showed no changes in total FAK protein levels in Cgnl1 silenced ECs (Sup.Fig. 9E). In contrast, a decline in phospho-Y397-FAK levels in siCgnl1-treated cells compared to sisham-treated controls was observed at 20 minutes after seeding (Fig. 7G), indicative of a reduction in FAK activation. Downstream activation of C-Src was impeded by Cgnl1 knockdown as well, shown by a decrease in phospho-Y418-C-Src at 40 minutes post-seeding, whereas total C-Src remained unaffected (Fig. 7H, and Sup.Fig. 9E). Combined, these data indicate that Cgnl1 silencing in endothelial cells diminishes focal adhesion assembly and FAK signalling in response to EC-ECM contact. These perturbations in the basic pathways of cell morphological adaption, in addition to the observed diminished assembly of Ve-cadherin adherens junctions, could induce instability of neovasculature and negatively affect the capacity of neovessels for further growth. To evaluate this concept, time lapse live imaging was conducted in the 3D collagen type I gel coculture system. GFP+ vascular structures were monitored for up to 125 time points post initiation of the assay (1 time point = 1 hour). Although in the early time points (<25 time points/hours), no difference in area per GFP+ structure between siCngl1 and sisham groups was observed, silencing of Cgnl1 in HUVECs-GFP at later time points (>25 time points/hours) significantly reduced the natural size increase per GFP+ vascular structure that was observed in sisham coculture conditions, indicating reduced tubule stability (Fig. 7I,J). Finally, these results were further confirmed by using a second set of siRNA that targeted Cgnl1 on different sequences (Sup.Fig. 9F).

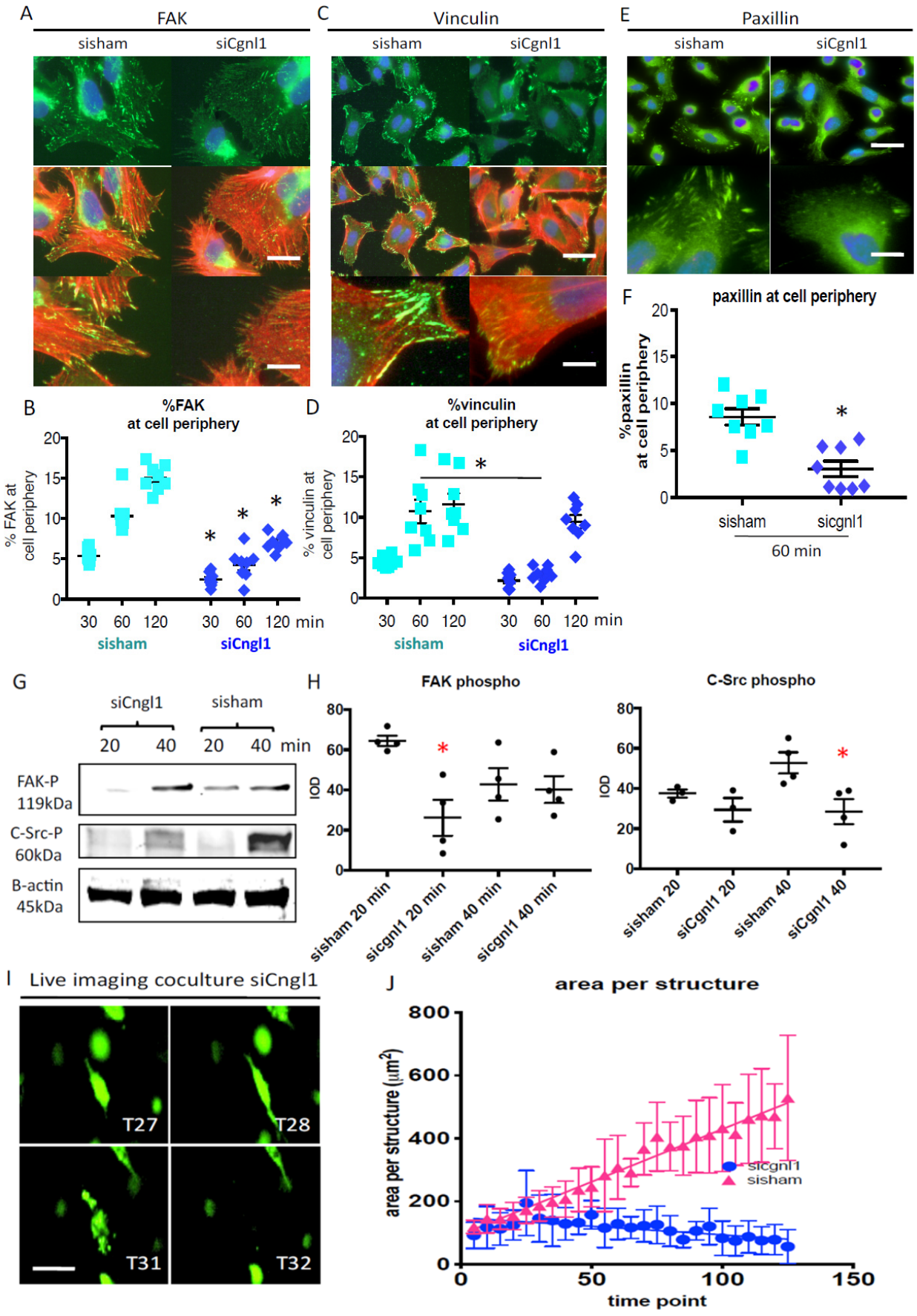
A
FAK
sisham
siCgnl1
C
Vinculin
sisham
siCgnl1
E
Paxillin
sisham
siCgnl1
B
%FAK
at cell periphery
% FAK at cell periphery
20
15
10
5
0
30 60 120 30 60 120 min
sisham
siCngl1
D
%vinculin
at cell periphery
% vinculin at cell periphery
20
15
10
5
0
30 60 120 30 60 120 min
sisham
siCngl1
F
paxillin at cell periphery
%paxillin at cell periphery
20
15
10
5
0
sisham
sicgnl1
60 min
G
siCngl1
sisham
20 40 20 40 min
FAK-P 119kDa
C-Src-P 60kDa
B-actin 45kDa
H
FAK phospho
IOD
80
60
40
20
0
sisham 20 min
sicgnl1 20 min
sisham 40 min
sicgnl1 40 min
C-Src phospho
IOD
80
60
40
20
0
sisham 20
siCgnl1 20
sisham 40
siCgnl1 40
I
Live imaging coculture siCngl1
T27
T28
T31
T32
J
area per structure
area per structure (μm²)
800
600
400
200
0
0
50
100
150
time point
sicgnl1
sisham

Figure 7: Cgnl1 inhibition hampers focal adhesion site assembly.
Representative micrographs of intracellular immunostaining in HUVECs for (A) focal adhesion signalling protein FAK (FITC) and the actin cytoskeleton (Phalloidin Rhodamine), for focal adhesion proteins (C) vinculin and (E) paxillin, in sisham and siCgnl1 tranfected HUVECs after 1 hour of adhesion to a gelatin/collagen coated underground. DAPI (blue signal). Upper two rows: Scale bar represents 5 μm. Lower rows show high magnification details. Scale bar represents 2 μm. Quantitative results of (B) %FAK, (D) % vinculin, and (F) %paxillin distribution at cell borders per image view adjusted for cell numbers at different time points of the adhesion assay. Values represent means ± SD. *p<0.05 versus time point matched sisham conditions. Data obtained from 8 different experiments with analysis of 12 different micrographs per group per experiment. Two-way ANOVA. Western blot analysis at 20 and 40 minutes after seeding of (G) FAK-phospho-Y397 and (H) C-Src-phospho-Y418 proteins level in siCgnl1-treated HUVECs compared to control groups. Quantified values in graph are shown in mean integrated optical density (IOD) ± SD corrected for β actin loading controls. *p<0.05 versus sisham and control of corresponding time points. n=3-4. Student's t-test for comparison within 1 time point. β actin protein level was assessed as a loading control and did not differ between the control, sisham and siCgnl1 samples (data not shown). (I) Serial images of time-lapse imaging of HUVECs GFP cells seeded in 3D collagen coculture with pericytes in siCgnl1 group. Different time points (T) are shown. 1 time point represents 1 hour post seeding. Scalebar represents 10 μm. (J) Quantification of area per HUVEC-GFP+ structure (from T = 0 to T = 125 post seeding). Each symbol represents average area per structure ± SD of 5 time points. Each time point is composed of 5 individual measurements. p<0.0001, siCngl1 versus sisham group, linear regression analysis, overall comparison.

Discussion

In the present study we report several findings: (1) Unlike cingulin, Cgnl1 expression is mainly enriched in endothelial cells during vascular growth. (2) Cgnl1 is pivotal for stable tubule structure formation during new vessel formation, as shown *in vitro* using loss-of function studies in a 3D matrix co-culture system that uses primary human endothelial cells and supporting mural cells. (3) Cgnl1 is critical for vascular growth *in vivo*, as shown in the murine retina vascularization model. (4) Cgnl1 in endothelial cells promotes Ve-cadherin association with the actin cytoskeleton and induces adherens junction stabilization. (5) Cgnl1 promotes focal adhesion assembly in response to endothelial cells-extracellular matrix contact. To our knowledge this is the first study to identify Cgnl1 as an important regulator of new vessel formation both *in vitro* and *in vivo*. It also provides new evidence for the involvement of Cngl1 in the regulation of Ve-cadherin assembly at adherens junctions in endothelial cells.

High level of expression of Cgnl1 in endothelial cells

Cgnl1 was reported to be highly expressed in renal epithelial cells.[12, 22] We detected significant higher Cgnl1 expression levels in Flk1+ (endothelial cells) versus Flk1- (non-endothelial cells) at different stages of mouse embryo development. Using *in situ* hybridization we showed that Cngl1 expression in developing zebrafish larvae is mainly observed in vascular structures. In human bloodvessels, we detected a strong endothelial Cngl1 signal by immunochemistry. Our observations are in line with the findings of Nurumiya *et al*., who reported that Cgnl1 was highly expressed in CD31+ (endothelial) cells in mouse embryos on embryonic day (E)8.5 and E9.5.[23] These data imply a role for Cngl1 in the regulation of endothelial cell function.

Cgnl1 regulates stable tubule structure formation and proves crucial for in vitro and in vivo angiogenesis

Cgnl1 has been implicated to be involved in the regulation of endothelial cell junctions: In a study focussed on the regulation of ZO-1 in cultured human dermal microvascular cells (HDMEC), Tornavaca *et al.* reported that Cgnl1 was located at tight junctions of confluent HDMEC monolayers. ZO-1 silencing in HDMECs led to reduced localization at tight junctions of Cngl1, whereas Cngl1 silencing led to redistribution of vinculin from cell junctions to focal adhesions and promoted stress fibers formation. ZO-1 and p114rhoGEF were shown to co-immunoprecipitate with Cgnl1, indicating direct binding between these proteins.[14] Combined, the data of Tornavaca *et al.* indicate that p114RhoGEF together with ZO-1 and Cngl1 stimulate junctional actomyosin activation, leading to coupling of mechanotransducers to the tight junction complex, thereby ensuring barrier function of the endothelium. However, no direct evidence was provided to demonstrate a role for cngl1 in the process of angiogenesis, and in particular tubule structure formation.

In our study, we provide for the first time both *in vitro* (3D coculture assay) and *in vivo data* (murine retina vascularization model) that demonstrate that Cgnl1 silencing significantly inhibits

the angiogenic capacity of vascular cells. Cgnl1 silencing greatly impaired tubule structure formation in the 3D coculture assay, and diminished the number of vascular structures formed during vascular expansion in the developing retina.

Cgnl1 in endothelial cells promotes Ve-cadherin association with the actin cytoskeleton and induces adherens junction stabilization.

The molecular mechanism of Cgnl1 has been mainly investigated *in vitro* in epithelial kidney cells, although it has also been shown in cultured urotherial cells that expression levels of Cngl1 is tightly regulated by miR-205.[24] In renal epithelial cells, Cgnl1 was identified as a cell-cell junctional complex adaptor protein.[10, 12] After recruitment of Cngnl1 to the tight junctions via ZO-1, Cgnl1 promotes Rac1 activation via Tiam1, and inhibits RhoA activity by GEFH1 inhibition[12]. Other studies have also indicated that Cgnl1 localizes in adherens junctions.[10, 25] Only one study reported the function of Cngl1 in vascular endothelial cells (HDMECs). Similar to the findings in epithelial kidney cells, this study in HDMECs demonstrated a regulatory role for ZO-1 in tight junction recruitment of Cgnl1.[14]

In our study, we focused on the regulation of Cgnl1 of adherens junctions via GTPases and actomyosin regulation. In line with the findings in renal epithelial cells, our data showed that Cgnl1 silencing in HUVECs inhibited Rac1 and promoted RhoA activity respectively, which led to impaired Ve-cadherin colocalization with actin filaments at adherens junction sites. The actin cytoskeleton at the cell periphery is composed of a highly organized meshwork of filamentous actin, which is closely associated with the nearby plasma membrane with cell-cell junction and ECM-cell focal adhesion complexes. Intracellular Cgnl1 co-localized with actin filaments,[10, 12] and Cgnl1 knockdown delayed cadherin recruitment and subsequent adherens junction assembly in epithelial cells. Our findings demonstrate that Cgnl1 is co-localized with the actin cytoskeleton and is enriched in the Triton-X100 insoluble (actin cytoskeleton-associated) fraction in endothelial cells. Knockdown of Cgnl1 induced Ve-cadherin-actin dissociation, implied by a decline in Ve-cadherin in the Triton-X100 insoluble compartment, and a decrease in Ve-cadherin accumulation at adherens junction sites. Combined with previous reported findings, the data demonstrate that Cgnl1 could affect vascular growth by promoting adherens junction stabilization.

Cgnl1 promotes focal adhesion assembly in response to endothelial cells-extracellular matrix contact.

Focal adhesions are dynamic protein complexes that provide a linkage point between the cells extra- and intra-cellular environment, playing a central role in migration and cell adhesion.[26, 27] Rac1 deletion significantly inhibited focal adhesion assembly in mouse embryonic fibroblasts, whereas overexpression of an active RhoA mutant failed to rescue the observed phenotype.[26] In a transgenic mouse model, expression of a constitutively active form of Rac1 altered focal adhesion structures.[28] The previous study in HDMECs demonstrated a regulatory role of Cgnl1 in

vinculin distribution to focal adhesions. In line with these observations, our study showed that Cgnl1 silencing impaired focal adhesion assembly, coinciding with a reduction in Rac1 activation.

Proposed mechanism for Cngl1 in neovessel formation

Based on our findings on the important role for Cgnl1 in vessel formation, we hypothesize that the main function of Cgnl1 during vascular growth is tubule formation by control of adherens junction and focal adhesion assembly via regulation of Rac1 activity. Initial contacts between ECs are relatively weak, with serrated Ve-cadherin junctions, providing ECs with high motility to respond to e.g. VEGFA gradients.[19, 29] In contrast, Notch signalling, provided either by neighbouring endothelial tip cells, or by pericytes via Notch ligand presentation, has been shown to promote the formation of strong cell-cell contacts with immobile straight Ve-cadherin junctions, that limit the migration capacity of the connected cells.[17, 19, 29] Based on our (live imaging) findings, which highlight the inhibitory effects of siCgnl1 on the capacity of ECs to undergo stable morphological adaptations to form and extend 3D neo tubule structures, Cngl1 could be mainly involved in the formation of strong Ve-cadherin junctions that promote immobile cell-cell connections in response to Notch signalling provided by pericytes, while it has a limited impact on initial weak (Ve-cadherin) bond formation. Indeed, our data demonstrate that Cngl1 expression in HUVECs is significantly enhanced by direct cell contact with pericytes. Furthermore, this induction of Cgnl1 expression in HUVECs is facilitated via Notch signalling, as knockdown of Notch1/4 and DLL4 in both cell types severely impeded the Cgnl1 induction in HUVECs in response to pericyte stimulation. Our data further demonstrate that Cngl1 upregulation in HUVECs by Notch signalling with pericytes enhances endothelial Rac1 activity. In further support of this concept, our analysis of the time lapse data indeed reveals that siCngl1 structures are more instable compared to sisham structures, negatively affecting the capacity of the individual neovessels for elongation beyond the 2-3 cell stage.

Thus, based on our current findings, we propose a working mechanism for Cngl1 in which pericyte-induced upregulation of Cngl1 in endothelial cells via Notch signalling promotes the formation of strong Ve-cadherin adherens junctions via Rac1 activation. Simultaneously, Cngl1 mediated Rac1 activation stimulates assembly of integrins-focal adhesion complexes. Combined, formation of both strong adherens junctions and focal adhesions ensures stabilization and further elongation of neovascular tubules (Sup.Fig. 10).

Limitations of the study

The use of siRNA to target Cgnl1 in the murine retinal vascularization model evokes a mild influx of IB4-possitive immune cells that may affect vascular growth. To be able to make a distinction between the effects that are the result of Cgnl1 inhibition and the effects that are linked to the use of siRNA, we injected the control retinas with a set of non-targeting siRNAs. As we compared non-targeting siRNA with Cgnl1 targeting siRNA treated conditions, we consider the observed vascular phenotype, at least in part, to be the direct result of Cngl1 silencing, and not

merely a side effect of immune cells activation by siRNA treatment itself. However, it cannot be entirely excluded that the observed effects of Cngl1 silencing in the murine retina model may have been facilitated by a background of increased immune activation. Although the Triton-X lysate separation method could help to distinguish soluble and insoluble fractions, our data set only provides evidence that Cngl1 is enriched in the same insoluble fraction as cytoskeletal actin, and does not show direct binding between Cngl1 and actin protein.

Conclusions

Cgnl1 mediates vascular growth by stabilizing newly formed vascular tubules via adherens junction stabilization in endothelial cells. Stimulation of neovessels by recruited pericytes via cross-cell type Notch signaling enhances the Cgnl1-mediated stabilization process in endothelial cells. Our findings support an important function of Cgnl1 in regulation of vascular growth during embryonic development and vascular-related disease in adulthood.

References

1. Carmeliet P. Angiogenesis in life, disease and medicine. *Nature*. 2005;438:932-6.
2. Jain RK. Molecular regulation of vessel maturation. *Nat Med*. 2003;9:685-93.
3. Spindler V, Schlegel N and Waschke J. Role of GTPases in control of microvascular permeability. *Cardiovasc Res*. 2010;87:243-53.
4. Fryer BH and Field J. Rho, Rac, Pak and angiogenesis: old roles and newly identified responsibilities in endothelial cells. *Cancer Lett*. 2005;229:13-23.
5. Heasman SJ and Ridley AJ. Mammalian Rho GTPases: new insights into their functions from in vivo studies. *Nat Rev Mol Cell Biol*. 2008;9:690-701.
6. Tan W, Palmby TR, Gavard J, Amornphimoltham P, Zheng Y and Gutkind JS. An essential role for Rac1 in endothelial cell function and vascular development. *FASEB J*. 2008;22:1829-38.
7. Dejana E, Orsenigo F and Lampugnani MG. The role of adherens junctions and VE-cadherin in the control of vascular permeability. *J Cell Sci*. 2008;121:2115-22.
8. Lampugnani MG and Dejana E. Adherens junctions in endothelial cells regulate vessel maintenance and angiogenesis. *Thromb Res*. 2007;120 Suppl 2:S1-6.
9. Hall A.Rho GTPases and the control of cell behaviour.*Biochem Soc Trans*. 2005;33:891-5.
10. Guillemot L, Guerrera D, Spadaro D, Tapia R, Jond L and Citi S. MgcRacGAP interacts with cingulin and paracingulin to regulate Rac1 activation and development of the tight junction barrier during epithelial junction assembly. *Mol Biol Cell*. 2014;25:1995-2005.
11. Guillemot L, Schneider Y, Brun P, Castagliuolo I, Pizzuti D, Martines D, Jond L, Bongiovanni M and Citi S. Cingulin is dispensable for epithelial barrier function and tight junction structure, and plays a role in the control of claudin-2 expression and response to duodenal mucosa injury. *J Cell Sci*. 2012;125:5005-14.
12. Guillemot L, Paschoud S, Jond L, Foglia A and Citi S. Paracingulin regulates the activity of Rac1 and RhoA GTPases by recruiting Tiam1 and GEF-H1 to epithelial junctions. *Mol Biol Cell*. 2008;19:4442-53.
13. Cheng C, Haasdijk R, Tempel D, van de Kamp EH, Herpers R, Bos F, Den Dekker WK, Blonden LA, de Jong R, Burgisser PE, Chrifi I, Biessen EA, Dimmeler S, Schulte-Merker S and Duckers HJ. Endothelial cell-specific FGD5 involvement in vascular pruning defines neovessel fate in mice. *Circulation*. 2012;125:3142-58.
14. Tornavaca O, Chia M, Dufton N, Almagro LO, Conway DE, Randi AM, Schwartz MA, Matter K and Balda MS. ZO-1 controls endothelial adherens junctions, cell-cell tension, angiogenesis, and barrier formation. *J Cell Biol*. 2015;208:821-38.
15. van Dijk CG, Nieuweboer FE, Pei JY, Xu YJ, Burgisser P, van Mulligen E, el Azzouzi H, Duncker DJ, Verhaar MC and Cheng C. The complex mural cell: pericyte function in health and disease. *Int J Cardiol*. 2015;190:75-89.

16. Kofler NM, Cuervo H, Uh MK, Murtomaki A and Kitajewski J. Combined deficiency of Notch1 and Notch3 causes pericyte dysfunction, models CADASIL, and results in arteriovenous malformations. *Sci Rep*. 2015;5:16449.
17. Winkler EA, Bell RD and Zlokovic BV. Central nervous system pericytes in health and disease. *Nat Neurosci*. 2011;14:1398-405.
18. Gaengel K, Genove G, Armulik A and Betsholtz C. Endothelial-mural cell signaling in vascular development and angiogenesis. *Arterioscler Thromb Vasc Biol*. 2009;29:630-8.
19. Bentley K, Franco CA, Philippides A, Blanco R, Dierkes M, Gebala V, Stanchi F, Jones M, Aspalter IM, Cagna G, Westrom S, Claesson-Welsh L, Vestweber D and Gerhardt H. The role of differential VE-cadherin dynamics in cell rearrangement during angiogenesis. *Nat Cell Biol*. 2014;16:309-21.
20. Kim SH, Cho YR, Kim HJ, Oh JS, Ahn EK, Ko HJ, Hwang BJ, Lee SJ, Cho Y, Kim YK, Stetler-Stevenson WG and Seo DW. Antagonism of VEGF-A-induced increase in vascular permeability by an integrin alpha3beta1-Shp-1-cAMP/PKA pathway. *Blood*. 2012;120:4892-902.
21. Chang F, Lemmon CA, Park D and Romer LH. FAK potentiates Rac1 activation and localization to matrix adhesion sites: a role for betaPIX. *Mol Biol Cell*. 2007;18:253-64.
22. Paschoud S, Yu D, Pulimeno P, Jond L, Turner JR and Citi S. Cingulin and paracingulin show similar dynamic behaviour, but are recruited independently to junctions. *Mol Membr Biol*. 2011;28:123-35.
23. Narumiya H, Hidaka K, Shirai M, Terami H, Aburatani H and Morisaki T. Endocardiogenesis in embryoid bodies: novel markers identified by gene expression profiling. *Biochem Biophys Res Commun*. 2007;357:896-902.
24. Chung PJ, Chi LM, Chen CL, Liang CL, Lin CT, Chang YX, Chen CH and Chang YS. MicroRNA-205 targets tight junction-related proteins during urothelial cellular differentiation. *Molecular & Cellular Proteomics*. 2014;13:2321–2336.
25. Ohnishi H, Nakahara T, Furuse K, Sasaki H, Tsukita S and Furuse M. JACOP, a novel plaque protein localizing at the apical junctional complex with sequence similarity to cingulin. *J Biol Chem*. 2004;279:46014-22.
26. Guo F, Debidda M, Yang L, Williams DA and Zheng Y. Genetic deletion of Rac1 GTPase reveals its critical role in actin stress fiber formation and focal adhesion complex assembly. *J Biol Chem*. 2006;281:18652-9.
27. Goetz JG. Bidirectional control of the inner dynamics of focal adhesions promotes cell migration. *Cell Adh Migr*. 2009;3:185-90.
28. Sussman MA, Welch S, Walker A, Klevitsky R, Hewett TE, Price RL, Schaefer E and Yager K. Altered focal adhesion regulation correlates with cardiomyopathy in mice expressing constitutively active rac1. *J Clin Invest*. 2000;105:875-86.
29. Choi CK and Chen CS. Jostling for position in angiogenic sprouts: continuous rearrangement of cells explained by differential adhesion dynamics. *EMBO J*. 2014;33:1089-90.

Supplement data

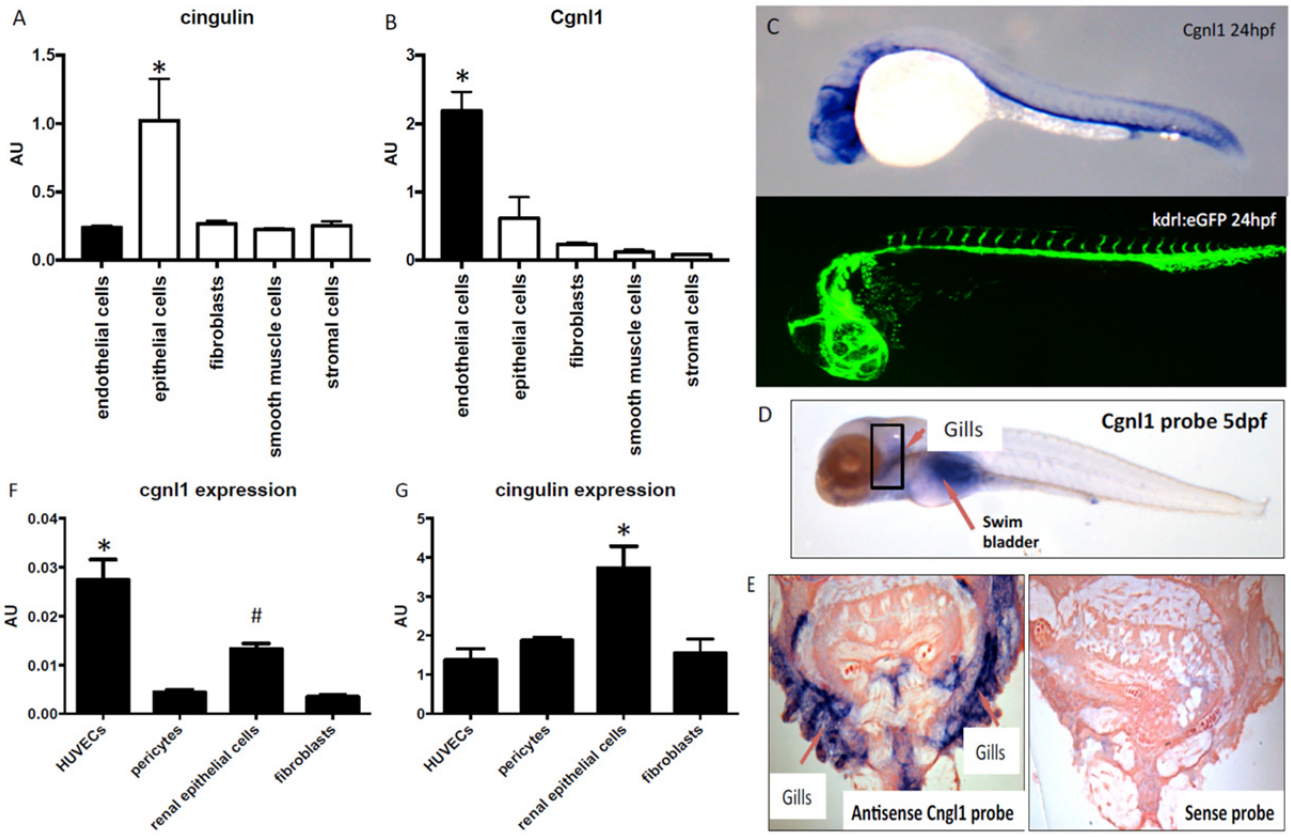

S.Figure 1: Data-mining of GEO-datasets show mRNA expression of different types of cultured human cells, including endothelial cells, epithelial cells, fibroblasts, smooth muscle cells and stromal cells, derived from different organs. Bar graphs indicate the expression levels of cingulin (A) and Cgnl1 (B). Shown are values of the mean ± SEM in arbitrary units (AU). *p<0.05 versus other cell types. (C) Upper image shows typical result of *in situ* hybridization (ISH) using an anti-sense probe specific for the zebrafish orthologue of Cgnl1 in developing zebrafish larvae at 24 hpf. The observed ISH pattern of the Cgnl1 anti-probe is very similar to the vascular GFP pattern (GFP expression driven by vascular kdrl promoter) observed in Tg(kdrl;eGFP)y1 zebrafish line at similar time point, shown in lower image. Lower and upper images do not display the same specimen. (D) Typical result of ISH using an anti-sense probe specific for the zebrafish orthologue of Cgnl1 in developing zebrafish larvae at 5 dpf. (E) Cross sections of the head region (gill area) showing the signal after ISH with anti-sense (Cngl1 detection) and sense (control) probe. Arrows point to Cngl1 ISH signal in gills. QPCR analysis of (F) Cgnl1 and (G) cingulin expression in human cells, including human venous endothelial cells (HUVECs compared to non-relevant cell types (pericytes, renal epithelial cells, and fibroblasts). Data obtained from 3 separate experiments, 2 samples per experiment. For F, *p<0.05 HUVECs versus pericytes, renal epithelial cells, and fibroblasts. #p<0.05 renal epithelial cells versus HUVECs, pericytes and fibroblasts. For G, *p<0.05 renal epithelial cells versus HUVECs, pericytes and fibroblasts. Values represent mean target/ house keeping gene ratio in AU ± SEM. One-way ANOVA.

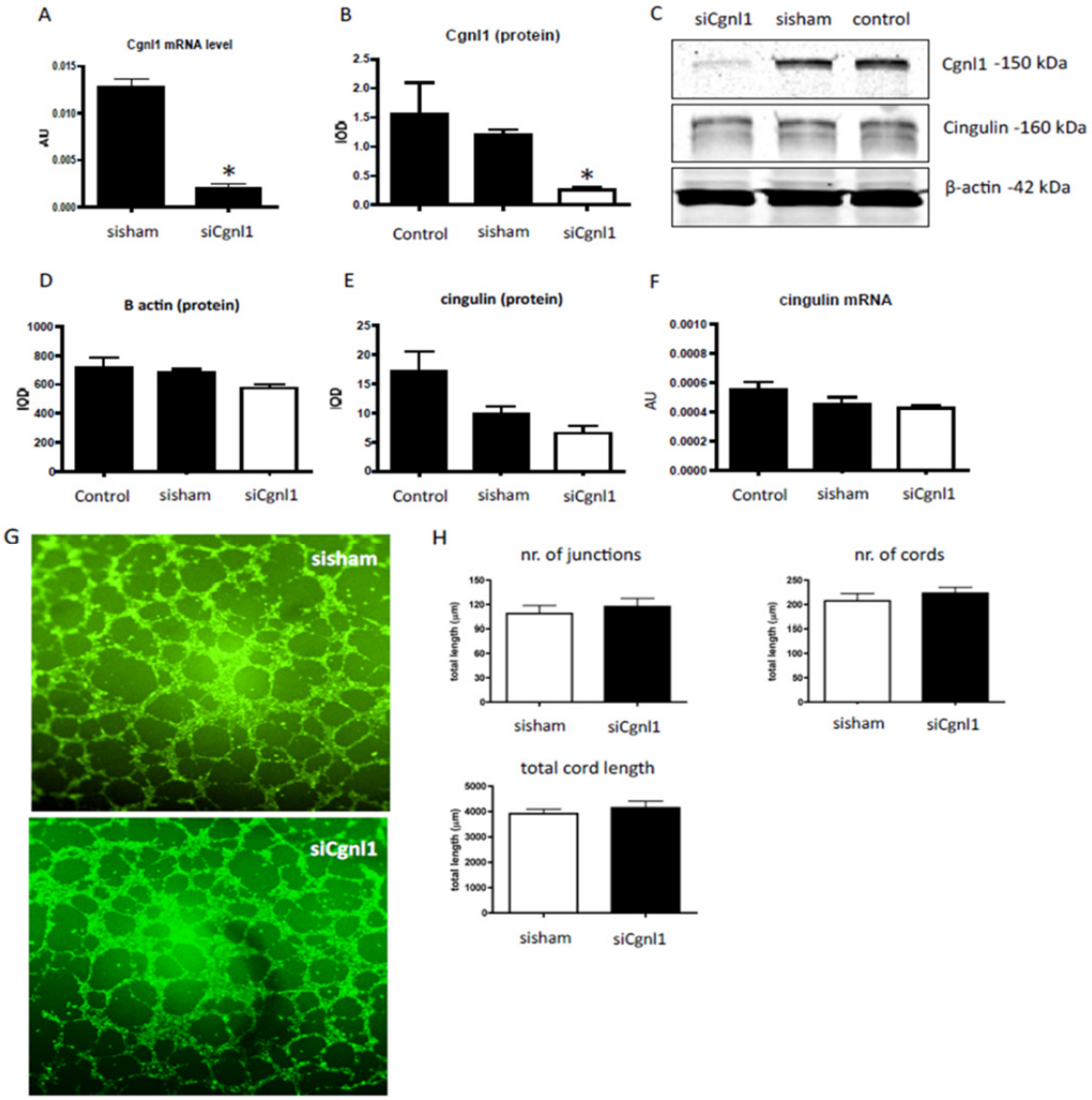

S.Figure 2: Validation of knockdown efficiency. (A) *In vitro* transfection of HUVECs Cgnl1-targeting siRNA followed by qPCR analysis at 2 days post-transfection demonstrates effect of Cgnl1 silencing on Cgnl1 expression compared to nontargeting scrambled siRNA (sisham) transfected HUVECs (~80% reduction) n=4. Student's t-test. (B) Western blot analysis of Cgnl1 protein signal in siCgnl1 as compared to sisham treated HUVECs or non-transfected cells. (C) A representative blot is shown of 3 separate experiments. (D) Quantified protein levels of ß actin loading control in the different groups. Effect of siRNA mediated knockdown of Cgnl1 on (E) cingulin protein (F) or mRNA levels. For protein quantification, values represent mean integrated optical density (IOD) ± SEM corrected for β-actin loading controls. For mRNA quantification, values represent mean target/ house keeping gene ratio in arbitrary units (AU) ± SEM.
*p<0.05 siCgnl1 versus control and sisham. One-way ANOVA. (G) Representative result of a cord formation assay in standard 2D Matrigel following Cgnl1 silencing or sham siRNA transfection in HUVECs. HUVECs were visualized by Calcein-AM uptake. 4X magnification. (H) Quantitative analysis of the Matrigel assays shows effect of Cgnl1 silencing on the number of junctions, cords, and total cord length compared to sishamtreated HUVECs. Data obtained from 3 individual experiments with >8 wells analyzed per group. Values represent means ± SEM. Student's t-test.

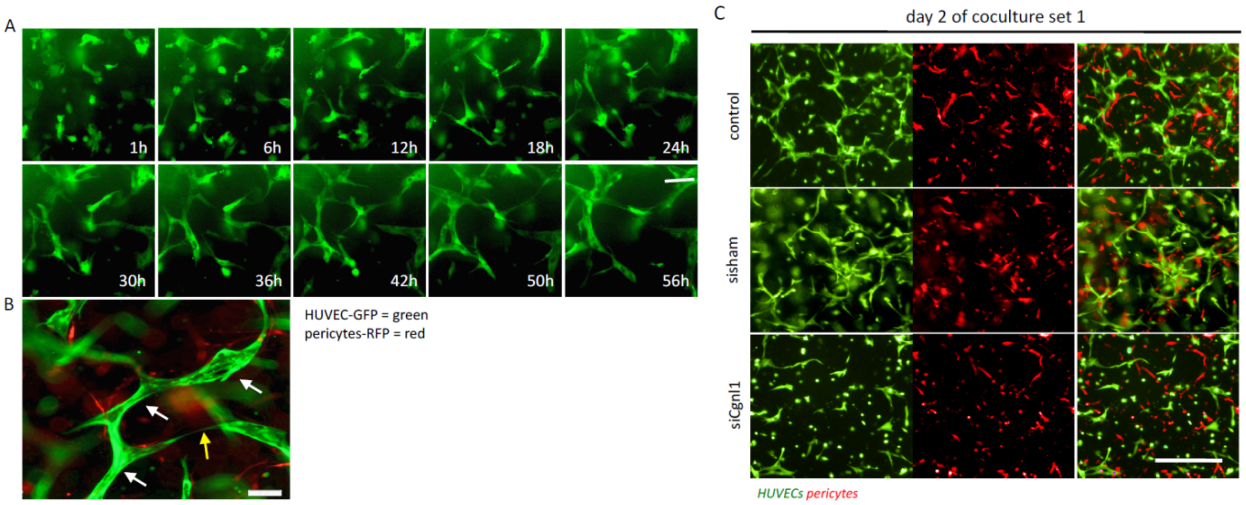

S.Figure 3: (A) Time series of a time lapse movie, showing angiogenesis in the 3D collagen coculture assay. Pericytes are present but not labelled. HUVECs are labelled with GFP marker. Indicated are hours post initiation of the assay. Scale bar represents 25 µm. (B) High magnification micrograph demonstrates lumenized vascular (GFP+) structures with pericyte (RFP+) coverage. Arrows indicate open (white) and closed (yellow) lumen areas. Scale bar represents 25 µm. (C) Representative results at day 2 in 3D collagen matrix coculture following Cgnl1 silencing or sham siRNA transfection in HUVEC-GFP (green). Pericytes are marked by RPF (red). Scale bar represents 100 µm.

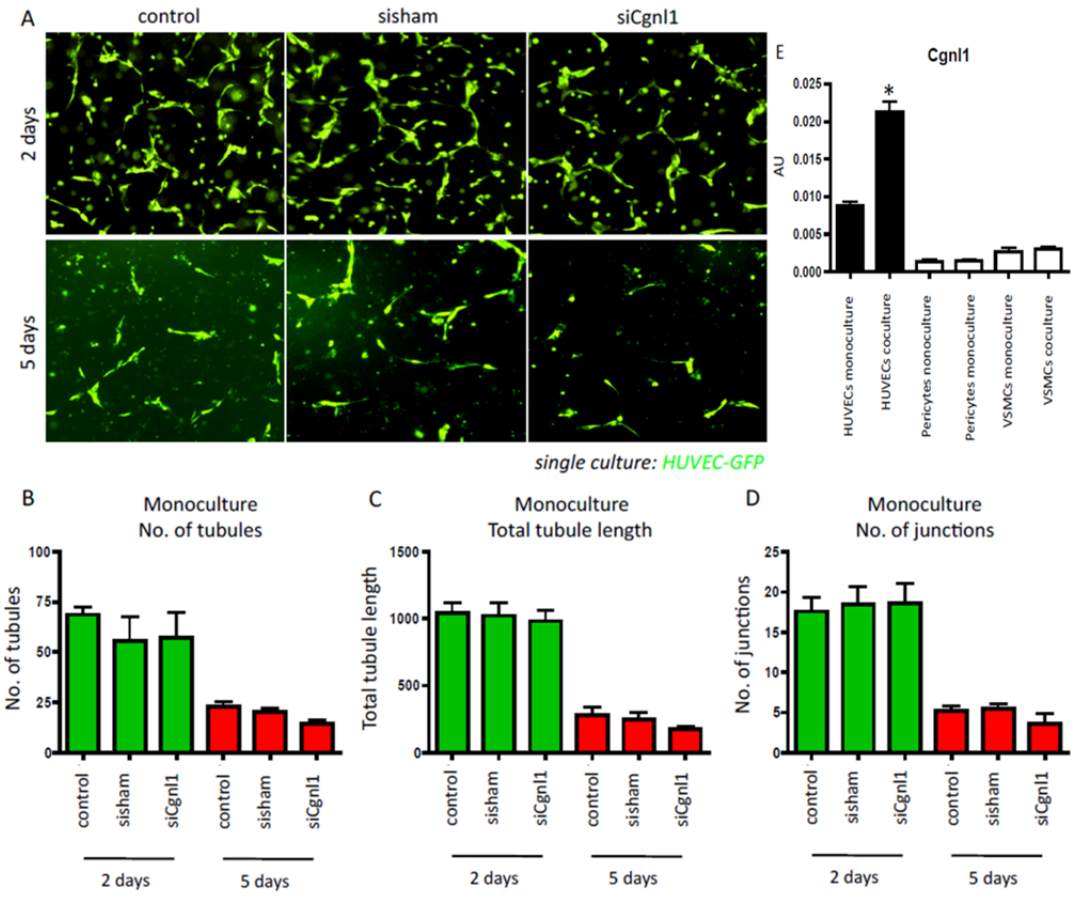

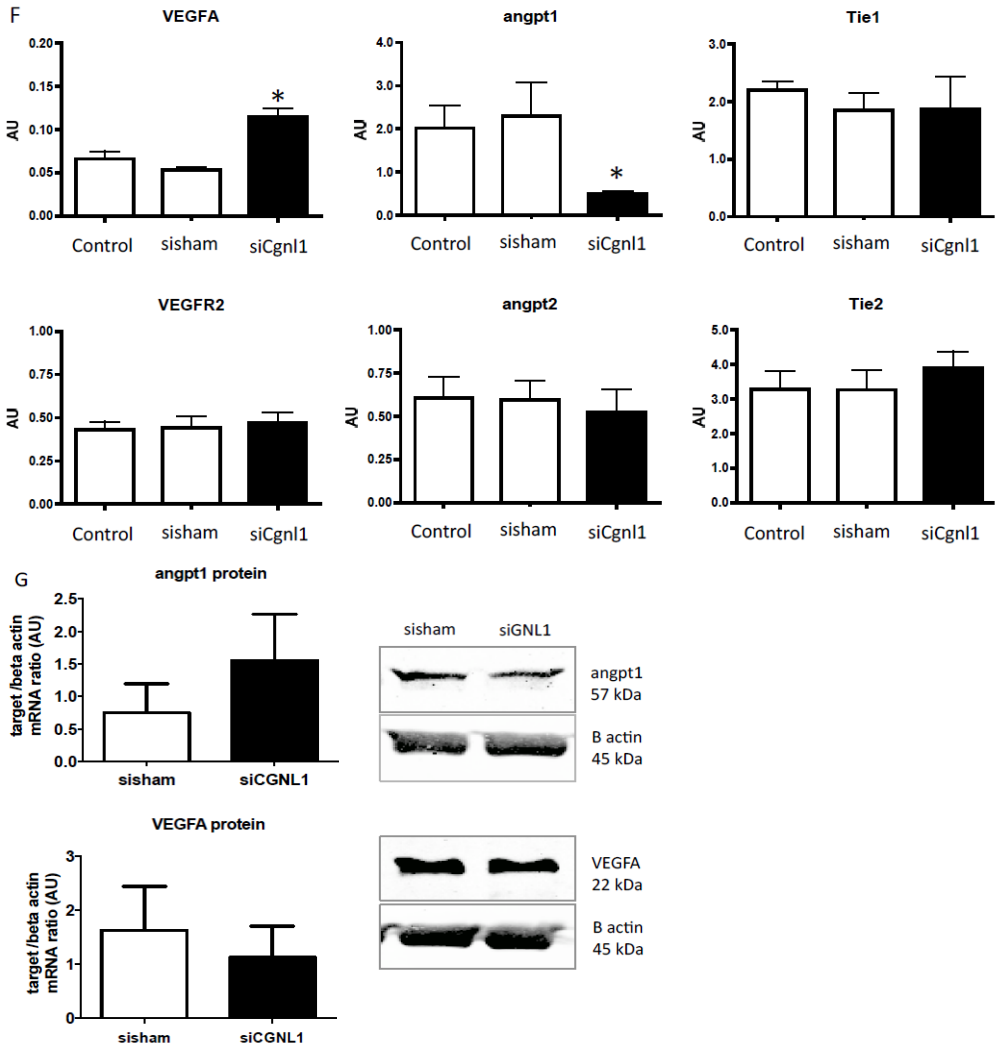

S.Figure 4: (A) Representative results at day 2 and 5 in 3D collagen assay without pericyte coculture, following Cgnl1 silencing or sham siRNA transfection in HUVEC-GFP. HUVECs are marked by GFP (green). 20X magnification. Quantitative analysis of assay results shows the effect of Cngnl1 silencing on the number of (B) tubules, (C) total tubule length, and number of (D) junctions compared to sisham-treated and non-transfected HUVEC-GFP in monoculture conditions. Data obtained from 3 individual experiments, with >8 wells analyzed per group, per experiment. Values represent means target/ house keeping gene ratio in AU ± SEM. Red bars indicate data obtained from 5 days coculture, and green bars indicate data obtained from 2 days coculture. One-way ANOVA for comparisons within one time point. (E) QPCR analysis of Cngnl1 mRNA levels in HUVEC monocultures and HUVECs cocultured with mural cells (pericytes or VMSCs). Values represent means ± SEM. *p<0.05 HUVECs coculture versus other conditions. One-way ANOVA. (F) Cgnl1 silencing induced changes in endothelial expression profile of VEGFA, angpt1, Tie1, VEGFR2, angpt2, Tie2. Values represent mean target/ house keeping gene ratio in AU ± SEM. *p<0.05 versus control and sisham. Data obtained from 3 different experiments with 2 samples per experiment. One-way ANOVA. (G) Quantified western blot results for VEGFA and angpt1 protein levels. Shown are representative immuno blots. Values represent mean integrated optical density (IOD) ± SD corrected for β-actin loading controls. (n=4). Student's t-test.

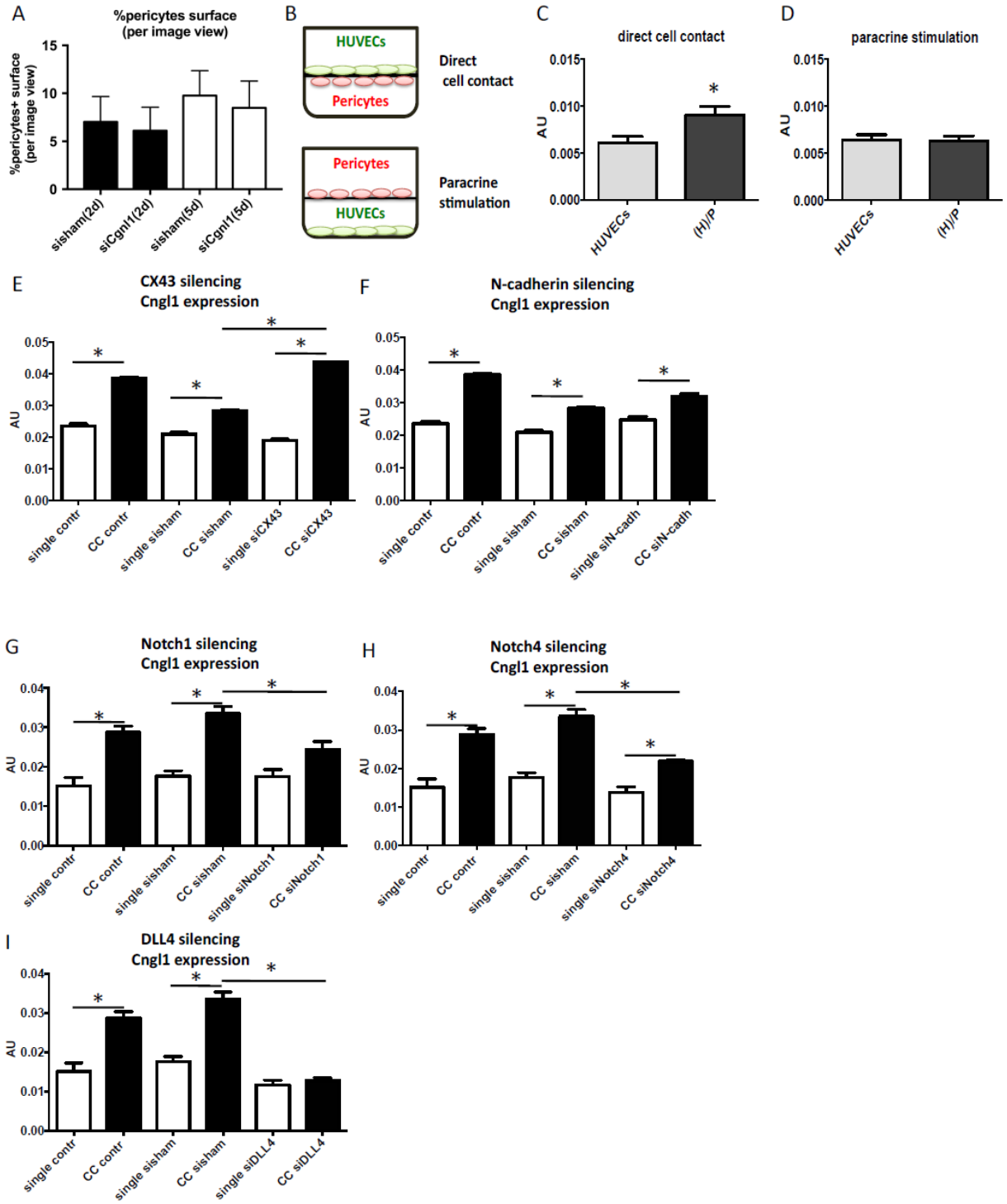

S.Figure 5: (A) Quantified results of %pericyte RFP surface per image view at day 2 (black bars) and day 5 (white bars) in the 3D collagen coculture assay, following Cgnl1 silencing or sham siRNA transfection in HUVEC-GFP. Values represent means ± SD (N>5). *p<0.05 siCgnl1 versus time-corresponding control and sisham. Student's t-test within 1 time point. (B) Diagrams showing the experimental setups of direct contact or paracrine stimulation of HUVECs by pericytes. (C) QPCR evaluation of Cngl1 mRNA levels in HUVECs without (HUVECs) and with direct cell contact with pericytes ((H)/P). (D) QPCR evaluation of Cngl1 mRNA levels in HUVECs without (HUVECs) and with paracrine stimulation by pericytes ((H)/P). For

C and D: n=3 *p<0.05 versus HUVECs without pericyte coculture. Values represent mean target/house keeping gene ratio in AU ± SEM. Student's t-test. (E) QPCR evaluation of Cngl1 mRNA levels in HUVECs without (single) and with direct contact stimulation by pericytes (CC) in HUVECs and pericytes untreated or treated with sisham or siCX43. (F) QPCR evaluation of Cngl1 mRNA levels in HUVECs without (single) and with direct contact stimulation by pericytes (CC) in HUVECs and pericytes untreated or treated with sisham or siN-cadherin. (G) QPCR evaluation of Cngl1 mRNA levels in HUVECs without (single) and with direct contact stimulation by pericytes (CC) in HUVECs and pericytes untreated or treated with sisham or siNotch1. (H) QPCR evaluation of Cngl1 mRNA levels in HUVECs without (single) and with direct contact stimulation by pericytes (CC) in HUVECs and pericytes untreated or treated with sisham or siNotch4. (I) QPCR evaluation of Cngl1 mRNA levels in HUVECs without (single) and with direct contact stimulation by pericytes (CC) in HUVECs and pericytes untreated or treated with sisham or siDLL4. For E-I: n>3 *p<0.05 Values represent mean target/house keeping gene ratio in AU ± SEM. One-way ANOVA.

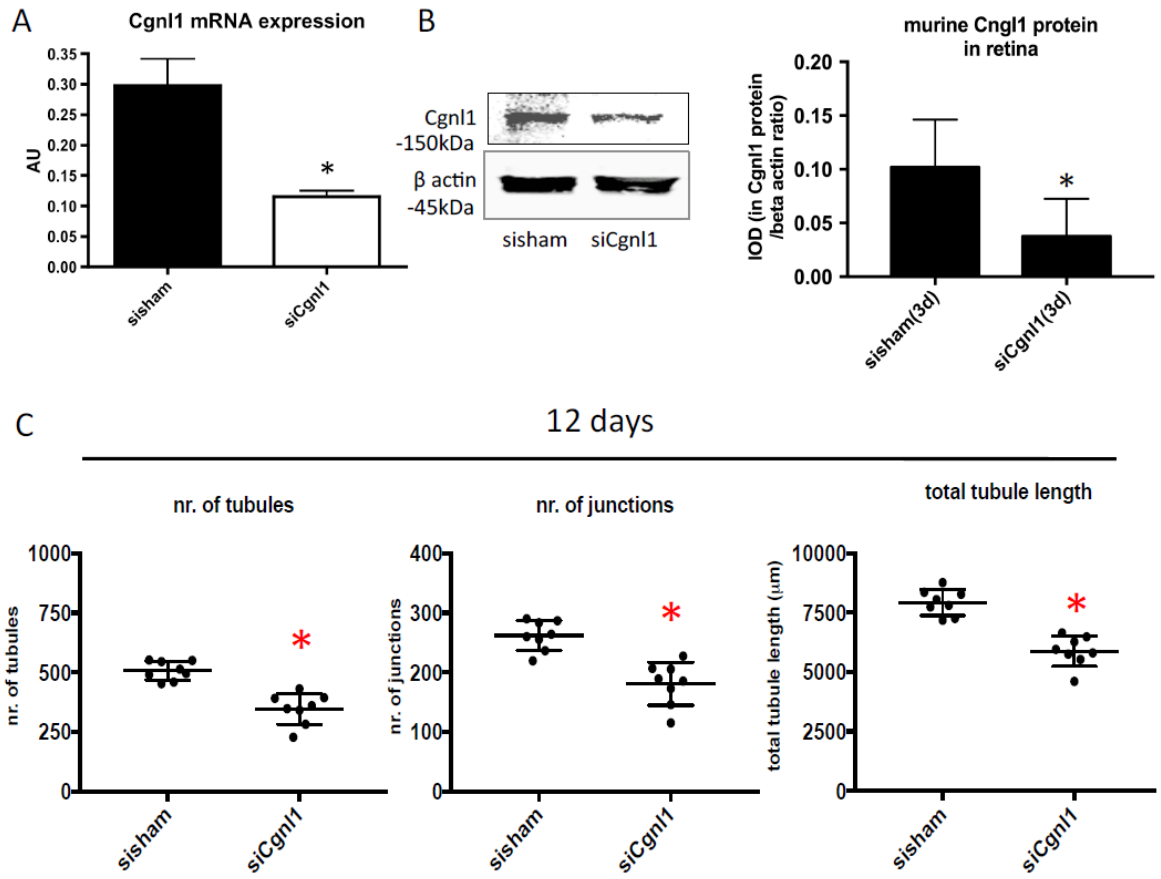

S.Figure 6: (A) QPCR validation of efficient knockdown in Accel siCgnl1 injected murine retina versus sisham treated samples. n=6 *p<0.05 versus sisham treated retinas. Values represent mean target/ house keeping gene ratio in AU ± SEM. Student's t-test. (B) Quantified western blot results for murine Cngl1 protein levels. Shown are representative immuno blots. Values represent mean integrated optical density (IOD) ±SD corrected for β actin loading controls. (n=6). Student's t-test. (C) Quantified results of retinal vascularization at day 12 after siCgnl1 injection at day 8 as compared to sisham injected controls. Mean ± SD per group is indicated in scatter plots. *p<0.05 versus sisham-injected eyes. n=8 pups per group. Student's t-test.

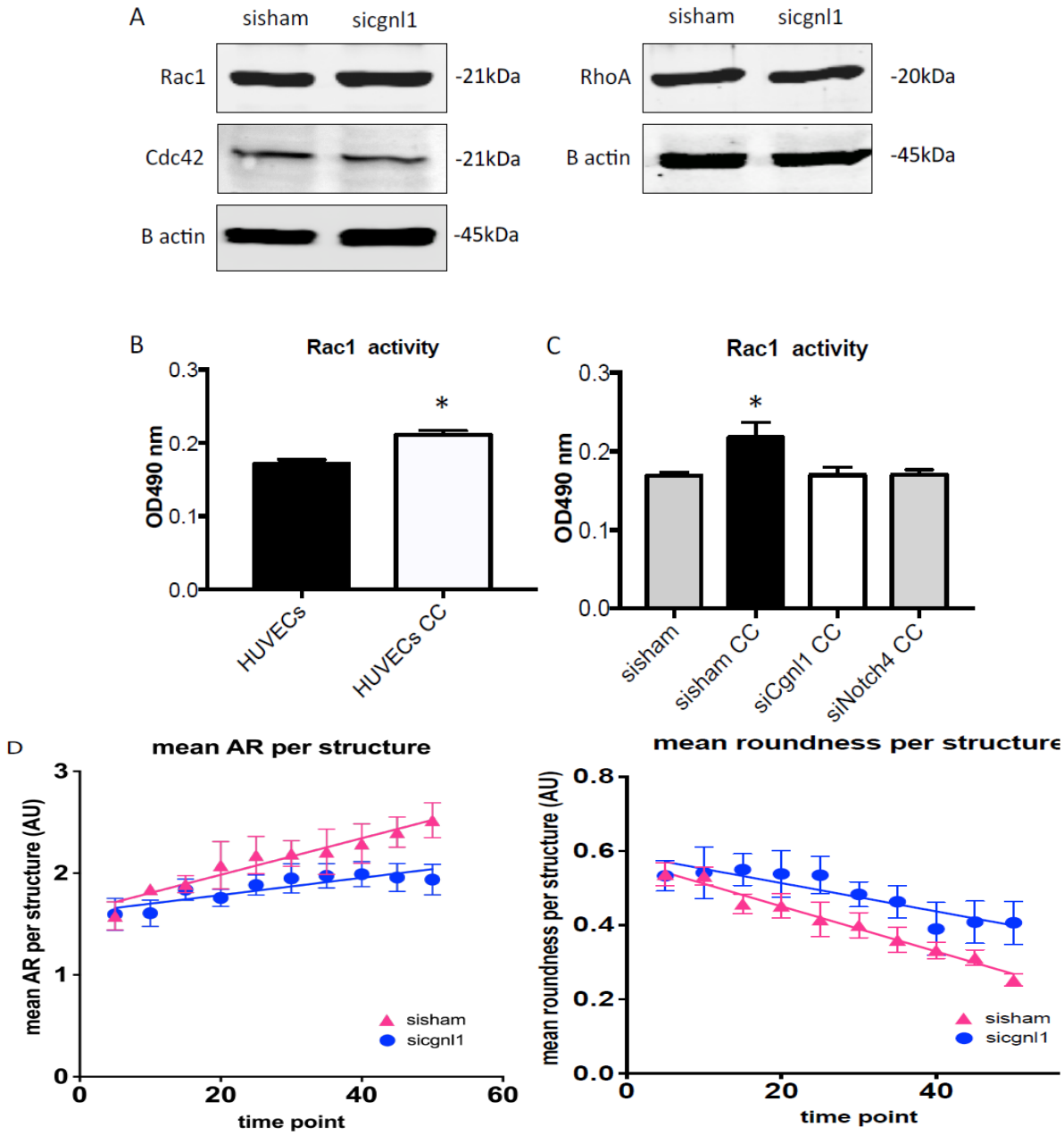

S.Figure 7: (A) Representative western blot for Rac1, Cdc42, RhoA, and β-actin, of sisham and siCgnl1 treated HUVECs. (B) Chemo-luminescence measurement of the GTP-bound small G-proteins in cell lysates from HUVECs in single and pericyte coculture conditions after 20 minutes of serum activation. Shown are the levels of GTP-Rac1. (C) Chemo-luminescence measurement in cell lysates from sisham, siCngl1, and siNotch4, transfected HUVECs cocultured with pericytes after 20 minutes of serum activation. Shown are the levels of GTP-Rac1. For B and C: Values represent means ± SEM.*P<0.05 other conditions, n=4. Student's t-test (B) and One-way ANOVA (C). (D) Serial images of time-lapse imaging of HUVECs GFP cells seeded in 3D collagen coculture with pericytes in siCgnl1 and sisham group. Different time points (T) are shown. 1 time point represents 1 hour post seeding. Quantification of aspect ratio (AR) and roundness per HUVEC-GFP+ structure (from T = 0 to T = 50 post seeding). Each symbol represents average ± SD of 5 time points. Each time point is composed of 5 individual measurements.

p<0.0001 for AR and roundness, siCngl1 versus sisham group, linear regression analysis, overall comparison.

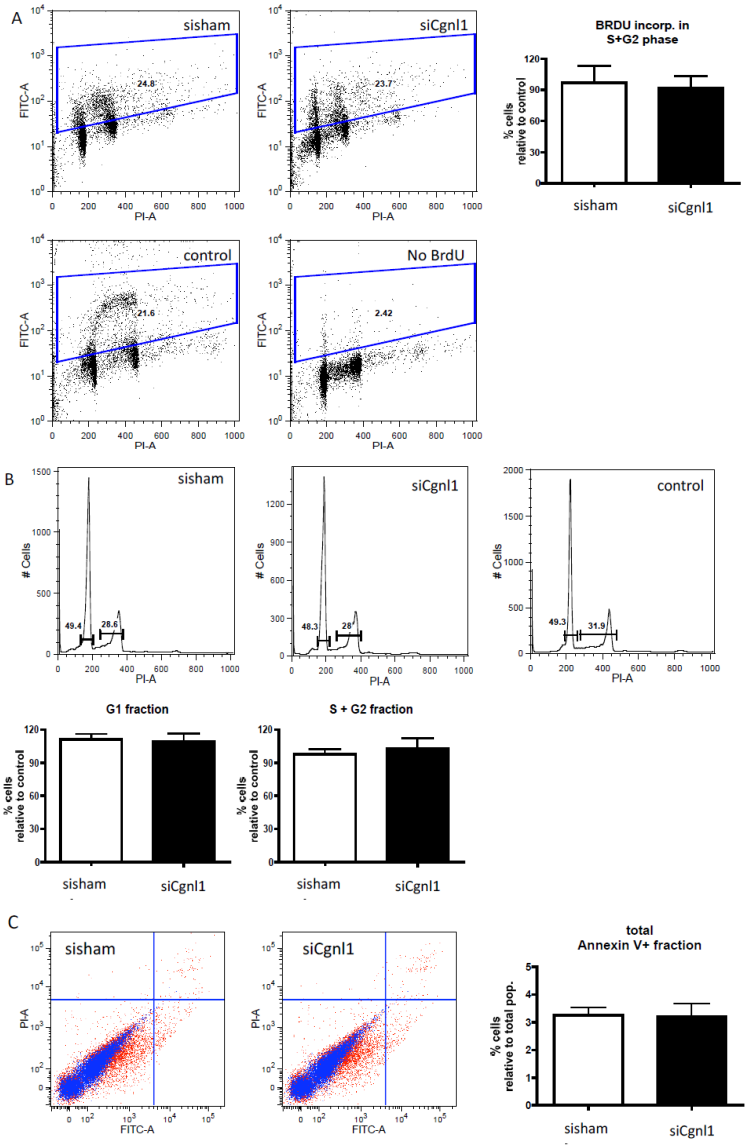

S.Figure 8: (A) Cell proliferation analysis was conducted by measuring BRDU incorporation using flow cytometry. (A) Representative dot blot graphs are shown for sisham, siCgnl1 transfected, and non-transfected HUVECs. The Y-axes show the BRDUFITC signal, the X-axes the PI signal. A negative control (HUVECs without BRDU incorportation) was used to define the gate settings. No difference was observed in BRDU signal was observed in the S+G_2 phase cell population between the different groups (n=3, values represent means ± SEM, student's t-test). Data shown are measured 4 hours post activation. (B) Analysis of cell cycle distribution of sisham, siCgnl1 transfected, and non-transfected HUVECs. Representative histograms show the G1 and the S+G2 region in the different groups. Quantification of the percentages of cells in the G1, and S+G2 fractions show no effect of Cgnl1 silencing on cell cycle progression n=3, values represent means ± SEM, student's t-test, data shown are measured at 12 hours post activation. (C) Flow cytometry analysis of apoptosis in HUVECs transfected with sisham and siCgnl1. Dead cells are PI+, apoptotic cells are Annexin V+, and alive cells are PI-/Annexin V-. Quantification of the percentage of

Annexin V+ cells show no difference between siCgnl1 or sisham treated HUVECs. n=3, values represent means ±SEM, student's t-test, data shown are measured at 4 hours post activation.

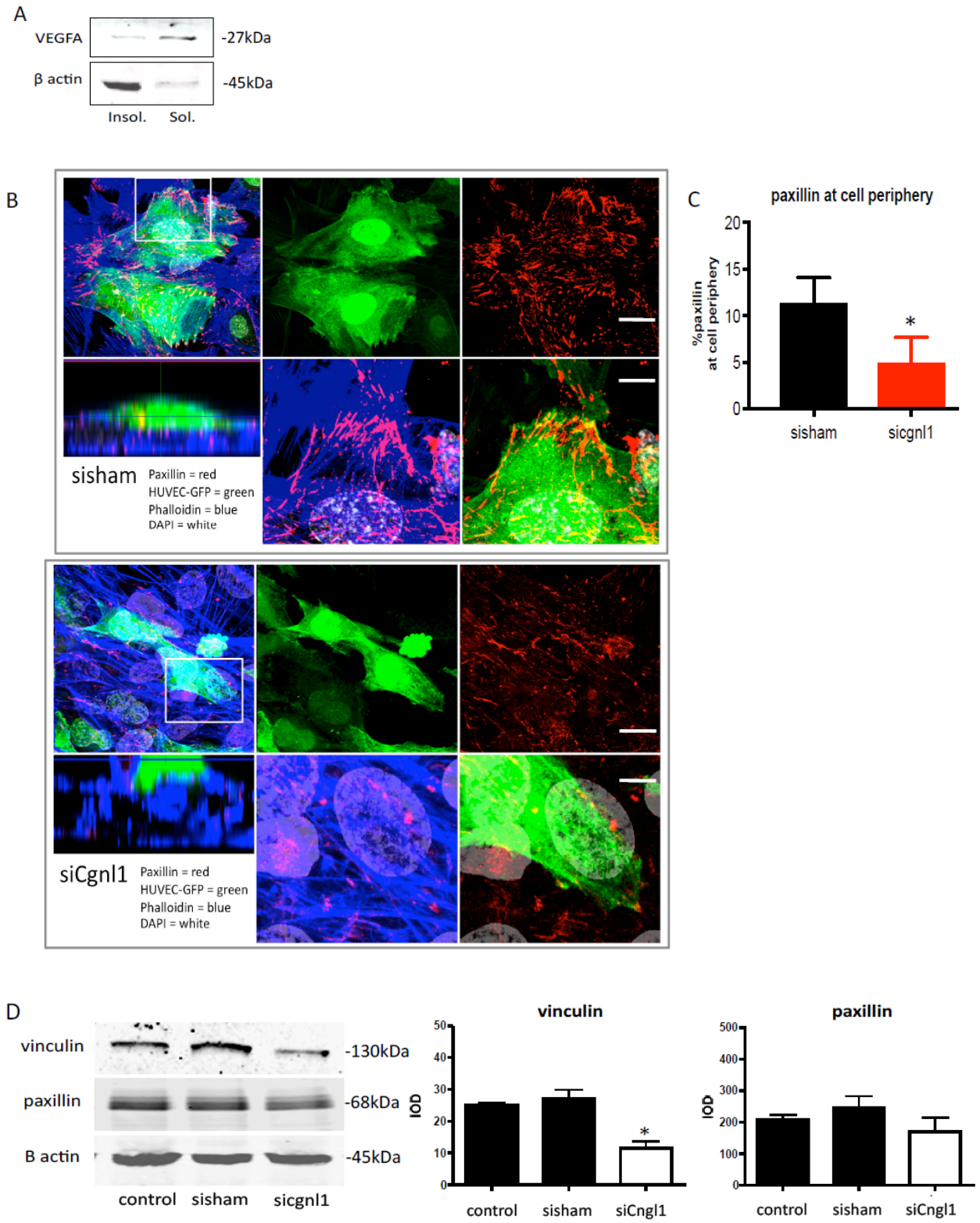

S.Figure 9: (A) Representative western blot results of 2 different experiments for VEGFA and β actin detection in Triton-X insoluble fraction (the actin cytoskeleton associated compartment) versus the

soluble fraction. (B) Representative images of intracellular staining of sisham (upper panel) and siCgnl1 (lower panel) treated HUVECs-GFP and human pericytes for paxillin (red signal), DAPI (white signal), and actin cytoskeleton (phalloidin blue signal). For both sisham and siCgnl1 panels: Upper row of images, scalebar represents 5 µm. Lower row of images; first image (left); Z stack showing HUVECs-GFP on top of phalloidin blue+ pericytes. 2nd and 3rd images; high magnification images of showing paxillin distribution HUVEC-GFP. Scale bar represents 2.5 µm. (C) Quantitative results of %paxillin distribution at cell borders of HUVECs-GFP per image view adjusted for cell numbers at 60 minutes post seeding on top of pericyte layer. Values represent means ± SD. *p<0.05 versus sisham. Data obtained from 4 different experiments with analysis of 12 different micrographs per group per experiment. Student's t-test. (D) Representative western blot results for vinculin, paxillin and β-actin detection in siCngl1 versus sisham and non-treated control HUVECs. Graphs (right) show quantified results of immuno blotting of vinculin and paxillin. Values represent mean integrated optical density (IOD) ± SEM corrected for β actin loading controls. (n=3). Oneway ANOVA.

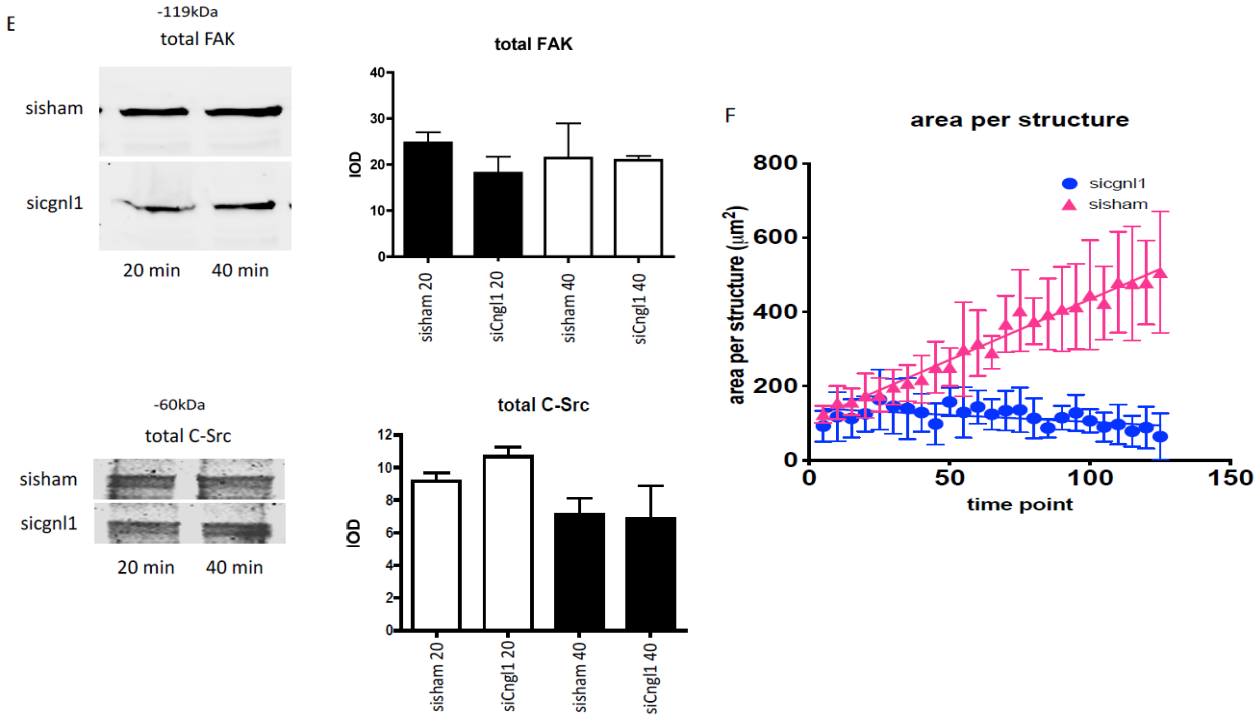

S.Figure 9: (E) Western blot analysis of total FAK and C-Src protein levels at 20 and 40 minutes after seeding of siCgnl1-treated compared to sisham-treated HUVECs. Graphs show quantified results. Values represent mean integrated optical density (IOD) ± SEM corrected for β actin loading controls. n=3. Student's t-test for comparison within corresponding time point. β actin protein level was assessed as a loading control and did not differ between the control, sisham and siCgnl1 samples (data not shown). (F) Quantification of area per HUVEC-GFP+ structure (from T = 0 to T = 125 post seeding). Each symbol represents average area per structure ± SD of 5 time points. Each time point is composed of 5 individual measurements. p<0.0001, siCngl1 versus sisham group, linear regression analysis, overall comparison.

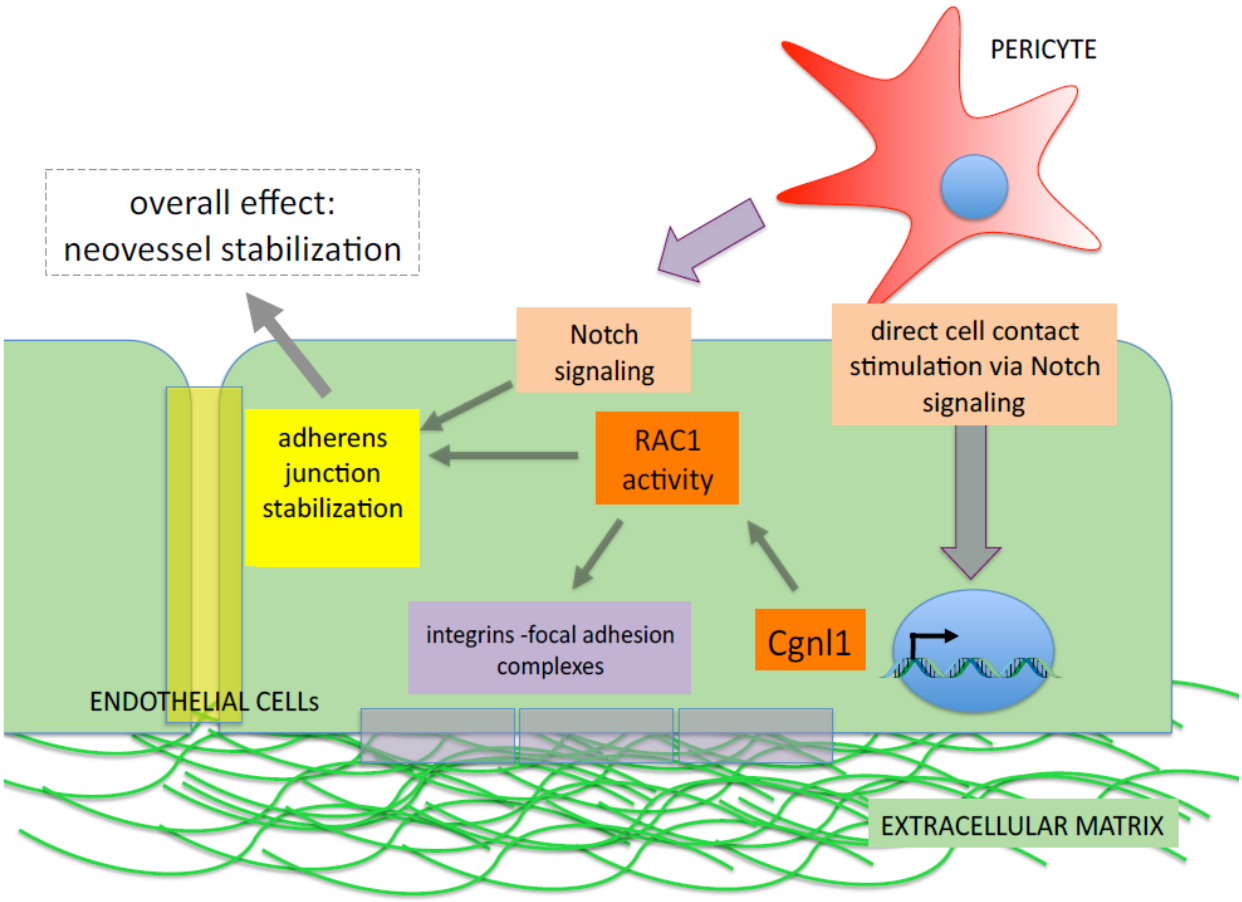

S.Figure 10: A proposed working mechanism for Cngl1 in which pericyte induced upregulation of Cngl1 in endothelial cells via Notch signalling promotes the formation of strong Ve-cadherin adherens junctions via Rac1 activation. Cross cell type Notch signalling may also provide adherens junction stabilization via other unknown mechanisms. Simultaneously, Cngl1 mediated Rac1 activation stimulates assembly of integrins-focal adhesion complexes. Combined, formation of both strong adherens junctions and focal adhesions ensures stabilization and further elongation of neovascular tubules.

Chapter 5 THSD1 preserves vascular integrity and protects against intraplaque haemorrhaging in ApoE−/− mice.

Remco A. Haasdijk*, Wijnand K. Dekker*, Caroline Cheng*, Denny Tempel†, Robert Szulcek†, Frank L. Bos†, Dorien M.A. Hermkens†, Ihsan Chrifi, Maarten Brandt, Christian G.M. van Dijk, Yan-Juan Xu, Esther H.M. van de Kamp, Lau A.J. Blonden, Jan van Bezu, Judith C. Sluimer, Erik A.L. Biessen, Geerten P. van Nieuw Amerongen, Henricus J. Duckers.

*These *first and † second authors contributed equally to the paper.*

Published: Cardiovascular Research 2016 May 1;110(1): 129-139

Abstract

Aim:
Impairment of the endothelial barrier leads to microvascular breakdown in cardiovascular disease and is involved in intraplaque haemorrhaging and the progression of advanced atherosclerotic lesions that are vulnerable to rupture. The exact mechanism that regulates vascular integrity requires further definition. Using a microarray screen for angiogenesis-associated genes during murine embryogenesis, we identified thrombospondin type I domain 1 (THSD1) as a new putative angiopotent factor with unknown biological function. We sought to characterize the role of THSD1 in endothelial cells during vascular development and cardiovascular disease.

Methods and results:
Functional knockdown of Thsd1 in zebrafish embryos and in a murine retina vascularization model induced severe haemorrhaging without affecting neovascular growth. In human carotid endarterectomy specimens, THSD1 expression by endothelial cells was detected in advanced atherosclerotic lesions with intraplaque haemorrhaging, but was absent in stable lesions, implying involvement of THSD1 in neovascular bleeding. In vitro, stimulation with pro-atherogenic factors (3% O2 and TNFα) decreased THSD1 expression in human endothelial cells, whereas stimulation with an anti-atherogenic factor (IL10) showed opposite effect. Therapeutic evaluation in a murine advanced atherosclerosis model showed that Thsd1 overexpression decreased plaque vulnerability by attenuating intraplaque vascular leakage, subsequently reducing macrophage accumulation and necrotic core size. Mechanistic studies in human endothelial cells demonstrated that THSD1 activates FAK-PI3K, leading to Rac1-mediated actin cytoskeleton regulation of adherens junctions and focal adhesion assembly.

Conclusion:
THSD1 is a new regulator of endothelial barrier function during vascular development and protects intraplaque microvessels against haemorrhaging in advanced atherosclerotic lesions.

Introduction

Vascular barrier integrity of the endothelium is actively controlled by dynamic interactions between the endothelial actin cytoskeleton, cell-to-cell junctions, and cell-to-extracellular matrix (ECM) focal adhesion contacts.[1,2] Loss of barrier function leads to passage of circulating cells and solutes and contributes to (micro)vascular haemorrhaging. Although intercellular contacts are established between endothelial cells during the earliest phases of vasculogenesis and angiogenesis, a functional barrier is only created after the critical process of junction maturation that is stringently controlled by members of the Rho family of GTPases.[3–6] In particular, Rac1 regulation of actin cytoskeleton dynamics prevents the build-up of actomyosin-mediated tension across VE-cadherin adhesion sites, which is crucial for the formation of stable adherens junctions that provide the mechanical cohesion of the intercellular bonds.[7] Disruption of the Rac1 regulatory pathway leads to loss of vascular integrity and is implicated to be an important contributing factor to vascular-related diseases, including atherosclerosis.[1,8]

In advanced atherosclerosis, lesions become characterized by intraplaque growth of microvessels that are phenotypically immature and are defined by lack of endothelial barrier function, making them susceptible to haemorrhaging and rupture.[9] Although the importance of loss of barrier integrity in the onset of cardiovascular disease has become increasingly evident, our knowledge of endothelial specific factors that orchestrate the key Rac1-mediated pathway in vascular barrier regulation remains limited. In this study, we report a new gene with a high level of endothelial specific expression that is a potent preservation factor of vascular barrier integrity.

Recently, we have carried out a genome-wide microarray analysis in search for genes involved in the regulation of new vessel formation and have identified thrombospondin type I domain 1 (*THSD1*), also known as transmembrane molecule with thrombospondin module (*TMTSP*), as a new candidate regulator of vascular development. *THSD1* has been described as an early marker of haematopoietic stem cells and ECs during embryonic development in mice.[10] *In silico* database analysis indicated that *THSD1* encodes for a putative protein structure that contains a signal sequence and a transmembrane and thrombospondin type 1 repeat (TSP1) domain. Currently, data that elucidate the vascular function of THSD1 are still lacking.

Here, we sought to characterize the function of THSD1 in ECs during blood vessel formation *in vitro*, using primary cell cultures, and *in vivo* in zebrafish and murine vascular development. Our studies identified, for the first time, THSD1 as a critical regulator of Rac1-mediated conservation of neovessel integrity. *Thsd1*knockdown induced microvascular ruptures and haemorrhaging during embryonic and postnatal vascular development, indicating that THSD1 is a beneficial factor for maintaining endothelial barrier function. The therapeutic potential of THSD1 was investigated in our well-validated murine ApoE-knockout model in which we induced growth of vulnerable plaque-like lesions by shear stress alteration.[11,12] *Thsd1* overexpression improved endothelial barrier function and reduced vascular bleeding of the neointimal microvasculature in the murine atherosclerotic plaques. Considering the potent vascular stabilizing function of the

gene, we propose that *THSD1* is an interesting drug target for the development of therapeutics in the treatment of vulnerable plaque or other (micro)vascular pathologies in which endothelial barrier function is compromised.

Materials

Ethics

The human samples were obtained from the Maastricht Pathology Tissue collection bank (MPTC). Collection and storage in the MPTC and patient data confidentiality as well as tissue usage were in accordance with the 'Code for Proper Secondary Use of Human Tissue in the Netherlands`. Collection and study of human samples were approved by institutional ethics committee and have been performed in full accordance with the ethical standards laid down in the 1964 Declaration of Helsinki and its later amendments. All animal studies were carried out in accordance with the Council of Europe Convention Directive (2010/63/EU) for the protection of vertebrate animals used for experimental and other scientific purposes with the approval of the National and Local Animal Care Committee.

Mouse model of retinal vascularization

Two-day-old murine C57BL/6J male and female pups were anaesthetized by placement on ice. One microlitre of *Thsd1* targeting siRNA (1.33 µg/µL) was injected into the left eye using a 33-Gauge needle (World Precision Instruments, Berlin, Germany). As control, one microlitre of scrambled non-targeting siRNA (1.33 µg/µL) was injected into the right eye. SiRNA was obtained from Thermo Fisher Scientific (Breda, The Netherlands). The following mix of mouse *Thsd1*targeting siRNA was used: 5'-GCA AGC AAG UUC CGA AUC A-3', 5'-AGU CAU UGC UUC UAC GGG A-3', 5'-GCU CCA ACG AAG AGG ACG A-3', 5'-UGA CUA UGU CCU CGG AGA A-3'. Mice pups were killed 5 days after intraocular injection by decapitation. The retinas were stained with Alexa Fluor® 488-conjugated isolectin GS-IB_4 1:200 (I21411; Invitrogen, Bleiswijk, The Netherlands) before assessment under a fluorescence microscope (Axiovert S100; Carl Zeiss, Sliedrecht, The Netherlands). Image analysis of number of junctions, tubules, and total tubule length was carried out using Angiosys Image Analysis Software 1.0 (TCS CellWorks, Buckingham, UK). Validation of adequate *Thsd1* knockdown in the retina (2 days after intra-ocular injection) was achieved by qPCR using the following mouse primers: 5'-AGA GCC AGC AAA AGG ACA AA-3' (forward) and 5'-CAA GGA GGT GGC AGT ACC AT-3' (reverse) (Biolegio, Nijmegen, The Netherlands). HPRT primers 5'-TCA GGA GAG AGA AAA GAT GTG ATT GA-3' (forward) and 5'-ACG CCA ACA CTGCTG AAA CA-3' (reverse) (Biolegio, Nijmegen, The Netherlands) were used for housekeeping gene detection.

ApoE-knockout mice vulnerable plaque model

Ten-week-old female ApoE$^{-/-}$/C57BL/J6 mice (Jackson Laboratory, UK) were put on a Western diet containing 15% (w/w) cacao and 0.25% (w/w) cholesterol (Arie Blok, Woerden, The Netherlands). Two weeks after start of the Western diet, mice were anaesthetized by ventilation of a 1:2 mixture of O_2/N_2O to which 2.3% isoflurane was added. The animals were maintained at 37°C on a heating pad during the operation; a neck incision was made and the right common carotid artery was dissected from connective tissue. A tapered cast was surgically implanted around the right common carotid artery. This device reduces flow shear stress upstream, triggering the growth of atherosclerotic lesions with a vulnerable plaque phenotype. Nine weeks after cast placement, mice were re-operated and locally transfected with either adenovirus-expressing murine Thsd1 or sham virus. At day 5, 1hr before sacrifice by cervical dislocation, FITC-labelled dextran (Sigma-Aldrich, Zwijndrecht, The Netherlands) was intravenously injected. The carotid artery was flushed and harvested. The carotids that were treated with the shear stress altering device were cut at the proximal and distal borders of the cast to separate the blood vessel into three different segments: Section 1, segment proximal from device (the vulnerable plaque section); Section 2, a segment distal from the device (the stable plaque section); and Section 3, a segment of the carotid that was encased by the device and which was discarded. Section 1 (proximal) and Section 2 (distal) were used for qPCR analysis of the vulnerable plaque and stable lesion area, respectively.

Mice

Plugged FVB/N mice (*Mus musculus*) were obtained from Harlan (Indianapolis, USA). C57BL/6.ApoE-knockout mice were obtained from The Jackson Laboratory (Bar Harbor, USA). C57BL/6J mice were obtained from laboratory stock. They were maintained under standard husbandry conditions.

Isolation of Flk1-positive and Flk1-negative cells from mouse embryos

From eight to sixteen days post-fertilization, embryos were collected from plugged FVB/N mice and homogenized. FVB/N mice were killed by cervical dislocation. Cells were stained with PE-conjugated anti-mouse Flk1 antibody 1:50 (555308; BD, Breda, The Netherlands). Hoechst (Sigma-Aldrich, Zwijndrecht, The Netherlands) was used to select dead cells. Flk1-positive/Hoechst-negative cells and Flk1-negative/Hoechstnegative cells were sorted on a BD FACSCantoTM (Breda, The Netherlands). Isolation of mRNA was carried out using the RNeasy Mini Kit from Qiagen (Venlo, The Netherlands).

Zebrafish

Zebrafish (*Danio rerio*) were maintained under standard laboratory conditions. The transgenic zebrafish lines used were Tg(fli1:eGFP)y1 and Tg(kdrl:eGFP x gata1:dsRed)y1.

Morpholino injection

Morpholinos (MO) were obtained from Gene Tools (Philomath, USA) and dissolved in Milli-Q water containing 0.2% phenol red. The following MO was used: 5'-AGA TTA AAG CAG ACT CAC TTG TAT G-3', which induces a non-functional splice variant of *thsd1*. Different doses of the MO were injected into single-cell stage zebrafish embryos. MO knockdown efficiency was tested by reverse transcriptase PCR using the following zebrafish primers: 5'-GGA AAG ATT CTG CTT TAC AAG G-3' (forward) and 5'-GCC TGA TCA GAG TTC TTT CTG-3' (reverse) (Biolegio, Nijmegen, The Netherlands).

Whole-mount in situ hybridization

As template for *in vitro* transcription, a *thsd1* cDNA fragment of at least 250 bp was used to ensure probe specificity. Antisense RNA probes of *thsd1* were generated by *in vitro* transcription using the digoxigenin RNA Labeling Mix from Roche (Woerden, The Netherlands). In situ hybridization was carried out as previously described1.

o-Dianisidine staining

Erythrocytes were stained by incubating embryos in a solution containing o-Dianisidine (Sigma-Aldrich, Zwijndrecht, The Netherlands) as previously described[1].

TER-119 staining

Retinas were incubated with anti-mouse TER-119 antibody 20µg/ml (NB100-77608; Novus Biologicals, Cambridge, UK) to stain erythrocytes.

Immunohistochemistry

The carotid artery region upstream of the cast was serially sectioned in 6µm sections. Histological and immunohistochemical analysis was carried out at 72µm intervals, covering the whole vulnerable plaque. Cryosections were routinely stained for haematoxylin and eosin, and lipid deposition (OilRed O; Sigma-Aldrich, Zwijndrecht, The Netherlands). The signal was visualized by bright field microscopy. Furthermore, coupes were stained for macrophages (CD68 antibody; AbD Serotec, Hercules, USA), ECs (CD31 antibody; BD, Breda, The Netherlands) and erythrocytes (TER-119 antibody; BD, Breda, The Netherlands). The signal was visualized by an immunofluorescence-labeled secondary antibody and recorded with an inverted laser scanning confocal microscope (LSM510LNO; Carl Zeiss, Sliedrecht, The Netherlands). Dextran-FITC staining was visualized directly without an secondary antibody. The different histological and immunohistological stainings were quantified using Clemex Vision Lite Image Analysis Software (Clemex Technologies, Longueuil, Canada).

THSD1 and CD31 analysis in human carotid endarterectomy specimens

Human carotid endarterectomy specimens were collected and processed by the Experimental Vascular Pathology group (Maastricht UMC+, The Netherlands). From all samples, three

randomly taken regions were studied for THSD1 and CD31 expression. All samples were stained with antibodies against THSD1 (Sigma-Aldrich, Zwijndrecht, The Netherlands) and CD31 (DakoCytomation, Glostrup, Denmark). An horseradish peroxidase (HRP)-labeled secondary antibody in combination with nickel-3,3'-diaminobenzidine (Sigma-Aldrich, Zwijndrecht, The Netherlands) was used to visualize the signal.

Cell cultures

Primary cultures of human umbilical endothelial cells (HUVEC) were obtained from Lonza (Breda, The Netherlands) and cultured in EBM®-2 medium supplemented with a commercial BulletKit, 10% fetal calf serum (FCS) and 1% penicillin/streptomycin (Lonza, Breda, The Netherlands). Primary aorta-derived human vascular smooth muscle cells (vSMC) and primary brain-derived human pericytes were cultured in SmGM®-2 medium supplemented with a commercial BulletKit, 10% FCS and 1% penicillin/streptomycin (Lonza, Breda, The Netherlands). Human skin-derived fibroblasts were cultured in Dulbecco's modified Eagle's medium (DMEM) supplemented with 5% FCS (Cambrex, Wiesbaden, Germany). Cells were cultured at 37°C in 5% CO_2. Passages three to six were used throughout the study.

Immunofluorescence microscopy of cell cultures

HUVECs transfected with scrambled non-targeting siRNA or THSD1 targeting siRNA were grown in gelatin-coated 48-wells. After 24 hours, the cells were fixed in 4% formaldehyde and permeabilized with 0.2% Triton® X-100. Cells were incubated overnight at 4°C with antibodies against THSD1 1:100 (HPA012611; Sigma-Aldrich, Zwijndrecht, The Netherlands), VE-cadherin 1:100 (sc-6458; Santa Cruz Biotechnology, Heidelberg, Germany), FITC-conjugated ZO-1 1:50 (339111; Invitrogen, Bleiswijk, The Netherlands), Paxillin 1:200 (ab32084; Abcam, Cambridge, UK), or Vinculin 1:25 (ab18058; Abcam, Cambridge, UK). For the detection of the primary antibodies Alexa Fluor® 488 1:100 (Invitrogen, Bleiswijk, The Netherlands) was used. Actin filaments were stained with rhodamin-phalloidin 1:40 (R415; Invitrogen, Bleiswijk, The Netherlands). The nucleus was stained with DAPI in Vectashield® mounting medium (H-1200; Vector Laboratories, Burlingame, USA). Cells were visualized with a fluorescence microscope (Axiovert S100; Carl Zeiss, Sliedrecht, The Netherlands).

Targeted siRNA knockdown

HUVECs were grown to 60-70% confluence. DharmaFECT1 Transfection Reagent was used to transfect 5 ng siRNA (Thermo Fisher Scientific, Breda, The Netherlands). The following mix of human THSD1 targeting siRNA was used: 5'-GCA AAC AAG UUC CGG AUC A-3' – 5'-UCA GGA GGA CAG CGA GUU U-3' – 5'-AAG AAA GGU CUG ACG GAA A-3' – 5'-AAG GAG GAG UGC AUG CUA A-3'. Scrambled non-targeting siRNA was used as a control. Knockdown of THSD1 was validated by qPCR analysis and Western blot two days post-transfection using the following human primers: 5'-AGA GAA CAG AGC CCC ACA GA-3' (forward) and 5'-CCC AAA ATA TCC TGG

GAG GT-3' (reverse) (Biolegio, Nijmegen, The Netherlands). Beta-actin primers 5'-TCC CTG GAG AAG AGC TAC GA-3' (forward) and 5'-AGC ACT GTG TTG GCG TAC AG-3' (reverse) (Biolegio, Nijmegen, The Netherlands) were used for housekeeping gene detection. Anti-human THSD1 antibody 1:125 (HPA012611; Sigma-Aldrich, Zwijndrecht, The Netherlands) was used for Western blot analysis. For validation of efficient *Thsd1* silencing in murine retinal endothelial cells, siRNA injected retinas were harvested and processed for magnetic bead isolation of PECAM1+ retinal endothelial cells following a previously described protocol2 using rat anti-mouse PECAM-1 monoclonal antibody MEC13.3 (BD Pharmingen, San Diego, CA). PECAM1 and Thsd1 expression in PECAM+ and PECAM- cell lysates were subsequently evaluated by qPCR analysis.

2D matrigel network-formation assay

To induce network-formation, HUVECs transfected with scrambled non-targeting siRNA or THSD1 targeting siRNA were cultured on a 2D MatrigelTM matrix (BD, Breda, The Netherlands). The tubules were stained by Calcein-AM (BD, Breda, The Netherlands) after 24 hours of network-formation. Each condition was assessed by fluorescence microscopy (Axiovert S100; Carl Zeiss, Sliedrecht, The Netherlands). Image analysis of the number of junctions, tubules and total tubule length was carried out using Angiosys Image Analysis Software 1.0 (TCS CellWorks, Buckingham, UK).

Transwell permeability assay and ECIS measurements

Endothelial barrier function *in vitro* was evaluated by culturing HUVECs on porous filters and measuring the passage of HRP as previously describes[3,4]. In short, HUVECs transfected with scrambled non-targeting siRNA or THSD1 targeting siRNA were seeded at high density on fibronectin-coated polycarbonate filters of the Transwellsystem (0.33cm^2, pore size 3.0µm, Corning Incorporated Life Sciences, Lowell, USA). Medium was refreshed the other day. At the start of the experiment, HRP (5µg/ml) was added to the upper compartment of the Transwell system. At time = 0 minutes, the first sample from the lower compartment was taken. The other samples from the lower compartment were taken at time = 15, 30, 45, 60, 90 and 120 minutes. At the end of the experiment, a sample was taken from the upper compartment. Filters were kept at 37°C in 5% CO_2 during the experiment. The concentration of HRP was derived from the HRP activity in each sample with peroxide and tetramethylbenzidine provided as a substrate. HRP passage as percentage of input was calculated. For ECIS measurements, cells were seeded on gelatin-coated electric cell-substrate impedance sensing arrays, each with 8 wells with 10 gold electrodes per well (Applied Biophysics, Troy, NY), experiments were carried out following standard protocols as previously described[5].

Western blot

To determine whether knockdown of THSD1 interfered with cellular processes, Western blot analysis was carried out using HUVEC protein lysates. At 72 hours post transfection, HUVECs were serum starved for 4 hours and replenished with EBM®-2 medium supplemented with a commercial BulletKit. Cells were lysed in NP40 Cell Lysis Buffer (Invitrogen, Bleiswijk, The Netherlands) and analyzed on a 12.5% SDS-PAGE gel, followed by immunoblotting using anti-human antibodies against focal adhesion kinase (FAK) 1:500, phosphorylated-FAK (Y397) (FAK-P) 1:500 (ab40794 and ab4803; Abcam, Cambridge, UK), phosphatidylinositol 3-kinase (PI3K) p85α 1:500 (#4292; Cell Signaling Technology, Leiden, The Netherlands), phosphorylated-PI3K p85α (Y508) (PI3K-P) 1:100 (sc-12929; Santa Cruz Biotechnology, Heidelberg, Germany) and Rac1 1:100 (ab71513; Abcam, Cambridge, UK). Beta-actin antibody 1:500 (ab8229; Abcam, Cambridge, UK) was used as a loading control. Protein bands were visualized by the Odyssey® Infrared Imaging System and analyzed by Odyssey 3.0 software (LI-COR Biotechnology, Cambridge, UK).

Rac1 activation assay

Rac1 activity was measured using the G-LISA® Rac Activation Assay Biochem KitTM from Cytoskeleton (Denver, USA) according to the instruction manual. HUVECs that were exposure to pro-and anti-atherogenic stimuli were used to examine the effect on THSD1 expression. For the pro-atherogenic stimulus, HUVECs were exposed to a low oxygen condition (3% O2) up to 4 days or to different concentrations of human recombinant TNFα (BD, Breda, The Netherlands) for 4 hours. For the anti-atherogenic stimulus, HUVECs were exposed to different concentrations of human recombinant IL 10 (Invitrogen, Bleiswijk, The Netherlands) for 4 hours. Samples were harvested at multiple time points and mRNA was isolated using an RNeasy Mini Kit from Qiagen (Venlo, The Netherlands), reversed transcribed to cDNA, and subsequently analyzed by qPCR.

Statistical analysis

Data were reported as mean ± standard error of the mean (SEM). Statistical significance was evaluated using Student's T-test, Mann Whitney U test, Repeated measurements ANOVA with Bonferroni post hoc test, or Kruskal-wallis test followed by Dunn's multiple comparison test, depending on sample size. Statistical significance was accepted when $P<0.05$.

Results

Vascular-specific mRNA expression of Thsd1 during mouse development

To identify new gene targets involved in angiogenesis, mRNA expression profiles of Flk1-positive angioblasts separated by flow cytometric sorting at various stages of murine embryonic development were compared with Flk1-negative cells. *Thsd1* was up-regulated in Flk1-positive angioblasts from 8 to 16 days post-fertilization. Expression levels peaked from 8 to 11 days post-

fertilization, which coincided with the period of early angiogenesis in murine development (*Figure 1A*).

Vascular-specific mRNA expression of Thsd1 during zebrafish development

In line with the findings from murine embryos indicating that *thsd1* is mainly expressed in the endothelial cell lineage, whole-mount *in situ* hybridization in developing zebrafish larvae showed expression of the *thsd1* zebrafish orthologue in the main axial vessels (dorsal aorta and posterior cardinal vein) and head vessels at 26hr post-fertilization. In addition, *thsd1* expression was also detected in the caudal and mid-cerebral veins, and in the somites (*Figure 1B*).

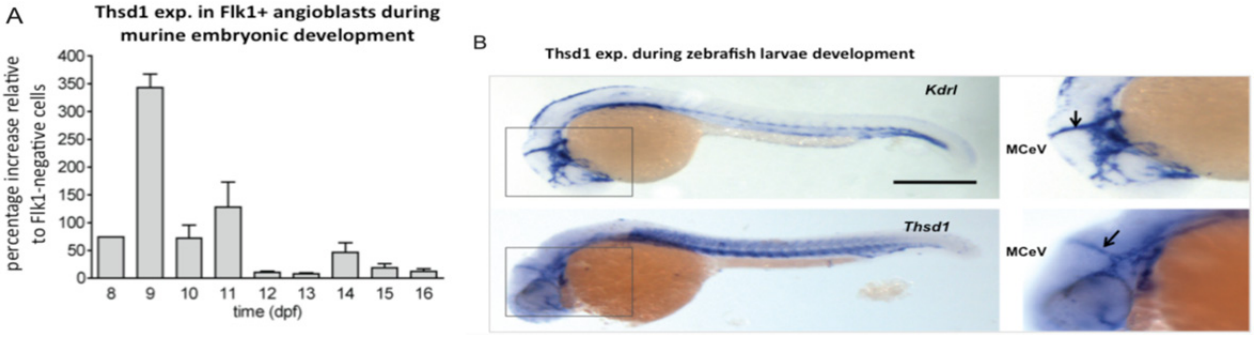

Figure 1 Vascular-specific expression of Thsd1 during mouse and zebrafish development. (A) Endogenous expression level of Thsd1 in Flk1-positive angioblasts during murine embryonic development from 8 to 16 days post-fertilization (dpf) vs. Flk1-negative cells, analysed by qPCR. Thsd1 mRNA level in Flk1-negative cells was set to baseline (n = 4; mean ± SEM). (B) Whole-mount in situ hybridization comparison of endothelial specific kdrl (upper panel) with thsd1 (lower panel) in zebrafish at 26 h post-fertilization (hpf), lateral view, anterior to the left. Like kdrl, thsd1 transcripts were localized in the developing vascular network, including the cerebral vasculature [indicated by black arrows are the caudal and mid-cerebral veins (MCeV)]. In addition, expression of thsd1 in the somites was observed. Right-hand panel shows high magnification images of the head region. Scale bar = 200 μm.

Knockdown of thsd1 *in zebrafish induces haemorrhaging of cerebral vessels*

For functional evaluation of *thsd1 in vivo*, the gene was silenced in developing zebrafish larvae of the transgenic zebrafish lines Tg(fli1:eGFP)^{y1} and Tg(kdrl:eGFP x gata1:dsRed)^{y1}, using morpholino (MO) knockdown technology. Successful targeting of *thsd1* was verified by qPCR analysis (see Supplementary material online, Figure S1). Silencing of *thsd1* had no effect on vascular growth (*Figure 2A*). However, time-lapse studies carried out during the first 48 h post-fertilization identified severe and frequent haemorrhaging in the cranial region, a known predilection site for vascular haemorrhaging in zebrafish,[13,14] which was observed in 24% of the injected embryos (*n* = 195) (*Figure 2B–E*). Haemorrhaging occurred as a sudden rupture of blood vessels, implying intrinsic weakness and lack of integrity of the endothelial barrier (*Figure 2B* and *C*). Cerebral haemorrhaging was further confirmed by an *o*-Dianisidine staining of iron/heme in red blood cells in *thsd1*-silenced wild-type zebrafish (*Figure 2D*). This phenotype

was consistently observed in the *thsd1*-silenced zebrafish after injections of different MO concentrations (*Figure 2E*).

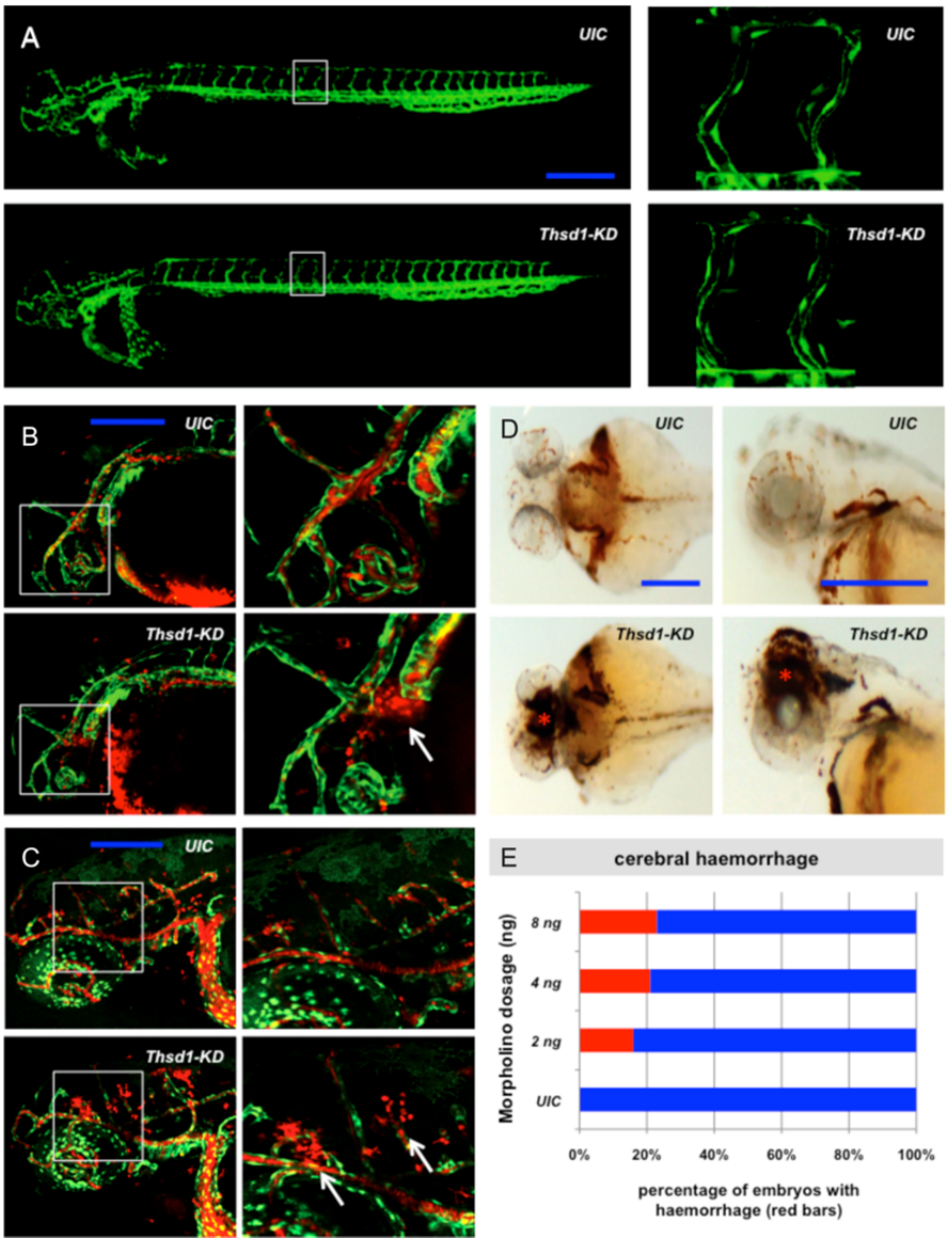

Figure 2 Morpholino-induced knockdown of thsd1 in zebrafish results in cerebral haemorrhages without affecting vascular growth. (A) Tg(fli1:eGFP)^{y1} embryos at 26 hpf, lateral view, anterior to the left. Scale bar = 200 µm. No apparent morphological abnormalities in the trunk or cerebral vasculature were observed between thsd1 targeting morpholino-injected (thsd1-KD) embryos and uninjected controls (UIC). Right-hand panel shows high magnification images of intersegmental outgrowth in the trunk region. Tg(kdrl:eGFP x gata1:dsRed)^{y1}thsd1-KD embryos around (B) 28 hpf (Scale bar = 200 µm) and (C) 2 dpf (Scale bar = 100 µm), lateral view, anterior to the left. ECs (green) and erythrocytes (red). Right-hand panel shows high magnification images of the head region. Haemorrhages were detected in the head region (white arrow). (D) o-Dianisidine stained embryos around 28 hpf (Scale bar = 200 µm), top view (left) lateral view (right), anterior to the left. Areas of

accumulated blood (red asterisk) in the head region were observed in thsd1-KD embryos. (E) Morpholino dose–response increase in the percentage of zebrafish with the cerebral haemorrhage phenotype (red bar) vs. the wild-type phenotype (no cerebral haemorrhaging, blue bar). (n = 195 larvae in total).

Thsd1 knockdown in the developing retinal vasculature of neonatal mice promotes vascular haemorrhages

In mice, vascularization of the retina takes place directly after birth, providing a 14-day time window to study the function of genes that are involved in angiogenesis in a non-embryonic setting. Here we used this neonatal retina vascularization model to study *Thsd1* following siRNA modulation of *Thsd1*expression. To determine the optimal moment of *Thsd1* knockdown, endogenous *Thsd1* mRNA expression in the murine retina during postnatal development was assessed by qPCR analysis. *Thsd1* mRNA levels were adjusted to CD31 mRNA levels to compensate for changes in percentage of ECs during vascular expansion. *Thsd1*expression was observed from 3 to 15 days post-partum in the murine retinas (*Figure 3A*). Therefore, *Thsd1* knockdown was induced in the first week of retinal vascular development by intra-ocular injection of a siRNA pool composed of four different *Thsd1* targeting siRNA sequences (*Thsd1-KD*) in 2-day-old wild-type C57BL/6J mouse pups and compared with controls injected with a scrambled non-targeting siRNA pool (sham). Efficient knockdown of *Thsd1* was observed 2 days after intraocular injection (see Supplementary material online, Figure S2A). More specifically, endogenous *Thsd1* expression was significant down-regulated after siRNA targeting of *Thsd1* in the retinal endothelial cell population (PECAM1+) compared with the PECAM1+ endothelial cell population obtained from retinas injected with the non-targeting siRNA pool, as shown by qPCR after magnetic bead isolation of PECAM1+ cells in collagenase-digested retina samples (see Supplementary material online, Figure S2B and C). Furthermore, the non-endothelial cell population (PECAM-) showed far lower endogenous expression levels of *Thsd1* compared with the PECAM1+ population, and no significant down-regulation of *Thsd1* was detected in PECAM− cells derived from *Thsd1*-KD retinas.

Quantification of the vascular network after visualization of ECs by isolectin GS-IB_4 staining showed no difference between *Thsd1-KD* and sham-injected eyes 5 days after intraocular injection (*Figure 3B–E*). However, double staining of retinas with isolectin GS-IB_4 (ECs in green) and TER-119 antibody (detecting erythrocytes in red) showed a higher frequency and larger areas of haemorrhaging in the *Thsd1-KD*-injected eyes, whereas retinal haemorrhaging was hardly observed in sham-injected controls (*Figure 3F* and *G*). Thus, like in the developing zebrafish, loss of *Thsd1* expression in the murine retinal vasculature had no effect on vascular growth, but induced high susceptibility to vascular haemorrhaging.

THSD1 is expressed in advanced human atherosclerotic lesions with neovascular intraplaque haemorrhaging and increased plaque vulnerability

Intimal neovascular growth with compromised vascular integrity is an important contributor to atherosclerotic lesion destabilization. We investigated the role of *THSD1* in the pathophysiology of the compromised neovasculature in advanced atherosclerotic lesions. Ten human

atherosclerotic plaques were obtained from patients with symptomatic carotid artery disease and were divided into a group of 5 stable lesions and a group of 5 advanced vulnerable plaques with pathological evidence of intraplaque haemorrhaging. *THSD1* and *CD31* expression was determined by immunohistological staining (see Supplementary material online, Figure S3A). THSD1 signal was co-localized with CD31+ ECs in vulnerable plaques with intraplaque haemorrhaging, whereas in stable plaques, *THSD1*expression by ECs was not detected (see Supplementary material online, Figure S3A). *THSD1* expression in human endothelial cells (s) *in vitro* could be decreased by two prominent pro-atherogenic stimuli, low oxygen (3% O_2) and TNFα (see Supplementary material online, Figure S3B and C), but was significantly up-regulated by the anti-atherogenic stimulus IL10 (see Supplementary material online, Figure S3D). *THSD1* expression appears to be sensitive to distinct transition points in TNFα and IL10 concentrations. These findings point towards a potential role for *THSD1* in endothelial barrier dysfunction in advanced atherosclerotic lesions vulnerable to rupture.

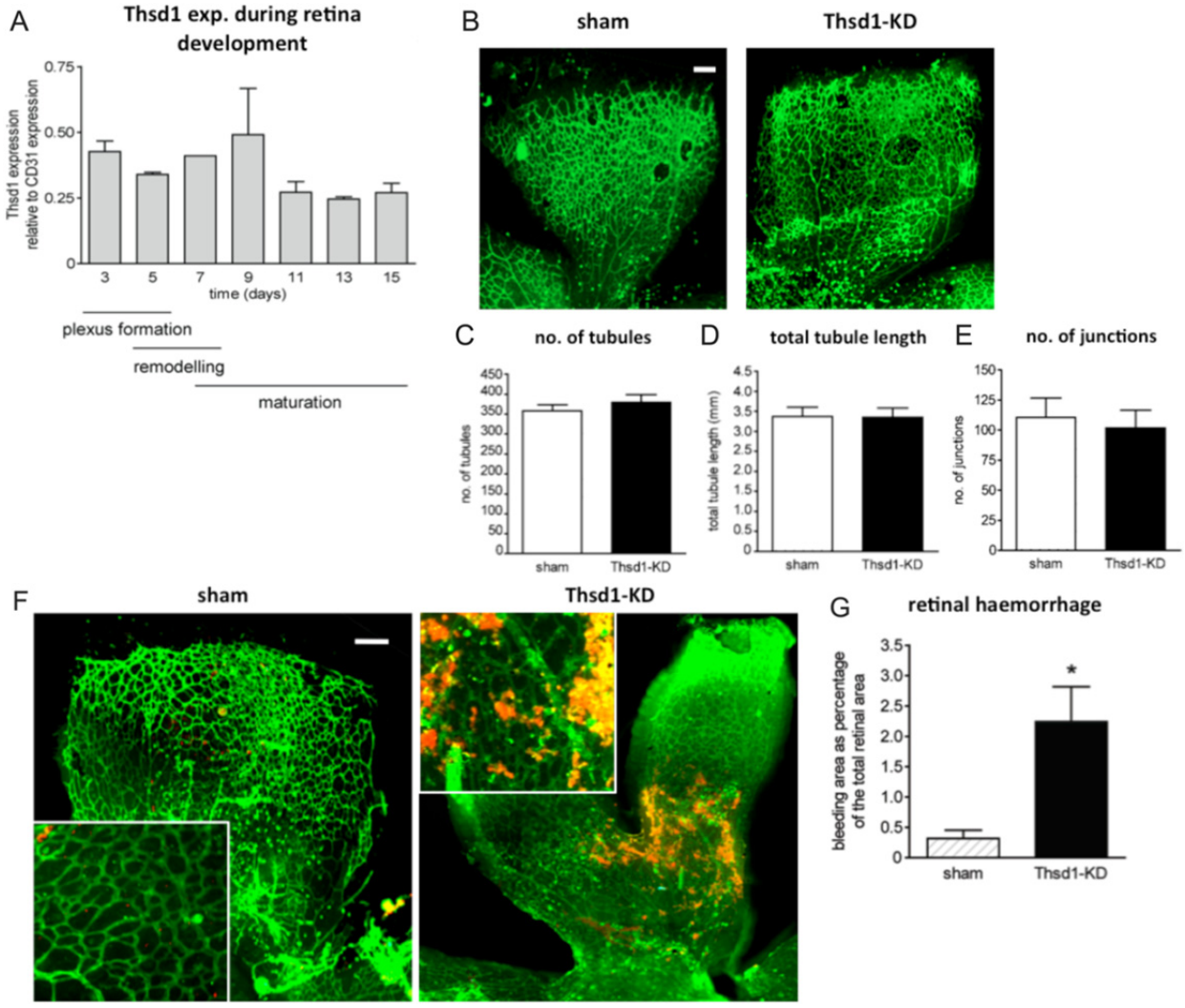

Figure 3 Thsd1 depletion during murine retinal vascular development results in vascular haemorrhaging without affecting vascular growth. (A) Endogenous expression level of Thsd1 in the

developing retinal vasculature of neonatal mice from 3 to 15 days after birth relative to CD31 expression (n = 3; mean ± SEM). Thsd1 is highly expressed from Day 3 to 9, which coincides with the period of plexus formation and vascular remodelling. (B) Retinas stained with isolectin GS-IB₄ for detection of ECs (representatives are shown from each group, n = 5; Scale bar = 300 μm). Quantification of the vascular network showed no morphological defects after Thsd1 knockdown (Thsd1-KD) regarding (C) number of tubules, (D) total tubule length, and (E) number of junctions. Double staining of retinas with isolectin GS-IB₄ (ECs green) and TER-119 (erythrocytes red) showed (F) significantly larger areas of vascular haemorrhaging in the THSD1-KD group. Inserted panels show high magnification details of the micrographs. (G) Quantification of retinal haemorrhage with the bleeding area expressed as percentage of the total retinal area in Thsd1-KD vs. sham retinas (n = 10; mean ± SEM). *P < 0.05 (Student's t-test), scale bar = 300 μm.

Thsd1 attenuates intraplaque haemorrhage and plaque destabilization without affecting neovascular growth

Findings in our zebrafish and murine retina models indicate that *Thsd1* is a beneficial factor for maintaining endothelial barrier function. We hypothesize that *Thsd1* expression in vulnerable plaque is part of an endogenous protective mechanism to counteract loss of endothelial integrity. The effect of *Thsd1*overexpression was assessed in our well-validated murine ApoE-knockout model in which we induced growth of carotid atherosclerotic lesions by shear stress alteration by implanting a tapered perivascular cast around the carotid artery.[11,12] In this murine model, a vulnerable plaque-like lesion develops in the low shear stimulated up-stream carotid region from the cast, whereas a stable plaque develops in the oscillatory shear stimulated downstream region from the cast.[11,12] Endogenous *Thsd1* expression in the normal carotid arteries of non-treated ApoE-knockout mice was already markedly increased in response to 1 week of feeding a high cholesterol, high fat diet (see Supplementary material online, Figure S4B). In line with the findings in the human samples, endogenous *Thsd1* mRNA level was significantly increased in the vulnerable plaque compared with the stable lesions derived from the murine cast model [*n* = 5; **P* < 0.05; Mann–Whitney *U* test; 23.0 ± 1.14 vs. 13.2 ± 0.86 (mean ± SEM); vulnerable vs. stable plaque, respectively, as determined by qPCR].

Peri-adventitial infection of an adenovirus expressing murine *Thsd1* (*adThsd1*) in the carotid artery resulted in a significant increase in *Thsd1* mRNA expression compared with infection with a sham virus (adsham) (see Supplementary material online, Figure S4A). Overexpression of *Thsd1* attenuated the vulnerable plaque phenotype at 9 weeks post shear stress-induced atherosclerosis induction: A 45% decrease in intimal accumulation of TER-119 erythrocytes was observed (*Figure 4A* and *B*). In addition, dextran-FITC extravasation was significantly reduced in the plaque intima (*Figure 4C*) and surrounding vasa vasorum of *adThsd1*-treated murine carotid arteries compared with adsham-treated controls (*Figure 4D*). These effects were independent of intimal neovascular growth, as no change in the number of CD31-positive cells was detected (*Figure 4E* and *F*).

Coincided with improved neovascular integrity, a 36% reduction in intraplaque macrophage accumulation in the *adThsd1* group was observed (*Figure 4G* and *H*), whereas intraplaque lipid accumulation remained unaffected (*Figure 4I* and *J*). This reduction in intraplaque macrophages did not affect lesion size as measured by intima/media ratio (*Figure 4K* and *L*). However, necrotic core area was significantly decreased in the *adThds1* group (*Figure 4K* and *M*). Together, these data demonstrate that *Thsd1* overexpression restores compromised endothelial barrier function of the intimal microvasculature in murine vulnerable plaque-like lesions.

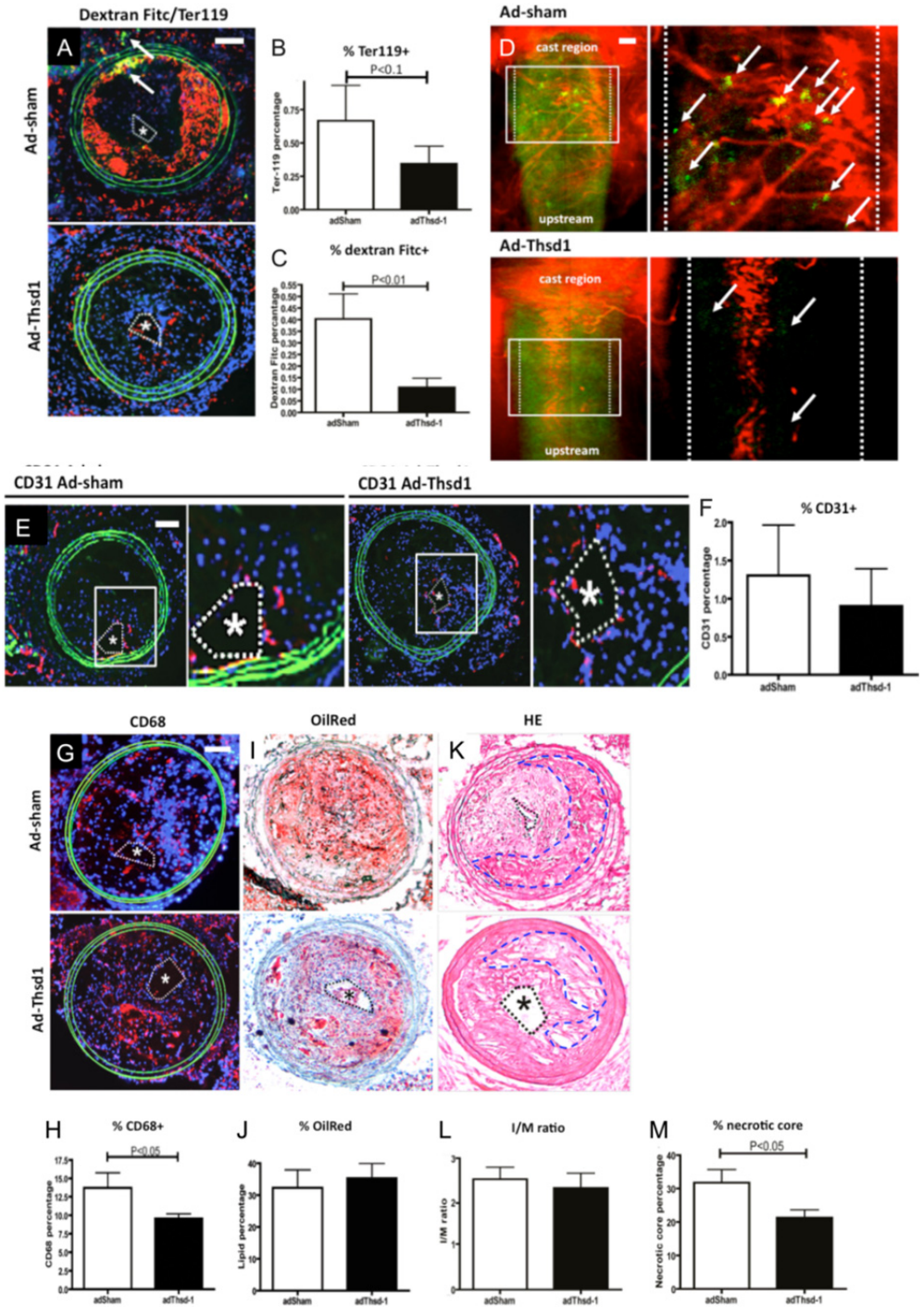

Figure 4. Overexpression of Thsd1 attenuates intraplaque haemorrhaging and stabilizes plaque vulnerability in murine vulnerable plaque-like lesions.
(A) Cryosections of adsham and AdThsd1-treated ApoE-knockout mice infused with dextran-FITC through the left heart ventricle during sacrifice with carotid plaque lesions stained for TER-119 (red) and visible dextran-FITC perivascular leakage in the intima and adventitia (white arrows). (B) Quantification of the percentage of TER-119+ area per carotid plaque cross-section. (C) Percentage of dextran-FITC+ area per carotid plaque cross-section. (D) Whole mount samples with adventitial vasculature stained for isolectin GS-IB₄ (ECs, red) with detection of dextran-FITC perivascular leakage (green, indicated by arrows) in the upstream (atherosclerotic) carotid region from the shear stress device. Dotted lines indicate vessel boundaries (representative micrograph of n = 6). Sections of adsham and AdThsd1-treated ApoE-knockout mice with carotid plaque lesions stained for (E) CD31+ endothelial cells, (G) CD68+ macrophages, (I) lipids, and (K) haematoxylin/eosin. Quantification of the percentage of (F) CD31+ area, (H) CD68+ area, (J) OilRed O+ area, (L) the intima/media ratio, and (M) necrotic core area (indicated by blue dotted lines in K) per cross-section. For all cross-sections, lumen areas are indicated by black dotted lines marked by an asterisk. For A, E, and G, elastin (autofluorescent green), dextran-FITC (green), DAPI (blue), TER-119, CD31 and CD68 (red) (n = 10; mean ± SEM; P-values based on Student's t-test). Scale bar = 200 μm.

THSD1 controls endothelial barrier function in vitro

Next we conducted *in vitro* assays to further define the mechanistic function of THSD1 in vascular cells. The expression level of *THSD1* was evaluated in different cell types. On comparing HUVEC, pericyte, VSMC, and fibroblast, the highest mRNA expression level of *THSD1* was observed in HUVECs (*Figure 5A*). In line with previous *in vivo* findings, siRNA-mediated knockdown of *THSD1* (*THSD1-KD*) in HUVECs did not affect network formation in a standard 2D Matrigel assay compared with cultures transfected with equimolar of non-targeting sham siRNA (sham) (*Figure 5B–E*). Adequate knockdown of the target gene was validated on both mRNA and protein level (see Supplementary material online, Figure S5A and B), and did not affect the expression of other genes that contain the TSP1 domain, such as Thrombospondin 1 (see Supplementary material online, Figure S5C).

A transwell permeability assay that measures HRP passage was carried out to determine the effect of *THSD1* on endothelial barrier function in HUVECs. In line with our *in vivo* findings, endothelial barrier function was significantly decreased in *THSD1* knockdown HUVECs as shown by increased permeability for HRP (*Figure 5F*). Evaluation of endothelial barrier function by ECIS (Electric Cell-substrate Impedance Sensing) also demonstrated that *THSD1* silencing in HUVEC monolayers impeded the build-up of endothelial electric resistance compared with sham treated cells (*Figure 5G*). These data indicate that endothelial barrier function in *THSD1* knockdown endothelial cells is compromised at the cell junction level.

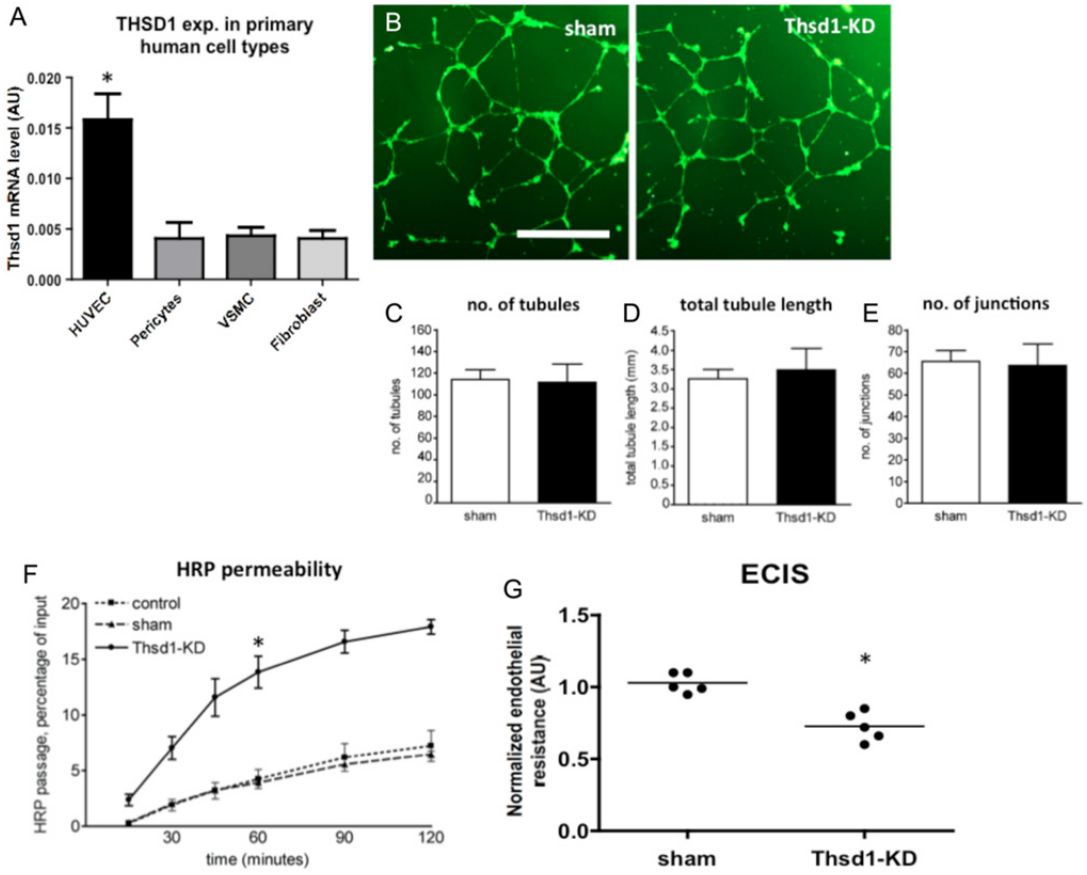

Figure 5 THSD1 knockdown in cultured endothelial cells impairs endothelial barrier function. (A) THSD1 was highly expressed in HUVEC vs. pericyte, VSMC, and fibroblast, as demonstrated by qPCR analysis. (n = 6); mean ± SEM normalized to housekeeping gene and indicated in arbitrary units (AU) *P < 0.05 vs. all; Kruskal–Wallis test followed by Dunn's multiple comparison test. (B) Assessment of network formation capacity of HUVECs transfected with THSD1 targeting siRNA (THSD1-KD) compared with HUVECs treated with non-targeting siRNA (sham) in a 2D Matrigel experiment. HUVECs were stained with Calcein-AM. Scale bar = 100 µm. Quantification of the vascular network showed no morphological defects after THSD1-KD regarding (C) number of tubules, (D) total tubule length, and (E) number of junctions (n = 4; mean ± SEM; Mann–Whitney U test). (F) Measurement of endothelial barrier function in vitro. Passage of horseradish peroxidase (HRP) over a confluent monolayer of HUVECs during thrombin (1 U/mL) stimulation for the different conditions over time. *P < 0.05 vs. control and si-sham; Bonferroni post hoc test of repeated-measures ANOVA. (n = 3; mean ± SEM) (G) ECIS measurement over a confluent monolayer of HUVECs shows a delay in electric resistance build-up after THSD1 knockdown at 45 h post seeding. *P < 0.05 vs. HUVECs treated with si-sham; Mann–Whitney U test (n = 5; mean ± SEM in arbitrary units (AU) after normalization for each well to the starting level of resistance measured at 4 h post seeding).

THSD1 mediates cell-to-cell interaction via activation of Rac1

Rac1 is an important mediator of endothelial barrier function as it enforces cell-to-cell and cell-ECM interaction via regulation of the actin cytoskeleton.[15,16] Here we evaluated the impact of *THSD1* knockdown on Rac1 activation via the FAK-PI3K pathway (*Figure 6A–G*). Knockdown

of *THSD1* significantly decreased total FAK protein levels and FAK phosphorylation at the Y397 site (*Figure 6A* and *B*) without affecting the FAK-phospho/total FAK ratio (**P* < 0.05, sham vs. *THSD1*-KD). PI3K phosphorylation at position Y508 was significantly diminished without affecting total PI3K protein levels (*Figure 6C* and *D*). Similarly, the PI3K-phospho/total PI3K ratio was decreased (**P* < 0.05, sham vs. *THSD1*-KD). Further downstream, *THSD1* silencing inhibited PI3K-mediated Rac1 activation, while total Rac1 protein levels remained unaffected (*Figure 6E* and *F*). These data indicate that *THSD1* acts through regulation of total FAK protein levels and by affecting PI3K phosphorylation levels.

To validate whether this *THSD1*-induced modulation of Rac1 activity is indeed a critical factor in the THSD1-mediated mechanisms, *THSD1*-silenced HUVECs were treated with a pharmaceutical activator for Rac1 in the *in vitro* transwell permeability assay. Rac1 stimulation decreased endothelial permeability after *THSD1* knockdown (see Supplementary material online, Figure S6A), confirming that loss of endothelial barrier function, as induced by *THSD1* knockdown, was indeed mediated via Rac1 inhibition. For further validation, a phenotype rescue experiment was carried out in the murine retina model: *Thsd1* was silenced in combination with treatment with the Rac1 activator and compared with controls with intra-ocular injection of *Thsd1* targeting siRNAs only. Rac1 activation reversed the effects of *Thsd1* silencing with a clear reduction in vascular haemorrhaging (**P* < 0.05; Mann–Whitney *U* test; 2.6 ± 0.18 vs. 0.91 ± 0.18 (mean ± SEM); *Thsd1*-KD vs. *Thsd1*-KD + Rac1 activator respectively; see Supplementary material online, Figure S6B).

To study the Rac1-mediated function of *THSD1* in actin dynamics, cell spreading, and actin filament distribution was evaluated at different time points after cell seeding (*Figure 6H* and *I*). Quantification and stratification of actin cytoskeleton surface per cell showed that *THSD1* knockdown induced a trend towards decrease in the number of cells with a large actin cytoskeleton surface (>1500 nm^2) at 30 min post seeding compared with sham transfected controls (*Figure 6I*). This decline in spreading efficiency was associated with a defect in ECM interaction: Visualization of focal adhesion sites showed a significant decline of Paxillin and Vinculin capping at actin stress fibre ends of *THSD1*-silenced cells (see Supplementary material online, Figure S7A–D).

Loss of association between VE-cadherin and the actin cytoskeleton at adherens junction sites promotes endothelial and thus vascular permeability.[3] The effect of *THSD1* knockdown on VE-cadherin-actin cytoskeleton association was assessed in confluent HUVEC monolayers. Knockdown of *THSD1* in HUVECs reduced co-localization of VE-cadherin with the actin cytoskeleton (*Figure 6J* and *K*). Taken together, these data suggest that *THSD1* modulates cell-to-cell interaction via a signalling mechanism that involves FAK-PI3K during Rac1-mediated regulation of the endothelial actin cytoskeleton.

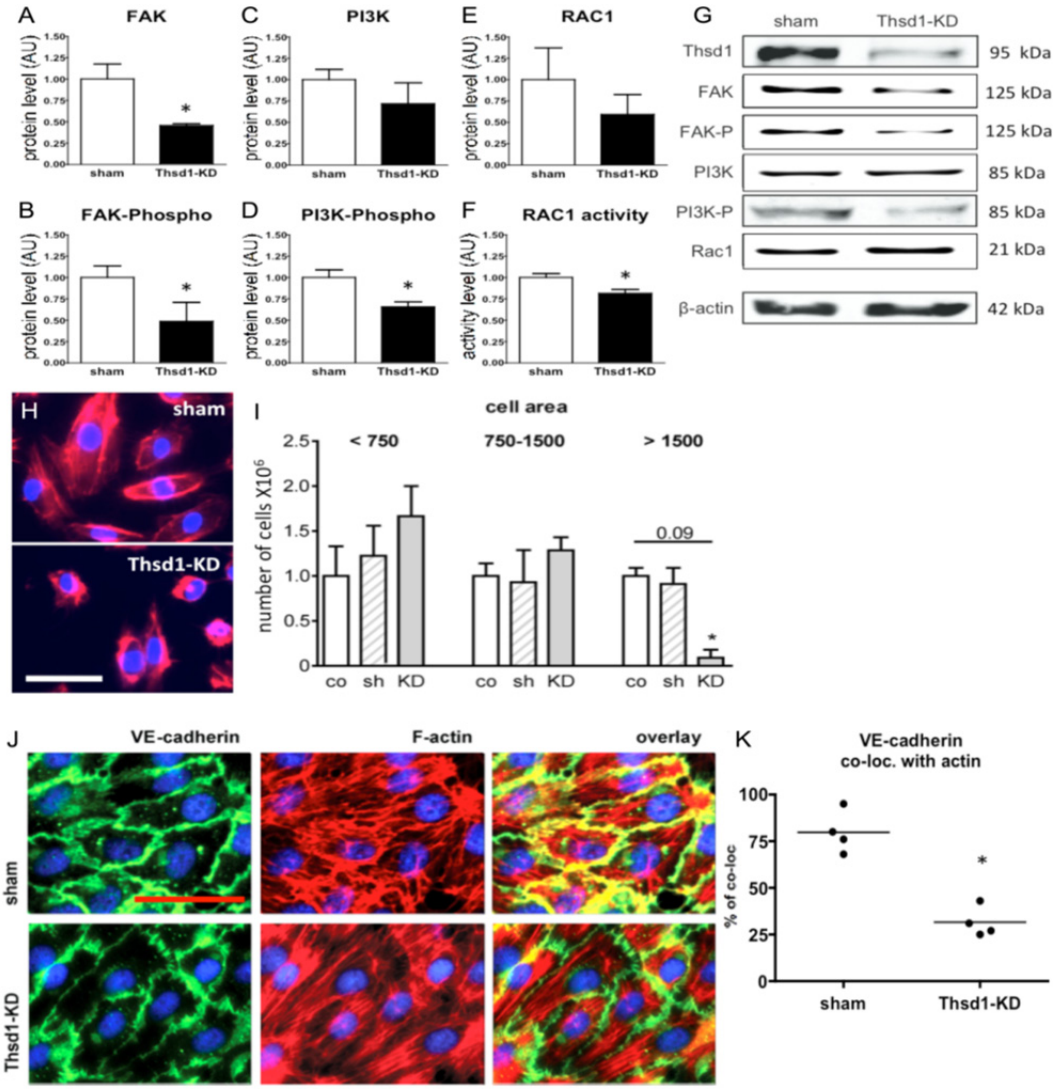

Figure 6 THSD1 induces actin cytoskeleton modulation via Rac1 activation. Western blot analysis of (A) FAK, (B) FAK-PhosphoY397 (C) PI3K, (D) PI3K-PhosphoY508, and (E) Rac1 protein levels normalized to ß-actin in THSD1-KD or sham conditions. (F) Rac1 GTPase activity levels as measured by G-lisa assays in sham and THSD1-KD conditions. (G) Representative western blot results for the assessed proteins with ß-actin loading control. [for A–F; n = 4; mean ± SEM in arbitrary units (AU)] *P < 0.05 vs. sham; Mann–Whitney U test. THSD1-KD impairs actin cytoskeleton dynamics during cell spreading. Actin mobility was assessed in a cell-spreading assay. (H) Thirty minutes after cell seeding, THSD1-KD showed a delay in actin cytoskeleton spreading. F-actin (red) and nuclei (blue). Scale bar = 50 µm. (I) Quantification of the actin cytoskeleton surface area per cell showed a decrease in the number of cells with a large actin cytoskeleton surface area (>1500 nm²) after THSD1 knockdown (n = 3; mean ± SEM). *P < 0.1 vs. sham or non-transfected control; Kruskal–Wallis test followed by Dunn's multiple comparison test. THSD1-KD impairs VE-cadherin-actin cytoskeleton colocalization. (J) THSD1-KD in HUVECs reduced co-localization of VE-cadherin with the actin cytoskeleton as demonstrated by immunofluorescent staining. VE-cadherin (green), F-actin (red), co-localized area (yellow), and nuclei (blue). (K) Quantification of the percentage of VE-cadherin that is co-localized with actin filaments (n = 4; mean ± SEM). Scale bar = 50 µm. *P < 0.05 vs. sham; Mann–Whitney U test.

Discussion

In this study, we identified *THSD1* as a new potent regulator of endothelial barrier function during physiological vascular development using *in vivo* zebrafish and mouse vascular growth models. In both embryonic zebrafish and postnatal murine pups, *Thsd1* silencing affected vascular integrity during angiogenesis, whereas vascular expansion remained effective. Mechanistically, our experiments with *THSD1*-silenced HUVECs in HRP and ECIS assays have demonstrated that endothelial barrier function was affected. Several mutant zebrafish lines have been described to display a similar vascular phenotype with hallmark haemorrhaging in the cranial region, including germ-line mutations in heg1, ccm1, ccm2, and ccm3.[14,17,18] Like *thsd1*, these genes appear to be involved in Rac1 activation and RhoA degradation.[19]

Activation of the small GTPase Rac1 in endothelial cells is a crucial factor in support of cell junction integrity and preservation of the endothelial barrier during vascular quiescence.[20–22] Rac1 activation promotes cell spreading by decreasing cell contractility via actomyosin suppression and by counteracting RhoA-induced actin stress fibre formation. Activation of Rac1 has also been reported to preserve VE-cadherin adherens junctions.[20,21,23] In contrast, inhibition of Rac1 by RhoA and Src through ß-integrin signalling induces actin stress fibre formation and disruption of VE-cadherin junctions.[22] We showed in this study that *THSD1* knockdown diminished Rac1 activity. This was coincided with a reduction in Rac1 downstream responses, including a decrease in actin cytoskeleton morphological adaptation during cell spreading in cell adhesion assays. Rac1-modulated cell spreading is part of the Rac1 and Cdc42 regulatory pathway to spatially control the formation of filopodia and lamellipodia, which favours the formation of barrier improvement.[2] Thus, THSD1 knockdown appears to directly inhibit this Rac1-mediated barrier stabilization pathway. Further downstream, decrease in Rac1 activation would lead to loss of actomyosin suppression and stress fibre formation, inducing endothelial cell contraction, and causing the formation of intercellular gaps and disruption of VE-cadherin junctions. In thrombin studies using confluent monolayers of HUVECs we showed that knockdown of *THSD1* significantly reduced co-localization of VE-cadherin with actin filaments, indicative of loss of functional adherens junctions.[3] Anchorage of VE-cadherin proteins to the actin cytoskeleton via a complex of adherens junction proteins plays a crucial role in controlling endothelial morphology and permeability.[2,24] However, the exact molecular basis of this regulation remains to be further clarified. Together the findings from our *in vitro* mechanistic studies demonstrate that *THSD1* regulates endothelial barrier function by Rac1 activation and the subsequent preservation of cell-to-cell junctions and cell-to-ECM focal adhesions via actin cytoskeleton dynamics. In our studies, *Thsd1* expression in the developing murine embryo was highest in Flk1-positive angioblasts compared with Flk1-negative cells, while whole mount *in situ* hybridization in developing zebrafish larvae validated the predominant vascular expression of *Thds1. THSD1* may thus be regarded as an endothelial regulator of Rac1 activity that plays a

prominent role in the preservation of endothelial barrier function, in particular during angiogenesis.

The current study has also highlighted the therapeutic potential of THSD1 in treatment of cardiovascular disease. Neovascular growth driven by intimal hypoxia often results in the formation of immature and fragile microvessels in advanced atherosclerotic lesions.[25] These intraplaque microvessels display extravasation of leucocytes and erythrocytes, which leads to intimal inflammation, expansion of the necrotic core, and intraplaque haemorrhaging. Recent evidence indicates that intraplaque haemorrhaging plays an important role in lesion progression towards a vulnerable plaque.[26,27] Restoration of endothelial integrity in compromised intraplaque vessels might prevent plaque destabilization and vulnerable plaque formation.[8] Assessment of human carotid endarterectomy specimens demonstrated *THSD1* expression by intimal microvascular ECs in advanced vulnerable lesions with intraplaque haemorrhaging. *THSD1* expression was absent in stable plaques. Furthermore, Thsd1 expression was significantly up-regulated in the vulnerable plaques compared with stable lesions in our murine vulnerable plaque model. These findings seem counterintuitive and difficult to integrate with the notion that *THSD1* is endothelial barrier protective. However, the findings of our *Thsd1* gain-of-function studies in our murine vulnerable plaque model further provide evidence that *Thsd1* promotes vascular integrity: Intraplaque haemorrhaging was decreased in advanced lesions in response to *Thsd1* overexpression. THSD1 expression in adults could be dependent on activation by micro-environmental factors. In support of this hypothesis, *THSD1* expression was induced by IL10, a secreted factor with plaque stabilizing properties and increased expressed in unstable lesions.[28,29]

Furthermore, THSD1 may be involved in regulating monocyte extravasation via activation of adhesion molecules and release of chemotactic cytokines. How different angiogenic modulators influence THSD1 function during vascular expansion and the effects of THSD1 on interaction between circulatory immune cells and the endothelium in adult condition remain to be further investigated.

In conclusion, in the current study, we have identified THSD1 as a new regulator of vascular integrity in vascular development and advanced vascular disease. To our knowledge, our findings are the first to report on the biological function of THSD1 in ECs during normal embryonic and early postnatal blood vessel formation. In advanced atherosclerotic lesions, overexpression of THSD1 can restore endothelial barrier function in the intraplaque neovasculature and protect the plaque from extensive haemorrhaging and further disease progression. In the light of our findings of the basic and pathophysiological function of *THSD1*, the gene may be considered to be an interesting target for the development of novel diagnostics and therapeutics in the treatment of atherosclerosis and other vascular-related diseases for which the pathophysiology involves loss of (micro)vascular integrity during angiogenic growth.

References

1 Klaassen I , Van Noorden CJ, Schlingemann RO. Molecular basis of the inner blood-retinal barrier and its breakdown in diabetic macular edema and other pathological conditions. Prog Retin Eye Res 2013;34:19–48.

2 Giannotta M , Trani M, Dejana E. VE-cadherin and endothelial adherens junctions: active guardians of vascular integrity. Dev Cell 2013;26:441–454.

3 Kim SH , Cho YR, Kim HJ, Oh JS, Ahn EK, Ko HJ, Hwang BJ, Lee SJ, Cho Y, Kim YK, Stetler-Stevenson WG, Seo DW. Antagonism of VEGF-A-induced increase in vascular permeability by an integrin alpha3beta1-Shp-1-cAMP/PKA pathway. Blood 2012;120:4892–4902.

4 Tian X , Tian Y, Sarich N, Wu T, Birukova AA. Novel role of stathmin in microtubule-dependent control of endothelial permeability. FASEB J 2012;26:3862–3874.

5 Spindler V , Schlegel N, Waschke J. Role of GTPases in control of microvascular permeability. Cardiovasc Res 2010;87:243–253.

6 Broman MT , Mehta D, Malik AB. Cdc42 regulates the restoration of endothelial adherens junctions and permeability. Trends Cardiovasc Med 2007;17:151–156.

7 Daneshjou N , Sieracki N, van Nieuw Amerongen GP, Conway DE, Schwartz MA, Komarova YA, Malik AB. Rac1 functions as a reversible tension modulator to stabilize VE-cadherin trans-interaction. J Cell Biol 2015;209:181.

8 Jain RK , Finn AV, Kolodgie FD, Gold HK, Virmani R. Antiangiogenic therapy for normalization of atherosclerotic plaque vasculature: a potential strategy for plaque stabilization. Nat Clin Pract Cardiovasc Med 2007;4:491–502.

9 Sluimer JC , Daemen MJ. Novel concepts in atherogenesis: angiogenesis and hypoxia in atherosclerosis. J Pathol 2009;218:7–29.

10 Takayanagi S , Hiroyama T, Yamazaki S, Nakajima T, Morita Y, Usui J, Eto K, Motohashi T, Shiomi K, Keino-Masu K, Masu M, Oike Y, Mori S, Yoshida N, Iwama A, Nakauchi H. Genetic marking of hematopoietic stem and endothelial cells: identification of the Tmtsp gene encoding a novel cell surface protein with the thrombospondin-1 domain. Blood 2006;107:4317–4325.

11 Cheng C , Tempel D, van Haperen R, de Boer HC, Segers D, Huisman M, van Zonneveld AJ, Leenen PJ, van der Steen A, Serruys PW, de Crom R, Krams R. Shear stress-induced changes in atherosclerotic plaque composition are modulated by chemokines. J Clin Invest 2007;117:616–626.

12 Cheng C , Noordeloos AM, Jeney V, Soares MP, Moll F, Pasterkamp G, Serruys PW, Duckers HJ. Heme oxygenase 1 determines atherosclerotic lesion progression into a vulnerable plaque. Circulation 2009;119:3017–3027.

13 Gjini E , Hekking LH, Kuchler A, Saharinen P, Wienholds E, Post JA, Alitalo K, Schulte-Merker S. Zebrafish Tie-2 shares a redundant role with Tie-1 in heart development and regulates vessel integrity. Dis Model Mech 2011;4:57–66.

14 Kleaveland B , Zheng X, Liu JJ, Blum Y, Tung JJ, Zou Z, Sweeney SM, Chen M, Guo L, Lu MM, Zhou D, Kitajewski J, Affolter M, Ginsberg MH, Kahn ML. Regulation of cardiovascular development and integrity by the heart of glass-cerebral cavernous malformation protein pathway. Nat Med 2009;15:169–176.

15 Huveneers S , Oldenburg J, Spanjaard E, van der Krogt G, Grigoriev I, Akhmanova A, Rehmann H, de Rooij J. Vinculin associates with endothelial VE-cadherin junctions to control force-dependent remodeling. J Cell Biol 2012;196:641–652.

16 Kraemer A , Goodwin M, Verma S, Yap AS, Ali RG. Rac is a dominant regulator of cadherin-directed actin assembly that is activated by adhesive ligation independently of Tiam1. Am J Physiol Cell Physiol 2007;292:C1061–9.

17 Voss K , Stahl S, Hogan BM, Reinders J, Schleider E, Schulte-Merker S, Felbor U. Functional analyses of human and zebrafish 18-amino acid in-frame deletion pave the way for domain mapping of the cerebral cavernous malformation 3 protein. Hum Mutat 2009;30:1003–1011.

18 Stainier DY , Fouquet B, Chen JN, Warren KS, Weinstein BM, Meiler SE, Mohideen MA, Neuhauss SC, Solnica-Krezel L, Schier AF, Zwartkruis F, Stemple DL, Malicki J, Driever W, Fishman MC. Mutations affecting the formation and function of the cardiovascular system in the zebrafish embryo. Development 1996;123:285–292.

19 Faurobert E , Albiges-Rizo C. Recent insights into cerebral cavernous malformations: a complex jigsaw puzzle under construction. FEBS J 2010;277:1084–1096.

Google ScholarCrossRefPubMed

20 Waschke J , Burger S, Curry FR, Drenckhahn D, Adamson RH. Activation of Rac-1 and Cdc42 stabilizes the microvascular endothelial barrier. Histochem Cell Biol 2006;125:397–406.

21 Wojciak-Stothard B , Potempa S, Eichholtz T, Ridley AJ. Rho and Rac but not Cdc42 regulate endothelial cell permeability. J Cell Sci 2001;114(Pt 7):1343–1355.

22 Davis GE , Senger DR. Endothelial extracellular matrix: biosynthesis, remodeling, and functions during vascular morphogenesis and neovessel stabilization. Circ Res 2005;97:1093–1107.

23 Good DJ , Polverini PJ, Rastinejad F, Le Beau MM, Lemons RS, Frazier WA, Bouck NP. A tumor suppressor-dependent inhibitor of angiogenesis is immunologically and functionally indistinguishable from a fragment of thrombospondin. Proc Natl Acad Sci USA 1990;87:6624–6628.

24 Dejana E , Orsenigo F, Lampugnani MG. The role of adherens junctions and VE-cadherin in the control of vascular permeability. J Cell Sci 2008;121(Pt 13):2115–2122.

25 Moreno PR , Purushothaman KR, Sirol M, Levy AP, Fuster V. Neovascularization in human atherosclerosis. Circulation 2006;113:2245–2252.

26 Kolodgie FD , Gold HK, Burke AP, Fowler DR, Kruth HS, Weber DK, Farb A, Guerrero LJ, Hayase M, Kutys R, Narula J, Finn AV, Virmani R. Intraplaque hemorrhage and progression of coronary atheroma. N Engl J Med 2003;349:2316–2325.

27 Michel JB , Virmani R, Arbustini E, Pasterkamp G. Intraplaque haemorrhages as the trigger of plaque vulnerability. Eur Heart J 2011;32:1977–1985, 1985a, 1985b, 1985c.

28 Mallat Z , Besnard S, Duriez M, Deleuze V, Emmanuel F, Bureau MF, Soubrier F, Esposito B, Duez H, Fievet C, Staels B, Duverger N, Scherman D, Tedgui A. Protective role of interleukin-10 in atherosclerosis. Circ Res 1999;85:e17–e24.

29 Nishihira K , Imamura T, Yamashita A, Hatakeyama K, Shibata Y, Nagatomo Y, Date H, Kita T, Eto T, Asada Y. Increased expression of interleukin-10 in unstable plaque obtained by directional coronary atherectomy. Eur Heart J 2006;27:1685–1689.

Supplement data

Supplemental Table 1. Patient characteristics

	stable plaque	*advanced vulnerable plaque*
gender	5 male/0 female	5 male/0 female
age (mean ± SEM)	74.6 ± 2.5	65.5 ± 6.4

N = 5; mean ± SEM, stable plaque versus advanced vulnerable plaque; Mann Whitney U test.

Supplemental figures

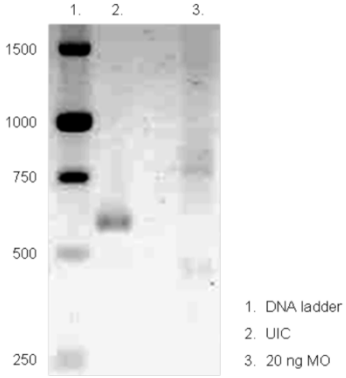

Supplemental figure 1. Morpholino-induced *thsd1* knockdown in zebrafish. Morpholino (MO) knockdown efficiency tested by PCR. After injection of 20 ng of *thsd1*splice donor MO (lane 3), *thsd1* mRNA was spliced incorrectly versus the uninjected control embryos (lane 2).

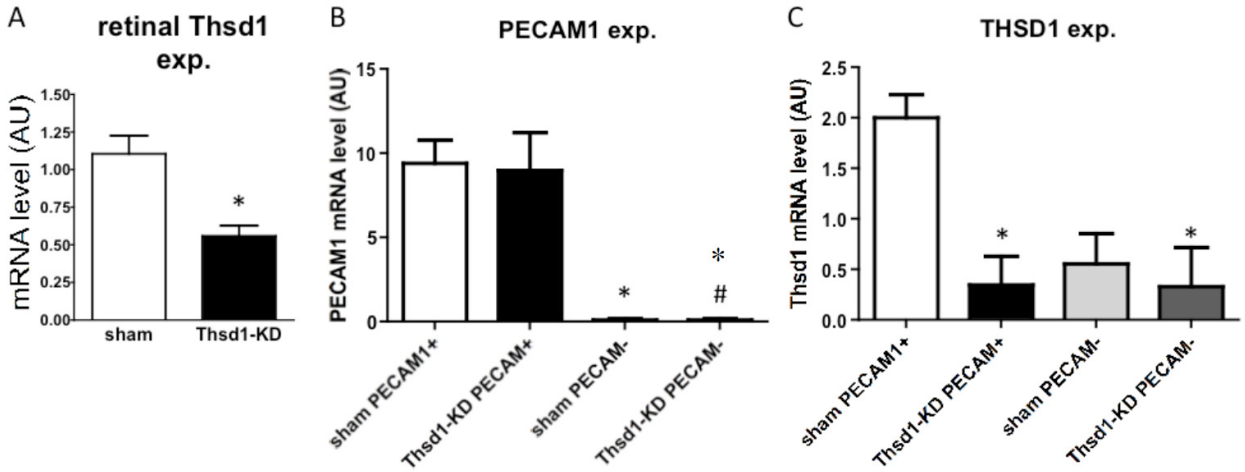

Supplemental figure 2. *Thsd1* depletion in the developing retinal vasculature of neonatal mice after siRNA targeting. (A) Endogenous expression level of *Thsd1* in the retina after intra-ocular injection of *Thsd1* targeting siRNA (*Thsd1-KD*) showed a reduction in expression levels of *Thsd1* as demonstrated by qPCR (n = 10; mean ± SEM, normalized to house keeping gene and indicated in arbitrary units (AU)). *P<0.05 versus sham; Student's T-test. (B) To validate efficient *Thsd1* silencing in retinal endothelial cells, PECAM+ retinal endothelial cells were isolated from collagenase treated retinas using magnetic beads

coated with anti-PECAM1 antibodies. PECAM1 expression in PECAM+ cells were compared to PECAM1- cells by qPCR in retina samples injected with non-targeting siRNAs (sham) or *Thsd1* targeting siRNAs (*Thsd1*-KD) at day 2 post injection (n = 5; mean ± SEM, normalized to house keeping gene and indicated in arbitrary units (AU)). *P<0.05 versus sham PECAM+ cells; #P<0.1 versus
Thsd1-KD PECAM+ cells; Kruskal-Wallis test followed by Dunn's multiple comparison test. (C) Endogenous *Thsd1* expression in sham PECAM+ cells were compared to *Thsd1*-KD PECAM1+ cells by qPCR in retina samples injected with non-targeting siRNAs (sham) or Thsd1 targeting siRNAs (Thsd1-KD) at day 2 post injection (n = 5;mean ± SEM, normalized to house keeping gene and indicated in arbitrary units (AU)).*P<0.05 versus sham PECAM+ cells; Kruskal-Wallis test followed by Dunn's multiple comparison test.

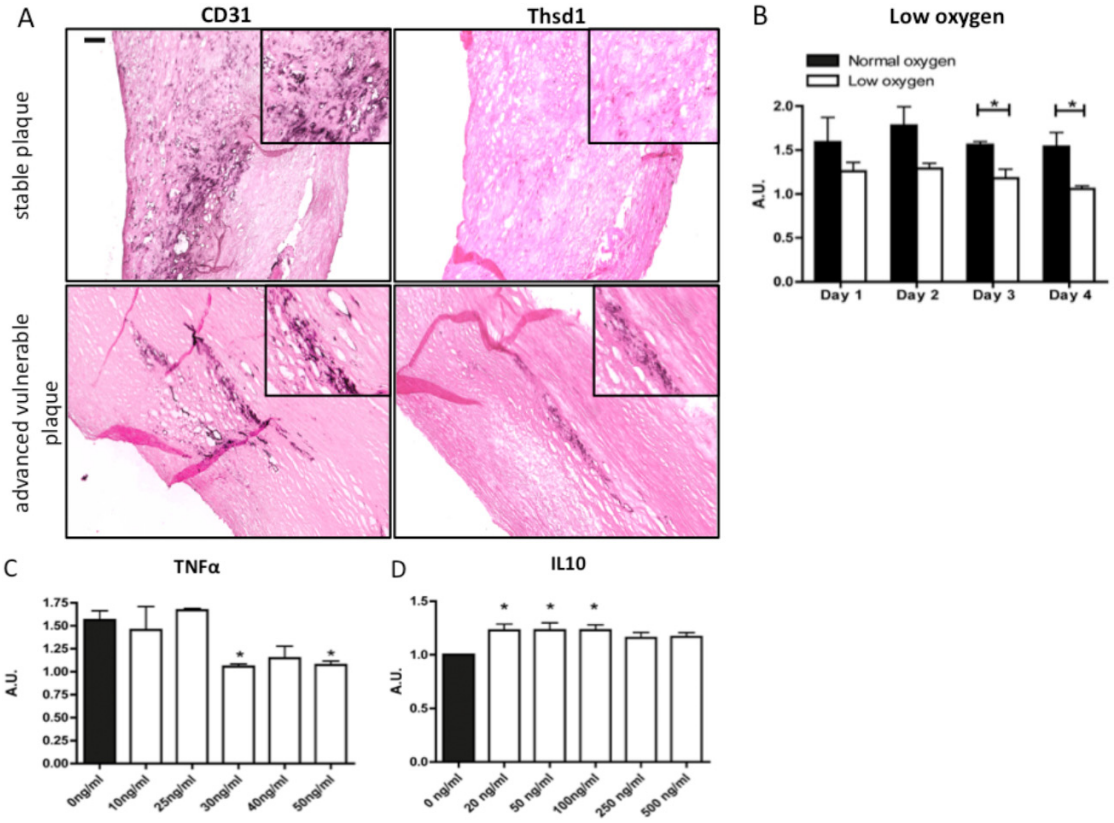

Supplemental figure 3. THSD1 expression in advanced human atherosclerotic lesions with neovascular intraplaque haemorrhaging. Human carotid endarterectomy specimens stained for (A) CD31 and THSD1. Specimens were divided in stable plaque (upper row) and vulnerable plaque with intraplaque haemorrhage (lower row). Inserted panels show high magnification details of the micrographs. Representative specimens from 5 in each group. Scale bar = 100µm. Pro-and anti-atherogenic stimuli determine THSD1 expression. Endogenous mRNA expression level of THSD1 in HUVECs in response to pro-atherogenic stimuli, including (B) low (3% O2) and normal (20% O2) oxygen conditions over time (*P<0.05 compared to normal oxygen; Mann Whitney U test per time point), and (C) different concentrations of TNFα (*P<0.05 compared to 0 ng/ml and 25 ng/ml; Kruskal-Wallis test followed by Dunn's multiple comparison test). Endogenous mRNA expression level of THSD1 in HUVECs in response to the anti-atherogenic stimulus (D) IL10 (*P<0.05 compared to 0ng/ml; Kruskal-Wallis test followed by Dunn's multiple comparison test). THSD1 expression in ECs was diminished by pro-atherogenic stimuli,

while an anti-atherogenic stimulus increased THSD1 mRNA expression (for B-D, n = 4; mean ± SEM, normalized to house keeping gene and indicated in arbitrary units (AU)).

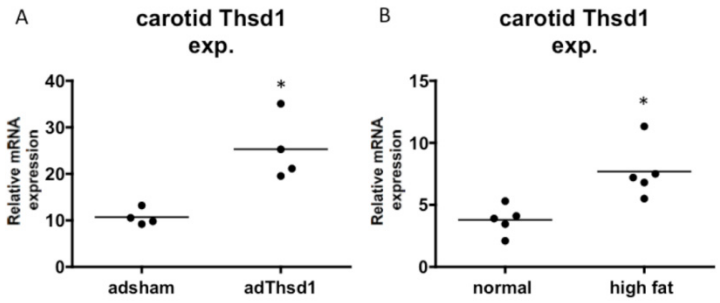

Supplemental figure 4. Adenovirus-mediated overexpression of Thsd1 in carotid arteries. (A) Carotid arteries transfected with an adenoviral expression plasmid for murine Thsd1 (AdThsd1) showed an elevation in mRNA expression levels of Thsd1 at day 3 post-infection compared to sham virus transfected arteries (adsham) as shown by qPCR (n = 4; mean ± SEM relative to house keeping gene expression). (B) Endogenous Thsd1 mRNA expression level in carotid arteries of ApoE-knockout mice fed on normal chow (normal) and high cholesterol, high fat diet (high fat) (n = 5respectively; indicated in mean ± SEM relative to housekeeping gene). *P<0.05 versus adsham or normal diet; Mann Whitney U test.

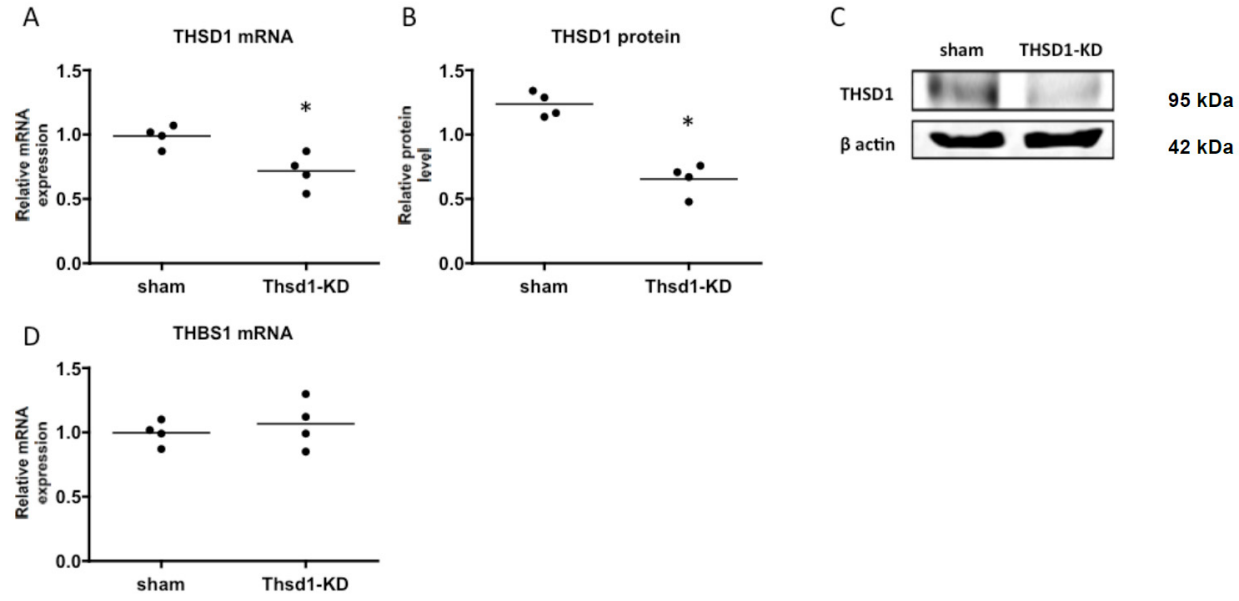

Supplemental figure 5. siRNA-mediated knockdown of THSD1 in cultured endothelial cells. (A) QPCR data of THSD1 mRNA levels in HUVECs transfected with THSD1 targeting siRNA (THSD1-KD) compared to HUVECs transfect with non-targeting siRNA (sham) relative to mRNA level of housekeeping gene. (B) Quantified THSD1 protein levels of HUVECs transfected with THSD1 targeting siRNA (THSD1-KD) compared to HUVECs transfect with non-targeting siRNA (sham) relative to ß actin loading control. (C) Representative Western blot result for the assessment of THSD1 protein with ß actin loading control. (D) The mRNA expression level of Thrombospondin 1 (THBS1) in HUVECs THSD1-KD versus sham relative to

mRNA level of housekeeping gene as shown by qPCR. (for A, B, and D; n = 4; mean ± SEM) *P<0.05 versus sham; Mann Whitney U test.

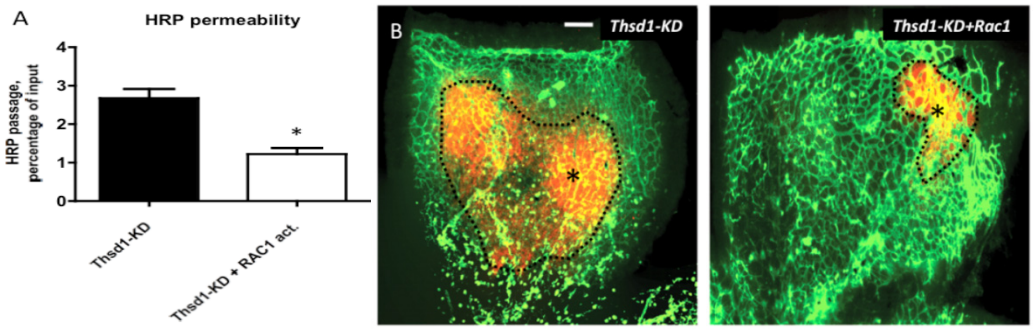

Supplemental figure 6. Rac1 stimulation rescues impaired endothelial integrity in THSD1-depleted cells. (A) Measurement of endothelial barrier function in vitro, showing differences in HRP passage in Rac1-stimulated HUVEC monolayers versus no Rac1 activation after 120 minutes of HRP passage. Control, sham and THSD1-KD conditions without Rac1 activation were set to zero. Bars indicate changes in HRP passage in response to Rac1 activation in the different groups. THSD1-KD shows a decrease in HRP passage with Rac1 activation compared to THSD1-KD without Rac1 activation *P<0.05 (n = 4; mean SEM; Mann Whitney U test). (B) Double-stained retinas with isolectin GS-IB4 (ECs, green) and TER-119 (erythrocytes, red). Rac1 stimulation reduced area size of extravascular TER-119 erythrocytes accumulation (dotted area marked by an asterisk) after Thsd1-KD (n = 5).

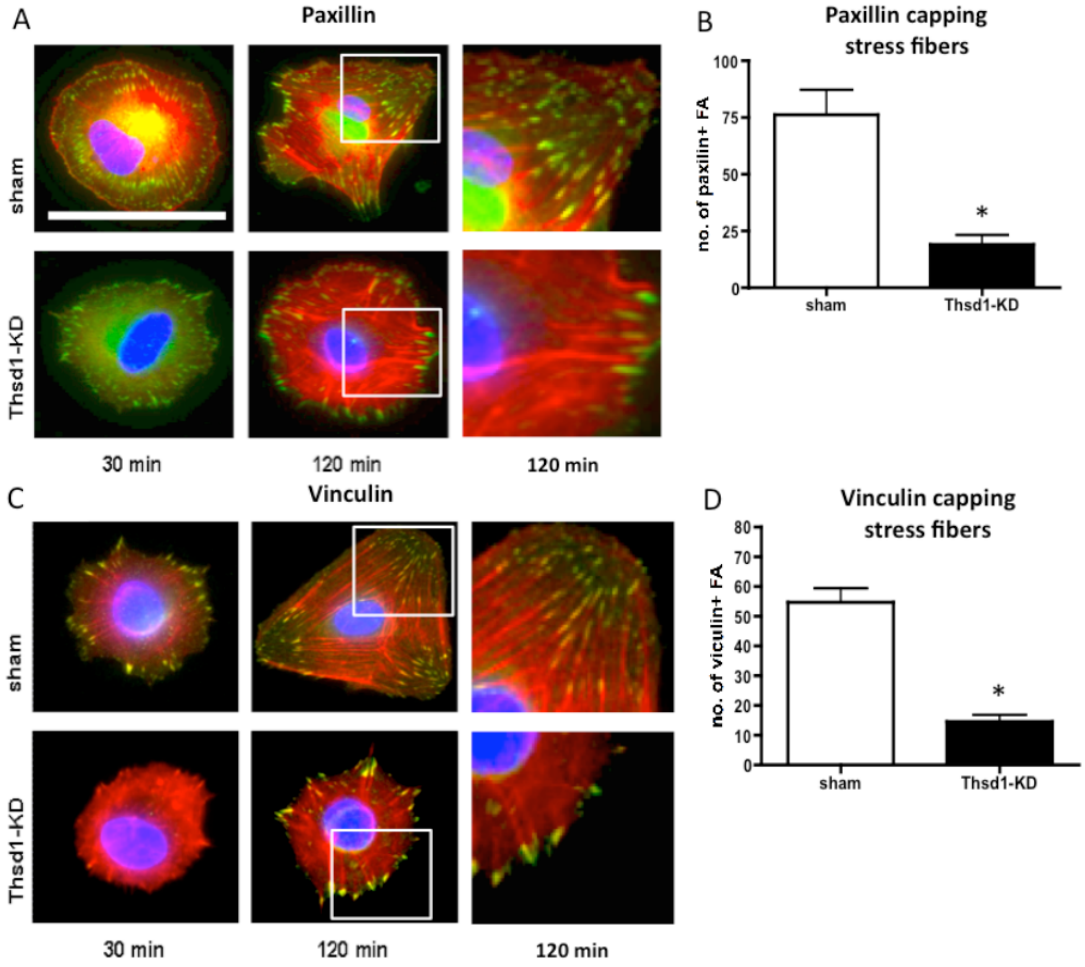

Supplemental figure 7. THSD1-KD impairs focal adhesion assembly. Micrograph panels show the distribution of the focal adhesion molecules (A) Paxillin and (C) Vinculin after 30 and 120 minutes of cell adhesion, as demonstrated by immunofluorescent staining in HUVECs transfected with THSD1 targeting siRNA (THSD1-KD, or non-targeting siRNA (sham). Paxillin or Vinculin (green), F-actin (red) and nuclei (blue). High magnification detail pictures of the 120 minutes micrograph series are shown in the right column. Quantified results of the number of (B) Paxillin or (D) Vinculin-positive focal adhesion sites capping the actin fibre ends, 120 minutes after cell seeding (for B and D; n = 5; mean ± SEM). Scale bar = 50 µm. *P<0.05 versus sham; Mann Whitney U test.

Chapter 6 Uridine adenosine tetraphosphate acts as a pro-angiogenic factor in vitro through purinergic P2Y receptors.

Zhichao Zhou [*], Ihsan Chrifi [*], Yanjuan Xu, John Pernow, Dirk J. Duncker, Daphne Merkus[†] and Caroline Cheng[†] *These *first and † last authors contributed equally to the paper.*

Published: American Journal Physiology Heart Circulation Physiology 2016 Jul 1;311(1):H299-309

Abstract

Aim:

Uridine adenosine tetraphosphate (Up_4A), a dinucleotide, exerts vascular influence via purinergic receptors (PR). We investigated the effects of Up_4A on angiogenesis and the putative PR involved.

Methods and Results:

Tubule formation assay was performed in a 3D system, in which human endothelial cells were co-cultured with pericytes with various Up_4A concentrations for 5 days. Expression of PR subtypes and angiogenic factors was assessed in human endothelial cells with and without $P2Y_6R$ antagonist. No difference in initial tubule formation was detected between Up_4A stimulation and control conditions at day 2. In contrast, a significant increase in vascular density in response to Up_4A was observed at day 5. Up_4A at an optimal concentration of 5 μM promoted total tubule length, number of tubules and number of junctions, all of which were inhibited by the $P2Y_6R$ antagonist MRS2578. Higher concentrations of Up_4A (10 μM) had no effects on angiogenesis parameters. Up_4A increased mRNA level of P2YRs ($P2Y_2R$, $P2Y_4R$ and $P2Y_6R$) but not P2XR ($P2X_4R$ and $P2X_7R$) or P1R ($A_{2A}R$ and $A_{2B}R$), while Up_4A upregulated VEGFA and ANGPT1, but not $VEGFR_2$, ANGPT2, Tie1 and Tie2. In addition, Up_4A increased VEGFA protein levels. Transcriptional upregulation of P2YRs by Up_4A was inhibited by MRS2578.

Conclusion:

In conclusion, Up_4A is functionally capable of promoting tubule formation in an *in vitro* co-culture system, which is likely mediated by pyrimidine-favoured P2YRs but not P2XRs or P1Rs, and involves upregulation of angiogenic factors.

Introduction

Extracellular nucleotides such as ATP, ADP, adenosine, UTP and UDP are increasingly recognized as important regulators of a variety vascular functions, including vascular tone (3), permeability (12), inflammation (6) and angiogenesis (7). All these vascular responses of extracellular nucleotides are initialized by activation of purinergic receptors (PRs) on the plasma membrane (7). PRs have been classified into two subtypes: P1 and P2 receptors, based on their pharmacological properties and molecular structures (10, 27). Four subtypes of P1 receptors (also termed adenosine receptors), all metabotropic, have been cloned, namely A1R, $A_{2A}R$, $A_{2B}R$ and A3R (33). The P2 receptors belong to two major families: ionotropic P2XR and metabotropic P2YR (1, 5). At least seven P2XR and eight P2YR have been cloned to date (4).

Angiogenesis, the formation of new capillaries from pre-existing blood vessels, occurs during normal embryonic development and in various physiological and pathological conditions (8). Several *in vitro* studies have shown that activation of all four subtypes of P1R by adenosine results in angiogenesis via release of angiogenic factors (18). Moreover, injection of an adenosine A_{2A} receptor agonist into diabetic mice has been shown to improve impaired wound healing and increase wound-breaking strength (13). In addition to P1R, activation of not only P2XR receptors by ATP (19) but also P2YR by ATP, ADP or UTP (2, 14, 35) have been reported to influence established angiogenic factors such as vascular endothelial growth factor (VEGF) leading to tubulogenesis, angiogenesis and wound repair. More recently, activation of $P2Y_4R$ receptors was shown to play an essential role in post-natal cardiac development (20). Together, these findings suggest that purinergic receptors activated by extracellular nucleotides may be involved in angiogenesis.

Uridine adenosine tetraphosphate (Up_4A), endogenously released from endothelial cells and biosynthesized by VEGF receptor type 2 ($VEGFR_2$) (23), has been identified as the first dinucleotide found in living organisms that contains both purine and pyrimidine moieties (25). This suggests that Up_4A is capable of activating both P1R and P2R (25, 44, 45). Indeed, early studies regarding the effect of Up_4A on vascular tone regulation found that Up_4A induces vasoconstriction through $P2X_1R$ (25, 46) and P2YR (17), but produces vasodilation through $A_{2A}R$ (44, 45), $P2X_1R$ and $P2Y_1R$ (44). Recent studies performed at the cellular level, showed that Up_4A induces human smooth muscle cell proliferation via activation of P2YR (16), and is a strong activator of migration in smooth muscle cell obtained from rat thoracic aorta through activation of $P2Y_2R$ (42).

To date, the effect of Up_4A on the angiogenic process has not been explored. Here, we investigated the angiogenic potential of Up_4A. Our data show that Up_4A stimulation promotes angiogenic tubule formation in a 3D matrix system *in vitro*, in which the neovascular growth process is more accurately mimicked by allowing interaction of human endothelial cells with pericytes. Since the biosynthesis of Up_4A is linked to $VEGFR_2$ in endothelial cells (23), we also investigated the effect of Up_4A on the expression of well-known angiogenic factors. In addition, we evaluated which putative PRs could be involved in the endothelial angiogenic response to

Up_4A. We found in the present study that Up_4A mainly affected pyrimidine-favoured P2YR ($P2Y_6R$). We subsequently tested the effect of $P2Y_6R$ blockade on Up_4A-mediated angiogenesis and the expression profile of PRs, as well as angiogenic factors.

Material and Methods

Cell culture

Human umbilical vein endothelial cells (HUVECs), human microvascular ECs (HMVECs), human aorta ECs (HAECs), and human carotid arterial endothelial cells (HCATECs) were obtained from Lonza (the Netherlands) and maintained in EGM™2 Bulletkit™ medium (Lonza, the Netherlands) with 100 Uml-1 penicillin-streptomycin (PS). Human brain vascular pericytes were obtained from ScienCell (the Netherlands) and maintained in DMEM supplemented with 10% FCS and 100 Uml-1 PS. All cells were used between passages 3 and 6 (9).

HUVECs-GFP, HMVECs-GFP and pericytes-dsRED were created by transfecting passage 1 HUVECs and pericytes at 60% confluency with lentiviral vectors encoding GFP and dsRED cDNA respectively at MOI 5 in the presence of 6 μg/ml polybrene in EBM medium with 0.2% FCS. After 6 hours of transduction, the cells were incubated for 72 hours in fresh growth medium and were exposed to Puromycin (1-2,5 μg/ml) selection for 10 days (38). HUVECs-GFP, HMVECs-GFP and pericytes-dsRED batches were stored by cryopreservation before use in experiments.

Collagen based 3D co-culture

Microvessel networks were established by seeding either HUVECs-GFP, HMVECs-GFP, and pericytes-dsRED at a density of 6×10^4 HUVECs- or HMVECs-GFP and 1.2×10^4 pericytes-dsRED in 50 μl of 2.0 mg/ml type 1 collagen (BD Bioscience, USA), supplemented with stem cell factor, stromal-derived factor-1α, and interleukin-3 (BD-Bioscience, USA), each added at a concentration of 400 ng/μl in the collagen matrix (39). Subsequently, the collagen was allowed to crosslink for 1 hour at 37°C and 5% CO_2. Depending on the test conditions, Up_4A (0 μM-1 μM-2.5 μM-5 μM-10 μM) and the potent/irreversible $P2Y_6R$ antagonist MRS2578 (10 μM) (30, 45) were added per well in EBM2 + 2%FCS + ascorbic acid + fibroblast growth factor-2 (obtained from the EGM2 bullitkit). After 2 days of co-culture, tubule formation, and after 5 days stabilization of the newly formed tubules was monitored by fluorescence microscopy. Total tubule length, mean tubule length and the amount of junctions were quantified with Angiosys software (UK). See Fig. 1A for a summary of methods.

Quantitative real-time PCR (q-PCR) analysis

q-PCR was conducted to determine the effect of Up_4A in the absence and presence of $P2Y_6R$ antagonist on mRNA expression levels of putative purinergic receptors and pro-angiogenic factors. Either HUVECs or HAECs were seeded at a density of 200.000 cells per well in a pre-coated (0.1% gelatin) 6 wells culture plate. HUVECs or HAECs were treated with Up_4A (0 μM-5

μM-10 μM) in the absence and presence of $P2Y_6R$ antagonist MRS2578 (10 μM) in EBM2 + 2%FCS + ascorbic acid + fibroblast growth factor-2. After 24 hours incubation at 37°C and 5% CO_2, cells were washed twice with ice cold PBS and harvested for total RNA extraction (9). RNA was isolated using RNAeasy kit (Qiagen, The Netherlands) and was checked for quality and quantity by spectophotometer (Nanodrop; ND-1000). Isolated RNA was reverse transcribed into cDNA according to manufacturer's instruction (Iscript, Bio-Rad, the Netherlands). q-PCR reactions were performed using iCycles iQ5 Detection System (Bio-Rad, the Netherlands) according to manufacturer's instructions. Sequences of the primers that were designed and used for these experiments are described in Table 1. The mRNA expression levels were analysed and normalized using the housekeeping gene β-actin or GAPDH.

Western blot analysis

HCATECs were seeded at a density of 200.000 cells per well in a pre-coated (0.1% gelatin) 6 wells culture plate. HCATECs were treated with Up_4A (0 μM-5 μM-10 μM) in EBM2 + 2%FCS + ascorbic acid + fibroblast growth factor-2. After 48 hours incubation at 37°C and 5% CO_2, cells were washed twice with ice cold PBS and harvested. Protein was extracted in RIPA Buffer (Thermo Scientific, USA) with protease inhibitors (Roche), and centrifuged for 15 min at 12000 g at 4^0C. Total protein content of the extracts was quantified by using a bicinchoninic acid protein assay kit (Pierce Biotechnology, Life Technologies Ltd). The proteins were separated on 12% SDS gel (30 μg per sample) and transferred onto PVDF membranes (Merck, Millipore, Solna, Sweden). Membranes were blocked with 5% milk for 1 h at room temperature and incubated overnight at 4^0C with primary antibodies against VEGFA (1:1000), ANGTP1 (1:500) and GAPDH (1:2500). Band densities were analyzed with Image Studio Lite Version 3.1 (LI-COR Bio-sciences) and the data obtained were normalized to GAPDH.

Statistical analysis

Statistical analysis of the 3D co-culture data was performed using GraphPad Prism statistical program (USA) or Microsoft Excel (Microsoft). Statistical significance was set at minimum with P less than 0.05. Data were analyzed by one-way ANOVA, followed by post hoc analysis using Bonferroni's test. Data are presented as mean±SEM, unless stated otherwise.

Results

Up_4A promotes vascular tubule formation

To assess the angiogenic potential of Up_4A, we used an *in vitro* co-culture assay. In this assay, GFP labeled human endothelial cells and human brain derived dsRED labeled pericytes were co-cultivated in a 3D collagen gel setting, enabling direct interaction between these two types of vascular cells. Vascular sprouting and initiation of tubule formation was observed after 1 day, with subsequent stabilization of the vascular structures till up to 5 days post-seeding. Imaging and quantification of the vascular structures were conducted at 2 and 5 days post-seeding (Fig. 1A). Different concentrations of Up_4A were added to the co-cultures at day 0, and the effect was evaluated in comparison to non-treated samples.

No difference in initial tubule formation was detected between Up_4A stimulation and control conditions at day 2. In contrast, a significant increase in vascular density in response to Up_4A was observed at day 5 in HUVEC-pericyte co-culture system (Fig. 1B and 1C). Up_4A at a concentration of 2.5 µM and 5 µM (but not at 10 µM) promoted total tubule length (by ~1.89 fold and ~2.23 fold), number of tubules (by ~1.71 fold and ~1.89 fold) as well as number of junctions (by ~2.24 fold and ~2.80 fold) (Fig. 1C). Similarly, Up_4A at a concentration of 5 µM significantly promoted angiogenesis in co-culture system of HMVECs at day 5 (Fig. 1D and 1E). However, increase in tubule formation was not detected at day 5 if Up_4A was added at day 2 (data not shown). These findings indicate that Up_4A is functionally capable of promoting tubule formation, and Up_4A stimulation during early sprouting in our co-culture setup is required to enhance vascular growth.

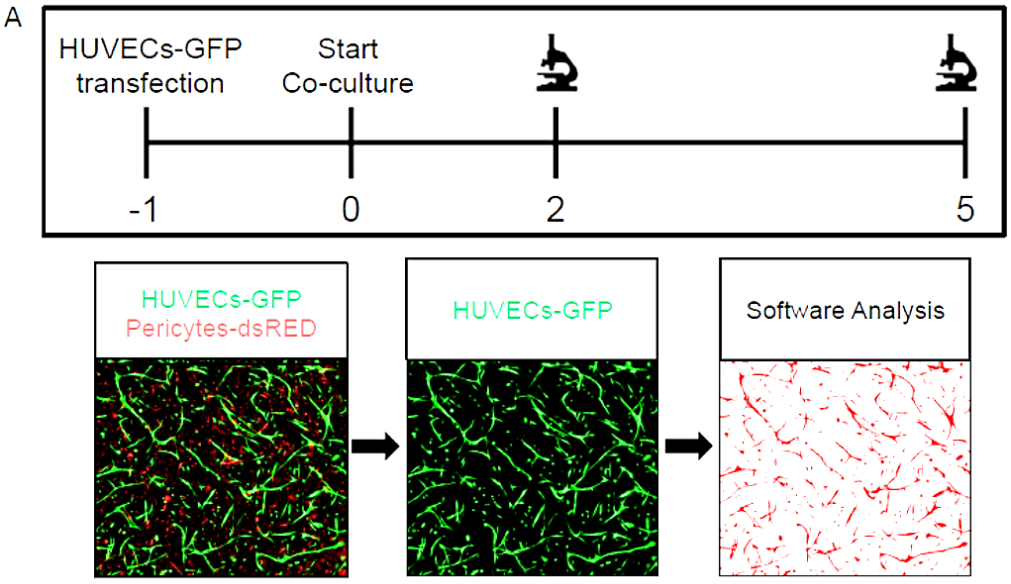

Figure 1: Endothelial cells and pericytes co-culture in response to different concentrations of Up_4A.

(A) Protocol of the co-culture assay. GFP labeled HUVECs and human brain derived dsRED labeled pericytes are co-cultivated in a 3D collagen gel setting and monitored at day 2 and day 5 post seeding. Up_4A was added at day 0 and compared to non-treated controls.

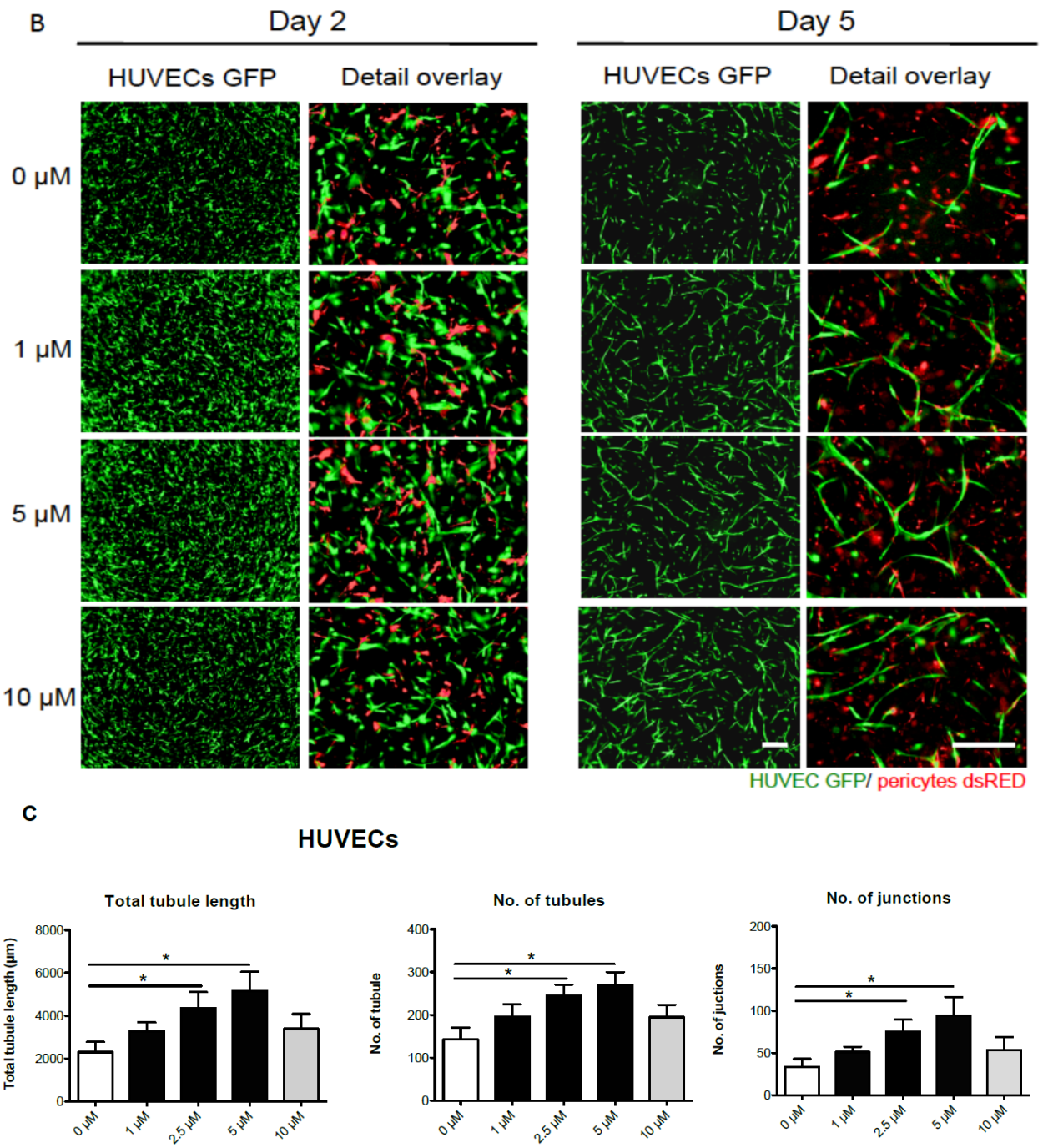

Figure 1: (B) Representative pictures of HUVECs and pericytes co-culture in a 3D matrix gel environment treated with 0, 1, 2.5, 5 or 10 µM Up_4A. Pictures were taken by fluorescent microscope on day 2 and 5. HUVECS are labeled with GFP (in green); Pericytes are labeled with dsRED (in red). (C) Quantification of total tubule length, number of tubules and junctions at day 5 of (HUVECs and pericytes) co-culture as shown in A. Scale bar: 50 µm. Values are mean ± SEM. * $P<0.05$ versus 0 µM. N=3 individual experiments.

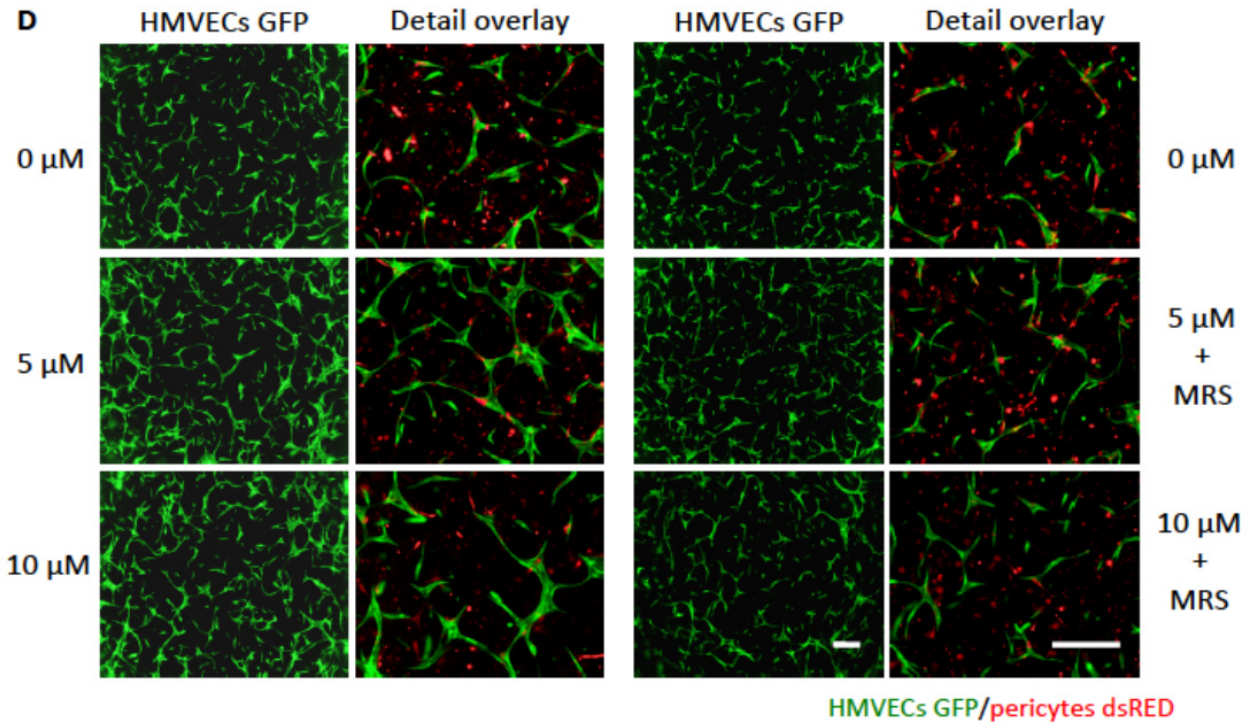

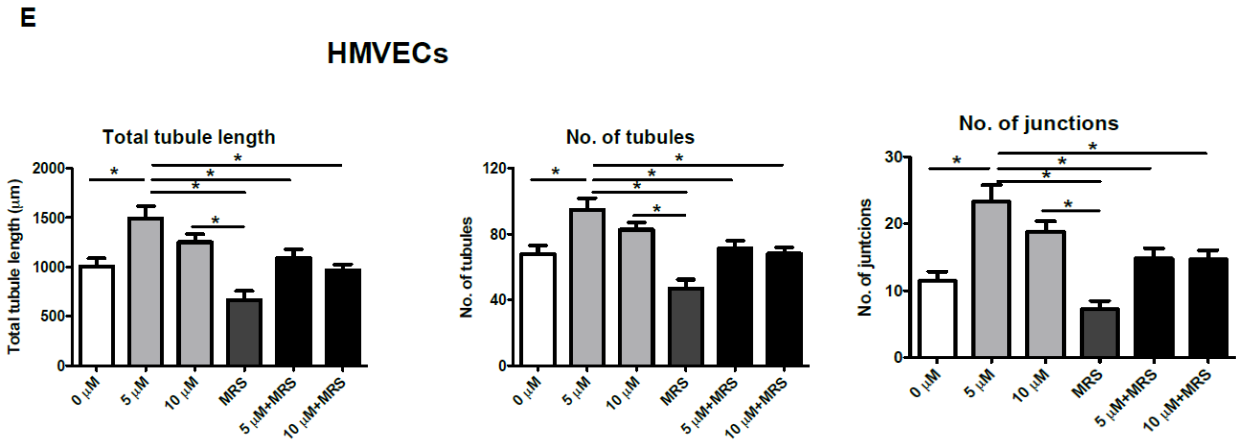

Figure 1 (D) Representative images of HMVECs and pericytes co-culture treated with Up_4A alone or in combination with $P2Y_6R$ antagonist MRS2578 (MRS, 10 µM). Pictures were taken by florescent microscope at day 5. HMVECs are labeled with GFP (in green); pericytes are labeled with dsRED (in red). (E) Quantification of fold increase in numbers of junctions, tubules and total tubule length of HMVECs and pericytes co-cultures at day 5. HMVECs were treated with 0, 5, or 10 µM Up_4A (as indicated in bar graph) with or without $P2Y_6R$ antagonist MRS2578 (10 µM). Scale bar: 50 µm. Values are represented as mean ± SEM. * $P<0.05$, N=3 individual experiments.

Effects of Up_4A on expression of purinergic receptors and angiogenic factors

Vascular tone regulation and other biological effects by Up_4A are mediated through activation of PRs (31). Next, we evaluated the effects of 24 hours of incubation with Up_4A on the mRNA expression profile of PRs in HUVECs. Up_4A at a concentration of 10 µM significantly increased mRNA levels of $P2Y_2R$, $P2Y_4R$ and $P2Y_6R$ (Fig. 2A). In contrast, mRNA levels of $A_{2A}R$, $A_{2B}R$, $P2X_4R$, and $P2X_7R$ were not affected by Up_4A, either at a concentration of 5 µM or 10 µM, as compared to non-treated controls (Fig. 2A). Further evaluation of Up_4A on expression levels of angiogenic factors showed that 10 µM of Up_4A significantly increased mRNA levels of VEGFA and ANGPT1, whereas 5 µM or 10 µM of Up_4A failed to increase mRNA levels of $VEGFR_2$, $PDGF_b$, ANGPT2, Tie1 and Tie2 (Fig. 2B). Western blot analysis of protein levels of VEGFA and ANGTP1 revealed that after 48 hours of treatment, Up_4A at a concentration of 10 µM significantly increased protein level of VEGFA, but not ANGPT1 in HCATECs (Fig. 2C).

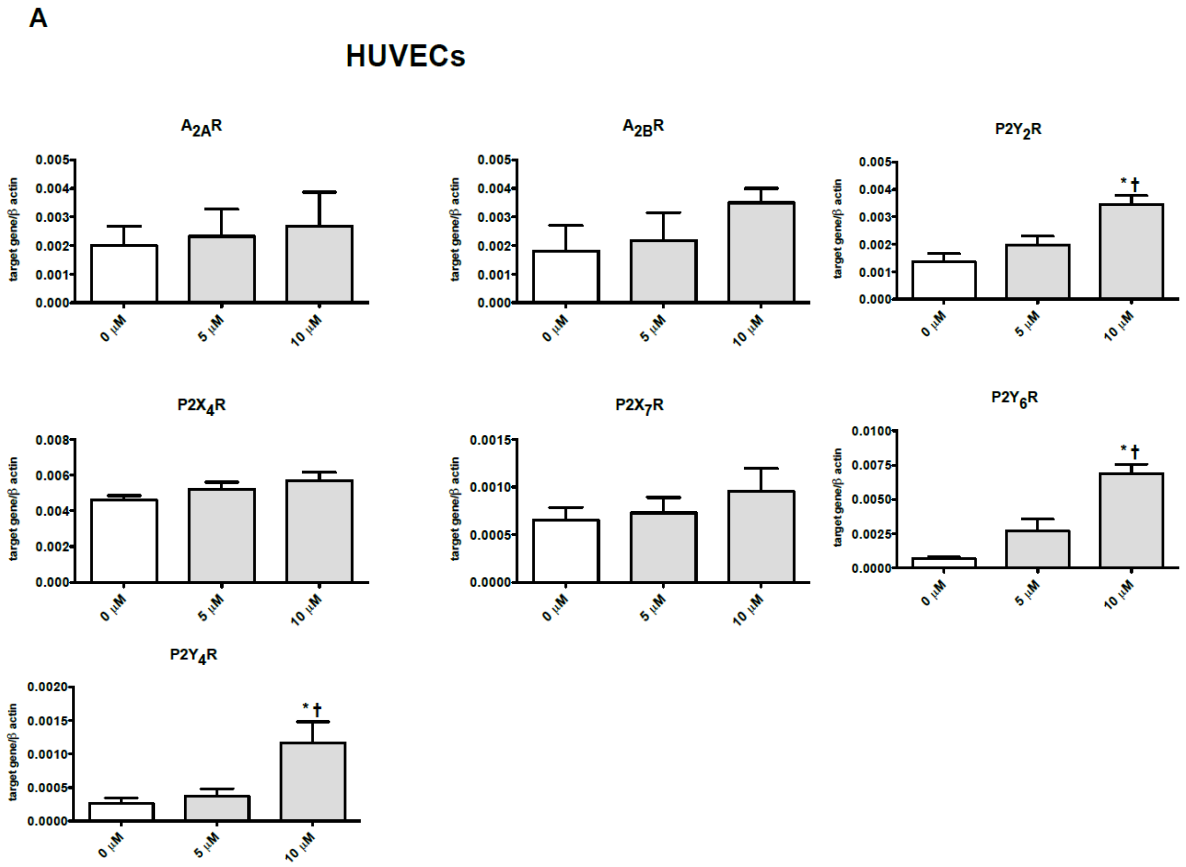

Figure 2: Expression of purinergic receptors and angiogenic factors in response to Up_4A treatment.

The expression of purinergic receptors in response to 24 hours of incubation with 0, 5 or 10 µM of Up_4A in HUVECs are shown in (A); mRNA levels of $A_{2A}R$, $A_{2B}R$, $P2X_4R$, $P2X_7R$, $P2Y_2R$, $P2Y_4R$ and $P2Y_6R$ were measured by q-PCR and normalized to ß-actin.

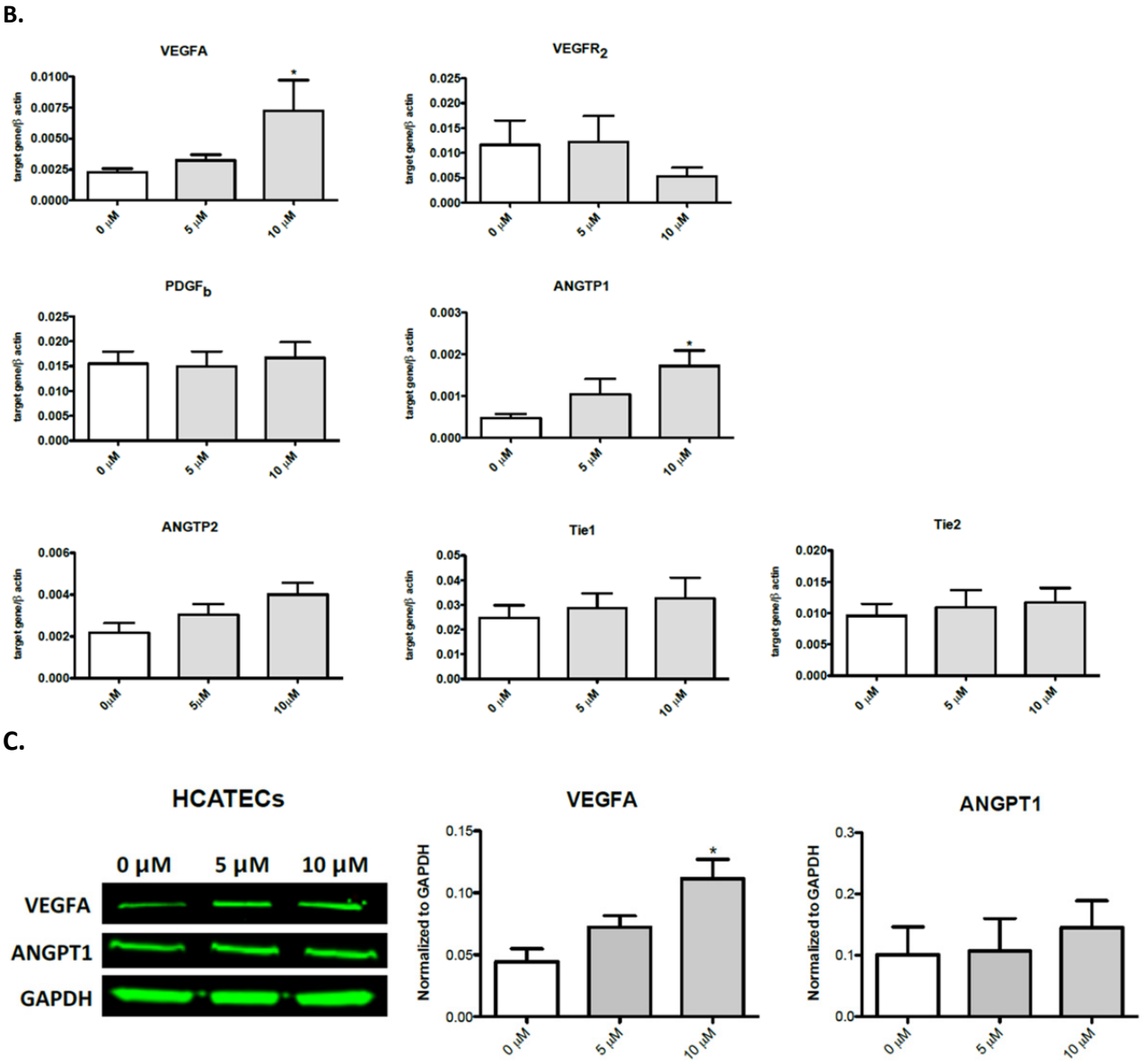

Figure 2: The expression of angiogenic factors in response to 0, 5 or 10 µM of Up_4A in HUVECs are shown in (B); mRNA levels of VEGFA, $VEGFR_2$, $PDGF_b$, ANGPT1, ANGPT2, Tie1 and Tie2 were detected by q-PCR and normalized to ß-actin. The protein expression of angiogenic factors in response to 48 hours of incubation with 0, 5 or 10 µM of Up_4A in HCATECs are shown in panel (C) Protein levels of VEGFA and ANGPT1 were detected by Western blot and normalized to GAPDH. Values are mean ± SEM. * P<0.05 versus 0 µM; † P<0.05 versus 5 µM. N=3-5.

$P2Y_6R$ blockade attenuated Up_4A-mediated vascular tubule formation

There is a lack of selective PR antagonists for many PR subtypes. Since Up_4A mainly affected P2YR subtypes in our setting, and MRS2578 is a selective antagonist for $P2Y_6R$ that previously has been well-validated by other studies, we used the MRS2578 to investigate the signalling pathway in the Up_4A-mediated angiogenic process, using the HUVECs and pericytes co-culture setup. Trace amounts of DMSO was used as a solvent for the MRS2578, but did not interfere

with the assay, as controls without and with DMSO did not differ in total tubule length (3357 ± 470 and 3470 ± 287), number of tubules (200 ± 27 and 213 ± 17), or number of junctions (66 ± 17 and 74 ± 7) in the absence and presence of DMSO, respectively. $P2Y_6R$ blockade markedly attenuated Up_4A-increased tubule formation at day 5 (Fig. 3A), as evidenced by a significant reduction in total tubule length, number of tubules, as well as number of junctions at a concentration of 1 µM and 5 µM Up_4A (Fig. 3B). Furthermore, co-culture experiments with GFP labelled HMVECs and dsRED-pericytes similarly showed that Up_4A (5 µM) could induce a significant pro-angiogenic response that was decreased by $P2Y_6R$ inhibition with MRS2578, thus validating our findings with HUVEC assays (Fig. 1D and 1E). These observations indicate that activation of $P2Y_6R$ is involved in Up_4A-mediated tubule formation and this mechanism is active in endothelial cells of different human vessel types origin.

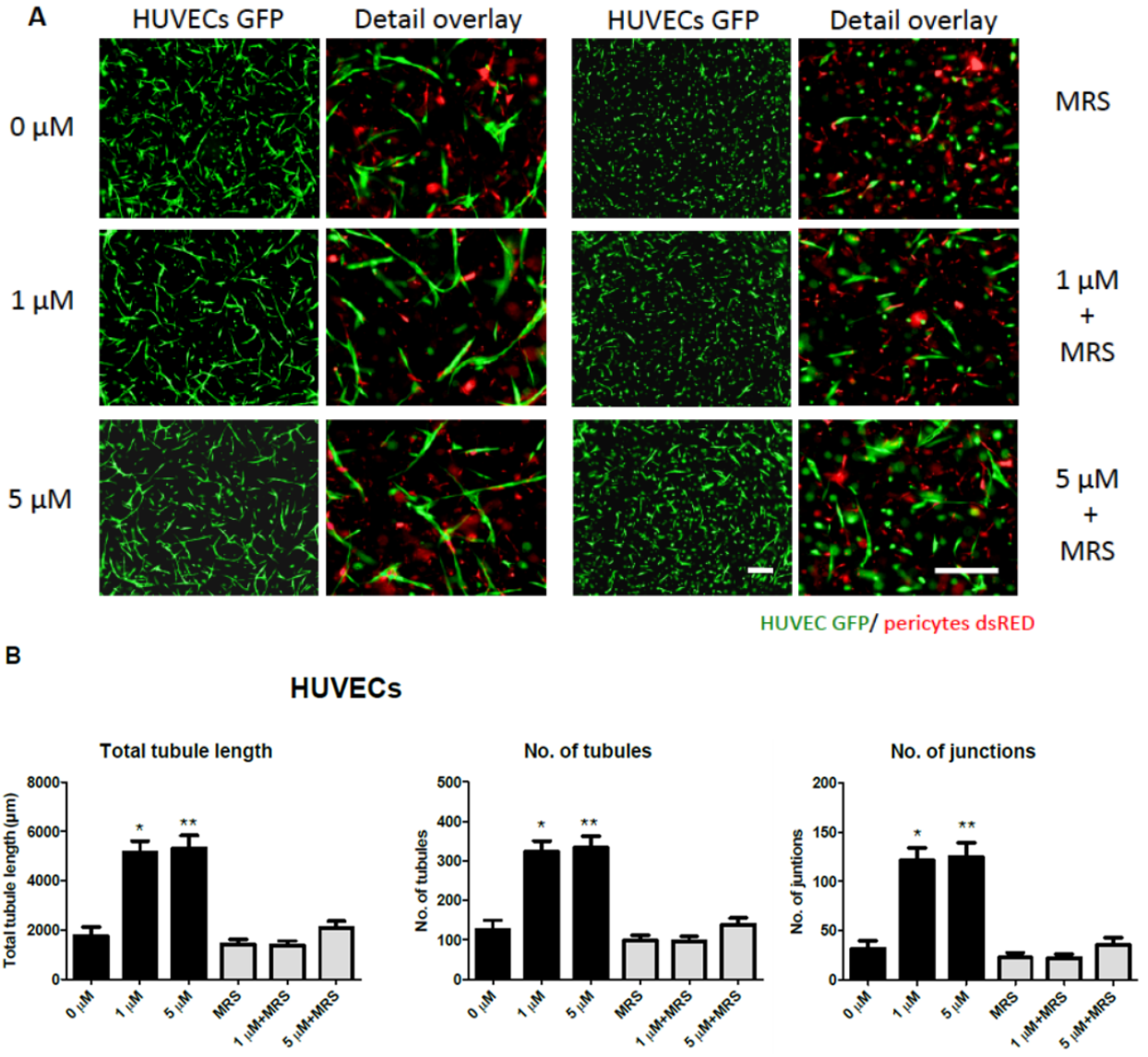

Figure 3: $P2Y_6R$ antagonist reverses the pro-angiogenic effects of Up_4A.

(A) Representative pictures of HUVECs and pericytes co-culture treated with Up_4A alone or in combination with $P2Y_6R$ antagonist MRS2578 (MRS, 10 µM). Pictures were taken by fluorescent microscope on day 5. HUVECS are labeled with GFP (in green); Pericytes are labeled with dsRED (in red). (B) Quantification of fold increase in total tubule length, numbers of tubules and junctions of HUVECs and pericytes co-cultures at day 5. HUVECs were treated with 0, 1 or 5 µM Up_4A with or without $P2Y_6R$ antagonist MRS2578 (10 µM). Scale bar: 50 µm. Values are represented as mean ± SEM. * $P<0.05$ versus all groups except 5 µM; ** $P<0.05$ versus all groups except 1 µM. N=3 individual experiments.

Effects of $P2Y_6R$ blockade on Up_4A-induced expression of purinergic receptors and angiogenic factors

$P2Y_6R$ blockade with MRS2578 significantly attenuated Up_4A (10 µM)-induced mRNA expression of $P2Y_6R$ in HUVECs (Fig. 4A). Moreover, $P2Y_6R$ blockade decreased Up_4A (10 µM)-induced mRNA expression of $P2Y_2R$, whereas $P2Y_6R$ blockade had no effect on the expression level of $A_{2A}R$, $A_{2B}R$, and $P2Y_4R$ (Fig. 4A). As for the angiogenic factors, $P2Y_6R$ blockade had no effect on VEGFA, ANGPT1, ANGPT2, Tie1 and Tie2 in response to Up_4A (Fig. 4B). Furthermore, q-PCR analysis using HAECs revealed that the transcriptional response of $P2Y_6R$ and ANGTP1 to Up_4A stimulation reflects the response in HUVECs (Fig. 4C). In contrast, VEGFA expression was not responsive to Up_4A in HAECs (0.0023 ± 0.0006, 0.0025 ± 0.0007, and 0.0028 ± 0.0007, for 0, 5 and 10 µM Up_4A respectively). This indicates that for the $P2Y_6R$ and ANGTP1, the trend of transcriptional regulation via Up_4A and $P2Y_6R$ antagonism is similar in endothelial cells of different vessel types origin.

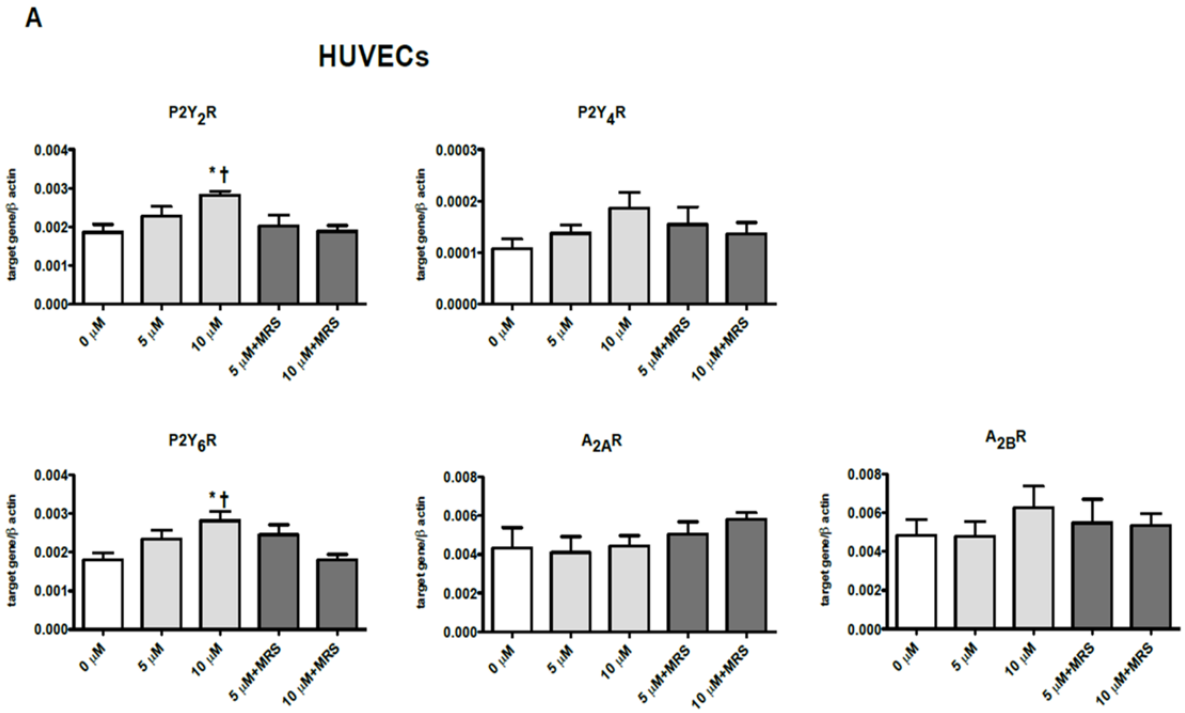

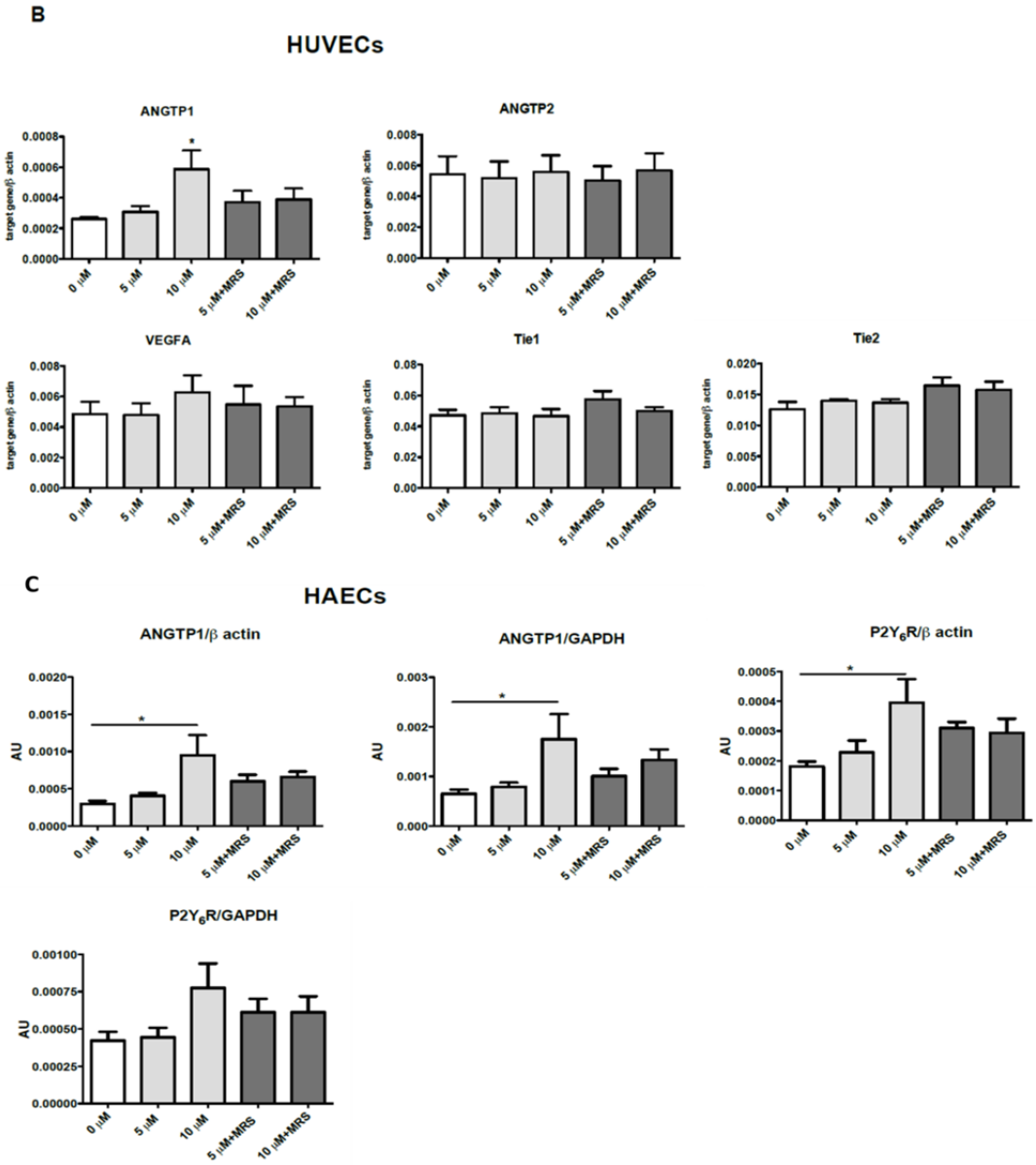

Figure 4: The effect of $P2Y_6R$ antagonist on mRNA expression levels of purinergic receptors and angiogenic factors.

(A) Effects of $P2Y_6R$ antagonist MRS2578 on purinergic receptor expression responses to Up_4A at 24 h. HUVECs were treated with 0, 5 or 10 μM Up_4A in combination with or without the $P2Y_6R$ antagonist MRS2578 (10 μM). The relative expression of $P2Y_2R$, $P2Y_4R$, $P2Y_6R$, $A_{2A}R$ and $A_{2B}R$ were measured by q-PCR followed by ß-actin normalization. Values are mean ± SEM. * P<0.05 versus 0 μM; † P<0.05 versus 10 μM Up_4A with $P2Y_6R$ antagonist MRS2578 (10 μM). N=6-7. (B) Effects of $P2Y_6R$ antagonist MRS2578 (10 μM) on angiogenic factor expression in response to Up_4A in HUVECs. Similar as (A), mRNA levels of ANGPT1, ANGPT2, VEGFA, Tie1 and Tie2 were detected by q-PCR and normalized with ß-actin. Values are mean ± SEM. * P<0.05 versus 0 μM. N=6-7. (C) Effects of $P2Y_6R$ antagonist MRS2578 (MRS, 10 μM) on $P2Y_6R$ and ANGTP1 expression in response to Up_4A at 24 h in HAECs. HAECs were treated with 0, 5 or 10 μM Up_4A with or without the $P2Y_6R$ antagonist MRS2578 (10 μM). The relative expression of ANGTP1 and $P2Y_6R$ measured by q-PCR followed by ß-actin or GAPDH normalization are shown. Values are mean ± SEM. * P<0.05, N=6.

Discussion

The main findings of the present study are that (*i*) Up_4A promotes angiogenesis, indicated by vascular tubule formation in our *in vitro* co-culture system. (*ii*) This pro-angiogenic effect of Up_4A was largely attenuated by $P2Y_6R$ inhibition. (*iii*) Moreover, Up_4A mainly influenced mRNA expression of P2YRs ($P2Y_2R$, $P2Y_4R$ and $P2Y_6R$) but not P2XRs ($P2X_4R$ and $P2X_7R$) or ARs ($A_{2A}R$ and $A_{2B}R$), whereas Up_4A increased mRNA levels of VEGFA (in HUVECs but not HAECs) and ANGPT1, but not $VEGFR_2$, $PDGF_b$, ANGPT2, Tie1 and Tie2. (*iv*) Up_4A significantly increased VEGFA protein levels. (*v*) Finally, inhibition of $P2Y_6R$ prohibited the induction of P2YRs ($P2Y_2R$ and $P2Y_6R$) by Up_4A. The implications of these findings are discussed below.

Up_4A, endogenously produced from endothelial cells as well as released upon mechanical (shear) stress and chemical challenges (25), is biosynthesized by activation of $VEGFR_2$ (23). The plasma concentrations of Up_4A detected in healthy subjects are in the vasoactive range (~4 nM) (25), which can be markedly elevated in diseased condition such as hypertension (~33 nM in juvenile hypertensive patients) (22). Thus, Up_4A has been shown to regulate vascular tone in various vascular beds (31, 45) and has been implicated in blood pressure regulation (22, 25). Moreover, the effects of Up_4A have been shown to induce human vascular smooth muscle cell proliferation (16), rat vascular smooth muscle migration (42) and vascular calcification in rats (37), suggesting a critical role of Up_4A in regulation of the homeostasis of blood vessels.

We hypothesize that Up_4A can be locally increased to a sufficient level to promote angiogenesis in tissues undergoing e.g. a hypoxic response or vascular strain (in case of hypertension). Indeed, (local) concentration of other nucleotides such as ATP, ADP and adenosine with angiogenic potential have been shown to be elevated during stress and injury conditions such as myocardial infarction and hypoxia (7, 18). Based on this assumption, we tested the potential angiogenic effect of Up_4A on human endothelial cells. We used HUVECs as the main experimental cell type together with other endothelial cell types including HMVECs, HCATECs, and HAECs to reveal a general capacity of Up_4A to induce angiogenesis in human endothelial cells of different origins. Indeed, Up_4A treatment stimulated vascular sprouting and initiation of tubule formation from 1 day in the co-culture setup. This was followed by subsequent stabilization of the vascular structures till up to 5 days post-seeding, as evidenced by an increase in vascular density in response to Up_4A at relatively low concentrations at day 5 (0 µM-5 µM). Interestingly, increase in tubule formation was not detected at day 5 in HMVECs if Up_4A was added at day 2, suggesting that Up_4A stimulation is required in early sprouting in our co-culture setup in order to induce angiogenic increase. Up_4A appears to have a dose optimum at 5 µM, after which the beneficial effects of Up_4A on tubule formation are diminished. These findings indicate that Up_4A is functionally involved in angiogenesis. Notably, another dinucleotide Up_4U, with two pyrimidine moieties, has been recently shown to be a potent angiogenic factor in human vascular endothelial cells, inducing migration, proliferation and tube formation, likely by activation of $P2Y_2R$ (24). Similarly to Up_4A, most of the cell responses induced by Up_4U showed a typical dose range effect with limited to no reaction beyond the optimal concentration (24).

Other dinucleotide polyphosphates, such as Ap_4A with two purine moieties, have been reported to be angiogenic inert (29). Since the pyrimidines UTP and UDP preferably activate $P2Y_2R$, $P2Y_4R$ and $P2Y_6R$ (33), these different observations for the dinucleotide polyphosphates group regarding angiogenic potential may be explained by the differences in binding properties of the purine and pyrimidine moieties. The four-phosphate groups do not vary between the dinucleotides and thus do not appear to be the decisive factor in compound-receptor signalling in the angiogenic process. In accordance with this concept, it is likely that the purine moieties from Up_4A do not have an effect on angiogenesis in HUVECs or HMVECs, even though Up_4A, with both purine and pyrimidine moieties, is capable of activating both P1Rs and P2Rs (25, 44, 45). In line with the concept that Up_4A mainly exerts pro-angiogenic actions via its pyrimidine moiety, tubule formation in the co-culture setup was significantly attenuated by $P2Y_6R$ inhibition. Furthermore, our q-PCR data revealed that Up_4A upregulated pyrimidine-favoured P2YRs ($P2Y_2R$, $P2Y_4R$ and $P2Y_6R$), but not P2XRs or P1Rs at mRNA levels. This Up_4A-induced expression response was in part blunted by $P2Y_6R$ inhibition, indicating a feed-forward loop in which Up_4A activation of $P2Y_6R$ amplifies gene expression of $P2Y_6R$. In addition, the observation that the potent and selective $P2Y_6R$ antagonist MRS2578 also significantly attenuated $P2Y_2R$ expression suggests a possible interaction between $P2Y_6R$ and $P2Y_2R$ (41). MRS2578 is well known to potently and selectively inhibit $P2Y_6R$-mediated actions in several cell types (21, 26, 30, 32, 34, 43), MRS2578 at 10 µM potently inhibits $P2Y_6R$, but has been shown to have very minimal effect on $P2Y_2R$ in 1321N astrocytoma cells (30). Future studies are needed to gain more insights into the interaction of PRs.

As shown in the data provided in Fig. 3B and Fig. 1C, MRS2578 stimulation alone significantly decreased all angiogenic parameters in both HUVECs and HMVECs co-culture systems compared to the 5 µM Up_4A condition. This is counteracted by stimulation with increasing concentrations of exogenous Up_4A (5 µM and 10 µM). We interpret these effects of MRS2578 as an indication that Up_4A is produced at low level by the HUVECs/HMVECs or pericytes under normal co-culture condition. In Fig. 2A and 4A, we show that stimulation with Up_4A significantly increases expression level of $P2Y_6R$. Thus, we further interpret the data in Fig. 3B and 1C as an indication that in the (10 µM) MRS + 5 µM Up_4A and (10 µM) MRS + 10 µM Up_4A conditions, the effect of the blocker is partially reversed by the effect of Up_4A, which leads to increased $P2Y_6R$ expression and receptor bio-availability, thereby counteracting the effect of the MRS2578 blocker. In the condition with only MRS2578 and no exogenous Up_4A stimulation, the anti-angiogenic effects of MRS2578 would therefore also be more severe.

All together, these findings suggest that P2YRs, particularly $P2Y_6R$ are involved in Up_4A-mediated angiogenic influence in human endothelial cells. Although Up_4A has been shown to activate not only P2YRs but also P1Rs and P2XRs, all of which appear to be involved in the regulation of vascular tone by Up_4A (31, 44), the concept that only pyrimidine but not purine moieties affect function in HUVECs and HMVECs is further supported by recent studies performed at the cellular level: Up_4A induces human vascular smooth muscle cell proliferation

via activation of P2Y receptors (16), and is a strong inductor of migration in vascular smooth muscle cell obtained from rat thoracic aorta through activation of $P2Y_2$ receptors (42). Moreover, Up_4A has been shown to influence phenotypic trans-differentiation of rat vascular smooth muscle cells to osteochondrogenic cells, likely via $P2Y_2$ and $P2Y_6$ receptors (37). Further studies are required to validate if pyrimidine moieties and endothelial P2YR signalling are indeed a vital requirement for the angiogenic potential for the different compounds of the nucleotide polyphosphates group.

In the present study, Up_4A also promoted mRNA expression of the pro-angiogenic genes ANGPT1 and VEGFA. Furthermore, Western blot analysis indicated that VEGFA protein levels were significantly increased in response to Up_4A stimulation. In contrast, ANGPT1 protein levels were not significantly altered. This poor correlation between ANGPT1 protein and mRNA level could be the result of a shorter half-life of the ANGPT1 protein compared to VEGFA protein, or could be associated with differences in post-transcriptional regulation between ANGPT1 and VEGFA protein levels (15). Previous reports demonstrated that purinergic receptor-induced angiogenesis could be mediated by autocrine stimulation of vascular cells by pro-angiogenic factors (2, 14, 35). Other studies have also indicated that Up_4A can be biosynthesized by activation of $VEGFR_2$ (23). An autocrine feed-forward loop exists, in which VEGFA signalling via $VEGFR_2$ promotes intracellular transport of $VEGFR_2$ to the plasma membrane, thus amplifying the bio-availability of this receptor tyrosine kinase on the endothelial cell surface (40). This intrinsic pathway may further enhance Up_4A synthesis and downstream vascular effects. New vascular growth is a complex, multiphasic process, during which both endothelial cells and mural cells (pericytes in the microvasculature and vascular smooth muscle cells in the macrovasculature) undergo activation, sprouting, and neovessel stabilization. VEGFA/$VEGFR_2$ signalling drives the typical initial response of vascular activation, and is critical for neovascular growth and survival (28). Up_4A may facilitate its pro-angiogenic function via upregulation of mRNA and protein levels of VEGFA in endothelial cells.

Methodological considerations

Since Up_4A mainly affected P2YR subtypes in our study, we used a pharmacological blocker of $P2Y_6R$ (MRS2578) to investigate the signalling pathway in the Up_4A-mediated angiogenic process. The potential pitfall of using pharmacological blockers is that while selectivity, i.e. the capability of blocking a particular receptor as compared to related receptors, is usually well-defined, specificity, i.e. the potential for discriminating between negative and positive interactions and the cross-reactivity with other (unrelated) targets, is less well established (36). However, MRS2578 has been reported to potently inhibit the response to 300 nM UDP in 1321N astrocytoma transfected with the human $P2Y_6R$, with an IC50 value of 37±16 nM (30). At the same time, MRS2578 at 10 µM did not affect the UTP (100 nM)-induced responses of cells expressing human $P2Y_2R$ or $P2Y_4R$, nor did it affect the 2-MeSADP (30 nM)-induced responses of

cells expressing the $P2Y_1R$ (30). In addition, MRS2578 did not affect the ATP (10 µM)-induced responses of cells expressing the $P2Y_{11}R$ (30).

The effects on tubule formation were mainly observed for 5 µM Up_4A, whereas mRNA expression of PRs and angiogenic factors responded mainly to 10 µM Up_4A. Similar to our HUVEC data, our additional experiments performed in HMVECs and HAECs showed a comparable pattern of tubule formation predominantly responding to 5 µM Up_4A, whereas mRNA of PRs and angiogenic factors responded mainly to 10 µM Up_4A (Fig. 1 and 4). Thus, the difference in responsive dose between co-culture and mRNA expression, was not endothelial cell type specific. This difference in effective dose may be attributed to the difference in our setup between normal (2D) endothelial cell culture (to yield samples for q-PCR) and our 3D collagen matrix endothelial-pericyte co-culture setup. For the 3D co-culture, HUVECs/HMVECs and pericytes were both prior the experiment lentivirally transfected with GFP and dsRED expression cassettes to obtain stable HUVEC/HUMVEC-GFP and pericyte-dsRED cells. These HUVEC/HMVEC-GFP and pericyte-dsRED cells have undergone several passages of selection to obtain a 99% pure marker expressing population. In contrast, for q-PCR analysis, we used HUVECs and HAECs that were not treated with lentivirus and were not selected for several passages on GFP or dsRED marker expression. This difference in treatment of the cells prior to the experiments could have affected their sensitivity and actual response to Up_4A stimulation (e.g. the GFP cells could have adapted to express higher levels of receptors, or have down-regulated inhibitory pathways that intervene with Up_4A receptor signaling). Furthermore, the co-culture assay was conducted in a 3D matrix environment, whereas for q-PCR, the cells were cultured under normal conditions without complex (ECM) extra cellular matrix support. This may also have affected the responsiveness of the vascular cells. For example, interaction of endothelial cells with complex ECM components such as collagen type 1 fibers via integrin interaction is known to aid activation of endothelial angiogenic sprouting (11). In addition, the phenotypical changes in the 3D co-culture assay were the result of transcriptional changes in multiple genes, which combined together, resulted in the phenotype (tubule formation). So even if transcriptional changes were slightly but non-significantly increased in response to 5 µM Up_4A stimulation, combined, this could have still contributed to the acquired phenotype.

Another limitation of our study is that different batches of HUVECs (GFP) and collagen were used for the experiments in Fig. 1 and Fig. 3, which may have resulted in the differences observed in tubule formation response to 1 µM Up_4A. However, Up_4A at 5 µM affected the tubule formation in a very similar pattern between these two experiments, indicating that Up_4A at 5 µM may be the optimal concentration for a more stable tubule formation response that surpasses these batch effects. Thus, although the optimal dose and the net amount of increase in angiogenesis varied, these experiments clearly showed that Up_4A could consistently induce a solid pro-angiogenic response. These finding were further verified by our HMVECs and pericytes co-culture assays. We therefore conclude that Up_4A has a strong angiogenic potential, but the optimal dose may vary between endothelial cell populations of different donors. For future

clinical use of Up_4A as a therapeutic agent in angiogenic stimulation, establishing the optimal dose range for specific subtypes of patients will be a crucial requirement.

Conclusions

We have identified, to our knowledge for the first time, the dinucleotide polyphosphate Up_4A as a novel angiogenic substance, which promotes sprouting and tubule formation in human vascular cells *in vitro*. This Up_4A pro-angiogenic function is mediated via $P2Y_6R$ signalling and is associated with upregulation of P2YRs and the pro-angiogenic factors.

References

1. Abbracchio MP, Burnstock G, Boeynaems JM, Barnard EA, Boyer JL, Kennedy C, Knight GE, Fumagalli M, Gachet C, Jacobson KA, and Weisman GA. International Union of Pharmacology LVIII: update on the P2Y G protein-coupled nucleotide receptors: from molecular mechanisms and pathophysiology to therapy. *Pharmacol Rev* 58: 281-341, 2006.

2. Bambace NM, Levis JE, and Holmes CE. The effect of P2Y-mediated platelet activation on the release of VEGF and endostatin from platelets. *Platelets* 21: 85-93, 2010.

3. Burnstock G. Control of vascular tone by purines and pyrimidines. *Br J Pharmacol* 161: 527-529, 2010.

4. Burnstock G. Introduction: P2 receptors. *Curr Top Med Chem* 4: 793-803, 2004.

5. Burnstock G. Purine and pyrimidine receptors. *Cell Mol Life Sci : CMLS* 64: 1471-1483, 2007.

6. Burnstock G, Brouns I, Adriaensen D, and Timmermans JP. Purinergic signaling in the airways. *Pharmacol Rev* 64: 834-868, 2012.

7. Burnstock G, and Ralevic V. Purinergic signaling and blood vessels in health and disease. *Pharmacol Rev* 66: 102-192, 2014.

8. Carmeliet P. Angiogenesis in life, disease and medicine. *Nature* 438: 932-936, 2005.

9. Cheng C, Haasdijk R, Tempel D, van de Kamp EH, Herpers R, Bos F, Den Dekker WK, Blonden LA, de Jong R, Burgisser PE, Chrifi I, Biessen EA, Dimmeler S, Schulte-Merker S, and Duckers HJ. Endothelial cell-specific FGD5 involvement in vascular pruning defines neovessel fate in mice. *Circulation* 125: 3142-3158, 2012.

10. Dalziel HH, and Westfall DP. Receptors for adenine nucleotides and nucleosides: subclassification, distribution, and molecular characterization. *Pharmacol Rev* 46: 449-466, 1994.

11. Davis GE, and Senger DR. Endothelial extracellular matrix: biosynthesis, remodeling, and functions during vascular morphogenesis and neovessel stabilization. *Circ Res* 97: 1093-1107, 2005.

12. Di Virgilio F, and Solini A. P2 receptors: new potential players in atherosclerosis. *Br J Pharmacol* 135: 831-842, 2002.

13. Galeano M, Bitto A, Altavilla D, Minutoli L, Polito F, Calo M, Lo Cascio P, Stagno d'Alcontres F, and Squadrito F. Polydeoxyribonucleotide stimulates angiogenesis and wound healing in the genetically diabetic mouse. *Wound Repair Regen* 16: 208-217, 2008.

14. Gerasimovskaya EV, Woodward HN, Tucker DA, and Stenmark KR. Extracellular ATP is a pro-angiogenic factor for pulmonary artery vasa vasorum endothelial cells. *Angiogenesis* 11: 169-182, 2008.

15. Greenbaum D, Colangelo C, Williams K, and Gerstein M. Comparing protein abundance and mRNA expression levels on a genomic scale. *Genome Biol* 4: 117, 2003.

16. Gui Y, He G, Walsh MP, and Zheng XL. Signaling mechanisms mediating uridine adenosine tetraphosphate-induced proliferation of human vascular smooth muscle cells. *J Cardiovasc Pharmacol* 58: 654-662, 2011.

17. Gui Y, Walsh MP, Jankowski V, Jankowski J, and Zheng XL. Up4A stimulates endothelium-independent contraction of isolated rat pulmonary artery. *Am J Physiol Lung Cellul Mol Physiol* 294: L733-738, 2008.

18. Headrick JP, Ashton KJ, Rose'meyer RB, and Peart JN. Cardiovascular adenosine receptors: expression, actions and interactions. *Pharmacol Ther* 140: 92-111, 2013.

19. Hill LM, Gavala ML, Lenertz LY, and Bertics PJ. Extracellular ATP may contribute to tissue repair by rapidly stimulating purinergic receptor X7-dependent vascular endothelial growth factor release from primary human monocytes. *J Immunol* 185: 3028-3034, 2010.

20. Horckmans M, Robaye B, Leon-Gomicronmez E, Lantz N, Unger P, Dol-Gleizes F, Clouet S, Cammarata D, Schaeffer P, Savi P, Gachet C, Balligand JL, Dessy C, Boeynaems JM, and Communi D. P2Y(4) nucleotide receptor: a novel actor in post-natal cardiac development. *Angiogenesis* 15: 349-360, 2012.

21. Ide S, Nishimaki N, Tsukimoto M, and Kojima S. Purine receptor P2Y6 mediates cellular response to gamma-ray-induced DNA damage. *J Toxicol Sci* 39: 15-23, 2014.

22. Jankowski V, Meyer AA, Schlattmann P, Gui Y, Zheng XL, Stamcou I, Radtke K, Tran TN, van der Giet M, Tolle M, Zidek W, and Jankowski J. Increased uridine adenosine tetraphosphate concentrations in plasma of juvenile hypertensives. *Arterioscler Thromb Vasc Biol* 27: 1776-1781, 2007.

23. Jankowski V, Schulz A, Kretschmer A, Mischak H, Boehringer F, van der Giet M, Janke D, Schuchardt M, Herwig R, Zidek W, and Jankowski J. The enzymatic activity of the VEGFR2 receptor for the biosynthesis of dinucleoside polyphosphates. *J Mol Med (Berl)* 91: 1095-1107, 2013.

24. Jankowski V, Tolle M, Tran TN, van der Giet M, Schuchardt M, Lehmann K, Janke D, Flick B, Ortiz A, Sanchez-Nino MD, Tepel M, Zidek W, and Jankowski J. Identification of a potent endothelium-derived angiogenic factor. *PloS one* 8: e68575, 2013.

25. Jankowski V, Tolle M, Vanholder R, Schonfelder G, van der Giet M, Henning L, Schluter H, Paul M, Zidek W, and Jankowski J. Uridine adenosine tetraphosphate: a novel endothelium- derived vasoconstrictive factor. *Nat Med* 11: 223-227, 2005.

26. Kim B, Jeong HK, Kim JH, Lee SY, Jou I, and Joe EH. Uridine 5'-diphosphate induces chemokine expression in microglia and astrocytes through activation of the P2Y6 receptor. *J Immunol* 186: 3701-3709, 2011.

27. Knight GE, and Burnstock G. Identification of P1 and P2 purinoceptors in the aorta of the lizard (Agama sp.). *Comp Biochem Physiol Toxicol Pharmacol : CBP* 128: 413-423, 2001.

28. Koch S, and Claesson-Welsh L. Signal transduction by vascular endothelial growth factor receptors. *Cold Spring Harb Perspect Med* 2: a006502, 2012.

29. Lyubchenko T, Woodward H, Veo KD, Burns N, Nijmeh H, Liubchenko GA, Stenmark KR, and Gerasimovskaya EV. P2Y1 and P2Y13 purinergic receptors mediate Ca2+ signaling and proliferative responses in pulmonary artery vasa vasorum endothelial cells. *Am J Physiol Cell Physiol* 300: C266-275, 2011.

30. Mamedova LK, Joshi BV, Gao ZG, von Kugelgen I, and Jacobson KA. Diisothiocyanate derivatives as potent, insurmountable antagonists of P2Y6 nucleotide receptors. *Biochem Pharmacol* 67: 1763-1770, 2004.

31. Matsumoto T, Tostes RC, and Webb RC. The role of uridine adenosine tetraphosphate in the vascular system. *Adv Pharmacol Sci* 2011: 435132, 2011.

32. Parandeh F, Abaraviciene SM, Amisten S, Erlinge D, and Salehi A. Uridine diphosphate (UDP) stimulates insulin secretion by activation of P2Y6 receptors. *Biochem Biophys Res Commun* 370: 499-503, 2008.

33. Ralevic V, and Burnstock G. Receptors for purines and pyrimidines. *Pharmacol Rev* 50: 413-492, 1998.

34. Rodrigues-Ribeiro R, Alvarenga EC, Calio ML, Paredes-Gamero EJ, and Ferreira AT. Dual role of P2 receptors during osteoblast differentiation. *Cell Biochem Biophys* 71: 1225-1233, 2015.

35. Rumjahn SM, Yokdang N, Baldwin KA, Thai J, and Buxton IL. Purinergic regulation of vascular endothelial growth factor signaling in angiogenesis. *Br J Cancer* 100: 1465-1470, 2009.

36. Salomone S, and Waeber C. Selectivity and specificity of sphingosine-1-phosphate receptor ligands: caveats and critical thinking in characterizing receptor-mediated effects. *Front Pharmacol* 2: 9, 2011.

37. Schuchardt M, Tolle M, Prufer J, Prufer N, Huang T, Jankowski V, Jankowski J, Zidek W, and van der Giet M. Uridine adenosine tetraphosphate activation of the purinergic receptor P2Y enhances in vitro vascular calcification. *Kidney Int* 81: 256-265, 2012.

38. Smith AO, Bowers SL, Stratman AN, and Davis GE. Hematopoietic stem cell cytokines and fibroblast growth factor-2 stimulate human endothelial cell-pericyte tube co-assembly in 3D fibrin matrices under serum-free defined conditions. *PloS one* 8: e85147, 2013.

39. Stratman AN, Schwindt AE, Malotte KM, and Davis GE. Endothelial-derived PDGF-BB and HB-EGF coordinately regulate pericyte recruitment during vasculogenic tube assembly and stabilization. *Blood* 116: 4720-4730, 2010.

40. Tiwari A, Jung JJ, Inamdar SM, Nihalani D, and Choudhury A. The myosin motor Myo1c is required for VEGFR2 delivery to the cell surface and for angiogenic signaling. *Am J Physiol Heart Circ Physiol* 304: H687-696.

41. Volonte C, Amadio S, D'Ambrosi N, Colpi M, and Burnstock G. P2 receptor web: complexity and fine-tuning. *Pharmacol Ther* 112: 264-280, 2006.

42. Wiedon A, Tolle M, Bastine J, Schuchardt M, Huang T, Jankowski V, Jankowski J, Zidek W, and van der Giet M. Uridine adenosine tetraphosphate (Up4A) is a strong inductor of smooth muscle cell migration via activation of the P2Y2 receptor and cross-communication to the PDGF receptor. *Biochem Biophys Res Commun* 417: 1035-1040, 2012.

43. Zhang Z, Wang Z, Ren H, Yue M, Huang K, Gu H, Liu M, Du B, and Qian M. P2Y(6) agonist uridine 5'-diphosphate promotes host defense against bacterial infection via monocyte chemoattractant protein-1-mediated monocytes/macrophages recruitment. *J Immunol* 186: 5376-5387, 2011.

44. Zhou Z, de Wijs-Meijler D, Lankhuizen I, Jankowski J, Jankowski V, Jan Danser AH, Duncker DJ, and Merkus D. Blunted coronary vasodilator response to uridine adenosine tetraphosphate in post-infarct remodeled myocardium is due to reduced P1 receptor activation. *Pharmacol Res* 77: 22-29, 2013.

45. Zhou Z, Merkus D, Cheng C, Duckers HJ, Jan Danser AH, and Duncker DJ. Uridine adenosine tetraphosphate is a novel vasodilator in the coronary microcirculation which acts through purinergic P1 but not P2 receptors. *Pharmacol Res* 67: 10-17, 2013.

46. Zhou Z, Sun C, Tilley SL, and Mustafa SJ. Mechanisms underlying uridine adenosine tetraphosphate-induced vascular contraction in mouse aorta: Role of thromboxane and purinergic receptors. *Vascul Pharmacol* 73: 78-85, 2015.

Supplement table 1

Table 1. Primer information

Genes	Sequences		Size
	Sense	Antisense	
A_{2A}	5′-CCAGACGTGAGCTCCTTAG-3′	5′-GGTCAAGCCAACCAGAAAGA-3′	161 bp
A_{2B}	5′-CAGTTGTTGGTGGCACTGTCTT-3′	5′-CTCACGCAGAGCTCCATCTTC-3′	200 bp
$P2X_4$	5′-CCGTGGAGGATGACACACAC-3′	5′-GGCTCTGTCCAGGTTGCAGT-3′	302 bp
$P2X_7$	5′-TAAAAGTCTTCGGGATCCGTTT-3′	5′-CTGGTTCACCATCCTAATGTGG-3′	334 bp
$P2Y_2$	5′-TCTACTTTGTCACCACCAGCG-3′	5′-TTGATGGCGTTGAGGGTGTG-3′	349 bp
$P2Y_4$	5′-TCGTGCCCAACCTGTTCTTT-3′	5′-TAAATGGTGCGGGTGATGTG-3′	304 bp
$P2Y_6$	5′-GCTGCCTGGCTAGTGTGTGT-3′	5′-AAGTAGAAGAGGATGGGCTCCA-3′	482 bp
$ANGPT_1$	5′-GCTGAACGGTCACACAGAGA-3′	5′-CTTTCCCCCTCAAAGAAAGC-3′	180 bp
$ANGPT_2$	5′-TTATCACAGCACCAGCAAGC-3′	5′-TTCGCGAGAACAAATGTGAG-3′	223 bp
Tie1	5′-GAGAGTGACCCAGCTTTTGC-3′	5′-CTGCAATCTTGGAGGCTAGG-3′	184 bp
Tie2	5′-TACACCTGCCTCATGCTCAG-3′	5′-TTCACAAGCCTTCTCACACG-3′	242 bp
VEGFA	5′-AAGGAGGAGGGCAGAATCAT-3′	5′-ATCTGCATGGTGATGTTGGA-3′	226 bp
$VEGFR_2$	5′-AGCGATGGCCTCTTCTGTAA-3′	5′-ACACGACTCCATGTTGGTCA-3′	172 bp
PDGFb	5′-CCCCACACTCCACTCTGATT-3′	5′-GCCCTGGCCTCTAGTCTTCT-3′	181 bp
β-actin	5′-TCCCTGGAGAAGAGCTACGA-3′	5′-AGCACTGTGTTGGCGTACAG-3′	194 bp
GAPDH	5′-TGCCAAATATGATGACATCAAGAA-3′	5′-GGAGTGGGTGTCGCTGTTG-3′	121 bp

Chapter 7 CECR1-mediated cross talk between macrophages and vascular mural cells promotes neovascularization in malignant glioma.

Changbin Zhu*; Ihsan Chrifi*; Dana Mustafa; Marcel van der Weiden; Pieter J.M. Leenen; Dirk J. Duncker; Johan M. Kros†; Caroline Cheng†.

**first and † last authors contributed equally to the paper.*

Published: Oncogene 2017 Sep 21:36(38):5356-5368

Abstract

Aim: Glioblastomas (GBM) are most malignant brain tumors characterized by profound vascularization. Activation of macrophages strongly contributes to tumor angiogenesis during GBM development. Previously, we showed that extracellular adenosine deaminase protein Cat Eye Syndrome Critical Region Protein 1(CECR1) is highly expressed by M2-like macrophages in GBM where it defines macrophage M2 polarization and contributes to tumor expansion. In this study, the effect of CECR1 in macrophages on tumor angiogenesis was investigated.

Methods and Results: Immunohistochemical evaluation of GBM tissue samples showed that the expression of CECR1 correlates with microvascular density in the tumors, confirming data from the TCGA set. In a 3D co-culture system consisting of human pericytes, HUVECs and THP1-derived macrophages, CECR1 knockdown by siRNA and CECR1 stimulation of macrophages inhibited and promoted new vessel formation respectively. Loss and gain of function studies demonstrated that PDGFB mRNA and protein levels in macrophages are modulated by CECR1. The pro-angiogenic properties of CECR1 in macrophages were partially mediated via paracrine activation of pericytes by PDGFB-PDGFRβ signaling. CECR1-PDGFB-PDGFRβ cross talk between macrophages and pericytes promoted pericyte migration, shown by transwell migration assay, and enhanced expression of periostin, a matrix component with pro-angiogenic properties.

Conclusions: CECR1 function in (M2-like) macrophages mediates cross talk between macrophages and pericytes in GBM via paracrine PDGFB-PDGFRβ signaling, promoting pericyte recruitment and migration, and tumor angiogenesis. Therefore, CECR1 offers a new target for anti-angiogenic therapy in GBM.

Introduction

Glioblastoma multiform (GBM) represents the highest grade of glioma and carries a dismal prognosis of merely 12-15 months, even after current standard chemo-radiotherapy and tumor resection regimes (1). Presently, our understanding of the exact mechanisms driving GBM pathogenesis remains limited and further research is essential for the design of more effective therapies. GBMs are highly vascularized tumors that are hall marked by vascular hyper-proliferative capacity (2) and vast myeloid infiltration (3).

So far, the therapeutic effects of anti-angiogenic regimes targeting VEGF were shown to be limited, due to rapid acquirement of resistance by the tumor cells (4). It has been proposed that the drug-resistance may be related to the activation of alternative angiogenic pathways such as FGF2-mediated and HIF1-independent mechanisms that bypass the need for VEGFA regulation of tumor angiogenesis (5). In addition, the recruitment and activation of bone marrow derived circulatory cells, including macrophages, could rescue tumor angiogenesis by secretion of these alternative pro-angiogenic factors (6).

Previous studies have well established the involvement of resident macrophages (microglia) and infiltrated macrophages, also called glioma-associated macrophages (GAMs), in tumor angiogenesis of GBM (7, 8). Although GAMs can produce VEGFA, alternative mechanisms including GAMs-induced RAGE (9), CXCL2 (10), and IGFBP1 (11) mediated regulation of tumor angiogenesis, have also been demonstrated. In addition to regulating angiogenesis, GAMs actively promote glioma growth, migration and invasion (12), and help maintain a glioma stem cell niche (13). Furthermore, findings of clinical studies imply an important functional contribution of GAMs to prognosis or recurrence of GBM (3, 8, 14, 15). Macrophages are classically distinguished into M1 and M2 phenotypes. M1 macrophages are primarily associated with a pro-inflammatory state, whereas M2 macrophages are associated with immune modulation and wound healing. Compared to M1 macrophages, M2 macrophages have been shown to act pro-angiogenic, both *in vitro* and *in vivo* (16-18). In line with these observations, recent studies have indicated that mainly tumor-associated macrophages with a M2-like phenotype can act as pro-angiogenic modulators, stimulating expansion of disorganized neovessels by e.g. paracrine release of PIGF (19) and CCL18 (20). In GBM, M2-like GAMs have been mainly described for their immune suppressive and tumor supportive function. As the majority of GAMs in GMB are known to have a M2-like phenotype, specific drug-targeting of M2 macrophages could become a viable alternative therapy for the inhibition of tumor angiogenesis in GBM (6).

Recently, the extracellular adenosine deaminase protein Cat Eye Syndrome Critical Region Protein 1(CECR1) has been shown to regulate macrophage maturation. In previous studies we demonstrated that CECR1 is consistently highly expressed by M2-type GAMs, particularly in high-grade glioma. In line with the findings presented by Zhou et al (21), we could validate that CECR1 is an important promoter of GAM polarization towards M2-like macrophages. Our previous study also demonstrated that CECR1-mediated paracrine activation of M2-like GAMs

directly affected the GBM cells, promoting tumor cell proliferation and migration. However, the effect of CECR1 regulation of GAMs on tumor angiogenesis remains to be investigated. Considering the important role that CECR1 plays in M2-like macrophage polarization, and the general pro-angiogenic function of GAMs, we hypothesize that CECR1 contributes to the paracrine pro-angiogenic function of (M2-like) GAMs.

In the present study we demonstrated that CECR1 expression correlated with microvascular density in GBM samples based analysis. Using a well-validated 3D co-culture system consisting of human pericytes, HUVECs and THP1-derived macrophages, we further demonstrated that gain and loss of function of CECR1 activity in macrophages inhibited and promoted new vessel formation respectively. Further investigation revealed that CECR1 modulated pericyte function (mainly migration), a process that was mediated by CECR1-PDGFB-PDGFRβ paracrine cross talk between macrophages and pericytes.

Material and Methods

Patient samples

Patient samples of glioblastoma were collected from the Department of Pathology, Erasmus Medical Center with the approval of committee of research ethics. All the samples were diagnosed as glioblastoma by a board certificated pathologist (J.M.K).

Cell culture

Human monocytic cell line THP-1, obtained from Department of Hematology, Erasmus Medical Center, was maintained in culture in RPMI-1640 (Lonza, Breda) supplemented with 10%FBS and 1% Penicillin/Streptomycin. THP-1 cells were differentiated into macrophage-like cells by PMA (Sigma, Sweden) at concentration of 100ng/ml for 48 hours. Recombinant human CECR1 protein (rhCECR1) was added to the macrophage cultures at a concentration gradient of 0, 12.5, 25, 50, 100, 200 nM for 96 hours. Human umbilical vein endothelial cells (HUVECs) (Lonza, Breda) and HUVECs transfected with a lentiviral vector encoding GFP were cultured in EGM-2 endothelial medium (Lonza, Breda) with 1% Penicillin/Streptomycin. Human brain vascular pericytes (HBVP) with and without lentiviral transfection of a vector encoding for dsRed, and GBM cell lines; U87, and U251 were maintained in DMEM (Lonza, Breda) with 10% FBS and 1% Penicillin/Streptomycin. Pericytes were treated with recombinant human PDGFB (Sigma, Sweden) at different concentrations according to the specifications of the different assays.

siRNA transfection

siCECR1 (5’-GUGCCAAAGGCUUGUCCUA-3’,5-CUUCCACGCCGGAGAAACA-3’,5’-GCCCAAAGCUAG UUAGUAC-3’;5’-UCGCAGAAUCCAUCCGAAU-3’); siPDGFβ (5’-CCGAGGAGCUUUAUGAGAU-3’, 5’-GAAGAAGGAGCCUGGGUUC-3’,5’-GCAAGCACCGGAAAUUCAA-3’, 5’-GGGCCGAGUUGGACCUGAA -3’), siPOSTN (5’-CCGAAGCUCUUAUGAAGUA-3’), and scrambled siRNA (siSham) (5’-

UGGUUUACAUGUCGACUAA-3',5'-UGGUUUACAUGUUGUGUGA-3',5'-UGGUUUACAUGUUUUCU GA-3', UGGUUUACAUGUUUUCCUA-3') were purchased from Dharmacon (GE health care, the Netherlands). Macrophages were transfected with SiCECR1 and siPDGFB using transfection buffer 2 (Dharmacon, GE, The Netherlands); pericytes or pericytes-dsRed were transfected with siPOSTN using transfection buffer 1 (Dharmacon, GE, the Netherlands) according to manufactural instructions (See supplementary material and methods for details).

RNA isolation and RT-qPCR

Total RNA was isolated from macrophages and pericytes using RNA isolation kit (Bio-line, UK) and cDNA was synthesized by sensi-fast cDNA synthesis kit (bio-line, UK). Transcripts of CECR1, PDGFB, and POSTN were measured and normalized to β-actin in macrophages and pericytes (For primers sequences see supplementary Table 1).

Trans-well co-culture

Macrophages were seeded in 0.4µm trans-well insert (Fisher scientific, USA) and were treated with U87-derived conditioned medium or recombinant human (rh)CECR1 protein for 48 hours followed by co-culture with pericytes for extra 72 hours. Pericytes were harvested afterwards for performing downstream assays.

Western blot

20 µg of total protein lysate derived from macrophages and pericytes was loaded onto 10% SDS-PAGE gel and blotted to Nitro cellulous membranes followed by blocking and incubation of primary antibody. Protein levels were assessed by immunoblotting using specific antibodies against CECR1 (Sigma, 1:200), Periostin (R&D, 1:200), PDGFRβ (Abcam, 1:10000), and β-actin (Abcam, 1:500) as a loading control, followed by incubation with secondary antibodies (IRdye 680 CW, IRDye 800 CW, Licor Bioscience, USA) and detection of signals using the Odyssey imaging system (Licor Bioscience, USA).

Immunostaining

4 µm of adjacent sections were used for immunohistochemical and immunofluorescence analysis. Immunostaining and slide scanning were performed according to the protocol described previously (43). Macrophages were fixed using 4% PFA/PBS, followed by antibody incubation. All fluorescence labeled samples was analyzed under the confocal microscope LSM 700 (Zeiss, The Netherlands). Five areas in high magnification field were randomly selected from each slide and quantified using Image J (Antibodies applied were listed in supplementary table2).

Transwell migration assay

7,000 Pericytes-dsRed with transfected with siPOSTN, siSham and non-transfected controls were seeded into the top compartment of the Fluor block 8 μm transwell inserts (Fisher Scientific, USA). Recombinant PDGFB protein was added in the lower chamber with serum free DMEM medium. Serum free macrophage conditioned medium from sisham, siCECR1, siPDGFB, and non-transfected control macrophages was added into the lower chamber. After 24 hours of migration, pictures from five randomly selected areas under 10x view were taken under a fluorescent microscope for image quantification by image J.

3D collagen tubule formation assay

HUVEC-GFP and Pericyte-dsRed were co-cultured in 96-well plate at 5:1 ratio within a 3D culture environment of bovine collagen type I (Gibco, USA) supplemented with SCF-1, SDF-1α, and IL-3, as described previously (44). 300 macrophages with different conditions were seeded on top of collagen gel and maintained for 5 days. At the 5^{th} day, tubule formation was captured by fluorescent microscope and quantified by Angiosys 1.0.

TCGA Database

Three GBM datasets were obtained from TCGA via the c-Bioportal provided by the Memorial Sloan Kettering Cancer Center. Genes that positively correlated with POSTN expression (cut off point: spearman r>0.4) in all three GBM database were selected for pathway analysis by String.

Statistics

Data from clinical samples were analyzed by Mann-Whitney U test and Spearman Correlation using SPSS 21.0. All *in vitro* data were tested using unpaired two-tailed student's T test (Significance levels $P<0.05$). All data are presented in Mean ± S.E.M. unless otherwise stated.

Results

CECR1 levels correlate with microvascular density in human GBM

Immuno-histochemisty analysis of human GBM samples indicated strong CECR1 intensity in GBM samples with high microvascular density, as shown by CD31+ staining of vascular endothelium (Figure 1a). The high level of CECR1 coincided with a strong signal of CD204+ M2 macrophages. In contrast, regions in GBM samples with weak CECR1 immunostaining showed limited numbers of CD204+ cells, and low microvascular density (Figure 1a). Quantitative analysis using ImageJ software confirmed the conclusions of the initial visual evaluation, with the mean percentage of CD31+ area per image field per GBM sample being significantly higher in the group of samples with high versus low CECR1 levels (Figure 1b). Further analysis revealed a significant positive correlation between the CD31 and CECR1 in the collection of GBM samples (Figure 1b). These data were in line with the findings obtained by data mining in the TCGA data set: significant positive correlations were identified between PECAM1 (endothelial cell marker), Endoglin (endothelial (progenitor) cell marker) and CECR1 expression in a set of 166 samples (Figure 1c, d). The findings were validated in a second TCGA GBM set (22) of 154 GBM samples (Figure 1c, d). Taken together, these observations indicate that high CECR1 levels in GBM relate to high microvascular density and the presence of CD204+ M2 macrophages.

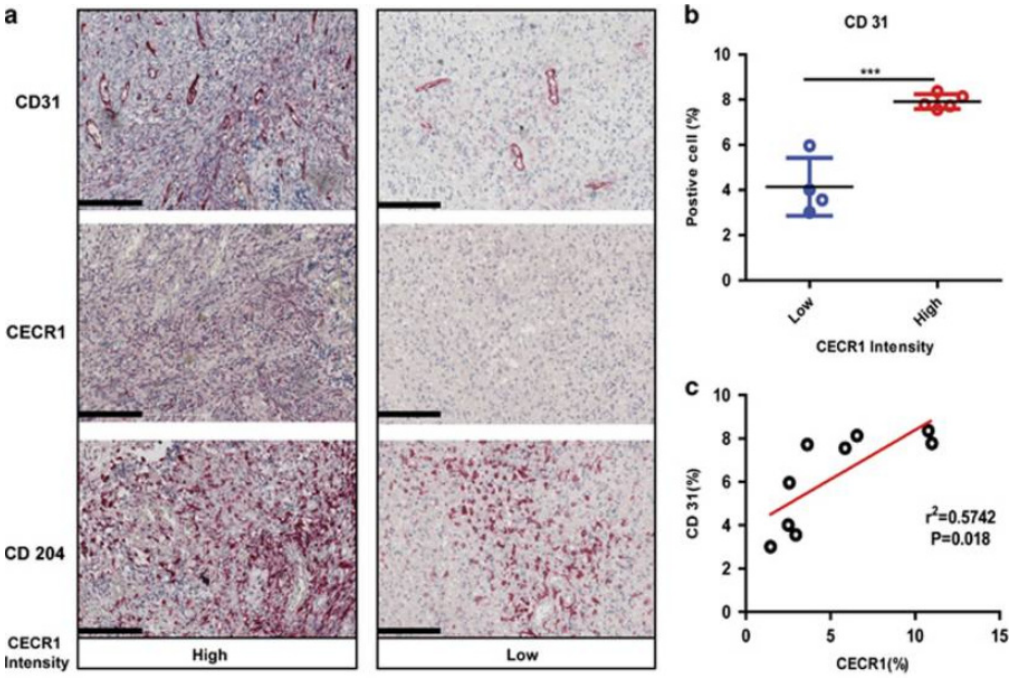

Fig.1. CECR1 levels correlates with microvascular density in human GBM

(a) Immuno-histological staining of human GBM cross-sections for CD31, CECR1 and CD204, in samples with high CECR1 signal (column High) and low CECR1 signal (column Low) (Scale bar: 200 µm).

(b) Upper graph shows the results of a quantitative analysis using ImageJ software of the mean percentage of CD31+ cells per image field per GBM patient in CECR1 low and high signal groups. Lower graph shows the correlation between mean %CD31+ cells and %CECR1+ cells per image field per GBM patient.

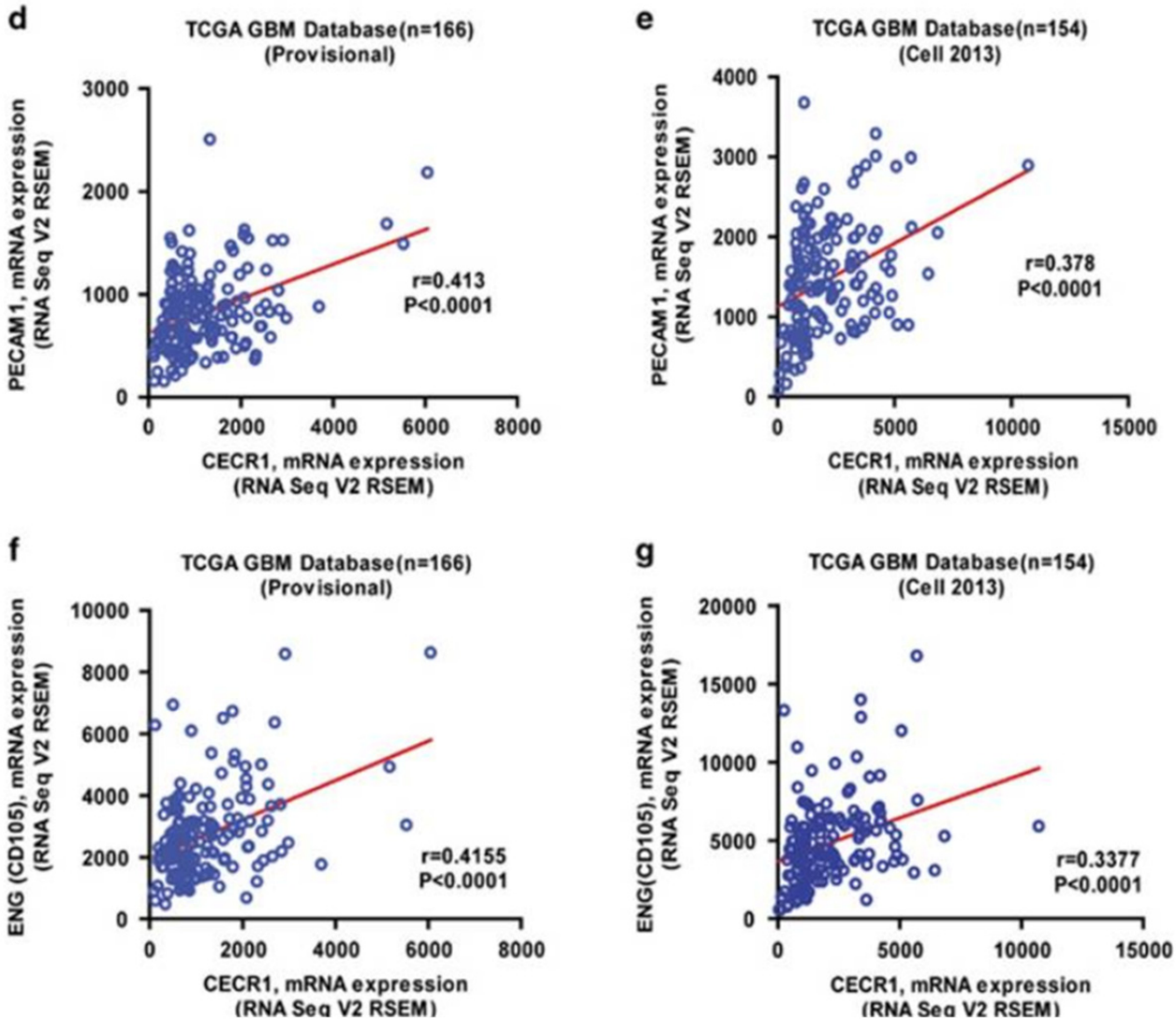

Fig.1. (c) Left graph: Correlation between PECAM1 and CECR1 mRNA levels in a set of 166 TCGA-dataset derived GBM samples. Right graph: Correlation between PECAM1 and CECR1 mRNA levels in a second set of 154 TCGA-dataset derived GBM samples. (d) Left graph: Correlation between Endoglin and CECR1 mRNA levels in a set of 166 TCGA-dataset derived GBM samples. Right graph: Correlation between Endoglin and CECR1 mRNA levels in a second set of 154 TCGA-dataset derived GBM samples.
***P<0.01.

CECR1 promotes the pro-angiogenic paracrine action of M2 macrophages

Previously we have identified M2-like macrophages as the main cell type in GBM to produce high levels of CECR1. We also showed that CECR1 promotes M0 to M2 macrophage polarization and determined M2 paracrine activity. Here we investigated the function of CECR1 in macrophage-mediated angiogenesis in a GBM-like environment. Angiogenesis was assessed in a 3D co-culture assay consisting of a collagen matrix in which GFP labeled HUVECs directly interact with dsRed labeled human-derived pericytes. This complex system mimics the complete sequence of events in microvasculature formation, allowing us to study vessel sprouting, vascular cell migration through a 3D matrix environment, multicellular vessel formation, lumenization, pericyte recruitment, perivascular coverage, and microvascular stabilization, all within a 5-day time range. To assess CECR1 function in GAMs in a GBM environment, THP1 monocytic cells were maturated by stimulation with PMA for 48 hours, before transfection with CECR1 targeting siRNA to obtain CECR1 silenced macrophages. These siCECR1 macrophages were further stimulated for 48 hours with or without U87 derived medium to assess the effect of a GBM paracrine environment. To assess the paracrine effect of the modified macrophages on angiogenesis, the THP1-derived macrophages were harvested and seeded on top of the co-culture system (Figure 2a). Stimulation of the co-cultures with THP1 macrophages significantly increased microvascular density, as observed by quantitative analysis of the number of tubules, total tubule length and number of junctions at day 5 (Figure 2b, c, f). Successful siRNA mediated knockdown CECR1 in THP1 macrophages, as validated by western blot and qPCR (Figure 2e), significantly reduced the response of the co-culture to the macrophages, as shown by a reduction in total tubule length compared to treatment with sisham and control macrophages. These effects were further amplified when the co-cultures were treated with THP1 macrophages stimulated with U87 supernatant during maturation, with CECR1-silenced + U87 supernatant-treated THP1 cells reducing the number of tubules and junctions and decreasing the total tubule length in the exposed co-cultures compared to the control groups (Figure 2d, f). In contrast, stimulation of co-cultures with the supernatant of THP1 macrophages that were stimulated with human recombinant CECR1 during maturation, showed a significant increase in all assessed vascular parameters (Supplementary figure 1a, b), demonstrating a dose-response relation.

Our previous studies demonstrated that M2 macrophages were the main producers of CECR1 in GBM. Here we investigated if the paracrine pro-angiogenic effects could be partially mediated by direct stimulation of vascular cells by CECR1. Indeed, stimulation of the co-cultures with recombinant CECR1 increased the number of junctions, tubules, and total tubule length, demonstrating that vascular cells can be directly stimulated by CECR1 (Supplemental figure 2a,b). Combined these data indicate that CECR1 plays an important role in regulating the pro-angiogenic function of macrophages.

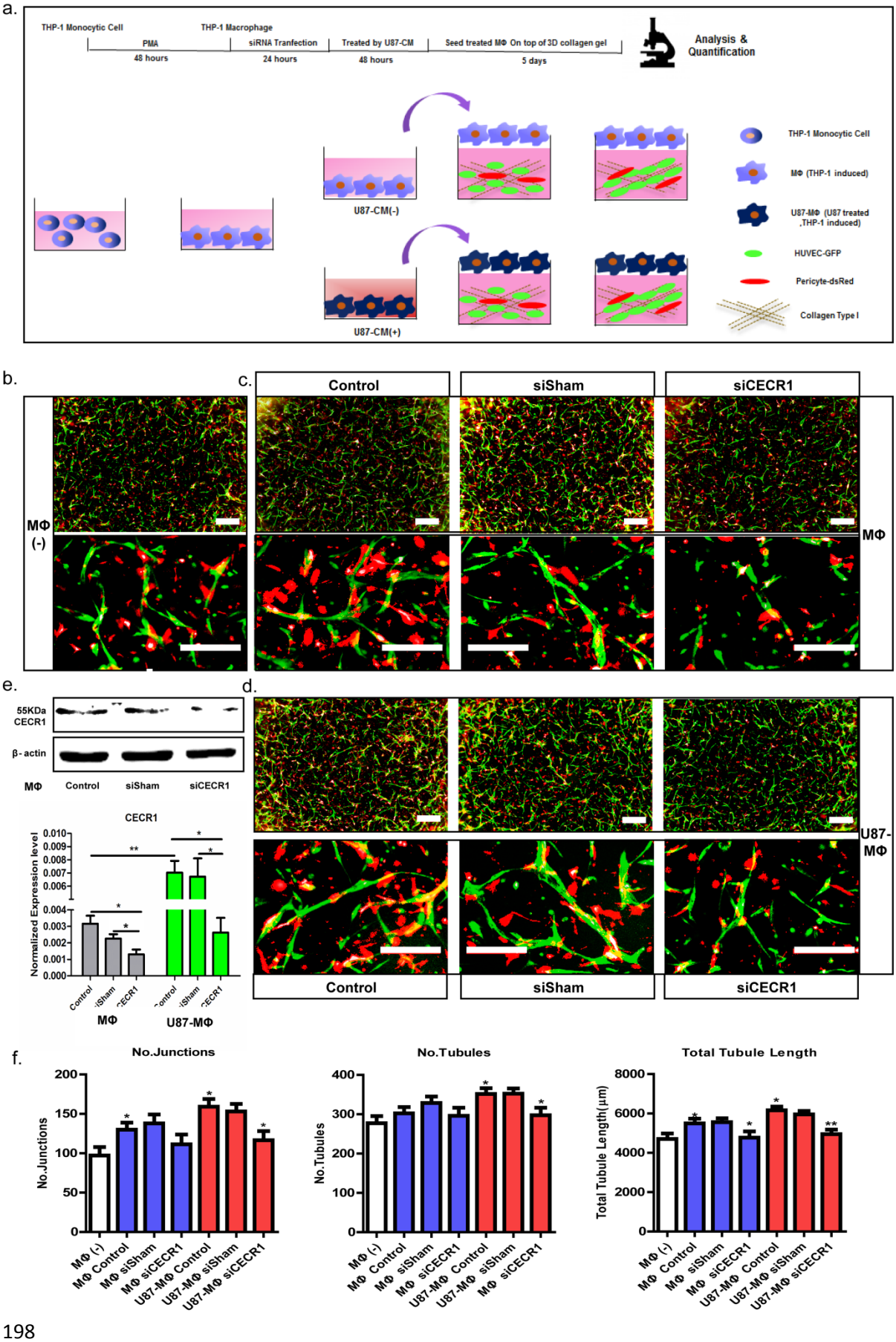
a.
THP-1 Monocytic Cell
THP-1 Macrophage
PMA
48 hours
siRNA Tranfection
24 hours
Treated by U87-CM
48 hours
Seed treated MΦ On top of 3D collagen gel
5 days
Analysis & Quantification
U87-CM(-)
U87-CM(+)
THP-1 Monocytic Cell
MΦ (THP-1 induced)
U87-MΦ (U87 treated ,THP-1 induced)
HUVEC-GFP
Pericyte-dsRed
Collagen Type I
b.
c.
Control
siSham
siCECR1
MΦ (-)
MΦ
e.
55KDa CECR1
β- actin
MΦ
Control
siSham
siCECR1
CECR1
Normalized Expression level
MΦ
U87-MΦ
d.
U87-MΦ
Control
siSham
siCECR1
f.
No.Junctions
No.Tubules
Total Tubule Length
Total Tubule Length(μm)
MΦ (-)
MΦ Control
MΦ siSham
MΦ siCECR1
U87-MΦ Control
U87-MΦ siSham
U87-MΦ siCECR1

Fig.2. CECR1 promotes the pro-angiogenic paracrine action of M2 macrophages
(a) Diagram showing the experimental setup of testing paracrine angiogenic activation of vascular cells in 3D co-cultures by THP1 macrophages. (b) Low and high magnification fluorescent images of neo-vessel formation by HUVECs (GFP-marked) and human derived pericytes (dsRed-marked) without THP1 marcrophage stimulation. (c) Low and high magnification fluorescent images of neo-vessel formation by HUVECs (GFP-marked) and human derived pericytes (dsRed-marked) with stimulation of non-treated (control), and sisham or siCECR1 treated THP1 macrophages. (d) Low and high magnification fluorescent images of neo-vessel formation by HUVECs (GFP-marked) and human derived pericytes (dsRed-marked) with stimulation of non-treated (control), and sisham or siCECR1 treated THP1 macrophages with U87 stimulation. (Scale bar: 100 μm for b, c, and d). (e) Upper image: Western blot of CECR1 protein and β actin loading control in THP1 macrophages. Blot represents results from three observations. Lower graph: QPCR results of CECR1 mRNA levels normalized to housekeeping genes in non-treated (control), and sisham or siCECR1 treated THP1 macrophages, without and with U87 stimulation. *P<0.05; **P<0.01. (f) Quantified results of the co-culture experiment. No. of junctions, tubules, and total tubule length data are shown. *P<0.05; **P<0.01. Representative graphs were taken from at least three experiments. Six wells were analyzed in each experiment.

PDGFB expression correlates with M2 GAMs and is enhanced by CECR1

In order to identify which particular known pro-angiogenic molecules are related to the expression of CECR1, qPCR was carried out on 6 common pro-angiogenic genes (VEGFA, TIE1, TIE2, ANGPT1, ANGPT2, PDGFB). QPCR analysis of macrophages silenced for CECR1 showed a significant decrease in PDGFB levels (Figure 3a), while expression levels of other pro-angiogenic genes were not affected (VEGFA, TIE1, TIE2, ANGPT1, ANGPT2, data not shown). Visa versa, stimulation of macrophages with recombinant human (rh)CECR1 significantly increased PDGFB in a dose-responsive manner (Figure 3b). These data were further validated by immuno-fluorescent staining of cytospin THP1 macrophages, showing a reduction in PDGFB signal that coincided with a reduction in CD163 (M2) marker signal in the CECR1 silenced versus control macrophages and sisham treated macrophages (Figure 3c). This effect was CECR1 knockdown specific, as knockdown of PDGFB in THP1 macrophages did not reduce the CD163 M2 marker signal, while the PDGFB signal was clearly decreased (Figure 3c). In contrast, treatment of macrophages with rhCECR1 increased both CD163 and PDGFB mean intensity signals (Figure 3e). Quantification of the mean intensity levels of PDGFB of the different groups confirmed that PDGFB was decreased and increased by CECR1 silencing, and rhCECR1 stimulation, respectively (Figure 3d). Stimulation of THP1 macrophages with U87 derived supernatant showed upregulation of PDGFβ signal in cytospin samples. This effect was significantly reduced in siCECR1 versus sisham treated THP1 macrophages (Figure 3f). A correlation between CECR1 and PDGFB levels was also found by analysis of TCGA datasets, which showed a positive correlation between PDGFB and CECR1 expression levels in a provisional set of 166 GBM samples, and was subsequently validated in a second set of 154 GBM samples (Figure 3h). Similar to CECR1,

immunostaining of GBM samples revealed that PDGFB+ cells were mainly GAMs that express pan macrophage and M2 markers such as CD68 and CD163 (Figure 3g).

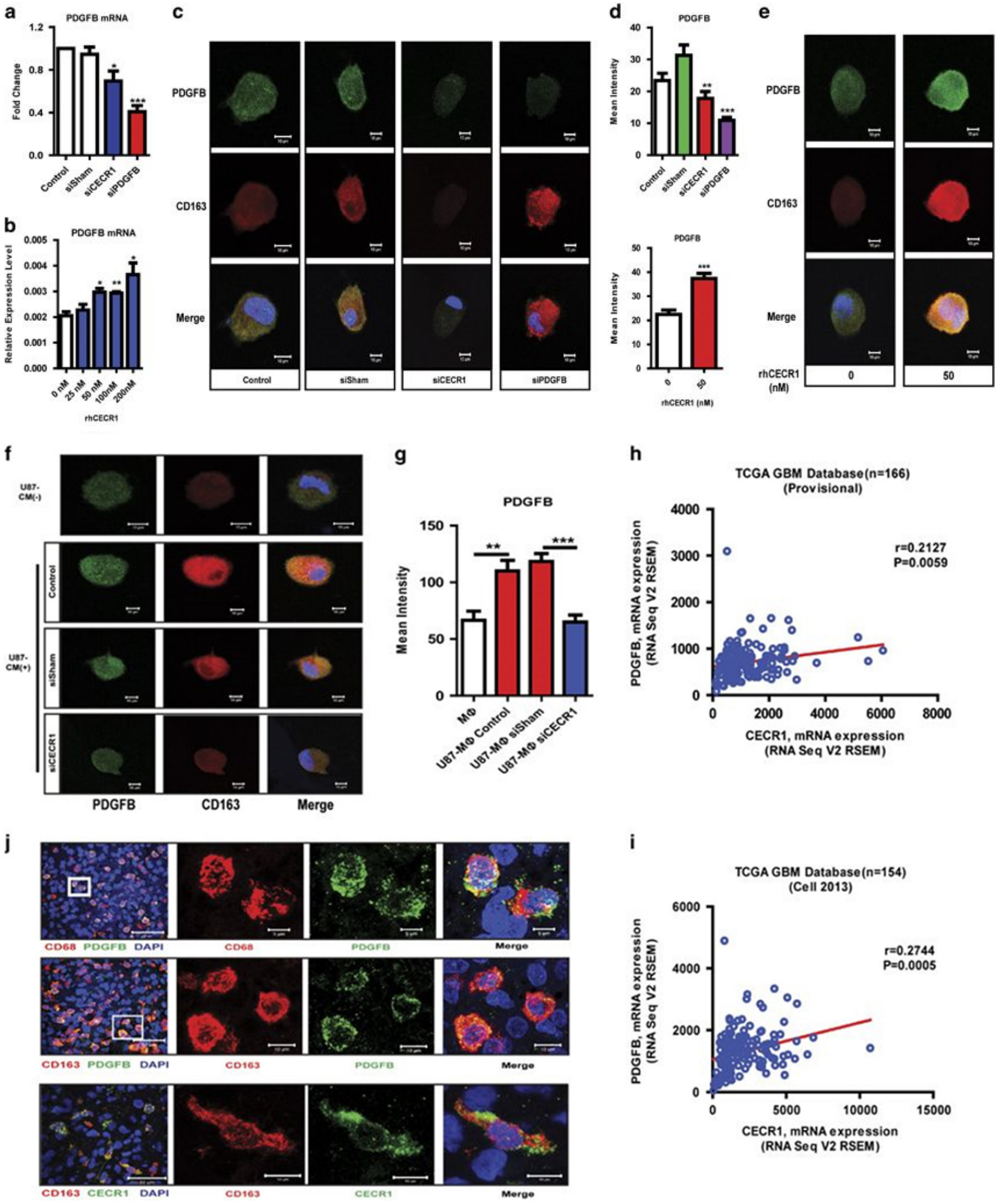

Fig.3. PDGFB expression correlates with M2 GAMs and is enhanced by CECR1

(a) QPCR analysis of PDGFβ mRNA levels normalized to housekeeping genes in non-treated (control), and sisham or siCECR1 or siPDGFB treated THP1 macrophages. *P<0.05; ***P<0.005. Experiments were repeated at least three times. (b) QPCR analysis of PDGFB mRNA levels normalized to housekeeping genes in THP1 macrophages treated with different concentrations of rhCECR1 from three experiments. *P<0.05; ***P<0.005. (c) Image panel shows immuno-fluorescent staining of PDGFB and CD163, and merged images of cytospin non-treated (control), and sisham or siCECR1 or siPDGFB treated THP1 macrophages (Scale bar: 10 μm).(d) Graph shows mean PDGFβ intensity of each treatment group. **P<0.01; ***P<0.005. Experiments were repeated at least three times. (e) Image panel shows immuno-fluorescent staining of PDGFB and CD163, and merged images of cytospun non-treated (control), and rhCECR1 treated THP1 macrophages (Scale bar: 10 μm) (f) Image panel shows immuno-fluorescent staining of PDGFB (green) and CD163 (red), and merged images of cytospin non-treated controls with exposure to U87 supernatant U87 conditioned medium (CM), and THP1 macrophages treated with sisham + U87 supernatant or siCECR1 + U87 supernatant. Graph shows mean PDGFB intensity of each treatment group from at least three experiments. **P<0.01; ***P<0.005. (g) Low and high magnification confocal images of double immuno-fluorescent staining of CD68, CD163 and PDGFB, CECR1 in human GBM sections (scale bar: Left panel, 50 μm, Right upper panel, 5 μm, right lower panel 10 μm). (h) Upper graph: Correlation between PDGFB and CECR1 mRNA levels in a set of 166 TCGA-dataset derived GBM samples. Right graph: Correlation between PDGFB and CECR1 mRNA levels in a second set of 154 TCGA-dataset derived GBM samples.

CECR1-mediated paracrine activation of macrophages promotes pericyte recruitment via PDGFB/PDGFβR signaling in GBM

To assess the role of PDGFB in CECR1 regulation of macrophages in angiogenesis, we conducted co-culture experiments with macrophages silenced for PDGFB. Co-cultures with PDGFB silenced macrophages seeded on top mimicked the phenotype of co-cultures that were treated by CECR1 silenced macrophages, demonstrating a general decrease of all parameters of active angiogenesis (Figure 4a b). Co-culture analysis of siPDGFB macrophages that differentiated with exposure to U87 supernatant showed a similar negative effect on angiogenic parameters (Supplemental data Figure 3a, b). This reduction was partially rescued by treating siPDGFβ macrophages with rhCECR1 (siPDGFB versus siPDGFB + rhCECR1, total tubule length), indicating that the paracrine pro-angiogenic effect of CECR1 in macrophages is partially mediated via PDGFB (Figure 4a, b). PDGFB mediates its activity via PDGFβ receptor (PDGFβR) signaling.

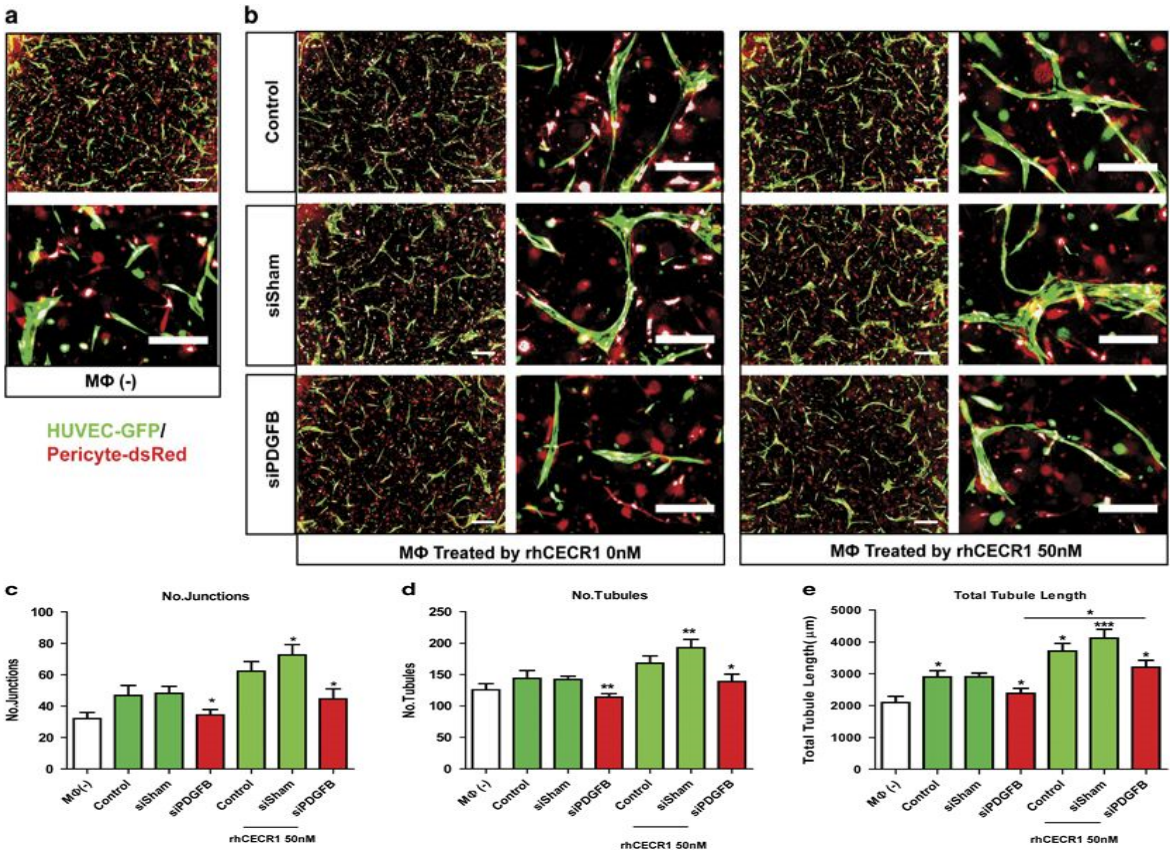

Fig.4. CECR1-mediated macrophage paracrine activation of angiogenesis is partially regulated via PDGFB (a) Low and high magnification fluorescent images of neovessel formation by HUVECs (GFP-marked) and human derived pericytes (dsRed-marked) without THP1 marcrophage stimulation, and with stimulation of non-treated (control), and sisham or siPDGFB treated THP1 macrophages, without or with rhCECR1 rescue. (b) Quantified results of the co-culture experiment. No. of junctions, tubules, and total tubule length data are shown. *P<0.05; **P<0.01 ***P<0.005. Scale bar: 100 μm. N>10 cocultures in total.

In GBM samples, immuno-staining revealed that PDGFβR+ cells are mainly perivascular mural cells that are closely located near CD163+ M2 macrophages (Figure 5a, b). QPCR analysis of different *in vitro* human cell types that have equivalents in GBM *in vivo*, including HUVECs, pericytes, U87, U251, and THP1 macrophages, demonstrated that PDGFβR was mainly expressed by pericytes (Figure 5c). Confocal imaging combined with double immuno-staining further confirms mural cell expression of PDGFβR and the close localization of CD163+ GAMs in human GBMs (Figure 5d). The PDGFB/PDGFRβ ligand/receptor signaling mechanism is well-known to promote mural cell proliferation and is critical for mural cell recruitment to newly formed vessels to ensure vascular coverage and stabilization. Next, we investigated the CECR1-mediated effects of THP1 macrophages on pericyte recruitment. Pericytes were evaluated for their migratory capacity in a transwell migration assay in response to paracrine factors that are present in macrophage-derived supernatants of the different groups (Figure 5e). Pericyte migration increased upon stimulation by supernatant of THP1 macrophages (Figure 5f, g). Pericyte migration significantly decreased in response to supernatant derived from CECR1

silenced THP1 macrophages (Figure 5e-g). This effect was mimicked by PDGFB silencing in THP1 macrophages in normal medium (Figure 5f, g). The data imply that CECR1-enhanced release of PDGFB by M2-like GAMs promotes pericyte recruitment to inflammatory pro-angiogenic sites via PDGFRβ signaling in GBM.

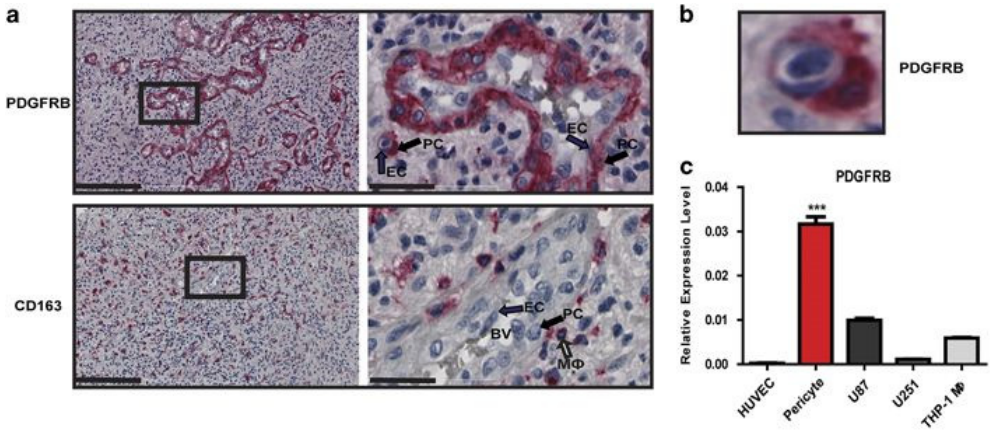

Fig.5. CECR1-mediated paracrine activation of macrophages may promote pericyte recruitment via PDGFB/PDGFRβ signaling in GBM

(a) Low (right panel) and high (left panel) immunohistological staining of PDGFRβ and CD163 in human GBM sections. Black arrows indicate pericytes and endothelial cells (EC) forming blood vessels (BV). White arrow indicates macrophages (Mφ) (Scale bar: Left panel, 200 μm, right panel, 40 μm). (b) High magnification image of PDGFRβ immunohistological staining in human GBM sections. (c) QPCR analysis of PDGFRβ mRNA expression levels normalized to housekeeping genes in HUVECs, pericytes, U87, U251, and THP1 macrophages from three experiments.

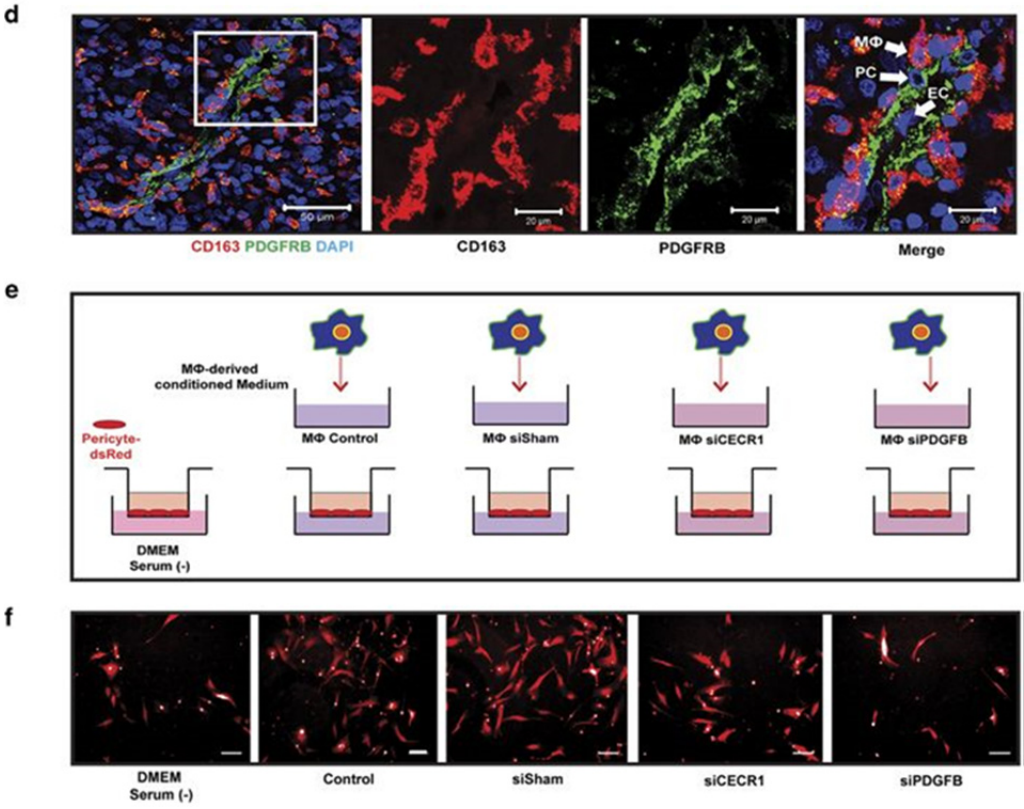

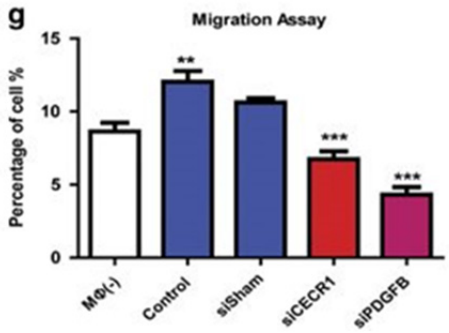

Fig.5. (d) Confocal images of CD163 and PDGFRβ double immuno-fluorescent staining in human GBM sections. White arrows indicate pericytes, endothelial cells (EC), and macrophages (Mφ). Scale bars: left panel, 50μm; right panel, 20 μm. (e) Diagram of the experimental setup of the transwell migration assay of pericytes (dsRed marked) seeded on top of the transwell. Cell migration aws towards a lower chamber with DMEM medium only, or with supernatant derived from non-treated (control) macrophages, and sisham or siCECR1 treated macrophages. (f) Panel of fluorescent images of dsRed marked pericytes that have migrated through the transwell setting in response to the different conditions (DMEM only, or in response to supernatant of non-treated macrophages (control), or sisham, siCECR1, or siPDGFRβ treated macrophages). (g) Quantified results of the transwell migration assay. **P<0.01; ***P<0.005, N>6 migration assays per condition.

CECR1 activation in THP1 macrophages promotes paracrine activation of periostin protein production in pericytes

Further confocal immuno-histochemical analysis of human GBM samples revealed colocalization of PDGFRβ+ perivascular mural cells with the extra cellular matrix component periostin (Figure 6a). Previously, we have detected enrichment of periostin in the microvasculature of GBMs using a proteomics screen (23). Work by others revealed an important role for periostin in recruitment of M2-like tumor associated macrophages and subsequent support of malignant growth (13). In line with these reports, periostin deposition was detected in close proximity of CD163+ M2 GAMs (Figure 6b). A significant positive correlation was also identified between CD163 and periostin expression in a set of 154 samples using the TCGA GBM database (Figure 6c). Similarly to PDGFRβ, qPCR analysis of different *in vitro* human cell types that can be found in GBM, including HUVECs, pericytes, U87, U251, and macrophages, demonstrated that periostin was mainly expressed by pericytes (Figure 6d). Paracrine stimulation of pericytes by THP1 macrophages enhanced periostin protein levels in the co-culture setup (Figure 6e, f). THP1 macrophages stimulated with U87 supernatant during maturation further enhanced periostin protein levels (Figure 6e, f), indicating that GAMs can significantly promote periostin protein production in pericytes.

Periostin expression correlates ($r=0.3015$; $p<0.0001$) with CECR1 expression levels in a set of 205 samples derived from the TCGA GBM database (Figure 6g). The periostin protein levels of pericytes exposed to the paracrine activity of THP1 macrophages dropped significantly following silencing the macrophages for CECR1 (Figure 6h). Similarly, silencing of PDGFB in the THP1

macrophages resulted in decreased periostin production by pericytes (Figure 6h). In support of these findings, THP1 macrophages that were treated with rhCECR1 during maturation, increased periostin protein levels produced by pericytes (Figure 6i). Similarly, periostin production by pericytes that were directly stimulated with physiological levels of PDGFB was significantly increased (Figure 6j). However, direct stimulation of pericytes with rhCECR1 did not enhance their periostin production (Figure 6k), indicating that the CECR1-mediated macrophage activation of periostin expression in pericytes is indirect and requires an intermediate paracrine factor, such PDGFB. In line with these findings, direct stimulation of pericytes with PDGFB promoted their migration, and silencing of periostin in pericytes inhibited this response (Figure 6l, m).

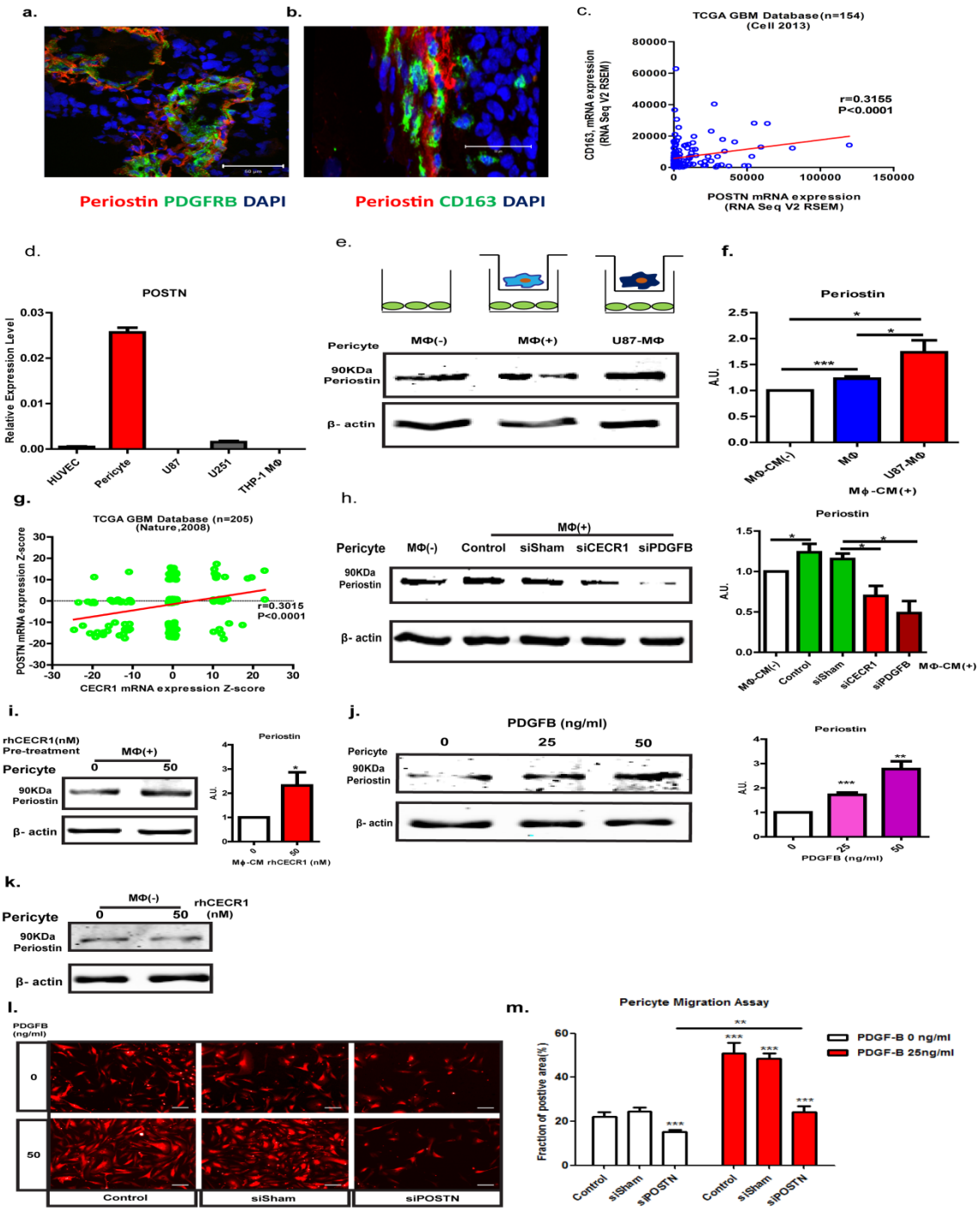

Fig. 6. CECR1 activation in THP1 macrophages promotes paracrine activation of periostin protein production in pericytes

(a, b) Confocal images of imunohistological stainings of periostin, PDGFRβ, and CD163 in human GBM sections. Scale bar: 50 µm. (c) Correlation between CD163 and periostin mRNA levels in a set of 154 TCGA-dataset derived GBM samples. (d) QPCR analysis of periostin mRNA expression levels normalized to housekeeping genes in HUVECs, pericytes, U87, U251, and THP1 macrophages from three experiments. (e) Diagram showing experimental setup with pericytes (green) cocultured with

macrophages without (light blue) and with U87 pre-stimulation (dark blue) seeded in filter insert. Western blot shows periostin and β actin protein levels in pericytes of the different treatment groups.
(f) Quantitative results of Western blot analysis normalized to β actin loading control from four experiments. *P<0.05; ***P<0.005.(g) Correlation between periostin and CECR1 mRNA levels in a set of 205 TCGA-dataset derived GBM samples. (h) Western blot shows periostin and β actin protein levels in pericytes treated with no macrophages, with non-transfected macrophages (control), and macrophages transfected with sisham, siCECR1, or siPDGFRβ. Graph shows quantitative results of Western blot analysis normalized to β actin loading control from four experiments. *P<0.05. (i) Western blot shows periostin and β actin protein levels in pericytes treated with macrophages with and without pre-treatment with rhCECR1. Graph shows quantitative results of Western blot analysis normalized to β actin loading control of at least four experiments. *P<0.05. (j) Western blot shows periostin and β actin protein levels in pericytes treated with different concentrations of PDGFB. Graph shows quantitative results of Western blot analysis normalized to β actin loading control from at least three experiments. ** P<0.01; ***P<0.005. (k) Representative western blot of three independent experiments, showing periostin and β actin protein levels in pericytes treated with rhCECR1. (l) Panel of fluorescent images of dsRed marked pericytes that have migrated through the transwell setting in response to the different conditions (in response to supernatant of non-treated macrophages (control), or sisham, or siperiostin treated macrophages), with and without PDGFB stimulation (Scale bar: 50 μm).(g) Quantified results of the transwell migration assay from three experiements. **P<0.01; ***P<0.005.

Further evidence for the involvement of periostin in angiogenesis and cell migration is provided by correlation analysis of periostin expression in three different TCGA derived human GBM data sets (Supplementary Figure 4a). Overlap analysis identified a set of 139 genes that was significantly correlated with periostin expression in the three GBM gene sets (Supplemental Figure 4b). Functional annotation of the 139 genes identified the top 20 of the significant biological processes including angiogenesis related GO terms such as "*blood vessel morphology*", "*angiogenesis*", "*blood vessel development*", and "*cardiovascular system development*" (Supplemental Figure 4c). Furthermore, GO terms associated with cell migration such as; "*cell adhesion*", and "*extracellular matrix disassembly*" were also identified (Supplemental Figure 4c). Taken together, the data reveal a link between periostin expression by pericytes and CECR1-mediated macrophage paracrine activity.

Discussion

The main findings of this study are: a) Expression of CECR1 is positively correlated with microvascular density in glioblastoma. b) CECR1 expression by GAMs promotes angiogenesis in a 3D co-culture assay. c) The level of CECR1 regulates PDGFB production in GAMs. d) The CECR1-PDGFB mediated cross talk between macrophages and pericytes promotes migration of pericytes and contributes to new vessel formation. e) Macrophage-pericyte CECR1-PDGFB-PDGFRβ signaling upregulates the expression of the pro-angiogenic extracellular matrix component periostin in pericytes.

Current knowledge of the proangiogenic capacities of GAMs mainly concerns the effects of these cells on vascular endothelial cells (24). The regulation of perivascular cells, such as pericytes, by GAMs, is rarely studied. In this study we describe the proangiogenic role of CECR1 that is mediated via an autocrine feedback loop in which CECR1 production in (M2) GAMs enhances PDGFB expression and secretion. PDGFB/PDGFRβ signaling is crucial for the vascular maturation process in angiogenesis, during which newly formed microvessels secrete PDGFB to guide perivasular coverage by pericytes. PDGFB secreted by (M2) GAMs promote both pericyte migration and angiogenesis, as shown by our migration and 3D co-culture data respectively. Periostin is an extracellular matrix protein that is specifically present in the basal membrane of the microvasculature of GBMs [19]. In the present study we identified periostin as a potent down-stream target of the macrophage CECR1-PDGFB paracrine signaling cascade (See Supplemental data Figure 5). Pericytes are defined by their singular perivascular position, their remarkable dendrite-like morphology and their expression of PDGFRβ and NG-2 (25), Pericytes are multifunctional cells (26), being vital cells for vessel construction, maintenance, and the regulation of the vascular physiology (27). Pericyte dysfunction could lead to delay in blood vessel maturation, and contributes to vascular instability and leakage (28). Pericytes also contribute to recruitment of immune cells, including monocytes, during inflammation (29). A process of mutual activation between GAMs and pericytes during tumorangiogenesis has been previously identified. In tumors the paracrine influence of GAMs leads to activation of the PDGFB-SOX17 axis, which is initiated by tumor cells and leads to pericyte production of IL-33 (30). In addition, tumor associated macrophages secrete MMP-9, which has been shown to enhance the recruitment of pericyte precursor cells into the tumor microenvironment (31). The present data demonstrate the pro-angiogenic function of CECR1 in macrophages, mediated via paracrine regulation of PDGFB. The relation between CECR1 and angiogenesis and vascular density is reflected by the hyper-inflammatory response in patients with a CECR1 loss of function mutation (32). One of the most prominent symptoms displayed by these patients was early-onset stroke and profound vasculopathy. Similarly, vascular instability was observed in zebrafish with CECR1 knockdown. In previous studies we pointed out that CECR1 in GBM is mainly expressed by M2-like GAMs. We also discovered that CECR1 acts as a potent polarizing factor in GAMs differentiation towards the M2-like phenotype. CECR1 activity also increased the pro-tumoral function of M2 macrophages in a paracrine fashion(33). In the current study, we

have shown that CECR1 activity in GAMs enhances PDGFB mRNA and protein production levels. In line with these findings, PDGFB was previously reported not only to be expressed by activated endothelial cells, but also by M2-like GAMs (34). Elevated levels of PDGFB produced in malignant cancers upregulate erythropoietin expression in stromal cells via activation of PDGRB that accelerates tumor angiogenesis (35). The CECR1-PDGFB-PDGFRβ axis that is revealed in this study points to a putative CECR1-mediated functional cross talk between macrophages and pericytes, guiding the process of vascular maturation and development. This process may be involved in the vascular symptoms observed in patients with CECR1 mutations (21).

Aberrant vessel morphology with abnormal pericyte coverage is considered as one of the classical hallmarks of tumor vasculature in malignant tumors including GBM. Recent studies in pericytes have revealed hyperplasia of this cell type in GBM (36). The function of pericytes in malignant tumors is not only restricted to support vascular growth. As a potent producer of VEGFA, perivascular pericytes protect the tumor microvasculature against disintegration during anti-VEGFA therapy by elevating local VEGFA levels (26). Furthermore, pericytes in glioma were shown to produce other angiogenic molecules like HGF, TGFβ1 and Prostaglandins. Pericytes also inhibit the activation of T cells and thereby induce immunosuppression in glioma (37), while expressing plasminogen urokinase in support of the self-renewal and invasion of glioma initiating cells (38). Based on these reports, we can conclude that pericytes play many significant roles in promoting angiogenesis and tumor progression in glial tumors.

In this study we have identified periostin as a down-stream target of PDGFB signaling in pericytes. Periostin was identified as a pro-angiogenic extracellular matrix component in glioma (23). As a multifunctional protein it is involved in various carcinogenic processes such as the regulation of cell migration and the epithelial-mesenchymal transition in cancer cells, mainly via activation of cell focal adhesion kinases through cell binding to integrins (39). Recently, periostin was shown to play a role in the recruitment of M2-like GAMs in GBM (13) and to mediate the resistance to anti-VEGFA therapy by increasing expression of caveolin-1, HIF-1α, and VEGFA (40). In addition, periostin is expressed by mammary stromal cells in breast cancer where it is involved in actively maintaining a breast cancer stem cell niche via the canonical WNT signaling pathway (41). In pancreatic carcinoma the expression of periostin was found upregulated in response to PDGFB stimulation (42). Our data provides evidence that the modulation of CECR1 in macrophages influences the expression of periostin in pericytes via PDGFB-mediated paracrine signaling.

In conclusion, this study demonstrates that in glioblastoma CECR1 produced by M2-like GAMs regulates the cross talk between macrophages and pericytes via paracrine PDGFB-PDGFRβ signaling, promoting pericyte recruitment and migration, and tumor angiogenesis. The pro-angiogenic function of the CECR1-PDGFB-PDGFRβ signaling cascade is related to the expression of periostin by pericytes. This new knowledge on complex interaction between immuno cells and vascular cells, in the process of tumor neo-angiogenesis could lead to better immune-modulatory and anti-angiogenic strategies for treatment of GBM in the future.

References

1. Wen PY, Kesari S. Malignant gliomas in adults. New England Journal of Medicine. 2008;359(5):492-507.
2. Das S, Marsden PA. Angiogenesis in glioblastoma. New England Journal of Medicine. 2013;369(16):1561-3.
3. Prosniak M, Harshyne LA, Andrews DW, Kenyon LC, Bedelbaeva K, Apanasovich TV, et al. Glioma grade is associated with the accumulation and activity of cells bearing M2 monocyte markers. Clin Cancer Res. 2013;19(14):3776-86.
4. Gilbert MR. Antiangiogenic Therapy for Glioblastoma: Complex Biology and Complicated Results. J Clin Oncol. 2016;34(14):1567-9.
5. Takano S. Glioblastoma angiogenesis: VEGF resistance solutions and new strategies based on molecular mechanisms of tumor vessel formation. Brain Tumor Pathol. 2012;29(2):73-86.
6. Ferrara N. Pathways mediating VEGF-independent tumor angiogenesis. Cytokine Growth Factor Rev. 2010;21(1):21-6.
7. Hambardzumyan D, Gutmann DH, Kettenmann H. The role of microglia and macrophages in glioma maintenance and progression. Nature Neuroscience. 2016;19(1):20-7.
8. Lu-Emerson C, Snuderl M, Kirkpatrick ND, Goveia J, Davidson C, Huang YH, et al. Increase in tumor-associated macrophages after antiangiogenic therapy is associated with poor survival among patients with recurrent glioblastoma. Neuro-Oncology. 2013;15(8):1079-87.
9. Chen X, Zhang L, Zhang IY, Liang J, Wang H, Ouyang M, et al. RAGE expression in tumor-associated macrophages promotes angiogenesis in glioma. Cancer Res. 2014;74(24):7285-97.
10. Brandenburg S, Müller A, Turkowski K, Radev Y, Rot S, Schmidt C, et al. Resident microglia rather than peripheral macrophages promote vascularization in brain tumors and are source of alternative pro-angiogenic factors. Acta Neuropathol. 2015:1-14.
11. Nijaguna MB, Patil V, Urbach S, Shwetha SD, Sravani K, Hegde AS, et al. Glioblastoma-derived Macrophage Colony-stimulating Factor (MCSF) Induces Microglial Release of Insulin-like Growth Factor-binding Protein 1 (IGFBP1) to Promote Angiogenesis. J Biol Chem. 2015;290(38):23401-15.
12. Li W, Graeber MB. The molecular profile of microglia under the influence of glioma. Neuro Oncol. 2012;14(8):958-78.
13. Squadrito ML, De Palma M. A niche role for periostin and macrophages in glioblastoma. Nat Cell Biol. 2015;17(2):107-9.
14. Pong WW, Walker J, Wylie T, Magrini V, Luo JQ, Emnett RJ, et al. F11R Is a Novel Monocyte Prognostic Biomarker for Malignant Glioma. Plos One. 2013;8(10).
15. Komohara Y, Ohnishi K, Kuratsu J, Takeya M. Possible involvement of the M2 anti-inflammatory macrophage phenotype in growth of human gliomas. J Pathol. 2008;216(1):15-24.
16. Roma-Lavisse C, Tagzirt M, Zawadzki C, Lorenzi R, Vincentelli A, Haulon S, et al. M1 and M2 macrophage proteolytic and angiogenic profile analysis in atherosclerotic patients reveals a distinctive profile in type 2 diabetes. Diab Vasc Dis Res. 2015;12(4):279-89.
17. Nakamura R, Sene A, Santeford A, Gdoura A, Kubota S, Zapata N, et al. IL10-driven STAT3 signalling in senescent macrophages promotes pathological eye angiogenesis. Nat Commun. 2015;6:7847.

18. Jetten N, Verbruggen S, Gijbels MJ, Post MJ, De Winther MP, Donners MM. Anti-inflammatory M2, but not pro-inflammatory M1 macrophages promote angiogenesis in vivo. Angiogenesis. 2014;17(1):109-18.
19. Potente M, Gerhardt H, Carmeliet P. Basic and Therapeutic Aspects of Angiogenesis. Cell.146(6):873-87.
20. Lin L, Chen YS, Yao YD, Chen JQ, Chen JN, Huang SY, et al. CCL18 from tumor-associated macrophages promotes angiogenesis in breast cancer. Oncotarget. 2015;6(33):34758-73.
21. Navon Elkan P, Pierce SB, Segel R, Walsh T, Barash J, Padeh S, et al. Mutant adenosine deaminase 2 in a polyarteritis nodosa vasculopathy. New England Journal of Medicine. 2014;370(10):921-31.
22. Brennan CW, Verhaak RG, McKenna A, Campos B, Noushmehr H, Salama SR, et al. The somatic genomic landscape of glioblastoma. Cell. 2013;155(2):462-77.
23. Mustafa DAM, Dekker LJ, Stingl C, Kremer A, Stoop M, Smitt PAES, et al. A Proteome Comparison Between Physiological Angiogenesis and Angiogenesis in Glioblastoma. Mol Cell Proteomics. 2012;11(6).
24. Riabov V, Gudima A, Wang N, Mickley A, Orekhov A, Kzhyshkowska J. Role of tumor associated macrophages in tumor angiogenesis and lymphangiogenesis. Front Physiol. 2014;5:75.
25. Armulik A, Genove G, Betsholtz C. Pericytes: developmental, physiological, and pathological perspectives, problems, and promises. Dev Cell. 2011;21(2):193-215.
26. Sweeney MD, Ayyadurai S, Zlokovic BV. Pericytes of the neurovascular unit: key functions and signaling pathways. Nat Neurosci. 2016;19(6):771-83.
27. Bergers G, Song S. The role of pericytes in blood-vessel formation and maintenance. Neuro Oncol. 2005;7(4):452-64.
28. Garcia-Quintans N, Sanchez-Ramos C, Prieto I, Tierrez A, Arza E, Alfranca A, et al. Oxidative stress induces loss of pericyte coverage and vascular instability in PGC-1 alpha-deficient mice. Angiogenesis. 2016;19(2):217-28.
29. Stark K, Eckart A, Haidari S, Tirniceriu A, Lorenz M, von Bruhl M-L, et al. Capillary and arteriolar pericytes attract innate leukocytes exiting through venules and 'instruct' them with pattern-recognition and motility programs. Nature Immunology. 2013;14(1):41-51.
30. Yang YL, Andersson P, Hosaka K, Zhang Y, Cao RH, Iwamoto H, et al. The PDGF-BB-SOX7 axis-modulated IL-33 in pericytes and stromal cells promotes metastasis through tumour-associated macrophages. Nature Communications. 2016;7.
31. Yang L, DeBusk LM, Fukuda K, Fingleton B, Green-Jarvis B, Shyr Y, et al. Expansion of myeloid immune suppressor Gr+CD11b+cells in tumor-bearing host directly promotes tumor angiogenesis. Cancer Cell. 2004;6(4):409-21.
32. Zhou Q, Yang D, Ombrello AK, Zavialov AV, Toro C, Zavialov AV, et al. Early-onset stroke and vasculopathy associated with mutations in ADA2. New England Journal of Medicine. 2014;370(10):911-20.
33. Zhu C, van der Weiden MM, Scchetti A, van den Bosch TPP, Chrifi I, Brandt MM, et al. Abstract 2348: Expression of CECR1 by activated M2-type macrophages in glioma. Cancer Research. 2015;75(15 Supplement):2348-.
34. Vignaud JM, Marie B, Klein N, Plenat F, Pech M, Borrelly J, et al. The Role of Platelet-Derived Growth-Factor Production by Tumor-Associated Macrophages in Tumor Stroma Formation in Lung-Cancer. Cancer Research. 1994;54(20):5455-63.

35. Xue Y, Lim S, Yang Y, Wang Z, Jensen LD, Hedlund EM, et al. PDGF-BB modulates hematopoiesis and tumor angiogenesis by inducing erythropoietin production in stromal cells. Nat Med. 2012;18(1):100-10.
36. Sun HQ, Guo DY, Su YP, Yu DM, Wang QL, Wang T, et al. Hyperplasia of Pericytes Is One of the Main Characteristics of Microvascular Architecture in Malignant Glioma. Plos One. 2014;9(12).
37. Ochs K, Sahm F, Opitz CA, Lanz TV, Oezen I, Couraud PO, et al. Immature mesenchymal stem cell-like pericytes as mediators of immunosuppression in human malignant glioma. Journal of Neuroimmunology. 2013;265(1-2):106-16.
38. Zhong X, Liu X, Li Y, Cheng M, Wang W, Tian K, et al. HMGA2 sustains self-renewal and invasiveness of glioma-initiating cells. Oncotarget. 2016.
39. Liu AY, Zheng H, Ouyang G. Periostin, a multifunctional matricellular protein in inflammatory and tumor microenvironments. Matrix Biol. 2014;37:150-6.
40. Park SY, Piao Y, Jeong KJ, Dong J, de Groot JF. Periostin (POSTN) regulates tumor resistance to antiangiogenic therapy in glioma models. Mol Cancer Ther. 2016.
41. Malanchi I, Santamaria-Martinez A, Susanto E, Peng H, Lehr HA, Delaloye JF, et al. Interactions between cancer stem cells and their niche govern metastatic colonization. Nature. 2012;481(7379):85-U95.
42. Erkan M, Kleeff J, Gorbachevski A, Reiser C, Mitkus T, Esposito I, et al. Periostin creates a tumor-supportive microenvironment in the pancreas by sustaining fibrogenic stellate cell activity. Gastroenterology. 2007;132(4):1447-64.
43. Zheng PP, van der Weiden M, Kros JM. Fast tracking of co-localization of multiple markers by using the nanozoomer slide scanner and NDPViewer. Journal of Cellular Physiology. 2014;229(8):967-73.
44. Koh W, Stratman AN, Sacharidou A, Davis GE. In vitro three dimensional collagen matrix models of endothelial lumen formation during vasculogenesis and angiogenesis. Methods Enzymol. 2008;443:83-101.

Supplemental figures

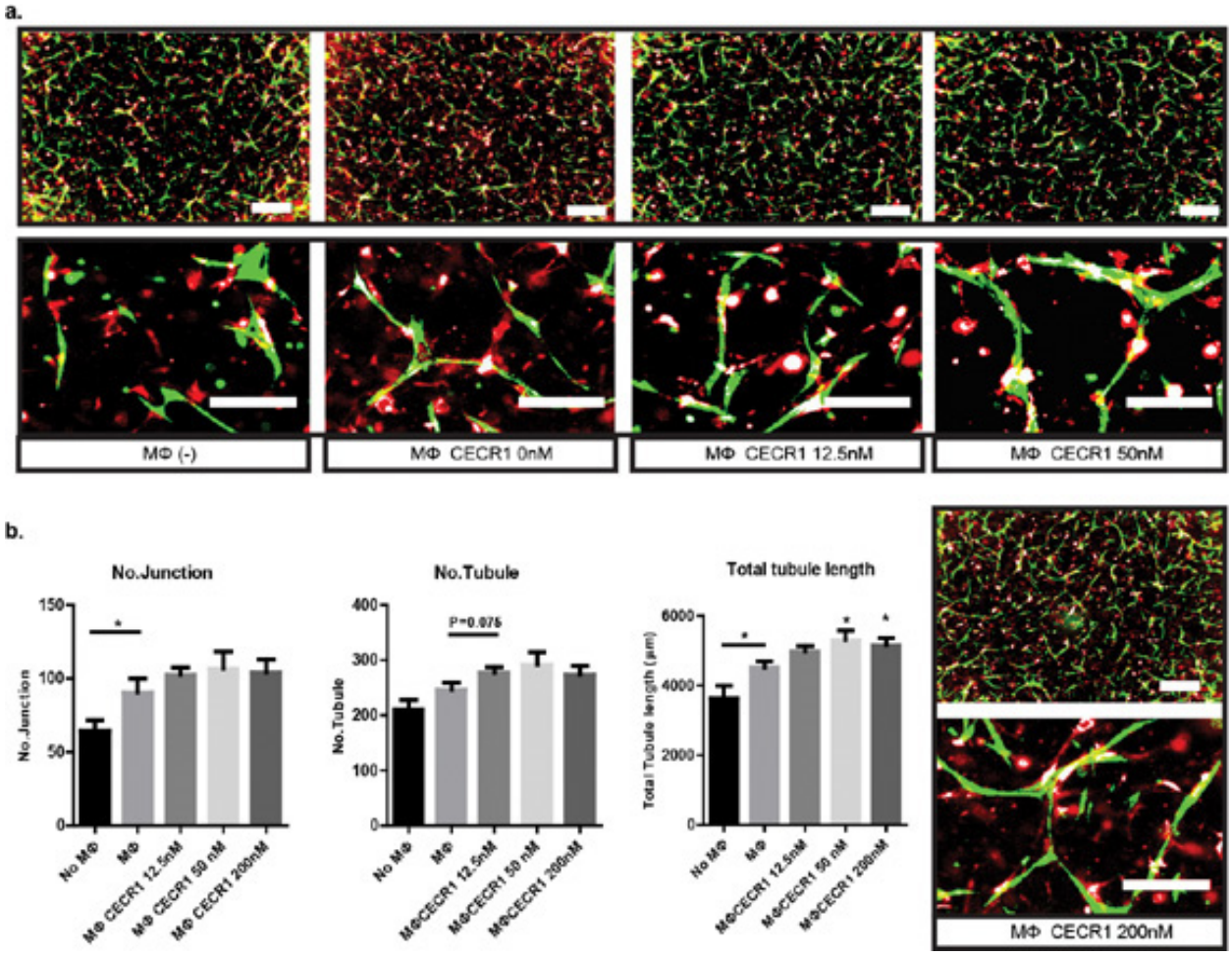

Sup. Fig.1. Macrophage Stimulated with rhCECR1 promotes angiogenesis in 3D coculture assays

(a) Low and high magnification fluorescent images of neovessel formation by HUVECs (GFP-marked) and human derived pericytes (dsRed-marked) with no macrophage stimulation (no Mϕ), with macrophage stimulation (Mϕ CECR1 0 nM), and with stimulation of macrophages that were exposed to different concentrations of CECR1 during maturation (Mϕ CECR1 12.5, 50 and 200 nM). (b) Quantified results of the co-culture experiment. No. of junctions, tubules, and total tubule length data are shown. Represented graphs were taken from at least three experiments. Six wells per condition were conducted in each experiment. * P<0.05. (Scale bar: 100 μm).

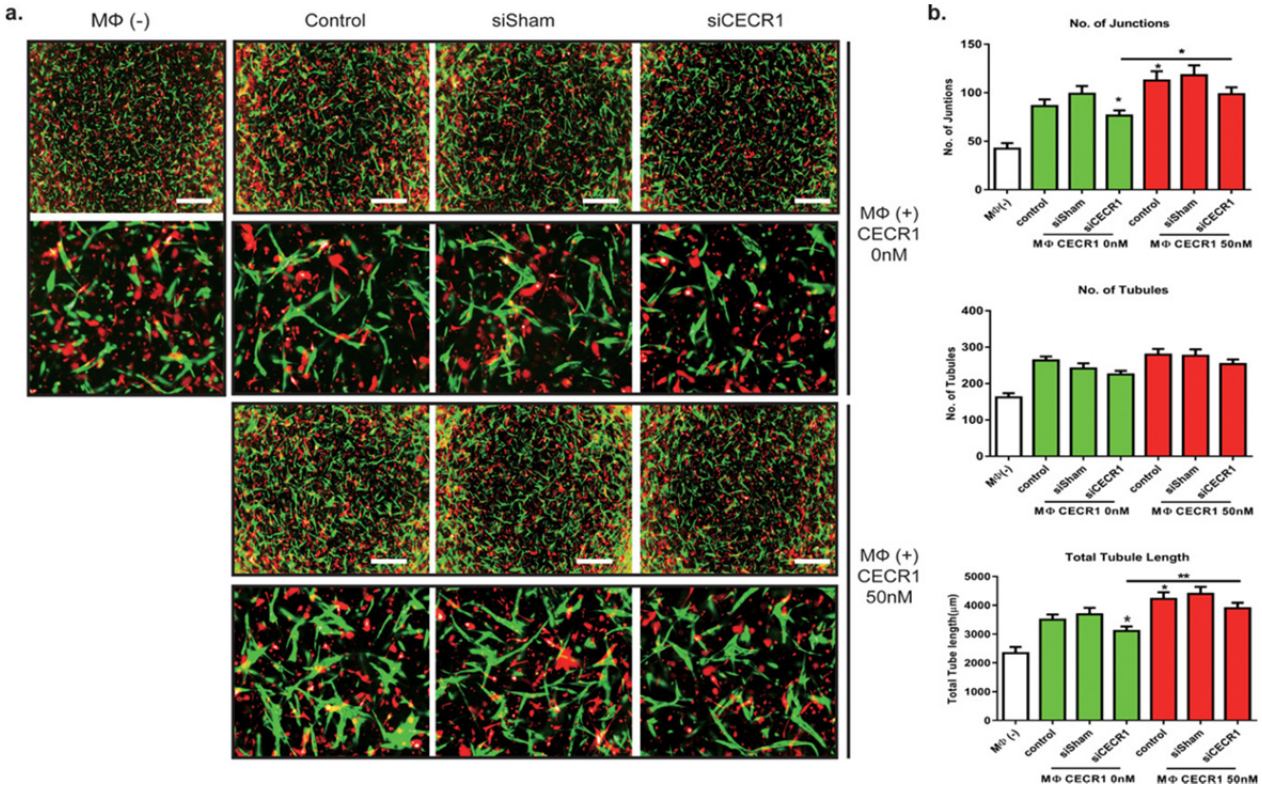

Sup. Fig.2. Stimulated with rhCECR1 recue attenuated tube formation induced by macrophages with CECR1 knockdown in 3D coculture assays

(a) Low and high magnification fluorescent images of neovessel formation by HUVECs (GFP-marked) and human derived pericytes (dsRed-marked) with no macrophage stimulation (no MΦ), with macrophage (Control, siSham, siCECR1) stimulation (MΦ CECR1 0 nM), and with stimulation of exogenous CECR1 (MΦ CECR1 50 nM) treated macrophages (Control, siSham, siCECR1) (Scale bar: 100 nM). (b) Quantified results of the co-culture experiment. No. of junctions, tubules, and total tubule length data are shown. Represented graphs were taken from at least three experiments. Six wells per condition were conducted in each experiment. * $P<0.05$ (siSham versus siCECR1; Control CECR1 0 nM versus CECR1 50 nM), **$P<0.01$ (siCECR1 CECR1 0 nM versus CECR1 50 nM).

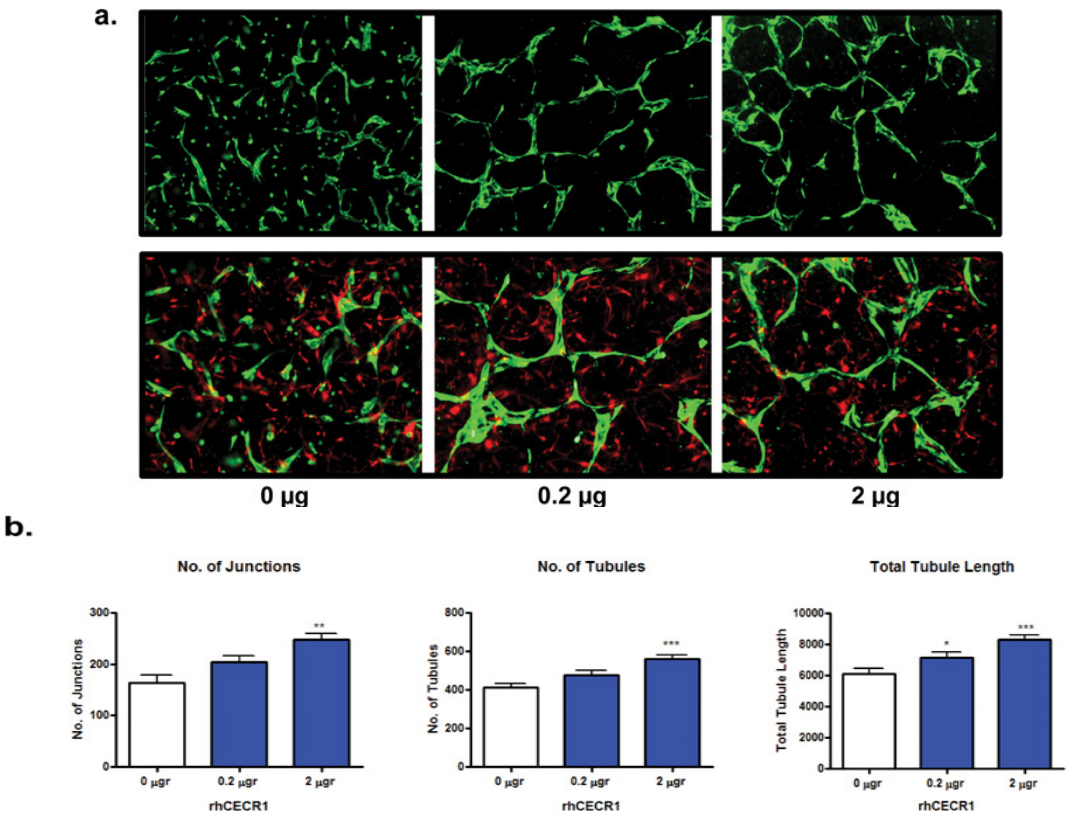

Sup. Fig.3. Stimulation with rhCECR1 promotes angiogenesis in 3D coculture assays

(a) Low and high magnification fluorescent images of neovessel formation by HUVECs (GFP-marked) and human derived pericytes (dsRed-marked) with stimulation of different concentrations of rhCECR1. (b) Quantified results of the co-culture experiment. No. of junctions, tubules, and total tubule length data are shown. * P<0.05 ***P<0.005.

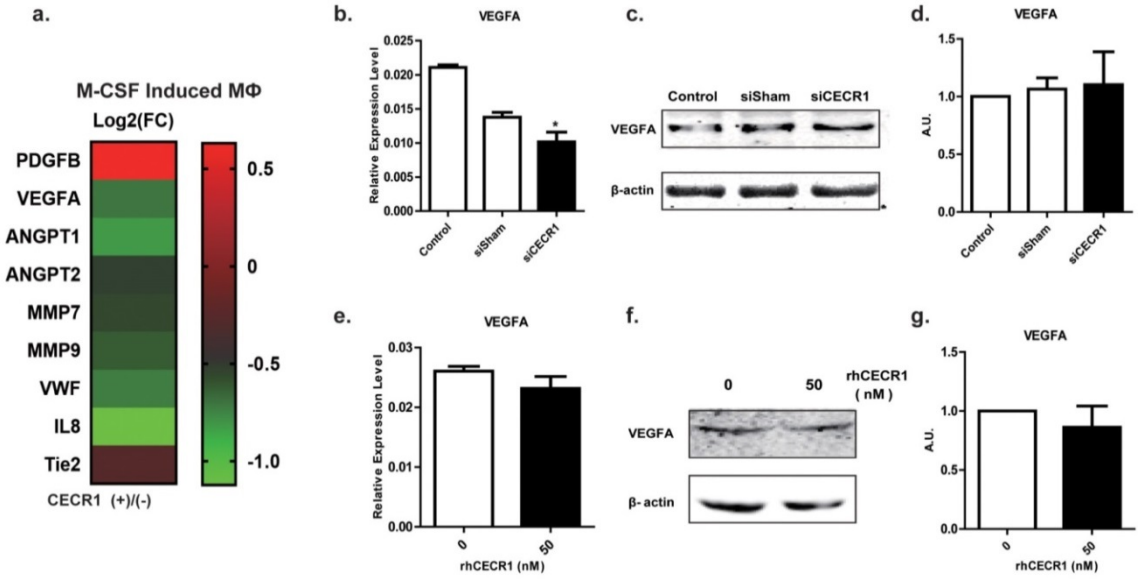

Sup. Fig.4. CECR1 directly promotes the expression of PDGFB, but not VEGFA and other pro-angiogenic molecules in macrophages

(a) Fold change (FC) of angiogenesis molecules in macrophages treated with 100 nM CECR1 shown in a heat map. Values are presented in Log_2 (FC). (b), (e) QPCR results of VEGFA mRNA levels normalized to housekeeping genes in non-treated (control), sisham, or siCECR1 treated THP1 macrophages and rhCECR1 treated macrophages. *P<0.05 (siSham versus siCECR1). (c), (f) Western blots of VEGFA protein and β-actin loading control in THP1 macrophages with various siRNA transfection and rhCECR1 treatment conditions. Blots represent results from three observations. (d), (g) Quantification of VEGFA bands normalized with β-actin loading control in THP1 macrophages with various siRNA transfection conditions and rhCECR1 treatment conditions.

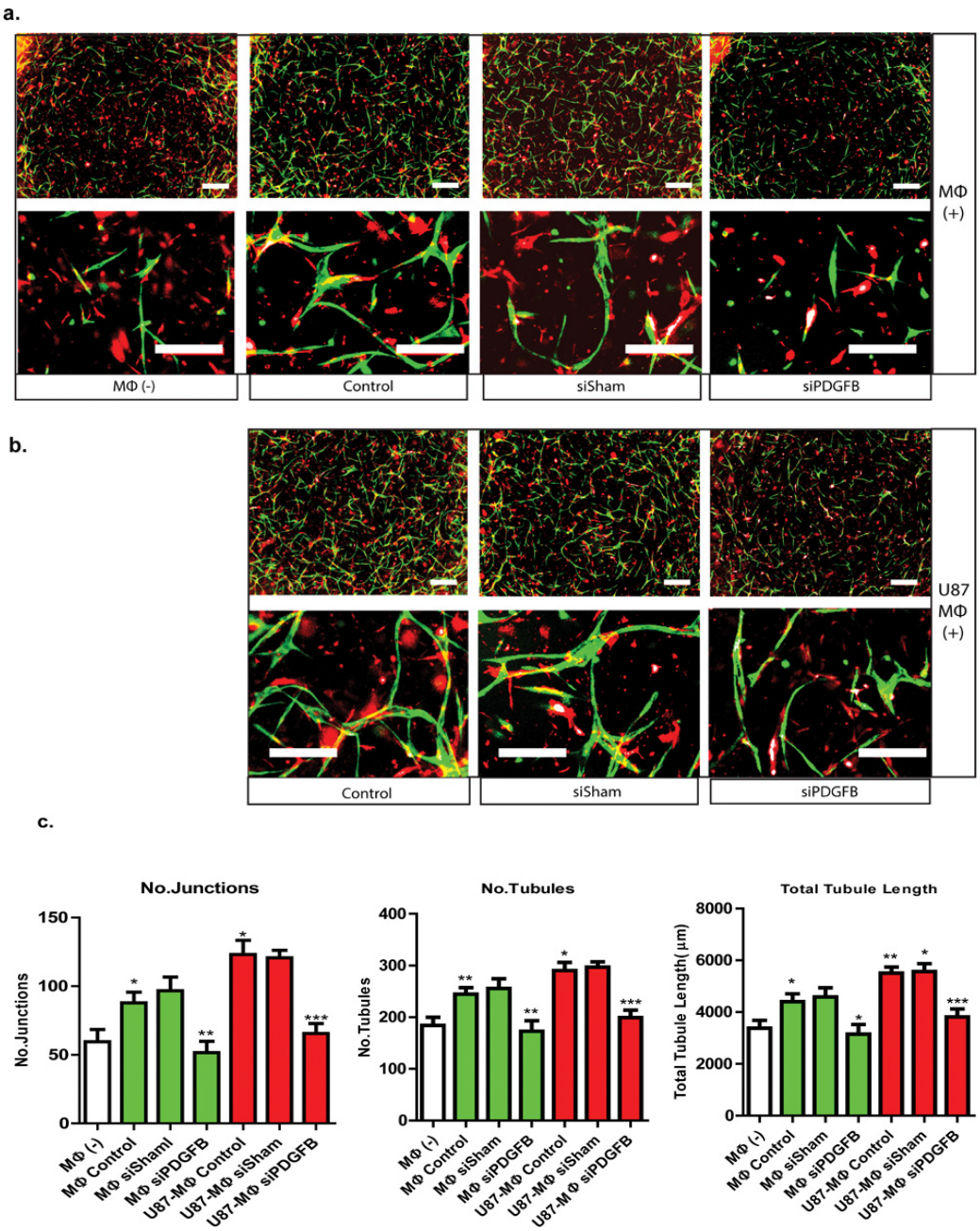

Sup. Fig.5. PDGFB silencing decreases macrophage paracrine activation of angiogenesis in 3D coculture assays

(a) Low and high magnification fluorescent images of neovessel formation by HUVECs (GFP-marked) and human derived pericytes (dsRed-marked) without macrophage stimulation, or with macrophage stimulation (non-treated control, sisham, or siPDGFB treated) that were pre-treated with or without U87 supernatant during differentiation.

(b) Quantified results of the co-culture experiment from three times. No. of junctions, tubules, and total tubule length data are shown. *P<0.05 **P<0.01 ***P<0.005. (Scale bar: 100 μm).

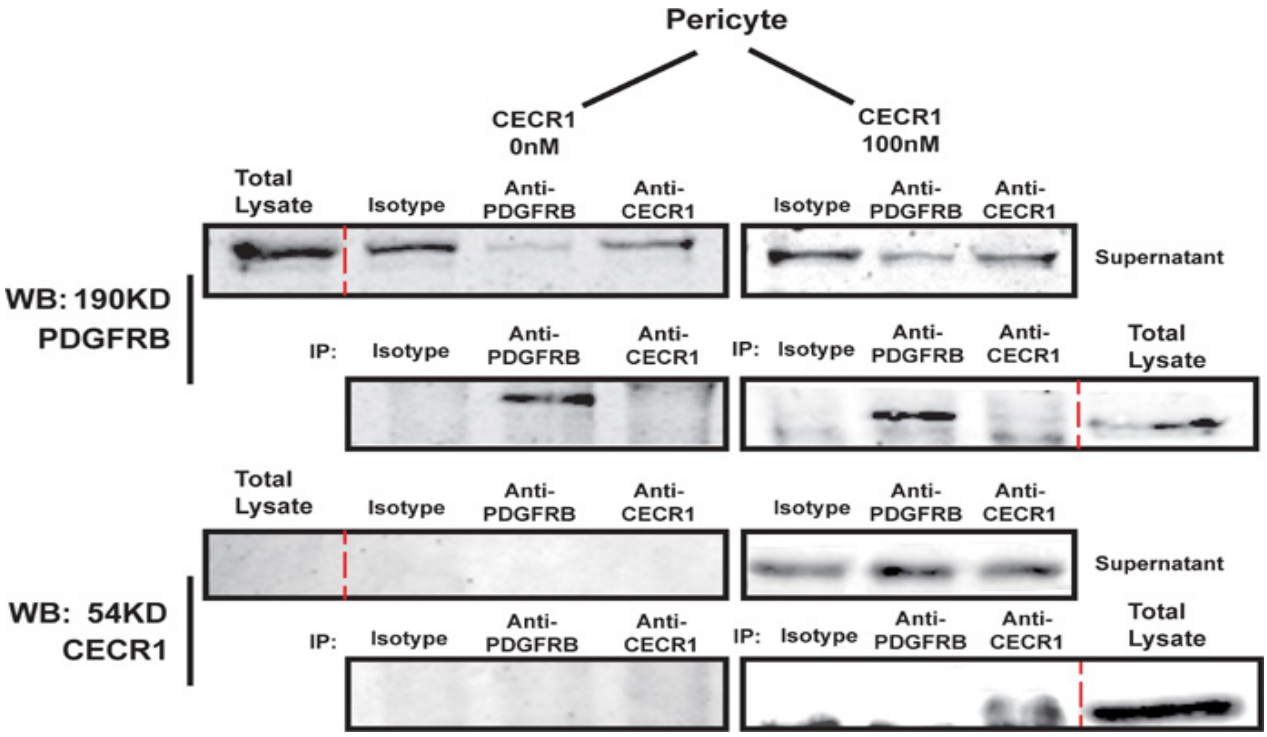

Sup. Fig.7. CECR1 does not bind to PDGFRβ on pericytes.

Pericyte lysates not treated and treated with CECR1 (100 nM). Western blot analysis showing PDGFRB protein levels in the upper 2 rows: Row 1; PDGFRβ signal in supernatants derived from pull down using isotype or anti-PDGFRβ or anti-CECR1 coated beads. Row 2: PDGFRβ signal in the co-IP pull down using isotype or anti-PDGFRβ or anti-CECR1 coated beads. Western blot analysis showing CECR1 protein levels in the lower 2 rows: Row 3; CECR1 signal in supernatants derived from pull down using isotype or anti-PDGFRβ or anti-CECR1 coated beads. Row 4: CECR1 signal in the co-IP pull down using isotype or anti-PDGFRβ or anti-CECR1 coated beads. For all 4 rows, PDGFRβ or CECR1 signals in whole lysate are shown for comparison. Results are representative of 4 different experiments.

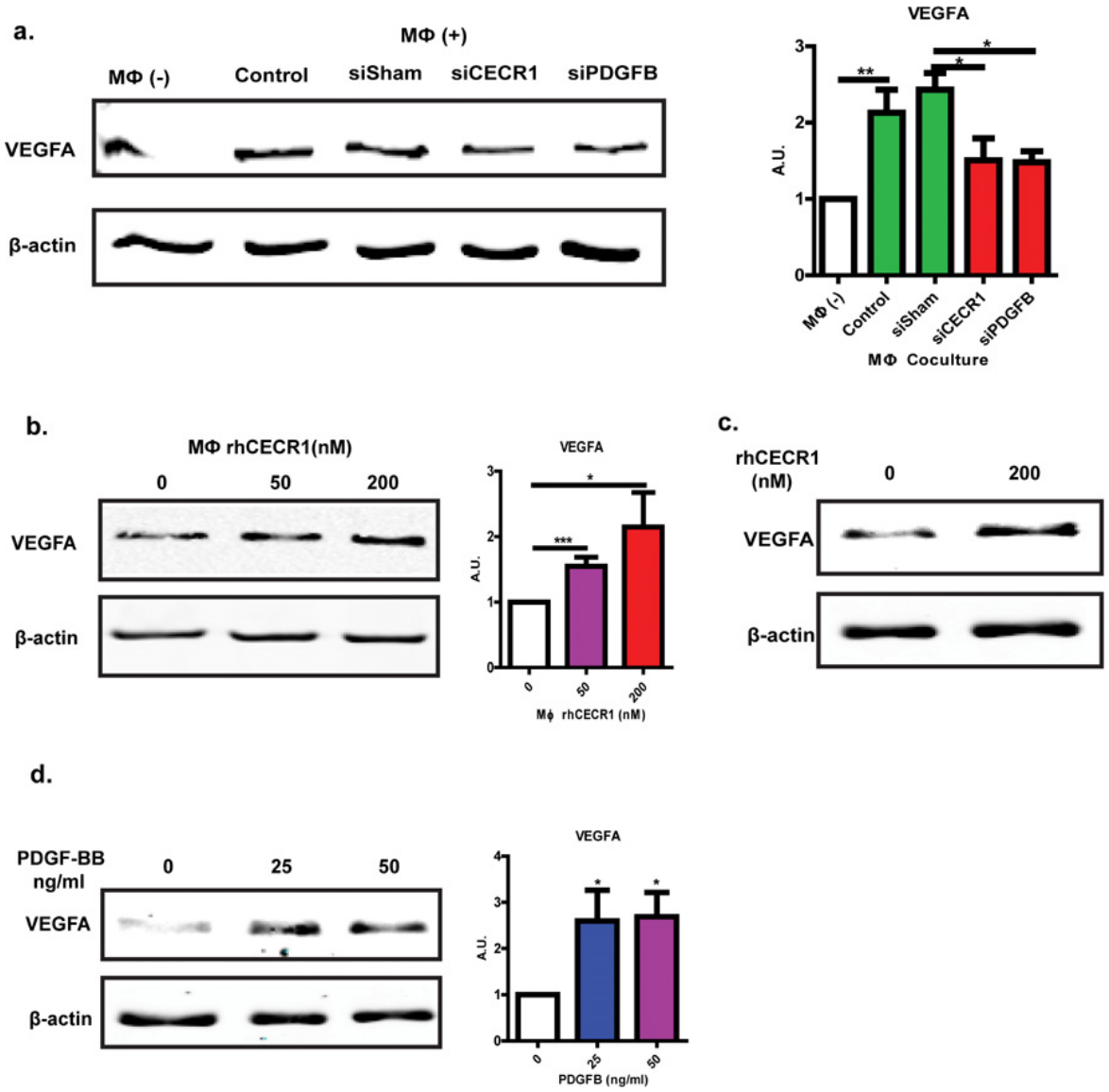

Sup. Fig.8. CECR1 in macrophages potentially regulates VEGFA expression in pericytes via PDGFB signaling.

a) Left hand side; Western blot shows VEGFA and β actin protein levels in pericytes of the different treatment groups. Right hand side; Quantitative results of Western blot analysis normalized to β actin loading control from three experiments. *P<0.05, **P<0.01. b) Western blot shows VEGFA and β actin protein levels in pericytes of the different macrophage treatment groups (Pretreated with different concentrations of CECR1, 0, 50, 200nM). Graph shows quantified intensity of VEGFA normalized to β actin protein levels. *P<0.05, ***P<0.005. c) Western blot shows VEGFA and β-actin protein levels in pericytes treated with different CECR1. D) Western blot shows VEGFA and β-actin protein levels in pericytes treated with different PDGFB concentrations. Graph shows quantified intensity of VEGFA normalized to β actin protein levels. *P<0.05 versus no treatment.

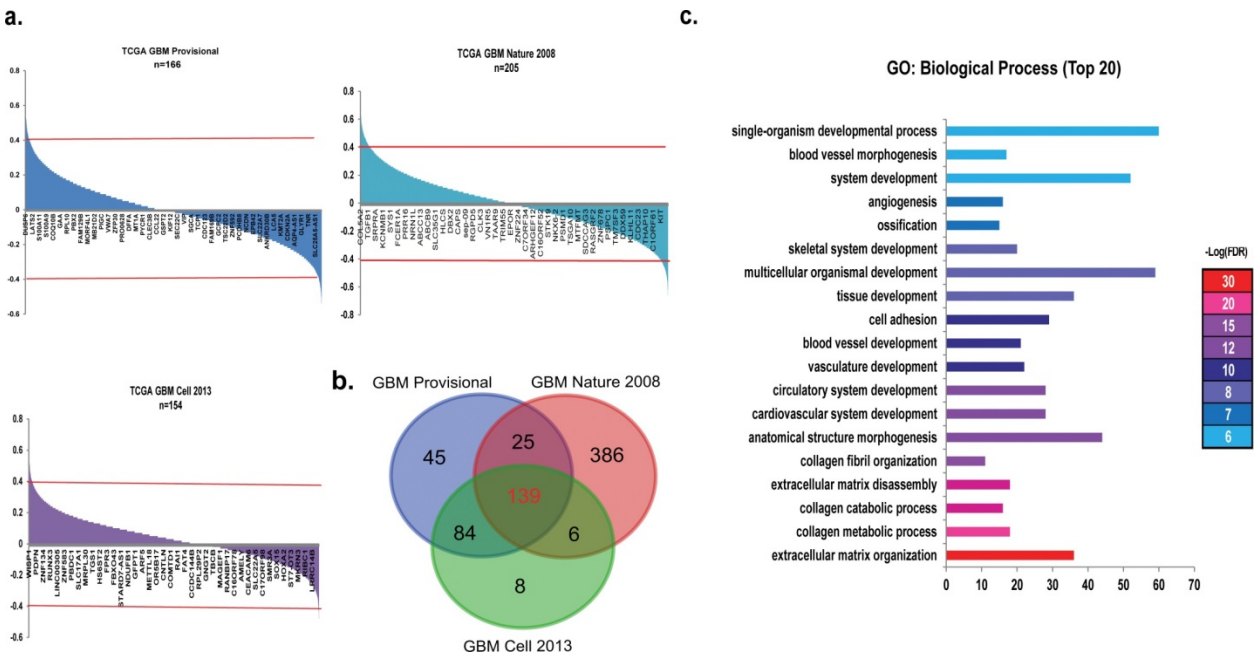

Sup. Fig.9. Periostin expression in TCGA human GBM samples correlates with a genetic profile that is associated with angiogenesis and cell migration.

(a) Correlation analysis of periostin mRNA levels with gene sets of three different TCGA human GBM data files. Graphs show r values on y-axis, and individual genes that significantly correlate with periostin on x-axis. (b) Venn graph demonstrating the overlap between the genes that significantly correlate with periostin expression in the three data sets. (c) Functional annotation of the 139 overlapping genes produced a list of top 20 significant biological processes. GO-terms are shown on the y-axis. No. of input genes per GO term are indicated on the x-axis.

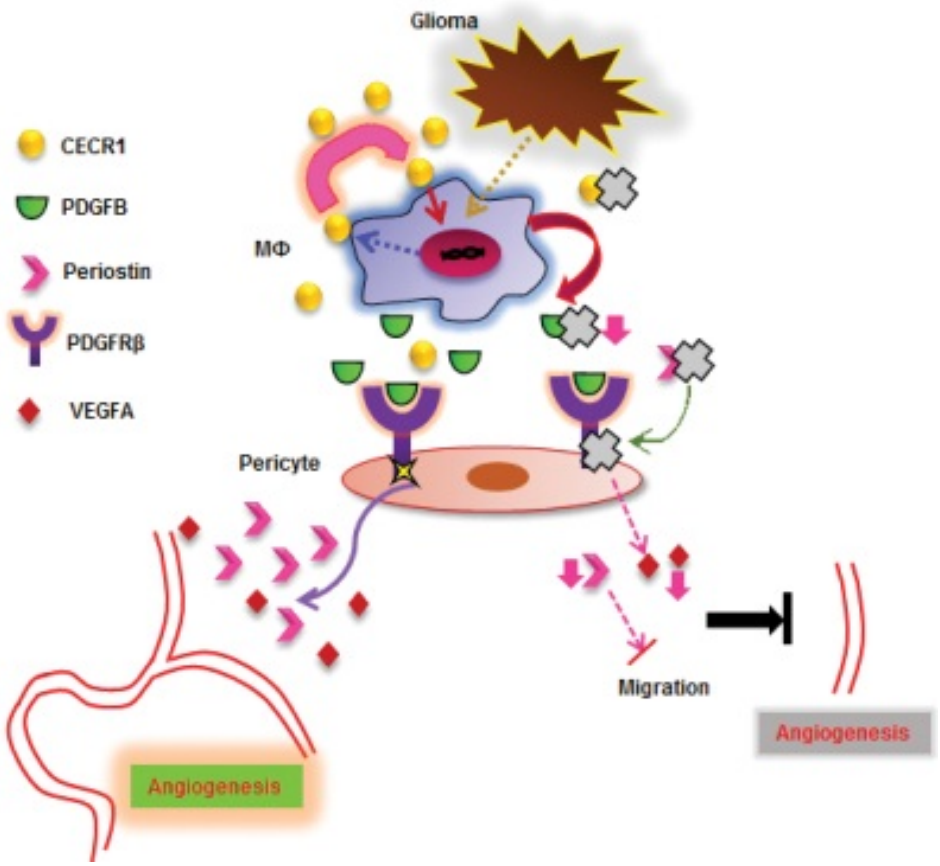

Sup. Fig.10. Proposed working mechanism of CECR1 in the cross talk between (M2-like) macrophages and pericytes.

The GBM environment promotes CECR1 production in (M2) TAMs, which enhances PDGFB expression and secretion. PDGFB/PDGFRβ signaling is crucial for the vascular maturation process in angiogenesis, during which newly formed microvessels secrete PDGFB to guide perivasular coverage by pericytes. PDGFB secreted by (M2) GAMs at perivascular locations activates PDGFRβ signaling and promotes both pericyte migration, and periostin production in support of angiogenesis. Therapeutic agents (indicated in the diagram as grey crosses) that target CECR1, PDGFB, PDGFRβ, or periostin, could interfere with macrophage-pericyte cross talk and subsequently counter tumor-angiogenesis. Supplementary Information accompanies the paper on the Oncogene website (http://www.nature.com/onc).

Chapter 8 General Discussion

General Discussion

Pathophysiological conditions such as cancer and cardiovascular diseases (CVD) have the highest rates of morbidity and mortality worldwide. These diseases shorten life expectancy, cause disability, and increase health care costs. In cancer and CVD, abnormal development of blood vessels plays a major role in disease progression. In case of cancer, abnormal angiogenesis promote tumour expansion and metastasis, which are characterized by formation of an abundant chaotic capillary network. Most of these blood vessels can`t be perfused because of their immature phenotype, which is characterised by a dysfunction of the endothelial barrier (leading to vascular leakage), focal obstruction in the lumen, and poor pericyte coverage. As a consequence, drug delivery is less efficient, although local drug permeability across the endothelium might be increased. Moreover, while mono-therapy targeting angiogenesis (in case of cancer) is successful in preclinical studies, in the clinical setting it may not be as effective because of the resistance observed through alternative pro-angiogenic escape pathways. Radiotherapy and systemic treatments (such as chemotherapy, targeted drugs, and immunotherapy) give promising short-term survival rates, but also undermine the quality of life during and after treatment. Research revealed a correlation between side-effects of radiation and chemotherapy with increased susceptibility to develop heart failure, as patients suffer from cardiotoxic side effects (1). In case of CVD, abnormal angiogenesis is characterised by obstruction of blood vessels, which results in insufficient oxygen transport to downstream areas, thereby leading to subsequent cell apoptosis and necrosis in e.g. cardiac tissue. In young healthy people, compensatory angiogenesis could bypass blood vessel obstruction to re-oxygenate hypoxic areas. However, most patients with CVD suffer from multiple cardiovascular risk-factors and show a poor response to ischemia with reduced pro-angiogenic response. Animal studies have shown that pro-angiogenic factors are impaired by advanced age, diabetes, and hypercholesterolemia (2). Novel therapies have been developed to supply ischemic tissues with collateral blood vessels by providing missing pro-angiogenic stimuli, which could bypass occluded arteries. However, the new vasculature formed in response to exogenous angiogenic stimuli is prone to regress when additional stimulatory cues for vessel maturation and stabilization are lacking (3). Accumulating evidence suggest, that angiogenic pathways are often redundant. So that therapeutic angiogenesis may require an even broader approach of inhibiting (in case of tumour angiogenesis) or stimulating (in case of neo-angiogenesis stimulation in response to CVD) multiple pathways simultaneously. However, many pathways of angiogenesis are still poorly understood and should be explored using gene function studies to yield a multitude of promising new factors for pro- and anti-angiogenic therapies.

To identify new genetic factors involved in angiogenesis, a genome-wide microarray screen was performed on the transcriptome of murine embryo`s. A list of genes that were significantly upregulated in FLK-positive cells was validated using whole-mount *in situ* hybridization in zebrafish larvae. Genes with a corresponding expression pattern in the vasculature were

selected for further investigation of their function both in *in vivo* and *in vitro* models. Thus, candidate knockdown assays were conducted targeting the development of vasculature in zebrafish and mural retina *in vivo*, while *in vitro* knockdown assays were also performed in 3D-collagen based co-culture of EC and pericytes to assess blood vessel formation. Candidate genes with validated angiogenic function were further investigated in the context of disease. In this thesis, we investigated the molecular mechanism of the following selected candidate genes: CMTM3, CMTM4, CGNL1, THSD1, and CECR1. We also investigated the angiogenic property of the nucleotide Up_4A as it is synthesised in response to VEGFR2 stimulation during stress conditions, such as hypoxia or in cancer conditions.

New characterisation of the CKLF1 Transmembrane Domain-containing region family in EC-endocytosis.

In angiogenesis, ECs are in constant communication with their environment through multiple paracrine factors and cell-to-cell and cell-to-matrix interactions. For these interactions, biological activity of growth factor receptor signalling and cell junctions is tightly regulated by the endocytic pathway. The endocytic pathway is a dynamic cellular process that alters the functions of the cell by modulating the cell surface proteins. It involves the uptake of cell surface proteins in transport vesicles and the distribution of vesicle cargo into recycling or degradation compartments. During sprouting angiogenesis differences in bioavailability of VEGFR2 on the ECs discriminates tip cells from stalk cells and adjust speed or direction of tip cell migration. Endocytosis is involved in regulating VEGFR2 availability on the cell surface and promotes stabilisation of vessels by inhibiting VE-cadherin internalisation at the adherence junctions side. Alterations in bio-availability and activation of endocytic adapter proteins and regulators are being recognised to be relevant to the process of neovascularisation in relation to disease conditions (4-6). For example, endothelial expressed epsins, a family of endocytic adaptor proteins that select specific cargos for clathrin-mediated internalisation of VEGFR2, was shown to impair tumorigenesis in epsin-knockout mouse tumour models (7). Defects were observed in the tumour vasculature, with blood vessels found to be enlarged, disorganised, poorly perfused and with poor pericyte coverage. Interestingly, under normal physiological conditions, the vasculature in these mice was unaffected indicating that the function of epsins affects explicitly diseased vasculature (7).

Moreover, defects in the regulators of vesicle trafficking, RAB-GTPases, are associated with numerous human genetic diseases, including cancer, neurodegeneration, and diabetes (5). Rab proteins are a large family (>60 members) of GTPases and each member has its specific function in regulating vesicle formation, transportation, cargo sorting and fusion of vesicles. Therefore up- or downregulation or modulation of RAB-GTPases will alter cell physiology, affect gene expression and contribute to disease pathology. For example, Lanahan et al. demonstrated that disrupting Rab5 positive early endosomes, via homozygous knockout of both synectin and myosin-VI expression in mice and zebrafish, resulted in decreased arterial morphogenesis and

poor arterial perfusion in adult tissue. The proposed molecular mechanism underlying these observations was slow trafficking of VEGFR2-positive endosomes that subsequently impaired activation of PLCγ-MAPK pathway, which is involved in arterial morphogenesis (8). Greater understanding of Rab-GTPases functions and affecters need to be acquired because of their essential role in genetic human diseases and in cellular and physiologic homeostasis.

In light of these considerations, we investigated in **chapter 2** and **3**, the potential new endocytic regulators CMTM3 and CMTM4. Both were discovered to be enriched in endothelial progenitor cells during development of mice and zebrafish, as well as in cultured human endothelial cells when co-cultured with human vascular pericytes. CMTM3 and CMTM4 are closely located on chromosome 16q22, an important tumour suppressor locus associated with the pathogenesis of multiple tumours. Genetic disruption of CMTM3 is known to be associated with poor prognosis of gastric cancers. CMTM3 inhibits metastasis via the STAT3/Twist1/EMT pathway which is known to promote cancer cell proliferation and invasion. Previous studies also discovered, that CMTM3 co-localizes with early endosomes RAB5 and EEA1 in gastric cancer cells, thereby promoting Rab5-mediated internalisation of epidermal growth factor receptor (EGFR), which subsequently attenuate cell migration and cell cycle (9, 10). The focus of previous studies was on the tumour suppressive qualities of CMTM3. However, high expression levels of CMTM3 in our microarray screen of murine endothelial progenitor cells suggested pro-angiogenic properties of CMTM3, which are elaborated **in chapter 2**. The results obtained in **chapter 2**, suggested that CMTM3 promotes sprouting angiogenesis by regulating the bioavailability of cell surface VE-cadherin by mediating the endocytosis pathway (figure 1). First, *in vivo* morpholino-based knockdown of CMTM3 in developing zebrafish larvae induced a significant reduction of intersegmental vessels sprouting from the dorsal aorta. This *in vivo* finding was supported by *in vitro* experiments in which CMTM3 silencing in ECs decreased the number of tubules formed in a 3-dimensional collagen matrix-based co-culture of primary vascular cells. To investigate the mechanism involved, we studied the function of CMTM3 in ECs using adenoviral overexpression or siRNA mediated silencing of CMTM3. In contrast, to previous reports on the function of CMTM3 in various cancer cell types, our data showed that neither cell cycle progression nor proliferation was altered by CMTM3 in ECs. Nevertheless, the finding that CMTM3 plays a role in early endosome trafficking in cancer cells could be similar to the endocytic pathway of ECs. Immunohistochemistry staining (IHC) of ECs showed that CMTM3 co-localized with endosome markers EEA1, clathrin, Rab 7 and Rab 11, which are involved in cargo sorting, vesicle transport, and fusion (9-11). Rab proteins specifically regulate each of these processes by binding to unique Rab-effector proteins to conduct each function. Rab-effector proteins like kinesin-like protein 16B (KIF16B) and Huntingtin (Htt) regulate the motility of early endosomes (EE) along the microtubule tracks. Interestingly, KIF16B overexpression causes relocation of EE to cell periphery and knockdown of KIF16B causes EE to cluster in the perinuclear region (12). Htt binds to microtubules and regulates clathrin-mediated endocytosis by detaching EE or moving them on the microtubule tracks (13). In **chapter 2** we observed that CMTM3 overexpression increased

and co-localized with clathrin -and EE-positive vesicles in clusters at the perinuclear regions. This indicated that CMTM3 stimulated relocation of EE carriers from the cell periphery towards the perinuclear regions via the microtubule tracks. At the perinuclear regions, the transition from EE to late endosomes occurs by conversion of RAB5+ vesicles into Rab7+ vesicles. Rab 7 is involved in the regulation of cell-cell adhesion by degrading cadherins in epithelia and neurons (14). In our study, CMTM3 overexpression promoted CMTM3 internalisation of VE-cadherin at the cell-cell adhesion (AJs) sites. VEGFa stimulation of ECs with abundant CMTM3 levels showed a higher VE-cadherin internalisation response, thereby weakening the endothelial barrier function. In the context of angiogenesis, we suggest that CMTM3 is involved in the vascular sprouting phase in which VEGFa-induced permeability decouples VE-cadherin from VEGFR2 allocating them into clathrin-coated compartments for recycling or degradation (figure 1). VE-cadherin remodelling is linked to loss of vascular homeostasis and endothelial integrity which causes phenotypes with compromised endothelial barrier function. Especially within the tumour vasculature this is often observed (15, 16). Expression of CMTM3 is known to be enhanced in tumours, which might be due to high local VEGFa levels. Tumour blood vessel networks are often irregular and leaky due to cell-cell contact destabilisation through VE-cadherin internalisation (15-17). Ultimately, this new biochemical route by which VEGF promotes endothelial permeability through CMTM3-dependent endocytosis of VE-cadherin may help identify new therapeutic targets for the treatment of many vascular diseases, including many forms of cancer in which tumour angiogenesis plays a critical role in disease progression.

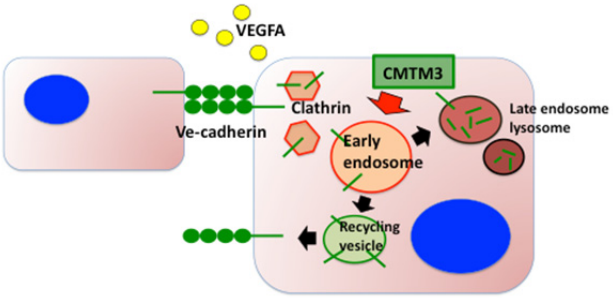

Figure 1: Proposed working mechanism of CMTM3. Simplified overview of CMTM3 involvement in the early stages of Ve-cadherin internalisation, induced by VEGFa, through allocating VE-cadherin into clathrin-coated compartments for recycling or degradation.

CMTM family members have a MARVEL domain of integral hexameric membrane proteins, which are associated with proteins involved in vesicle trafficking and membrane linking (18). Previous studies have linked CMTM5, CMTM7 and CMTM8 to endosomal trafficking in cancer cells (19-21). However, the function of CMTM4 had not yet been explored in the context of endosomal trafficking. Hence in **chapter 3** the function of CMTM4 was investigated, demonstrating that CMTM4 shares many similar features with CMTM3 both *in vivo* and *in vitro*. The main observed difference was that CMTM4 strongly localizes with Rab4 and VE-cadherin,

suggesting that CMTM4 is involved in regulating the rapid recycling of VE-cadherin back to the plasma membrane at AJs. These findings indicate a quicker restoration of the endothelial barrier function, which is crucial after sprouting angiogenesis to establish a mature vessel network. CMTM4 may thus function as a Rab-effector protein by creating Rab4 domains in rapid and slow recycling endosome populations. Moreover, CMTM4 may also serve as an adaptor protein for targeting and positioning VE-cadherin into recycling vesicles. More research is needed to increase our understanding about the regulation of EC-barrier function through maintaining the balance of Rab-effector proteins, and to explore these mechanisms as possible therapeutic targets. Alterations in the Rab-GTPases and associated regulatory proteins have been correlated with disease pathogenesis of cancers, vascular, lung, and thyroid diseases (22-27). To modulate the Rab function, more research is required to determine the specificity of Rab members on healthy and diseased tissue and to determine the specific effectors regulating the Rab expression in healthy and diseased tissue (5).

Maintenance and disruption of endothelial barrier function by CGNL1

A crucial feature of VE-cadherin is maintaining the endothelial barrier during vascular stabilization and maturation, by modulating the focal adhesion junction between cell-cell interactions or between ECs and the extracellular matrix (ECM). Changes in the ECM environment due to pericytes attachment trigger focal adhesion assembly on the immature vessel sprout, which is controlled by PDGFβ and ANGPT1 signalling. Small GTPases of the Rho family (Rho, Rac, and CDC42) stimulate interaction between the actin cytoskeleton and junctional proteins like VE-cadherin, to assemble adherence junctions (p120, β-catenin, and plakoglobin) (28). This interplay between cadherin and actin cytoskeleton is an important process to maintain the endothelial barrier on the one hand and on the other hand to regulate endothelial cell proliferation, migration and differentiation during sprouting angiogenesis. The molecular basis of adherens junction-actin interactions still requires further investigation to provide a full understanding of endothelial barrier function. In particular, the exact trigger of the interplay of Rho-proteins with VE-cadherin in a stage-specific manner during the angiogenesis process remains to be investigated (29). In **chapter 4** we identified CGNL1 to promote Rac1 activation to assemble integrins-focal adhesion complexes. Previous study in epithelia cells, observed CGNL1 to be localized in both adherence and tight junctions, implying that it could link intercellular junction assembly to the actin cytoskeleton (30, 31). Based on IHC staining we observed that focal adhesion proteins FAK, Vinculin, Paxallin, and Src recruitment were delayed when CGNL1 was silenced in ECs, coinciding with a reduction of Rac1 activation, post seeding. Disassociation of the cytoskeleton linker proteins (Vinculin, Paxallin and FAK) from VE-cadherin is known to contribute to internalisation of VE-cadherin and thus weakening of the endothelial barrier function (32). In line with these findings, a decline in VE-cadherin accumulation at the adherens junction site was observed in ECs.

We also observed that the expression of CGNL1 was endothelium specific, which was preserved in mice and zebrafish. Furthermore, CGNL1 expression in ECs was significantly enhanced by direct cell contact with pericytes, previously only known to be expressed in epithelial cells (33). The induction of CGNL1 in ECs was facilitated via Notch signalling in response to pericytes stimulation. Cgnl1 knockdown impaired tubule formation in a 3D co-culture assay and delayed vascular expansion in the developing retina of mice. Our findings indicate that, during angiogenesis pericytes interaction with ECs stimulates CGNL1 expression via Notch signaling (provided by the pericytes), to strengthen the VE-cadherins junctions thereby stabilizing the endothelial barrier of the neo-vessel. In **chapter 4,** supplement figure 10 a graphic abstract is made to give an overview of the proposed mechanism of CGNL1. CGNL-1 is recruited towards tight junctions by forming a complex with the tight junction protein ZO-1 and the adherens junction protein PLEKHA7. Depletion of ZO-1 or PLEKHA7 is known to result in a loss of CGNL1 expression and junctional localization. Subsequently, during junctional formation CGNL1 promotes the activation of Rac1 upon calcium switch, by recruiting the Rac1 activator TIAM1 to the junctions (33). Our findings support an important role of Cgnl1 in the regulation of vascular growth during embryonic development as well as in vasculature-related diseases in adulthood.

THSD1 attenuate vulnerable plaque by maintaining endothelial barrier function during atherosclerosis in mice

An example of vascular disease that is initiated by poor endothelial barrier function is atherosclerosis. As atherosclerosis progresses, plaques become characterised by the neovascular growth of microvessels which are phenotypically immature as defined by lack of endothelial barrier function (i.e. haemorrhage) and increased susceptibility to rupture (34). Neovascularisation in atherosclerosis is the result of intraplaque hypoxia and inflammation, leading to up-regulation of pro-angiogenic growth factors such as VEGFa and AGNPT2 (35). Despite improved insight into disease pathogenesis and therapeutic options, additional treatment strategies are required to block mechanisms involved in plaque destabilization. In **chapter 5** we investigated Thsd1 as a possible pro-angiogenic factor that is able to normalize the vascular integrity in the advanced atherosclerotic lesion. Thsd1 has been described as an early marker of haematopoietic stem cells and ECs during embryonic development (36). Our microarray screen confirmed this finding, as Thsd1 was overexpressed in Flk+ angioblast during murine embryonic development compared to FLK- angioblasts. Loss of function studies *in vivo* revealed that Thsd1 affected vascular integrity, which coincided with haemorrhage, during physiological angiogenesis in embryonic zebrafish as well as in the retina of neonatal mice. A similar vascular phenotype of haemorrhage in the cranial region was described in a previous study and was linked to the mutation in cerebral cavernous malformation (CMM) proteins (37). Mechanistically the authors hypothesized that these proteins are involved in Rac1 activation and RhoA degradation. In line with these observations, we found that Thsd1 knockdown in ECs directly inhibits Rac1-mediated endothelial barrier function. As a result, reduced VE-cadherin

co-localization with the actin cytoskeleton at the adherence junctions was observed, thereby weakening the cell-cell junctions. Anchorage of VE-cadherin proteins to the actin cytoskeleton via a complex of adherence junction proteins plays a crucial role in controlling vascular morphology and permeability (38). Bearing this mechanistic overview in mind, we hypothesized that Thsd1 reduces vascular bleeding of the neointimal microvasculature in our well-validated murine atherosclerotic plaque model. Adenoviral overexpression of Thsd1 attenuated the vulnerable plaque phenotype post shear stress-induced atherosclerosis. Conversely, loss of Thsd-1 resulted in a worsening of vulnerable plaque instability contributing to extensive intraplaque haemorrhage and inflammation. From a therapeutic perspective, plaque neovascularization should ideally be blocked to prevent extravasation of red blood cells enriched in cholesterol, leucocytes and plasma lipids. Based on our findings, Thsd-1 emerges as a potential therapeutic target to induce normalization of vulnerable atherosclerotic lesions or other (micro)vascular pathologies in which endothelial barrier function is compromised.

Uridine adenosine tetraphosphate (Up_4A) stimulates tubule formation *in vitro*

Extracellular nucleotides represent another biological mechanism of regulating angiogenesis and maintaining vessel function. As a result of hypoxia, tissue damage or cell death extracellular nucleotides are released into the ECM and activate purinergic receptors on recipient cells. Alterations in the purinergic receptor signalling have been increasingly recognised to be relevant as therapeutic targets of pathological neovascularisation. In those studies, it was shown that purinergic signalling contributed to improving impaired wound healing in diabetic mice, activation of VEGFR2-mediated angiogenesis in the absence of VEGF in tumours, and transactivation of receptor kinases to generate an inflammatory response associated with atherosclerosis (39-41). In **chapter 6** we investigate the function of a relatively unknown extracellular dinucleotide, uridine adenosine tetraphosphate (Up_4A), in the angiogenesis process. In stress conditions, Up_4A is endogenously released from ECs and biosynthesized via VEGFR2 stimulation. Up_4A contains purine and pyrimidine moieties, which make it capable of activating P1 and P2 receptors. The vasoactive role of Up_4A was studied in coronary microvessels in swine and induced vasodilation via activation of the P1 receptors (A_{2A}) (42). To our knowledge, we investigated for the first time, the pro-angiogenic effect of Up_4A. Based on our 3D collagen co-culture we observed that Up_4A addition increases tubule sprouting and stabilization and this proangiogenic affect is largely attenuated by $P2Y_6r$ inhibition. Stimulating ECs with Up_4A revealed that the pro-angiogenic function was mainly regulated via P2Yrs signal transduction, in particularly $P2Y_6r$, and upregulated mRNA and protein levels of VEGFa. We propose that Up_4A increases VEGFa levels to stimulate VEGFR2 signalling, which may further enhance Up_4A synthesis in an autocrine feed-forward loop. P2Yr is known to promote ECs tubulogenesis through another breast cancer cell-secreted extracellular nucleotide, namely nucleoside diphosphate kinase, which subsequently activate VEGFR2 signalling and thus angiogenesis (40). The authors of that study proposed the inhibition of P2Yr and VEGFR2 as an

effective approach for anti-angiogenic therapy. Clearly, more knowledge is required in order to use extracellular nucleotides effectively as a therapeutic agent. A primary focus of future studies should be to determine the optimal dose range for specific subtypes of patients, as we observed clear differences in dose effects between different donors of primary ECs *in vitro*.

Glioma based CECR1 crosstalk between M2-macrophages and pericytes promotes neovascularisation.

In **chapter 7** we describe CECR1 as a new potent target for anti-angiogenic therapy in glioblastoma multiform (GBM), which has a particularly high density of microvasculature. In part, tumour angiogenesis in GBM is heavily regulated by glioma-associated macrophages (GAM). In our study, we could positively correlate CECR1 expression with microvascular density in GBM. In one of our previous studies, we showed that CECR1 co-localizes with M2-type macrophages in GBM using IHC. Further characterisation of CECR1 expression led to the finding that THP-1 cells polarise into M2-macrophage after addition of CECR1 (43). We validated the function of the polarized M2-macrophages in our 3D collagen co-culture model and observed an increase in tubule formation, compared to vascular cells treated with unpolarised M1-macrophages and premature monocytes. To further explore the mechanism involved in this pro-angiogenic effect, we screened various angiogenic genes (VEGFa, ANGPT1&2, PDGFβ) on macrophages treated with and without CECR1. Interestingly, only PDGFβ appeared to be significantly influenced by CECR1. PDGFβ is an essential factor in recruiting pericytes during vessel stabilization. Indicating that CECR1 may mediate cross talk between GAMs and pericytes, as shown by our migration and 3D co-culture data. The regulation of perivascular cells (pericytes) by GAMs is rarely studied, although previous studies have mentioned that GAMs recruit pericytes by secreting SOX17 or MMP9, PDGFβ was not mentioned (44, 45). Gene and protein expression analysis of CECR1 mediated cross talk between GAMs and pericytes showed that upon PDGFβ-PDGFβr activation, pericytes upregulate periostin expression. Moreover, IHC staining showed increased periostin deposition into the ECM close to M2 GAMs. Periostin is a pro-angiogenic extracellular matrix component, which is known to be enriched in the microvasculature of GBM (46). It also plays an important role in the recruitment of M2-like TAM and supports inflammatory cell infiltration, activates FAK, and stimulates the release of pro-angiogenic factors (47-49). Our data suggest that the pro-angiogenic function of the CECR1-PDGFβ-PDGFβR signalling cascade, promotes pericytes recruitment and migration, and tumour angiogenesis. In supplementary figure 10 of **chapter 7** a graphic overview is made of all the findings mentioned previously. The complex cross talk between different cell types in the microenvironment of GBM as mediated via CECR1 and associated pathways could yield interesting targets for future anti-angiogenic strategies.

Future perspectives

For more than 20 years scientist have accumulated data on therapeutic angiogenesis by gene therapy, including preclinical and clinical studies (50-53). Several growth factors, like vascular

endothelial growth factor, fibroblast growth factors and hepatocyte growth factor have been tested in clinical trials (50, 54). However, apart from observed increased vascularity, very few resulted with significant increase in life expectancy (51-53). Clinical trials encountered problems with gene transfer efficacy, dosage of transgene expression, patient selection criteria, and endpoint measurements (54). They all concluded that gene therapy efficacy should be researched more in large animal models that mimic human pathology with their comorbidities, to determine the dosage and duration of exposure of the delivery system. Also, personalized medicine should be implicated to define which gene therapy is suitable for an individual (50, 54). Also, lack of understanding of the molecular basis of angiogenesis in CVD and cancer contributes and complicates these problems even more. In this thesis we identified novel molecular pathways to contribute to the basic knowledge of the fundaments of angiogenesis. Downstream research showed that CMTM3, CMTM4, Thsd1, Cgnl1, Cecr1 signaling are activated in *in vivo* derived progenitor ECs and upon co-culture of vascular ECs and pericytes. Indicating that these pathways are not redundant during angiogenesis. The scientific results observed in the CMTM3, CMTM4, Cgnl1 and Thsd1 chapters add to our knowledge the possible downstream (escape) routes of gene therapy and potential biomarkers. Further investigation is needed to explore which molecules upstream trigger their activation, by screening pericytes for their paracrine factors, while in close contact with ECs. Also, it would be beneficial to use current gene delivery therapy compounds of e.g. VEGF and FGF in our *in vitro* and *in vivo* vascular models, to determine wheather they affect vascular integrity through CMTM3, CMTM4, Thsd1 and Cgnl1.

The paracrine factor CECR1 could be a promising new factor for gene therapy. Because, it can be used in gene delivery systems to recruit pericytes to activate and stabilize newly formed vessels. Interestingly, gene therapy uses genes that encode proteins that are naturally secreted (like VEGFa) so that a biological effect can be achieved by transfecting limited numbers of cells. Subsequently, transfected cells secrete substantial amounts of the inserted gene product into the extra cellular matrix. The paracrine effect of the secreted gene product may then modulate the bioactivity of a large number of target cells (e.g. pericytes and ECs) (55). The proposed gene therapy will use CECR1 as a pro-angiogenic factor to increase the survival rate of ECs by recruitment of pericytes to the ischemic tissue. Cecr1 can also shed new light on the development of resistance during anti-VEGF therapy. It has been proposed that pericyte induce resistance to ant-VEGF drugs, because of the strong paracrine relationship between pericyte and ECs. The supporting pericytes protect the underlying endothelial cells such that it is only the immature vessels that appear to be susceptible to treatment, thus rendering anti-VEGF therapy potentially less effective in established advanced disease (56, 57). It appears that these supporting pericytes are driven by the tumour and endothelial cell production of Platelet Derived Growth Factor β (PDGF-β) and indeed upon blockade of PDGF-β and VEGF in combination, results in a more effective treatment (57-59). In our study, we propose that in glioblastoma CECR1 activates PDGF-β signaling to recruit pericytes towards the immature

neovasculature. Inactivating Cecr1 using therapeutic anti-Cecr1 antibodies might provide a new anti-angiogenic therapy.
In chapter 6 Up_4A was found to be pro-angiogenic through stimulating $p2Y_6$ receptor signalling. It is known that P2Yr can activate angiogenesis by the absence of VEGF through activating VEGFR-2 intracellular signalling (40). Surrounding cells secrete nucleotides into extracellular matrix as a result of low VEGF levels during stress conditions like hypoxia or even during anti-VEGF therapy. This potential escape route makes the tumour cells resistant to anti-VEGF therapy. Therefore a dual inhibition of VEGF and P2Yr might be a new anti-angiogenic drug target (40). The involvement of different purinergic receptors in response to Up_4A is altered in various cardiovascular diseases (60). The plasma levels of Up_4A may serve as a diagnostic biomarker to different forms of cardiovascular diseases (60).

In conclusion, our fundamental findings of novel pathways involved in angiogenesis hold promising therapeutic perspectives to understand and treat vascular diseases. Therefore, more research is needed to translate the provided basic molecular knowledge into drug targets.

Literature

1. Ewer MS, Ewer SM. Cardiotoxicity of anticancer treatments. Nat Rev Cardiol. 2015;12(9):547-58.
2. Hoeben A, Landuyt B, Highley MS, Wildiers H, Van Oosterom AT, De Bruijn EA. Vascular endothelial growth factor and angiogenesis. Pharmacol Rev. 2004;56(4):549-80.
3. Yoo SY, Kwon SM. Angiogenesis and its therapeutic opportunities. Mediators Inflamm. 2013;2013:127170.
4. Yin H, Flynn AD. Drugging Membrane Protein Interactions. Annu Rev Biomed Eng. 2016;18:51-76.
5. Agola JO, Jim PA, Ward HH, Basuray S, Wandinger-Ness A. Rab GTPases as regulators of endocytosis, targets of disease and therapeutic opportunities. Clin Genet. 2011;80(4):305-18.
6. Jopling HM, Odell AF, Hooper NM, Zachary IC, Walker JH, Ponnambalam S. Rab GTPase regulation of VEGFR2 trafficking and signaling in endothelial cells. Arterioscler Thromb Vasc Biol. 2009;29(7):1119-24.
7. Song K, Wu H, Rahman HN, Dong Y, Wen A, Brophy ML, et al. Endothelial epsins as regulators and potential therapeutic targets of tumor angiogenesis. Cell Mol Life Sci. 2017;74(3):393-8.
8. Lanahan AA, Hermans K, Claes F, Kerley-Hamilton JS, Zhuang ZW, Giordano FJ, et al. VEGF receptor 2 endocytic trafficking regulates arterial morphogenesis. Dev Cell. 2010;18(5):713-24.
9. Christoforidis S, McBride HM, Burgoyne RD, Zerial M. The Rab5 effector EEA1 is a core component of endosome docking. Nature. 1999;397(6720):621-5.
10. McLauchlan H, Newell J, Morrice N, Osborne A, West M, Smythe E. A novel role for Rab5-GDI in ligand sequestration into clathrin-coated pits. Curr Biol. 1998;8(1):34-45.
11. Echard A, Jollivet F, Martinez O, Lacapere JJ, Rousselet A, Janoueix-Lerosey I, et al. Interaction of a Golgi-associated kinesin-like protein with Rab6. Science. 1998;279(5350):580-5.
12. Hoepfner S, Severin F, Cabezas A, Habermann B, Runge A, Gillooly D, et al. Modulation of receptor recycling and degradation by the endosomal kinesin KIF16B. Cell. 2005;121(3):437-50.
13. Pal A, Severin F, Lommer B, Shevchenko A, Zerial M. Huntingtin-HAP40 complex is a novel Rab5 effector that regulates early endosome motility and is up-regulated in Huntington's disease. J Cell Biol. 2006;172(4):605-18.
14. Tabata K, Matsunaga K, Sakane A, Sasaki T, Noda T, Yoshimori T. Rubicon and PLEKHM1 negatively regulate the endocytic/autophagic pathway via a novel Rab7-binding domain. Mol Biol Cell. 2010;21(23):4162-72.
15. Corada M, Zanetta L, Orsenigo F, Breviario F, Lampugnani MG, Bernasconi S, et al. A monoclonal antibody to vascular endothelial-cadherin inhibits tumor angiogenesis without side effects on endothelial permeability. Blood. 2002;100(3):905-11.
16. May C, Doody JF, Abdullah R, Balderes P, Xu X, Chen CP, et al. Identification of a transiently exposed VE-cadherin epitope that allows for specific targeting of an antibody to the tumor neovasculature. Blood. 2005;105(11):4337-44.
17. Carmeliet P, Lampugnani MG, Moons L, Breviario F, Compernolle V, Bono F, et al. Targeted deficiency or cytosolic truncation of the VE-cadherin gene in mice impairs VEGF-mediated endothelial survival and angiogenesis. Cell. 1999;98(2):147-57.
18. Arthur CP, Stowell MH. Structure of synaptophysin: a hexameric MARVEL-domain channel protein. Structure. 2007;15(6):707-14.
19. Li H, Guo X, Shao L, Plate M, Mo X, Wang Y, et al. CMTM5-v1, a four-transmembrane protein, presents a secreted form released via a vesicle-mediated secretory pathway. BMB Rep. 2010;43(3):182-7.
20. Li H, Li J, Su Y, Fan Y, Guo X, Li L, et al. A novel 3p22.3 gene CMTM7 represses oncogenic EGFR signaling and inhibits cancer cell growth. Oncogene. 2014;33(24):3109-18.
21. Jin C, Ding P, Wang Y, Ma D. Regulation of EGF receptor signaling by the MARVEL domain-containing protein CKLFSF8. FEBS Lett. 2005;579(28):6375-82.

22. Croizet-Berger K, Daumerie C, Couvreur M, Courtoy PJ, van den Hove MF. The endocytic catalysts, Rab5a and Rab7, are tandem regulators of thyroid hormone production. Proc Natl Acad Sci U S A. 2002;99(12):8277-82.
23. Wu G, Yussman MG, Barrett TJ, Hahn HS, Osinska H, Hilliard GM, et al. Increased myocardial Rab GTPase expression: a consequence and cause of cardiomyopathy. Circ Res. 2001;89(12):1130-7.
24. Yao R, Wang Y, Lubet RA, You M. Differentially expressed genes associated with mouse lung tumor progression. Oncogene. 2002;21(37):5814-21.
25. Calvo A, Xiao N, Kang J, Best CJ, Leiva I, Emmert-Buck MR, et al. Alterations in gene expression profiles during prostate cancer progression: functional correlations to tumorigenicity and down-regulation of selenoprotein-P in mouse and human tumors. Cancer Res. 2002;62(18):5325-35.
26. He H, Dai F, Yu L, She X, Zhao Y, Jiang J, et al. Identification and characterization of nine novel human small GTPases showing variable expressions in liver cancer tissues. Gene Expr. 2002;10(5-6):231-42.
27. Kim JY, Jang MK, Lee SS, Choi MS, Bok SH, Oh GT, et al. Rab7 gene is up-regulated by cholesterol-rich diet in the liver and artery. Biochem Biophys Res Commun. 2002;293(1):375-82.
28. Fryer BH, Field J. Rho, Rac, Pak and angiogenesis: old roles and newly identified responsibilities in endothelial cells. Cancer Lett. 2005;229(1):13-23.
29. Bryan BA, D'Amore PA. What tangled webs they weave: Rho-GTPase control of angiogenesis. Cell Mol Life Sci. 2007;64(16):2053-65.
30. Guillemot L, Guerrera D, Spadaro D, Tapia R, Jond L, Citi S. MgcRacGAP interacts with cingulin and paracingulin to regulate Rac1 activation and development of the tight junction barrier during epithelial junction assembly. Mol Biol Cell. 2014;25(13):1995-2005.
31. Guillemot L, Paschoud S, Jond L, Foglia A, Citi S. Paracingulin regulates the activity of Rac1 and RhoA GTPases by recruiting Tiam1 and GEF-H1 to epithelial junctions. Mol Biol Cell. 2008;19(10):4442-53.
32. Rahimi N. Defenders and Challengers of Endothelial Barrier Function. Front Immunol. 2017;8:1847.
33. Pulimeno P, Paschoud S, Citi S. A role for ZO-1 and PLEKHA7 in recruiting paracingulin to tight and adherens junctions of epithelial cells. J Biol Chem. 2011;286(19):16743-50.
34. Jain RK, Finn AV, Kolodgie FD, Gold HK, Virmani R. Antiangiogenic therapy for normalization of atherosclerotic plaque vasculature: a potential strategy for plaque stabilization. Nat Clin Pract Cardiovasc Med. 2007;4(9):491-502.
35. Sluimer JC, Daemen MJ. Novel concepts in atherogenesis: angiogenesis and hypoxia in atherosclerosis. J Pathol. 2009;218(1):7-29.
36. Takayanagi S, Hiroyama T, Yamazaki S, Nakajima T, Morita Y, Usui J, et al. Genetic marking of hematopoietic stem and endothelial cells: identification of the Tmtsp gene encoding a novel cell surface protein with the thrombospondin-1 domain. Blood. 2006;107(11):4317-25.
37. Faurobert E, Albiges-Rizo C. Recent insights into cerebral cavernous malformations: a complex jigsaw puzzle under construction. FEBS J. 2010;277(5):1084-96.
38. Giannotta M, Trani M, Dejana E. VE-cadherin and endothelial adherens junctions: active guardians of vascular integrity. Dev Cell. 2013;26(5):441-54.
39. Seye CI, Yu N, Gonzalez FA, Erb L, Weisman GA. The P2Y2 nucleotide receptor mediates vascular cell adhesion molecule-1 expression through interaction with VEGF receptor-2 (KDR/Flk-1). J Biol Chem. 2004;279(34):35679-86.
40. Rumjahn SM, Yokdang N, Baldwin KA, Thai J, Buxton IL. Purinergic regulation of vascular endothelial growth factor signaling in angiogenesis. Br J Cancer. 2009;100(9):1465-70.
41. Galeano M, Bitto A, Altavilla D, Minutoli L, Polito F, Calo M, et al. Polydeoxyribonucleotide stimulates angiogenesis and wound healing in the genetically diabetic mouse. Wound Repair Regen. 2008;16(2):208-17.

42. Zhou Z, Merkus D, Cheng C, Duckers HJ, Jan Danser AH, Duncker DJ. Uridine adenosine tetraphosphate is a novel vasodilator in the coronary microcirculation which acts through purinergic P1 but not P2 receptors. Pharmacol Res. 2013;67(1):10-7.
43. Zhu C, Mustafa D, Zheng PP, van der Weiden M, Sacchetti A, Brandt M, et al. Activation of CECR1 in M2-like TAMs promotes paracrine stimulation-mediated glial tumor progression. Neuro Oncol. 2017;19(5):648-59.
44. Yang Y, Andersson P, Hosaka K, Zhang Y, Cao R, Iwamoto H, et al. The PDGF-BB-SOX7 axis-modulated IL-33 in pericytes and stromal cells promotes metastasis through tumour-associated macrophages. Nat Commun. 2016;7:11385.
45. Yang L, DeBusk LM, Fukuda K, Fingleton B, Green-Jarvis B, Shyr Y, et al. Expansion of myeloid immune suppressor Gr+CD11b+ cells in tumor-bearing host directly promotes tumor angiogenesis. Cancer Cell. 2004;6(4):409-21.
46. Mustafa DA, Dekker LJ, Stingl C, Kremer A, Stoop M, Sillevis Smitt PA, et al. A proteome comparison between physiological angiogenesis and angiogenesis in glioblastoma. Mol Cell Proteomics. 2012;11(6):M111 008466.
47. Squadrito ML, De Palma M. A niche role for periostin and macrophages in glioblastoma. Nat Cell Biol. 2015;17(2):107-9.
48. Liu AY, Zheng H, Ouyang G. Periostin, a multifunctional matricellular protein in inflammatory and tumor microenvironments. Matrix Biol. 2014;37:150-6.
49. Park SY, Piao Y, Jeong KJ, Dong J, de Groot JF. Periostin (POSTN) Regulates Tumor Resistance to Antiangiogenic Therapy in Glioma Models. Mol Cancer Ther. 2016;15(9):2187-97.
50. Sanada F, Taniyama Y, Muratsu J, Otsu R, Shimizu H, Rakugi H, et al. Gene-Therapeutic Strategies Targeting Angiogenesis in Peripheral Artery Disease. Medicines (Basel). 2018;5(2).
51. Kastrup J, Jorgensen E, Ruck A, Tagil K, Glogar D, Ruzyllo W, et al. Direct intramyocardial plasmid vascular endothelial growth factor-A165 gene therapy in patients with stable severe angina pectoris A randomized double-blind placebo-controlled study: the Euroinject One trial. J Am Coll Cardiol. 2005;45(7)
52. Hedman M, Hartikainen J, Syvanne M, Stjernvall J, Hedman A, Kivela A, et al. Safety and feasibility of catheter-based local intracoronary vascular endothelial growth factor gene transfer in the prevention of postangioplasty and in-stent restenosis and in the treatment of chronic myocardial ischemia: phase II results of the Kuopio Angiogenesis Trial (KAT). Circulation. 2003;107(21):2677-83.
53. Stewart DJ, Kutryk MJ, Fitchett D, Freeman M, Camack N, Su Y, et al. VEGF gene therapy fails to improve perfusion of ischemic myocardium in patients with advanced coronary disease: results of the NORTHERN trial. Mol Ther. 2009;17(6):1109-15.
54. Yla-Herttuala S, Bridges C, Katz MG, Korpisalo P. Angiogenic gene therapy in cardiovascular diseases: dream or vision? Eur Heart J. 2017;38(18):1365-71.
55. Isner JM, Vale PR, Symes JF, Losordo DW. Assessment of risks associated with cardiovascular gene therapy in human subjects. Circ Res. 2001;89(5):389-400.
56. Emmett MS, Dewing D, Pritchard-Jones RO. Angiogenesis and melanoma - from basic science to clinical trials. Am J Cancer Res. 2011;1(7):852-68.
57. Liu W, Ahmad SA, Reinmuth N, Shaheen RM, Jung YD, Fan F, et al. Endothelial cell survival and apoptosis in the tumor vasculature. Apoptosis. 2000;5(4):323-8.
58. Reinmuth N, Liu W, Jung YD, Ahmad SA, Shaheen RM, Fan F, et al. Induction of VEGF in perivascular cells defines a potential paracrine mechanism for endothelial cell survival. FASEB J. 2001;15(7):1239-41.
59. Shaheen RM, Tseng WW, Davis DW, Liu W, Reinmuth N, Vellagas R, et al. Tyrosine kinase inhibition of multiple angiogenic growth factor receptors improves survival in mice bearing colon cancer liver metastases by inhibition of endothelial cell survival mechanisms. Cancer Res. 2001;61(4):1464-8.
60. Zhou Z, Matsumoto T, Jankowski V, Pernow J, Mustafa SJ, Duncker DJ, et al. Uridine adenosine tetraphosphate and purinergic signaling in cardiovascular system: an update. Pharmacol Res. 2018.

Appendix

Nederlandse Samenvatting

Curriculum Vitae

List op Publications

PhD portfolio

Dankwoord

Nederlandse samenvatting

Alle cellen in het lichaam hebben zuurstof en voedingstoffen nodig om hun metabolisme in gang te houden. De toevoer van zuurstof en voedingstoffen wordt geleverd via een hiërarchisch netwerk van bloedvaten. Tijdens lichamelijke processen als weefselgroei, menstruatie en wondgenezing neemt de diffusie afstand en de vraag naar zuurstof en voedingstoffen toe, waardoor het bloedvatenstelsel zich moet uitbreiden. Dit proces wordt angiogenese genoemd. Het angiogenese proces bestaat uit verschillende signaal transductie routes die stuk voor stuk cruciaal zijn om bloedvaten te laten groeien uit het al bestaande netwerk van bloedvaten. Echter kan de aanmaak van nieuwe bloedvaten gemanipuleerd worden door verschillende cardiovasculaire ziekten en tumoren. Bij cardiovasculaire ziekten is er meestal een gebrek aan angiogenese wat er voor zorgt dat cellen geen zuurstof en voedingstoffen krijgen en daardoor afsterven. Bijvoorbeeld, tijdens een hartinfarct ontstaat er een verstopping (aderverkalking) in een van de kransslagaderen die het hart voorziet van zuurstof en voedingstoffen, waardoor het bloed niet meer efficiënt kan worden rond gepompt. Daardoor is de kans groot dat een deel van het hartweefsel afsterft en vervolgens niet meer de capaciteit heeft om de bloed volledig rond te pompen. In de ergste gevallen leidt tot hartstilstand met de dood als gevolg. Door angiogenese te stimuleren zou herstel kunnen op treden in het zuurstofarme hartweefsel en de aangerichte schade doen verminderen. In het geval van tumoren, zorgt de ongeremde groei van tumorcellen er voor dat angiogenese gestimuleerd moet worden, om aan de groeiende vraag van zuurstof en voedingstoffen te voldoen. Door angiogenese te remmen in dit proces, zou tumorgroei en metastasering geremd kunnen worden. Om meer inzicht te krijgen in het ontstaan van deze ziekten, is het cruciaal om de normale ontwikkeling van bloedvaten te onderzoeken. Angiogenese vindt voornamelijk plaats in de kleinste bloedvaten van het lichaam, ook wel capillairen (haarvaten) genoemd. De capillairen zijn opgebouwd uit endotheelcellen (ECs) en pericyten die nauw met elkaar in contact zijn via hun basaal membraan. De ECs en de pericyten communiceren met elkaar en met de zuurstof arme omgeving, om zo een stabiele capillaire netwerk van bloedvaten te genereren en te onderhouden. Deze communicatie wordt gekenmerkt, doordat op moleculair niveau biologische factoren worden aangemaakt die remming (anti-angiogenetisch) of stimulatie (pro-angiogenetisch) van vaatvorming stimuleren. Echter is er nog vrij weinig bekend over de fundamentele biologie en de moleculaire mechanismen die de communicatie bevorderd. Het moleculaire onderzoek beschreven in deze thesis beschrijft de ontdekking van vrijwel onbekende angiogenetische factoren die communicatie bevorderen tussen ECs en pericyten en biedt daarbij nieuwe gedetailleerde inzichten in de werking van het angiogenese proces. Dit kan leiden tot nieuwe perspectieven in de ontwikkeling van innoverende behandelingen van vaat gerelateerde ziekten.

In dit onderzoek werden biologische factoren (genen) ontdekt, door naar de genexpressie te kijken van premature endotheelcellen. Die afkomstig waren uit de bloedvatwand van muizenembryo's, nadat ze een bepaalde tijdstip bereikt hadden waarbij angiogenese het actiefst was. De genen werden vervolgens gevalideerd aan de hand van een *in vitro* model van

ECs die in direct contact stonden met pericyten. De genexpressie van ECs in co-cultuur werden vergeleken met de ECs in singel cultuur. Hieruit waren er target genen geselecteerd. In deze thesis werden 5 target genen gevalideerd door ze uit te schakelen in ECs en getoetst op angiogenetische eigenschappen in *in vitro* als *in vivo* modellen. Tevens werd er voor het eerst een veelbelovende metaboliet Up_4A, onderzocht op angiogenetische eigenschappen.

In **hoofdstuk 2** wordt het target gen CMTM3 geïdentificeerd als een mogelijk pro-angiogenetische factor. Door de genexpressie te verlagen in ECs zagen we een afname in bloedvatvorming tijdens de ontwikkeling van zebravissen (*in vivo)*. Hetzelfde effect werd ook geobserveerd *in vitro*, in een 3D co-cultuur kweekmodel waarin humane ECs en pericyten minuscule bloedvaten ontwikkelen. Aanvullend onderzoek in een kweekopstelling van HUVECs liet zien dat CMTM3 cel-cel contacten kon beheren door de aanwezigheid van het aanhechtingseiwit VE-cadherin te reguleren. VE-cadherin hecht de ECs als een rits aan elkaar waardoor er een ondoordringbare endotheelcel barrière ontstaat. Speciale Rab eiwitten zorgen ervoor dat er via endocytose aanhechtingseiwitten als VE-cadherin worden getransporteerd van het membraan naar het cytoplasma, om enerzijds gerecycled of anderzijds afgebroken te worden. Hierdoor raakt de endotheelcel barrière permeabel waardoor ECs worden geactiveerd om te migreren en/of te prolifereren, om zo een nieuw bloedvat te vormen. Door CMTM3 expressie te verhogen in ECs, bleek VE-cadherin te worden geïnternaliseerd via stimulatie van specifieke Rab eiwitten, namelijk clatherin, EEA1, Rab11, Rab 5 en Rab7. Vanuit de literatuur is bekend dat bloedvaten met weinig VE-cadherin op het membraan, zorgen dat bloedvaten permeabel worden en gaan lekken. Dit concept zou kunnen toegepast worden om meer inzicht te krijgen in de begin fase van angiogenese waarbij ECs los moeten komen van elkaar, om te kunnen prolifereren en migreren naar de zuurstofarme omgeving. In ziekten als kanker kan het nieuwe inzichten geven in de reden waarom bloedvaten rondom een tumor zo permeabel zijn. Dit zorgt er namelijk voor dat medicijnen niet de vaatwand kunnen passeren.
Het volgende target gen dat onderzocht wordt in **hoofdstuk 3** is CMTM4, een familielid van CMTM3. CMTM4 heeft bijna dezelfde pro-angiogenetische eigenschappen als CMTM3. Door de CMTM4 expressie te verhogen in ECs is er echter een verschil ontdekt in vergelijking met de functie van CMTM3. CMTM4 is sterk betrokken bij het internaliseren en recyclen van de VE-cadherin terug naar het plasma membraan, via RAB4 stimulatie. Dit impliceert dat CMTM4 een belangrijke rol speelt in het stabiliseren van premature bloedvaten door de EC barrière te herstellen. Al met al, biedt de CMTM-familie een nieuwe inkijk op de signaaltransductie van RAB-eiwitten die de endotheel cel barrière kunnen moduleren om zo het angiogenese proces te stimuleren.
De endotheel cel barrière wordt niet alleen in stand gehouden door VE-cadherin maar ook door zo geheten adherens junction eiwitten. Deze zorgen voor mechanische verbindingen tussen cytoskelet filamenten en het plasmamembraan via specifieke eiwitten gekoppeld aan transmembraan eiwitten (zoals cadherin eiwitten). Deze transmembraan eiwitten staan

vervolgens gekoppeld met naburige cellen en/of met het extra cellulaire matrix (ECM). Gedurende angiogenese zullen pericyten veranderingen in het ECM brengen waardoor adherens junctions zoals focal adhesion kinasen (FAK) worden gestimuleerd om het immature bloedvat te stabiliseren. In **hoofdstuk 4** wordt de endotheel specifieke CGNL1 geïdentificeerd als een belangrijke speler in het stabiliseren van bloedvaten door opbouw van focal adhesion junctions en adherens junctions te stimuleren, waarmee de endotheel cel barrière versterkt kan worden. Uitschakeling van CGNL1 in de retina van de muis zorgde voor een significante vermindering van bloedvaten. Dezelfde afname van bloedvaten werd geobserveerd in ons 3D co-cultuur kweekmodel van ECs en pericyten. Uit vervolg experimenten blijkt dat CGNL1 angiogenese reguleert door VE-cadherin te koppelen aan het actine cytoskelet, om zo de adherens junctions te stabiliseren. Vermindering van Cgnl1 zorgt namelijk voor een reductie in RAC1 (cytoskelet eiwit) activatie, waardoor FAK eiwitten als Vinculin, Paxallin en SRC te laat aangetrokken worden naar de junction plekken. Dit heeft negatieve gevolgen voor VE-cadherin accumulatie op de adherens sites, waardoor de endotheel cel barrière permeabel wordt. Echter, gedurende stabilisatie van bloedvaten communiceren de pericyten met de ECs door de Notch signaaltransductie route te activeren, die tevens ook de CGNL1 expressie verhoogd. Dit zorgt ervoor dat RAC1 wordt geactiveerd en de activatie van adherens junctions en tight junctions, om zo de endotheel cel barrière te versterken.

In **hoofdstuk 5** wordt er basaal gekeken naar de klinische toepasbaarheid van een ander endotheel specifieke target gen, die ook de endotheel cel barrière kan versterken, namelijk THSD1. Uit *in vivo* onderzoek in de retina van de muis en de zebravis, is er gebleken dat bloedingen optreden wanneer THSD1 werd uitgeschakeld in de cellen. Wat kan komen door een verslechterd endotheel cel barrière functie. Moleculair onderzoek in ECs toonde aan dat afname van THSD1 de koppeling verstoort tussen RAC1 en de CRT-LRP1 eiwitcomplex (die als secundaire boodschapper dient om RAC1 te activeren). Hierdoor raakt de bouw van het cytoskelet verstoord als mede de connectie met de naburige cellen en de ECM, waardoor er een verstoord endotheel cel barrière ontstaat met als gevolg bloedingen die optreden. Om dit effect te onderzoeken op klinische toepasbaarheid werd in muizen gekeken naar het effect van THSD1 op de groei van bloedvaten in de instabiele plaque (aderverkalking). Naarmate de plaque groter wordt, ontstaat er zuurstofarme omgeving in de plaque, dit zorgt ervoor dat angiogenese wordt getriggerd. Echter zijn de ontwikkelde bloedvaten in de plaque prematuur en zeer permeabel. Dit kan leiden tot intra-plaque bloedingen en in ergste geval plaque ruptuur met als gevolg een acuut hartinfarct. Het verlagen van de expressie van THSD1 in muizen met aderverkalking verergert de plaque groei, doordat de endotheel cel integriteit verslechtert wat leidt tot ernstige intra-plaque bloedingen. Het verhogen van THSD1 expressie bevordert de stabilisatie van de plaque en een afname in intra-plaque bloedingen vanwege het herstellen van de EC integriteit. THSD1 zou mogelijk nieuw inzicht kunnen geven om instabiele plaque vorming te voorkomen.

In **hoofdstuk 6** hebben we onderzoek gedaan naar de potentiële angiogenetische eigenschappen van het metaboliet Up_4A. Up_4A is een extracellulaire nucleotide die in stresscondities (hypoxie) gesynthetiseerd wordt door VEGFR2 in ECs. Vanwege het feit dat Up_4A een purine- en pyrimidine groep bezit, kan het purinergic receptoren activeren. *In vitro* onderzoek in een 3D co-cultuur model van ECs en pericyten liet een toename zien van bloedvaten na toevoeging van Up_4A. Moleculair onderzoek bevestigt dat de signaaltransductie via de pyrimidine receptoren gaat die vervolgens de activatie van angiogenetische factoren als VEGFa en ANGPT1 stimuleren. Dit maakt Up_4A een interessant metaboliet voor therapeutische toepassing om bij cardiovasculaire ziekten vaatgroei te stimuleren.

Het immuunsysteem speelt een belangrijke rol in angiogenese vooral in ziekten als glioma blastoma multiforme (GBM, tumorgroei in de hersenen). De polarisatie van glioma-geassocieerde-macrofagen (GAM) in M2-macrofagen, bepaalt de dichtheid van het vaatwerk in GBM. In **hoofdstuk 7** beschrijven we de functie van CECR1 op de vaatgroei in GBM. CECR1 polariseert monocyten in M2-macrofagen waardoor ze in de 3D co-cultuur model van ECs en pericyten veel vaatgroei en maturatie initiëren. Moleculair onderzoek in M2-macrofagen liet zien dat PDGFβ expressie toenam naarmate de GAM beïnvloedt werd door CECR1. Hiermee zorgt CECR1 er indirect voor dat de pericyten periostin gaan aanmaken. Periostin is een extracellulair eiwit dat veelal aanwezig is in GBM waar het angiogenese stimuleert en M2-GAM rekruteert. Dit zorgt voor verergering en uitbreiding van GBM. CECR1 kan hiermee een nieuw therapeutische target zijn voor het behandelen van GBM. Door CECR1 expressie te verlagen is het mogelijk om angiogenese te remmen, waardoor de glioma cellen zich niet kunnen kunnen uitbreiden en mogelijk afsterven vanwege een tekort aan zuurstof en voedingstoffen.

Concluderend, het onderzoek uitgevoerd in dit proefschrift beschrijft de ontdekking van potentiële target genen die allemaal een specifieke rol spelen in angiogenese. Daarnaast geeft het een basaal beeld van nieuwe signaaltransductie routes die nog niet eerder zijn geïdentificeerd en waarop dit moment nog geen focus op ligt, om nieuwe therapieën mee te ontwikkelen. Aangezien beschikbare therapieën met pro- of anti-angiogenetische factoren nog niet doeltreffend genoeg zijn en alleen gericht zijn op een specifieke signaaltransductie route, is het belangrijk om onderzoek te doen naar de samenwerking tussen meerdere signaaltransductie routen. Angiogenese is namelijk een complex proces en heeft bij elk ziekte een andere werking. Ook zouden de target genen kunnen bijdragen aan erfelijkheidsonderzoek om te bepalen of patiënten aanleg hebben voor bepaalde vasculaire ziekten.

Curriculum Vitae

Ihsane Chrifi is geboren op 13 april 1987 te Breda, Nederland. Op de Nassau scholengemeenschap behaalde hij zijn VWO diploma. Nadat hij uitgeloot was voor de studie Geneeskunde vervolgde hij zijn studie loopbaan aan het Erasmus Universiteit Rotterdam en volgde hierbij de opleiding Beleid Management in de Gezondheidszorg. Na 1 jaar de studie te volgen en nogmaals uitgeloot te zijn voor de studie Geneeskunde, veranderde hij zijn studierichting naar Biologie en Medisch Laboratoriumonderzoek. Hiervan behaalde hij zijn bachelor diploma aan de Avans Hogeschool te Breda, in 2010. Gedurende deze studie liep hij stage op de afdeling Experimentele Cardiologie in het Erasmus MC te Rotterdam, onder supervisie van dr. Caroline Cheng. Dat onderzoek richtte zich op atherosclerose en vaatwand biologie in angiogenese. Direct na afstuderen startte hij als research analist op dezelfde afdeling onder de supervisie van Caroline Cheng. In 2012 startte hij als onderzoeker in opleiding (OIO) bij dezelfde groep met als promotor prof. dr. Dirk-Jan Duncker en als co-promotor dr. Caroline Cheng. De resultaten van dit onderzoek staan beschreven in dit proefschrift.

List of publications

Kool HM, Bürgisser PE, De Kleer I, De Laat I, **Chrifi I**, Cheng C, Van Cappellen WA, Kremers GJ, Tibboel D, Rottier RJ. Inhibition of retinoic acid signaling induces aberrant pericyte coverage and differentiation resulting in vascular defects in congenital diaphragmatic hernia.
In revision American Journal of Physiology-Lung Cellular and Molecular Physiology.

Zhu C, Mustafa D*, Krebber MM*, **Chrifi I**, Leenen PJ, Duncker DJ, Zeneyedpour L, Dekker L, Luider T, Kros JM*, Cheng C*. Comparative proteomic analysis of the cat eye syndrome critical region protein 1- function in tumor-associated macrophages and immune response of glial tumors.
OncoTarget. 2018 Sep 11;9(71):33500-33514.

Chrifi I, Louzao-Martinez L, Brandt MM, van Dijk CGM, Bürgisser PE, Zhu C, Kros JM, Verhaar MC, Duncker DJ, Cheng C. CMTM4 regulates angiogenesis by promoting cell surface recycling of VE-cadherin to endothelial adherens junctions.
Angiogenesis. 2018 Aug 10; ahead of print.

Brandt MM, van Dijk CGM, **Chrifi I**, Kool HM, Bürgisser PE, Louzao-Martinez L, Pei J, Rottier RJ, Verhaar MC, Duncker DJ, Cheng C. Endothelial loss of FZD5 stimulates PKC/Ets1-mediated transcription of Angpt2 and Flt1.
Angiogenesis. 2018 Nov;21(4):805-821.

Chrifi I*, Hermkens D*, Brandt MM, van Dijk CGM, Bürgisser PE, Haasdijk R, Van de Kamp E, Zhu C, Blonden L, Kros JM, Duckers HJ*, Cheng C*. CGNL1, an endothelial junction complex protein, regulates GTPase mediated angiogenesis.
Cardiovascular Research. 2017 Dec 1;113(14):1776-1788.

Octavia Y*, Kararigas G*, de Boer M, **Chrifi I**, Kietadisorn R, Swinnen M, Duimel H, Verheyen FK, Brandt MM, Fliegner D, Cheng C, Janssens S, Duncker DJ[#], Moens AL[#]. Folic acid reduces doxorubicin-induced cardiomyopathy by modulating endothelial nitric oxide synthase.
Journal of Cellular and Molecular Medicine. 2017 Dec;21(12):3277-3287.

Chrifi I*, Zhu C*, Mustafa D, Van de Weiden M, Leenen JM, Duncker DJ, Kros JM[#], Cheng C[#]. Cecr1-mediated crosstalk between macrophages and vascular mural cells promotes neo-vascularization in malignant glioma.
Oncogene. 2017 Sep 21;36(38):5356-5368.

Zhu C, Mustafa D, Zheng PP, van der Weiden M, Sacchetti A, Brandt M, **Chrifi I**, Tempel D, Leenen PJM, Duncker DJ, Cheng C*, Kros JM*. Activation of CECR1 in M2-like TAMs promotes paracrine stimulation-mediated glial tumor progression.

Neuro-Oncology. 2017 May 1;19(5):648-659.

Chrifi I, Louzao-Martinez L, Brandt MM, Van Dijk CGM, Bürgisser P, Zhu C, Kros JM, Duncker DJ, Cheng C. CMTM3 (CKLF-Like Marvel Transmembrane Domain 3) mediates angiogenesis by regulating cell surface availability of VE-cadherin in endothelial adherens juntions.
Arteriosclerosis Thrombosis Vascular Biology. 2017 Jun;37(6):1098-1114.

Chrifi I*, Zhou Z*, Xu Y, Pernow J, Duncker DJ, Merkus D*, Cheng C*. Uridine adenosine tetraphosphate acts as a proangiogenic factor *in vitro* through purinergic P2Y receptors.
American Journal of Physiology Heart Circulation Physiology. 2016 Jul 1;311(1):H299-309.

Haasdijk RA*, Den Dekker WK*, Cheng C*, Tempel D#, Szulcek R, Bos FL#, Hermkens DM#, **Chrifi I,** Brandt MM, Van Dijk C, Xu YJ, Van de Kamp EH, Blonden LA, Van Bezu J, Sluimer JC, Biessen EA, Van nieuw Amerongen GP, Duckers HJ. THSD1 preserves vascular integrity and protects against intraplaque haemorrhaging in ApoE-/- mice.
Cardiovascular Research. 2016 May 1;110(1):129-139.

Chrifi I*, Cheng C*, Pasterkamp G, Duckers HJ. Biological mechanisms of microvessel formation in advanced atherosclerosis: the big five.
Trends in Cardiovascular Medine. 2013 Jul;23(5):153-64.

Cheng C, Haasdijk R, Tempel D, van de Kamp EH, Herpers R, Bos F, Den Dekker WK, Blonden LA, de Jong R, Bürgisser PE, **Chrifi I,** Biessen EA, Dimmeler S, Schulte-Merker S, Duckers HJ. Endothelial cell-specific FGD5 involvement in vascular pruning defines neovessel fate in mice. *Circulation. 2012 Jun 26;125(25):3142-3158.*

Cheng C, Haasdijk RA, Tempel D, Den Dekker WK, **Chrifi I,** Blonden LA, van de Kamp EH, de Boer M, Bürgisser PE, Noorderloos A, Rens JA, Ten Hagen TL, Duckers HJ. PDGF-induced migration of vascular smooth muscle cells is inhibited by heme oxygenase-1 via VEGFR2 upregulation and subsequent assembly of inactive VEGFR2/PDGFRβ heterodimers.
Arteriosclerosis Thrombosis Vascular Biology. 2012 May;32(5):1289-98.

Cheng C, Tempel D, Den Dekker WK, Haasdijk R, **Chrifi I,** Bos FL, Wagtmans K, Van de Kamp EH, Blonden L, Biessen EA, Moll F, Pasterkamp G, Serruys PW, Schulte-Merker S, Duckers HJ. Ets2 determines the inflammatory state of endothelial cells in advanced atherosclerotic lesions.
Circulation Research. 2011 Aug 5;109(4):382-395.

*/#Authors contributed equally to the study.

PhD portfolio

Naam PhD student :Ihsane Chrifi
Erasmus MC Department :Experimental Cardiology
Research School :COEUR
PhD period :2012-2018
Promotor :dr. C. Cheng, prof. dr. D.J.G.M. Duncker
Supervisor :dr. C.Cheng

General academic skills	Year	ECTS
Biomedical English writing and communication.	2015	1.5

Research skills	Year	ECTS
Training Flowcytometry .	2011	0.4
Training GGO.	2012	0.1
Optical Image Centre practical introduction to laser scanning microscopy.	2013	0.1
IncuCyte video imaging.	2015	0.1

In-depth courses	Year	ECTS
COEUR Molecular biology in atherosclerosis and cardiovascular research.	2011	1.5
NHF Vascular biology Papendal.	2012	2.0
NHF Cardiac function and adaptation Papendal.	2013	2.0
Cardiovascular regenerative medicine	2013	0.5
COEUR Hearth Failure research.	2014	1.5

National and international conferences	Year	ECTS
Vascular and cell biology in health and disease meeting (NvvC + FEDERA), Amsterdam.	2011	0.4
Cardio vascular conference (CVC), Noordwijkerhout.	2013	1
5th International Meeting on angiogenesis, Amsterdam.	2014	0.4
Cardio vascular conference (CVC), Heerlickheijd van Ermelo.	2014	0.6
DEBS, Amsterdam.	2014	0.6
Frontiers in cardiovascular biology (FCVB), Florence, Italy.	2016	1
American Heart Association (AHA) Scientific sessions, New Orleans, America.	2016	1.2
NHS 1st translational cardiovascular research meeting, Utrecht.	2017	0.4
ANZMS and AVBS conference, Mooloolaba, Australia.	2017	1

Dutch German meeting, Amsterdam.	2018	0.6

Presentations	**Year**	**ECTS**
Poster + oral presentation, NHF Papendal	2012	1.0
Poster presentation, NHF Papendal.	2013	0.5
Oral presentation, CVC.	2013	1.5
Poster presentation, Angiogenesis.	2014	0.5
Poster presentaion CVC.	2014	0.5
Oral presentation DEBS.	2014	1.5
Poster presentation FCVB.	2016	0.5
Poster presentation AHA.	2016	0.5
Oral presentation ANZMS and AVBS conference.	2017	1.5
Dutch German meeting, Amsterdam.	2018	0.5
Journal clubs.	2011-2018	1

Seminars and workshops	**Year**	**ECTS**
New strategegies for post infarction left ventricle dysfuntion.	2012	0.1
Endothelin in the picture.	2012	0.5
COEUR PhD day. (poster presentation).	2012	0.5
Biomarkers in cardiovascular diseases.	2013	0.5
COEUR PhD day. (poster presentation).	2013	0.5
Molecular and cellular mechanisms of remodeling.	2014	0.1
Current cardiac and vascular aging research.	2014	0.4
Specific molecular pathways and targeted therapy of right heart failure.	2014	0.1
JNI oncology lecture: principles of vascular patterning in development and disease.	2015	0.1
PhD day.	2016	0.4
Pharmacology department seminar of prof. Widdop Monash University.	2017	0.1
Rotterdam Science tower Postdoc network event.	2018	0.4

Supervision of students	**Year**	**ECTS**
M. Anandbahadoer: BMO bachelor student of Hogeschool Rotterdam.	2011	1
M. Rijken: BMO bachelor student of Avans Hogeschool Breda.	2011	1
H Meijer: BMO bachelor student of Avans Hogeschool Breda.	2011	1

H. Saleem: BMO bachelor student of Hogeschool Rotterdam	2012	1.3
M. Brandt: BMO bachelor student of Hogeschool Rotterdam.	2012	1.3
E. Salcedo Plazas: BMO bachelor student of Hogeschool Rotterdam.	2013	1
R. van Es: BMO bachelor student of Hogeschool Rotterdam.	2013	1
P. Sarikaya: BMO bachelor student of Hogeschool Rotterdam.	2013	1
M. Snelder: BMO bachelor student of Avans Hogeschool Breda.	2015	1.3
S. David: BMO bachelor student of Avans Hogeschool Breda.	2015	1.3
C. da luz: BMO bachelor student of Hogeschool Rotterdam.	2016	1

Total	**42.3**

Dankwoord

Dit proefschrift zou niet tot stand zijn gekomen zonder hulp van mijn collega`s, vrienden en familie. Jullie hebben me gemotiveerd om mijn wetenschappelijke verlangens uit te laten komen. Ik ben jullie dankbaar en vandaar deze ode.

Allereerst wil ik mijn promotor prof. Dirk Duncker bedanken. Als een ware mentor en uitdager heb je me gemotiveerd om vanuit een ander perspectief naar mijn onderzoek te kijken. De tijd en het vertrouwen dat je in mij persoonlijk en mijn onderzoek hebt gestoken, zal me altijd bijblijven. De manier hoe je me stimuleerde om aan mijn competenties te werken op een positieve toon, was een verlichting voor mij. Ik zal nooit vergeten dat je me de vertrouwen had gegeven om onze afdeling te vertegenwoordigen op een congres in Australië. Bovendien was je nauwkeurigheid in het nakijken van mijn abstracts, presentaties en manuscript en de gehele thesis, een bron van inspiratie.

Mijn co-promotor, Caroline. Ik ben je eeuwig dankbaar voor mijn aanstellen. Eerst als onervaren stagiaire, later als research analist en daarna als PhD-student. De tijd en energie die je in me investeerde heeft mij gemaakt tot de onderzoeker die ik nu ben. Je bent inspirerend en soms ook grappig, wetenschappelijk en ook pragmatisch wanneer nodig, zakelijk maar zeker niet afstandelijk. De interpretatie van resultaten en de vindingrijkheid van oplossingen elke keer weer, daar heb ik veel van geleerd. Je bent ook heel erg belangrijk geweest in de ontwikkeling van mijn schrijfstijl en mijn manier van presenteren. Zonder je eindeloze inzet en onvermoeibare voorkomen zou mijn proefschrift incompleet zijn.

De leden van mijn promotiecommissie, prof. Anton Horrevoets, prof. Max Kros en dr. Daphne Merkus wil ik bedanken voor het lezen en beoordelen van mijn proefschrift. Ook ben ik dankbaar dat zij zitting willen nemen in mijn promotiecommissie. Max, bedankt voor de leerzame samenwerking die we hebben gehad tijdens het CECR1 project. Daphne, ondanks dat je expertise in een ander gebied dan mijn onderzoek ligt, heb je toch de moeite genomen mij te adviseren en te beoordelen bij presentaties en mijn proefschrift. Ik ben je hier zeer dankbaar voor.

Mijn paranimf, Maarten, de oud-BeijerlanderT die ik heb zien opbloeien van mijn student tot aan mijn successor. Wij hebben veel van elkaar geleerd en daarbij een ware vriendschap opgebouwd, wat ons door de eindeloze PhD-tijd heen heeft gesleept. De fiets, de gastvrijheid (BBQ`s bij je thuis), het slakken symbool, de congressen, borrels, koffiemomenten en al die andere leuke momenten zullen me altijd bij blijven. Waaronder ook je ‘zangtalent’, die je wel eens in de problemen heeft gebracht. Je hebt daarmee een aantal collega`s behoorlijk van het werk afgehouden. Je bracht het zelfs zo ver, dat je je zelfs moest verstoppen. Je passie voor

Frizzled en de drang om altijd je resultaten aan me te laten zien en uit te leggen waren bijzonder. Met grote bewondering heb ik aanschouwd hoe je mijn adviezen implementeerde, dat deed je niet direct maar een maand later, wanneer je het zelf pas inzag. Onze samenwerkingen en steun wanneer nodig, zowel theoretisch als praktisch, waren mij een waar genoegen. Mooi dat je mij zelfs als paranimf wil blijven steunen. Ook jij zal binnenkort promoveren, met jouw passie voor wetenschap hoef je je helemaal niet druk te maken. Ik wens jou, jouw prachtige gezin en Feyenoord het beste toe.

Het MCL-lab zou niets zijn zonder de ervaren Esther en Lau. Esther (Essie) bedankt dat ik altijd bij je terecht kon voor praktische zaken en dat je meteen klaar stond voor mij als er iets geregeld moest worden. Jij bent diegene die me gemotiveerd heeft, toen nog als student, om mijn minor proefdierkunde te gaan halen. In mijn PhD-periode betrapte je me op allerlei zaken die ik beter anders had kunnen doen. Door jouw adviezen op sociaal en werk niveau, leerde ik mijn praktische handelingen te verbeteren. Lau (the Law), je hield ons in het gareel door ons de regels van het lab te leren, zodat er een sociaal werk milieu zou ontstaan. Wat helaas, tot jouw grote frustratie, niet altijd werkte. Met originele waarschuwingsbrieven voor elke apparaat zorgde je voor orde in de soms chaotische werk sfeer. Waar ik je het meest dankbaar voor ben, is voor de in mijn ogen onuitputtelijke kennis die je bezit en je vermogen om elk apparaat dat niet functioneert te herstellen. Dankzij jou werden mijn protocollen gepolijst, wat mij verder hielp om niet werkende protocollen aan de gang te krijgen, zoals de Co-IP.
Eric Duckers, ik ben je dankbaar voor alle financiële support die je me hebt gegeven als analist en aan het begin van mijn PhD-periode. Als beginnende stagiaire had ik Kim (Kimmie) om me wegwijs te maken in het lab en me te introduceren aan mijn collega`s. Heel erg bedankt voor alle tips en tricks! Pinar (π), abi bedankt voor de periode dat je een dag in de week over had, om mij een helpende hand te bieden. Jouw inzet, creativiteit en enthousiasme, zowel op sociaal als op werk niveau, zullen me altijd bijblijven.

De promotiekandidaten die voor mij zijn gepromoveerd, hebben elk een steentje bijgedragen aan mijn ontwikkeling als PhD-student. Dennie (“…on a stick!!!’’) en Vincent (dr. de Beer) ik heb veel gehad aan jullie manier van motiveren, ook wel afbouwende kritiek genoemd. Jullie wijsheden hebben er persoonlijk voor gezorgd dat ik bij elk onderzoek nog dieper moet graven om mijn onderzoek te verbeteren. De eenzijdige discussie over mijn resultaten, waar ik snel tevreden mee was, hebben mij kritischer gemaakt op mijn eigen manier van werken. Ik bewonder jullie daarvoor en voor het feit dat jullie altijd voor me klaar stonden. Wijnand, dankzij jouw manier van scherpe vragen stellen in mijn begin periode, werd ik gemotiveerd om mijn onderzoek beter te interpreteren. Veel succes met het afronden van je opleiding als interventie cardioloog. Renate, mijn Duckers-tijdperk was niet half zo leuk geweest zonder jou. We hadden een luisterend oor aan elkaar, in zowel leuke als moeilijke momenten. Ik wens je ontzettend veel succes met de afronding van je opleiding als anesthesioloog. Remco, we hadden

een kleine samenwerking voor het Thsd1 project en daar ben ik je dankbaar voor. Jouw doorzettingsvermogen gedurende tegenslagen, netheid op het lab en straffe looppas zullen me bijblijven. Changbin, without the CECR1 project we would never have met and I am glad that we worked together on this project. You are a smart hardworking man, who survived the MCL-lab culture. You even started to sing and make the same jokes as us. It was my pleasure to teach you as my grasshopper and always remember: you have to look into yourself to save yourself from the other self only then your true self will reveal itself. Zhichao, I am glad and thankful for persuading me to look into the molecular mechanism of a promising nucleotide Up_4A, hence we started working together and published an interesting article about it. André, bedankt voor je hulp en het beantwoorden voor al mijn bezorgde vragen over de promotieprocedures. Elza, bedankt voor je advies om meer vragen te stellen tijdens een werkbespreking, om me meer te betrekken bij andermans onderzoek. Ook bedankt voor het boek dat afspeelde in de tijd van de Andalusiërs. Mark, bedankt voor de grappige en de ooh zo bijdehante gesprekken en het uitleggen van het programma Endnote.

Mijn kamergenoten na mijn Duckers-tijd ben ik dankbaar voor de steun, gezelligheid en medeleven naar mijn promotie toe. Oana ik ben je dankbaar dat je Maarten en mij hebt “geadopteerd” toen het MCL-lab uit elkaar viel. Het spijt ons voor de drukte die daarbij gepaard ging, maar gelukkig kon je ons wel temmen als het moest. Je hield je prima staande tussen alle mannelijke collega`s en daar heb ik bewondering voor. Ruben als een protegé van Oana heb jij je prima ontwikkeld tot vaste waarde. Jouw levensfilosofie kwam bijna overeen met die van mij en dat zorgde voor aangename gesprekken. Nu daag ik je alleen nog uit om mijn tijd van de bruggenloop te evenaren of zelfs te verbeteren. Jens (Djens), als de nieuwe lichting AIO, waait er een frisse wind door de kamer. Jouw gedrevenheid en ambitie zal je zeker goed doen in je PhD-periode. Plus, iemand moet Maarten zo nu en dan van zijn wolkje halen.

Ik ben mijn stagiaires uitermate zeer dankbaar voor het harde werk dat ze geleverd hebben. Manisha, Mikel, Hans, Hamza, Estefania, Stephan, Matthijs, Pinar, Robert, Stephan en Celia, het was me een waar genoegen om jullie begeleider te zijn en jullie te zien afstuderen. Jullie hebben mij geleerd om mijn onderzoek op een universelere manier toe te lichten.

Om soms even te ontsnappen aan het moleculaire onderzoek, hoefde ik alleen de befaamde klapdeuren voorbij te lopen. Monique, wat is een afdeling zonder secretaresse die alles in een belletje of mailtje voor je kan regelen. Zonder jou zou ik nog steeds wachten op antwoord van de service desk of waren mijn formulieren nooit of niet op tijd ingevuld. Mijn dank is groot! Martine, als ik een pep-talk nodig had dan stond jij voor me klaar en dan niet alleen met advies maar ook met oplossingen. Van mijn stagetijd tot aan nu, heb je me altijd klaar proberen te stomen om vervolg stappen te maken. De congres uitnodiging, het stimuleren om voor mezelf op te komen, de praktische hulp als ik wat weefsel nodig had, het contact leggen met de

grafisch ontwerper, de gedrevenheid en nauwkeurigheid, heb ik heel erg gewaardeerd van je. Natuurlijk ook het slap lullen over de mooie reizen die je gemaakt hebt en nog wil gaan maken. Het is bijna jouw beurt om te gaan promoveren, ik heb er alle vertrouwen in dat het je goed af gaat, heel veel succes. Inge, bedankt voor het regelen van leuke uitjes, zoals de zevenkamp en het labuitje. Als jij iets organiseert dan is het altijd genieten. Yanti (sweet-harmless-Asian-girl), I had a great time teaching you Co-Ip and western blotting and I am glad that our teamwork was rewarded by publishing a very nice article. Your career driven mindset and hard work amazed me. I will always support you and I hope that one day you will be satisfied with all that you have and are going to accomplish. Als we het over Brabantse gezelligheid hebben dan moet ik bij Marion zijn. Bedankt voor de leuke herinneringen op het werk en daarbuiten. Mijn dag kon niet meer stuk toen ik eindelijk de man had ontmoet, waar bijna al jouw gesprekken over gaan. Ik hoop dat jij en Joris voor altijd gelukkig zullen blijven. Richard (Richie) de gesprekken die wij gehad hadden zal ik hier niet beschrijven, maar wat hadden wij een lol en respect daarvoor. Het was altijd fijn om even het werk los te laten en met jou levenswijsheden te delen. Ook jij gaat binnenkort promoveren, heel veel succes daarmee.

Mijn co-auteurs van het UMCU wil ik graag ook in het zonnetje zetten, zonder Christian en Laura waren een aantal van mijn hoofdstukken onvolledig. Christian, ik ben daadwerkelijk trots op de onderzoeker die jij bent geworden. Ik ken je al sinds we studeerden aan de Avans Hogeschool en ik heb je alleen maar zien groeien. Ik was ook heel erg blij dat je op mijn aandringen aangenomen werd op onze afdeling. Jouw passie en werkethos, dat je natuurlijk van ons hebt overgenomen, heeft er voor gezorgd dat je van onschatbare waarde bent in Utrecht. Ik ben je heel erg dankbaar voor de zebravis werk die je hebt gedaan voor mijn projecten en voor alle epische momenten buiten werktijd. Laura, bedankt voor de CMTM3 en -4 samenwerking die we zijn aangegaan. Mede door jouw inzet, energie en schrijftalent hebben we twee prachtige artikelen gepubliceerd. Beiden wens ik jullie veel succes met het afronden van je PhD.

My paranimf Adil (Omani) and my brother from another mother, Zouhair (Berkani). I wish I met you two sooner. I sincerely thank you guys for supporting me in finishing my PhD. You guys made working overtime fun. As soon as we had to work overtime we contacted each other to have dinner together or just help each other with stuff. Our trips to Luxembourg and Tunisia were epic and impossible to forget. Hope we can do that more often in the future. Both of you are almost finished with your PhD, I wish you all the best in writing your thesis and defending it.

Voor de rest wil ik Jeroen, Jelmer, Ilia, Shin, Tirza, Petra, Dorien, Mieke, Stijn, Jaco, Stefan, Metin, Jarno, Ilona, Annemarie, Zongye, Sena, Heleen, Anouchka, Kelly, Jelle, Nienke, Bibi, Tom, Leah, Do, Fasha, Bri, Erna, Yvette, Naomi, Klazina, Kim, Geraldine, Ayla, Anette, Eric, Mahnaz, Stephanie, Sam, Harold, Sophinese, Yuan, Hendrik bedanken voor de gezellige momenten op de werkvloer.

Mijn grafisch ontwerper Maarten, je hebt waarlijk een meesterwerk gemaakt van mijn kaft. Als een magiër die vele opties bezit, heb jij een kaft ontworpen waar ik alleen maar blij van wordt. De omgang, de inzet, de oog voor detail en de vertaling van mijn onderzoek in simpele vormen, had niemand beter kunnen doen. Bedankt held!

Om me echt af te sluiten van werk, hielp het om met vrienden af te spreken. In het bijzonder met de “Beertjes”: Lizanne, Sanne, Frank, Roel, Kathy, Arjan, Hazal, Stefanie (bedankt voor het nakijken van mijn dankwoord en samenvatting), Christian, Martijn, Lisanne, Renier en Sabine, maar ook buiten die groep kreeg ik steun van Rudolf, Bavo, Bastiaan, Johan om maar wat namen op te noemen. Bedankt voor alle ontstress momenten.

Mijn familie: papa, mama (moge Allah je ziel in vrede laten doen rusten en insha Allah het paradijs laten betreden), Manal, Ilhame, Hicham, Rachid, Ritaj en Fatima. De onvoorwaardelijke steun en liefde die ik van jullie heb gekregen om mijn grenzen te verzetten en te mikken op het hoogst haalbare, is voor mij van onschatbare waarde geweest. Ik kan jullie niet genoeg bedanken, jullie zijn erg belangrijk voor mij. Hoop dat jullie kinderen mij kunnen evenaren of zelf voorbij stevenen, insha Allah.

En als laatste, degene die mijn leven een doel geeft en mij stimuleert om het beste uit mijn zelf te halen. Om het leven te onderzoeken in al haar facetten, om zo te appreciëren wat de Schepper gemaakt heeft. Ash-Ha-Du An Laa illa-ha il Allah wa Ash-ha-du anna Muhammadan rasoel Allah. A salaam alaikum wa rahmatoelah wa barakatoehoe.